UNIVERSIDADE FEDERAL DO CEARÁ

CENTRO DE CIÊNCIAS

DEPARTAMENTO DE QUÍMICA ORGÂNICA E INORGÂNICA

PROGRAMA DE PÓS-GRADUAÇÃO EM QUÍMICA

KÉSYA AMANDA DANTAS ROCHA

VITANOLÍDEOS ANTIPROLIFERATIVOS E ANTI-INFLAMATÓRIOS ISOLADOS DAS FOLHAS DE Athenaea velutina (Sendtn.) D'Arcy - SOLANACEAE

FORTALEZA

2023

KÉSYA AMANDA DANTAS ROCHA

VITANOLÍDEOS ANTIPROLIFERATIVOS E ANTI-INFLAMATÓRIOS ISOLADOS
DAS FOLHAS DE *Athenaea velutina* (Sendtn.) D'Arcy - SOLANACEAE

Tese apresentada ao Programa de Pós-Graduação em Química da Universidade Federal do Ceará como parte dos requisitos para obtenção do título de Doutor em Química. Área de concentração: Química orgânica.

Orientadora: Professora Doutora Otília Deusdênia Loiola Pessoa.

FORTALEZA

2023

KÉSYA AMANDA DANTAS ROCHA

VITANOLÍDEOS ANTIPROLIFERATIVOS E ANTI-INFLAMATÓRIOS ISOLADOS
DAS FOLHAS DE *Athenaea velutina* (Sendtn.) D'Arcy - SOLANACEAE

Tese apresentada ao Programa de Pós-Graduação em Química da Universidade Federal do Ceará como parte dos requisitos para obtenção do título de Doutor em Química. Área de concentração: Química orgânica.

Aprovação em: 18/04/2023.

BANCA EXAMINADORA

_____
Profa. Dra. Otília Deusdênia Loiola Pessoa (Orientador)
Universidade Federal do Ceará (UFC)

_____
Profa. Dra. Mary Anne Sousa Lima
Universidade Federal do Ceará (UFC)

_____
Profa. Dra. Maria da Conceição Ferreira de Oliveira
Universidade Federal do Ceará (UFC)

_____
Prof. Dr. Joao Henrique Ghilardi Lago
Universidade Federal do ABC (UFABC)

_____
Prof. Dr. Jackson Roberto Guedes da Silva Almeida
Universidade Federal do Vale do São Francisco (UNIVASF)

A Deus, pela vida e perseverança nos estudos.

Aos meus pais, irmãs, esposo, filho e professores que participaram dessa conquista.

AGRADECIMENTOS

A Deus, porque sem ele nada seria possível. Aos meus pais, Onofre e Rosane, pelo amor e dedicação, que me conduziu na direção correta. As minhas irmãs Keidy e Ketley pela amizade e apoio, dividindo lágrimas e sorrisos comigo.

Ao meu esposo Lucas pelo amor, companheirismo e compreensão nos momentos em que estive ausente para a realização deste trabalho.

A minha avó Vina pelo carinho e atenção, aos meus tios, tias e primos pelos conselhos. Aos amigos do Passaredo que se tornaram minha família no Ceará.

Aos meus colegas de laboratório e agora Doutores, Chaguinha, Álison, Kaline, Herbert, Patrícia e Luana, pela convivência, experiências trocadas e pela disponibilidade em ajudar e somar sempre. Aos alunos de iniciação científica e mestrado que me ajudaram e que pude retribuir, Lucas, Joana e Lavosier.

A professora Dra. Otília Deusdênia Loiola Pessoa pela amizade, compreensão, dedicação e orientação na realização e elaboração do trabalho.

Ao Dr. Edilberto Rocha Silveira pelos conselhos e conhecimentos que enriqueceram o trabalho.

Ao Dr. Francisco das Chagas (Chaguinha) que me auxiliou em todo o mestrado, participou da coleta do material vegetal e ainda acompanhou todo o trabalho.

A todos os professores da trajetória pelo conhecimento e saber compartilhado, principalmente aos professores da Pós-Graduação em química pelos ensinamentos, os quais foram imprescindíveis para o desenvolvimento desse trabalho.

Ao programa da Pós-Graduação e aos seus funcionários, principalmente a Célia e a Lana, pelo apoio e amizade.

"Natural products still hold out the best options for finding novel agents/active templates, which when worked on in conjunction with synthetic chemists and biologists, offer the potential to discover novel structures that can lead to effective agents in a variety of human diseases" (Newman; Cragg, 2020).

RESUMO

Os vitanolídeos, lactonas esteroidas derivadas do ergostano, são uma classe de metabólitos secundários de grandes potencialidades farmacológicas, em especial contra doenças cancerígenas, autoimunes, inflamatórias e neurodegenerativas. A ocorrência dessa classe de compostos é comum em plantas da subfamília Solanoideae (Solanaceae). A investigação química do extrato das folhas de *Athenaea velutina* resultou no isolamento de quatorze novos vitanolídeos, incluindo três vitajardins, e outros conhecidos como 27-desidroxivitaferina A, 2,3-dihidro-27-desidroxivitaferina A, tuboanosigenina e vitaferina A. Os fracionamentos cromatográficos e a purificação dos compostos foram realizados por cromatografia em coluna aberta utilizando gel de sílica e cromatografia líquida de alta eficiência (CLAE). As estruturas dos compostos foram determinadas por técnicas espectroscópicas de infravermelho e ressonância magnética nuclear (1D e 2D), e espectrometria de massas. A configuração absoluta foi determinada por cristalografia de raio-X e dicroísmo circular. A atividade citotóxica dos compostos foi avaliada em quatro linhagens de células de câncer humano: SNB-19 (glioblastoma), PC-3 (próstata), HCT-116 (cólon), HL-60 (leucemia). A maioria dos vitanolídeos exibiram atividade citotóxica com valores de IC_{50} variando de 0,19 a 8,96 µg/mL. A atividade antii-nflamatória dos vitajardins foi avaliada através da quantificação da liberação de óxido nítrico (NO) induzida por lipopolissacarídeo (LPS) e citocinas pró-inflamatórias TNF-α e IL-6, em células RAW 264,7. Os vitajardins apresentaram valores de IC_{50} de 74,43 a 354,40 µM em células RAW 264,7 e atenuaram a liberação de NO induzida por LPS, além de diminuir as citocinas pró-inflamatórias TNF-α e IL-6. Para alguns dos vitanolídeos, foi realizado estudos de docking molecular e de dinâmica molecular contra o novo coronavírus (SARS-CoV-2) e os resultados sugeriram que vitanolídeos podem ser candidatos naturais contra o COVID-19.

Palavras-chave: *Athenaea velutina*; Solanaceae; vitanolídeos; atividade citotóxica; atividade anti-inflamatória; coronavírus; docking molecular.

ABSTRACT

Withanolides, steroidal lactones derived from ergostane, are a class of secondary metabolites with important potential pharmacological, particularly against cancer and autoimmune, inflammatory, and neurogenerative diseases. The occurrence of this class of compounds is common in plants of the subfamily Solanoideae (Solanaceaee). The chemical investigation from leave extract of *Athenaea velutina* resulted in the isolation of fourteen unreported withanolides, including three withajardins and four known withanolides: 27-dehydroxywithaferin A, 2,3-dihydro-27-dehydroxywithaferin A, tuboanesigenin, and withaferin A. The compounds isolation and purification were performed by chromatographic fractionation on sílica gel and high-performance liquid chromatography (HPLC). The compound structures were determined by spectroscopic methods such as IR and NMR (1D and 2D), and mass spectrometry. The absolute configuration was determined by X-ray diffraction and circular dichroism analyses. The antiproliferative properties of the withanolides were evaluated against four human cancer cell lines: SNB-19 (glioblastoma), PC-3 (prostate), HCT-116 (colon), and HL-60 (leukemia). Compounds displayed cytotoxic activity with IC_{50} values ranging from 0.19 to 8.96 µM. The anti-inflammatory activity of withajardins was evaluated by quantifying the release of nitric oxide (NO) induced by lipopolysaccharide (LPS) and the pro-inflammatory cytokines TNF-α and IL-6, in RAW 264,7 cells. The withajardins showed IC_{50} values from 74.43 to 354.40 µM in RAW 264.7 cells. In addition, attenuated the release of NO induced by LPS, and decreased the pro-inflammatory cytokines TNF-α and IL-6. Moreover, for some of the withanolides, molecular docking and dynamics studies against the new coronavírus (SARS-CoV-2) were carried out. The binding free energy results suggested that withanolides can be natural candidates against COVID-19 disease.

Keywords: *Athenaea velutina*; Solanaceae; withanolides; cytotoxic activity; anti-inflammatory activity; coronavírus; molecular docking.

LISTA DE ILUSTRAÇÕES

LISTA DE TABELAS

LISTA DE ABREVIATURAS E SIGLAS

AcOEt	Acetato de etila
APT	*Attached Proton Test*
BB	*Broad Band*
CCD	Cromatografia em camada delgada
COSY	*Correlation Spectroscopy*
AVFH/A	Extrato hexâno/Acetato de etila das folhas de *Aureliana velutina*
AVFE	Extrato etanólico das folhas de *Aureliana velutina*
HRESIMS	*High Resolution Electrospray Ionization Mass Spectrometer*
HMBC	*Heteronuclear Multiple Bond Correlation*
HSQC	*Heteronuclear Single Quantun Coherence*
Hz	Hertz
IDH	Índice de deficiência de hidrogênio
IV	Infravermelho
MeOH	Metanol
RMN ^{13}C	Ressonância magnética nuclear de carbono 13
RMN ^{1}H	Ressonância magnética nuclear de prótio
UV	Ultravioleta
Ortep	*Oak Ridge Thermal-Ellipsoid Plot Program*

LISTA DE SÍMBOLOS

J	Constante de acoplamento
α	Alfa
β	Beta
γ	Gama
δ	Delta
Δ	Delta

SUMÁRIO

1 INTRODUÇÃO

Os vitanolídeos pertencem a uma classe de metabólitos secundários conhecidos principalmente por suas potencialidades farmacológicas, incluindo doenças cancerígenas, autoimunes, inflamatórias e neurodegenerativas (WHITE et al., 2016), e como resultado, tornaram-se substâncias de grande interesse, com destaque na área oncológica (XU et al., 2016; DOM et al., 2020).

O relato de isolamento do primeiro vitanolídeo foi publicado em 1965, isolado das folhas *Withania somnifera* (família Solanaceaee), uma planta medicinal de origem indiana, popularmente conhecida como "ashwagandha" ou "ginseng indiano" e usada no sistema ayurvédico há mais de 3.000 anos (YOUSEFIAN et al., 2018; KIM et al., 2019).

No sistema Ayurveda, esta planta tem propriedades afrodisíacas, eficaz no rejuvenescimento e prolongamento da vida. Possui habilidades de renovação e regeneração, usado no tratamento de exaustão nervosa, insônia, condições relacionadas à memória, aprendizado e concentração, além de problemas de pele, cansaço e tosse (KHANCHANDANI et al., 2019). A aplicação tópica das bagas e folhas desta planta tem sido usada como remédio caseiro para úlceras e tumores. É utilizado como tônico hepático, anti-inflamatório, antioxidante, anti-stress e antidepressiva (SINGH et al., 2022)

Das oito espécies que compreende o gênero *Withania* (BAKRIN et al., 2022), *W. somnifera* é domimante, com centenas de trabalhos que incluem atividades de impacto na medicina, entre elas, as atividades anti-inflamatória, antibacteriana, antifúngica, antiviral, antitumoral, imunomoduladora, antiestresse, anticonvulsivante, neurofarmacológica, hepatoprotetora, espasmolítica, antioxidante, anti-hiperglicêmica. Além disso, foram observados efeitos de tolerância à morfina e inibidor da dependência química (KHANCHANDANI et al., 2019).

Em decorrência do valor medicinal e baixa toxicidade, a farmacopeia indiana documenta oficialmente a planta como um medicamento, desde 1985, sendo seu valor medicinal atribuído, principalmente, aos vitanolídeos (CHAUHAN et al., 2022).

Segundo Zamberlam (2012), a ocorrência de vitanolídeos é restrita a alguns gêneros da família Solanaceae, com ocorrência em todos os gêneros da subtribo Withaninae, na qual os gêneros *Withania* e *Athenaea* fazem parte.

Apesar da diferença geográfica de ocorrência dos gêneros, uma análise filogenética baseada nas sequências de genes, revelou que os gêneros *Withania* e *Athenaea* devem permanecer agrupados por suas semelhanças botânicas (ZAMBERLAM, 2012).

Enquanto o gênero *Withania* é endêmico do continente asiático, *Athenaea* spp. apresenta centro de diversidade principalmente no Brasil, com uma única espécie identificada no estado do Ceará, *Athenaea velutina* (Sendtn) D´Arcy.

Nesse contexto, este trabalho descreve o estudo fitoquímico do extrato orgânico das folhas de *A. velutina,* concentrando-se no isolamento, caracterização, e avaliação da atividade farmacológica de seus principais metabólitos secundários, os vitanolídeos.

1.1 Objetivos

1.1.1. Objetivo geral

Investigar o extrato hexano/AcOEt das folhas de *A. velutina* com vistas ao isolamento e caracterização química de seus metabólitos secundários, bem como avaliar atividades farmacológicas.

1.1.2. Objetivos específicos

✓ Isolar novos metabólitos secundários, particularmente, vitanolídeos;
✓ Caracterizar de forma inequívoca suas estruturas químicas, incluindo os aspectos estereoquímicos;
✓ Avaliar atividades farmacológicas, em particular, citotóxica e anti-inflamatória.

2 CONSIDERAÇÕES GERAIS

2.1 A família Solanaceaee e o gênero *Athenaea*

Solanaceaee é uma das maiores famílias entre as angiospermas eudicotiledôneas, compreendendo cerca de 100 gêneros e 2.500 espécies, distribuídas em todo o mundo, embora com maior diversidade e concentração na região Neotropical (SAMPAIO et al., 2019).

A América do Sul contém o maior número de gêneros e espécies de Solanaceaee, podendo ser encontrados em *habitats* que variam drasticamente como as regiões dos Andes e Amazônia (MISICO et al., 2011), sendo este último, considerado um dos principais centros de diversidade taxonômica e endemismo (SAMPAIO et al., 2019).

De acordo com Misico e colaboradores (2011), Solanaceaee é a terceira família mais importante economicamente e a mais valiosa, em vegetais comestíveis, como *Solanum tuberosum* (batata), *S. muricatum* (melão), *S. lycopersicum* (tomate), *S. melongena* (berinjela), *S. aethiopicum* (jiló) e especies do gênero *Capsicum* (pimentas e pimentão).

Entre os gêneros produtores de plantas medicinais, se destacam: *Solanum*, *Atropa*, *Capsicum*, *Datura*, *Withania* e *Nicotiana*. Solanaceaes tambem possuem um grande elenco de plantas ornamentais, representado pelos gêneros *Brunfelsia*, *Cestrum*, *Datura*, *Petunia* e *Calibrachoa*. Por fim, *Nicotiana tabacum* (tabaco) também apresenta grande impacto econômico, tanto pelos recursos gerados com seu cultivo e industrialização, como em despesas geradas na saúde pública (ZAMBERLAM, 2012).

Além da importância ecomômica dos gêneros *Nicotiana*, *Solanum* e *Capsicum*, algumas espécies dos gêneros *Withania* e *Physalis* são reconhecidas por suas propriedades medicinais, atribuídas à presença dos vitanolídeos (SINGH et al., 2022).

A ocorrência de vitanolídeos é restrita à subfamília Solanoideae, na qual incluem os gêneros *Acnistus*, *Jaborosa*, *Datura*, *Physalis*, e *Nicandra,* além dos gêneros da subtribo Withaninae, *Athenaea*, *Aureliana*, *Deprea*, *Tubocapsicum*, *Discopodium*, *Nothocestrum*, *Mellissia* e *Withania*. Uma análise filogenética, baseada em sequências de genes e fragmentos de restrição do DNA plastidial, revelou que dois dos gêneros acima mencionados, isto é, *Athenaea* e *Withania* são muito próximos do ponto de vista morfológico e possuem como grupo irmão, o gênero *Tubocapsicum* (ZAMBERLAM, 2012).

Os gêneros *Aureliana* e *Athenaea* foram simultaneamente descritos na Flora brasiliensis de Martius pelo botânico Alemão Otto Sendtner em 1846. Ambos são exclusivamente neotropicais com centros de diversidade pricipalmente no sudeste do Brasil

(RODRIGUES; KNAPP; STEHMANN, 2019). Apesar das similaridades morfológicas desses gêneros, estes se diferenciam pelo cálice crescente em frutos (RODRIGUES et al., 2016).

As plantas dos gêneros *Athenaea* e *Aureliana* são arbustos ou pequenas árvores com altura entre 1,5 a 8 m. As folhas são geminadas, ovadas, elípticas ou lanceoladas. Suas flores são axilares, pentâmeras e corola rotada com 5 a 17 mm de altura, apresentam máculas esverdeadas, arroxeadas ou amarronzadas na superfície interior das pétalas acordo com a espécie. Os frutos são pequenos (1 a 1,5 cm de diâmetro), de forma ovoides com diversas sementes (ZAMBERLAM, 2012).

Os gêneros *Athenaea* e *Aureliana* apresentavam sete e oito espécies, respectivamente, mas, após uma recente revisão botânica realizada por Rodrigues e colaboradores (2019), baseados em aspectos morfológicos do cálice e pólen e estudos filogenéticos relaccionados na sequência de DNA, revelaram que as espécies de *Athenaea* e *Aureliana* não são distintas, e assim, todos os táxons reconhecidos como *Aureliana* foram transferidos para *Athenaea* Sendtn.

O gênero *Athenaea* contempla 14 espécies (TABELA 1, pag. 18) duas delas descritas recentemente por Rodrigues e colaboradores (2021), *A. altoserranae* I.M.C. Rodrigues & Stehmann (São Paulo) e *A. hunzikeriana* I.M.C. Rodrigues & Stehmann (nordeste de Minas Gerais e sul da Bahia).

Athenaea é um pequeno gênero sul-americano, com espécies endêmicas da Mata Atlântica brasileira, com distribuição geográfica nos estados da Bahia, Espírito Santo, Minas Gerais, Rio de Janeiro, São Paulo, Paraná e Santa Catarina, exceto *A. fasciculata* (Vell.) I.M.C. Rodrigues & Stehmann, espécie que ocorre tanto no Brasil como na Argentina, Bolívia, Paraguai e Peru (RODRIGUES; KNAPP; STEHMANN, 2021).

O gênero é composto pelas espécies *A. angustifolia* (Alm.-Lafetá) I.M.C. Rodrigues & Stehmann, *A. anonacea* Sendtn., *A. brasiliana* Hunz., *A. cuspidata* Witasek, *A. picta* (Mart.) Sendtn., *A. pogogena* (Moric.) Sendtn., *A. sellowiana* (Sendtn.) I.M. Rodrigues & Stehmann, *A. tomentosa* (Sendtn.) I.M.C Rodrigues & Stehmann, *A. velutina* (Sendtn.) D'Arcy e *A. wettsteiniana* (Witasek) I.M.C. Rodrigues & Stehmann.

Tabela 1 - Ilustração das espécies de *Athenaea* e sua distribuição geográfica

Espécies	Distribuição Geográfica
1. *Athenaea altoserranae*	Brasil (São Paulo).
2. *Athenaea angustifolia*	Brasil (Minas Gerais e Espírito Santo).
3. *Athenaea anonacea*	Brasil (Minas Gerais, Rio de Janeiro e São Paulo).
4. *Athenaea brasiliana*	Brasil (Minas Gerais, Rio de Janeiro e São Paulo).

5. *Athenaea cuspidata*

Brasil (Bahia, Espírito Santo, Minas Gerais e São Paulo).

6. *Athenaea fasciculata*
A. fasciculata var. *fasciculata* (Sendtn.) Hunz. & Barboza

A. fasciculata var. *longifolia* (Sendtn.) Hunz. & Barboza

Argentina (Misiones),
Bolivia (Pando),
Brasil (Acre, Alagoas, Bahia,
Distrito Federal,
Espírito Santo, Minas Gerais,
Pará, Paraná, Pernambuco,
Rio de Janeiro,
Rio Grande do Sul, São Paulo
e Santa Catarina),
Paraguai (Alto Paraná,
Caazapá) e Peru (Madre de
Dios).

A. fasciculata var. *tomentella* (Sendtn.) Hunz. & Barboza.

7. *Athenaea hunzikeriana*

Brasil (nordeste de Minas Gerais e sul da Bahia)

8. *Athenaea martiana* Sendtn.

Brasil (Espírito Santo, Minas Gerais e Rio de Janeiro).

9. *Athenaea picta* (Mart.) Sendtn.

Brasil (Espírito Santo, Minas Gerais, Paraná, Rio de Janeiro, Rio Grande do Sul, Santa Catarina e São Paulo).

10. *Athenaea pogogena* (Moric.) Sendtn.

Brasil (Bahia, Espírito Santo, Minas Gerais, Rio de Janeiro e São Paulo).

11. *Athenaea sellowiana*   Brasil (São Paulo).

12. *Athenaea tomentosa*	Brasil (Espírito Santo, Minas Gerais, Rio de Janeiro e São Paulo).
13. *Athenaea velutina*	Brazil (Bahia, Ceará, Distrito Federal, Goiás e Minas Gerais).
14. *Athenaea wettsteiniana*	Brasil (Paraná, Rio Grande do Sul, São Paulo e Santa Catarina).

Fonte: Adaptado de RODRIGUES et al., 2019; 2021

Como mencionado, a ocorrência de vitanolídeos é restrita a plantas da subfamília Solanoideae, sendo *W. somnifera* (L.) Dunal a mais relevante, por ser uma planta medicinal de grande importância na medicina ayurvédica. Esta é mundialmente reconhecida em virtude de suas atividades farmacológicas (KHANCHANDANI et al., 2019). As substâncias isoladas de *W. somnifera* sempre foram de grande interesse para a comunidade científica desde o isolamento de do primeiro vitanolídeo, vitaferina A.
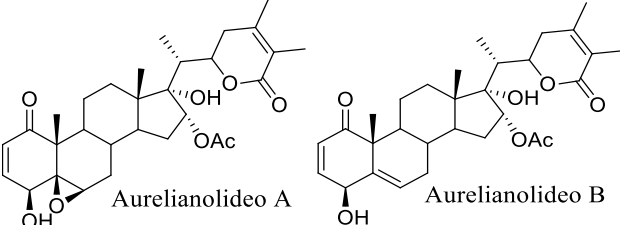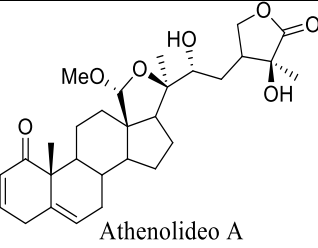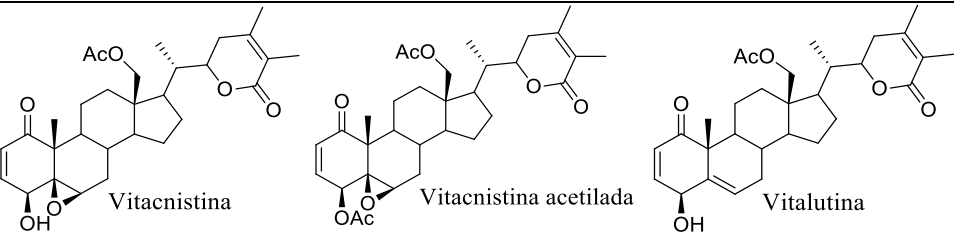
Além dos vitanolídeos (vitasomniferina A, vitanolides A-Y, vitasomniferols A-C, vitasomniferina, vitanone, Vitanolídeo A e vitaferina A), outros compostos biologicamente ativos, como os alcaloides ashwagandhina, anahigrina, cuscohigrine e tropina foram descritos em *W. somnifera* (KHANCHANDANI et al., 2019).

Devido à grande semelhança entre os gêneros *Withania* e *Athenaea* (ZAMBERLAM, 2012), pressupõe-se que espécies do gênero *Athenaea* sejam, também, fontes promissoras dos vitanolídeos. Portanto, embora a localização geográfica de *W. somnifera* seja

na África, Europa e Ásia enquanto *Athenaea* spp. apresenta centro de diversidade principalmente no Brasil, espera-se que o perfil metabólico das espécies *Athenaea* sejam similares aos encontrados em *W. somnifera* (ZAMBERLAM, 2012).

Das 14 espécies descritas para o gênero, apenas para 3 delas, há relatos de estudos fitoquímicos: *A. fasciculata* (ALMEIDA-LAFETA´ et al., 2010), *A. martiana* (SILVA et al., 2018) e, recentemente, *A. velutina* (ALMEIDA et al., 2022), Tabela 2. Dos seis vitanolídeos descritos para o gênero *Athenaea*, apenas vitacnistina e seu derivado acetilado já haviam sidos previamente isolados de *Acnistus arborescens* (KUPCHAN et al., 1969). Estes estudos corroboram com o trabalho descrito por Zambelam et al. 2012 e quimiotaxonomia dos gêneros que compõe a subfamília Solanoideae.

Tabela 2 - Vitanolídeos identificados/isolados de plantas do gênero *Athenaea*

Espécie	Compostos identificados ou isolados
A. fasciculata	Aurelianolideo A Aurelianolideo B
A. martiana	Athenolideo A
A. velutina	Vitacnistina Vitacnistina acetilada Vitalutina

Fonte: próprio autor.

Um estudo realizado por Almeida e colaborades (2020), mostrou que dos 196 extratos preparados por maceração com solventes orgânicos e água destilada, de plantas nativas da Mata Atlântica brasileira, o extrato das folhas de *A. velutina* mostrou maior atividade citotóxica e antimetastática, na qual inibiu a migração, adesão, invasão e formação de colônias celulares em células B16F10 (melanoma murino) (FIGURA 1).

Figura 1 - Avaliação histológica do melanoma B16F10 em camundongos.
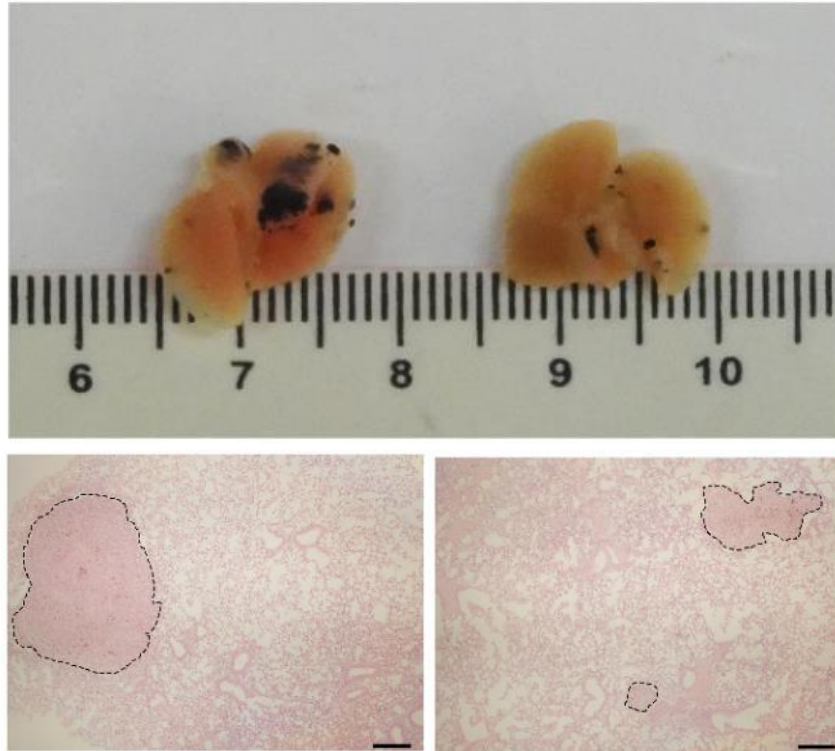
Fonte: ALMEIDA et al., 2020

O tratamento com o extrato foi realizado durante 21 dias após a inoculação das células tumorais. Após o tratamento, a área ocupada pela metástase interna, foi quatro vezes menor após o tratamento (ALMEIDA et al., 2020). Esses resultados mostram a importância dos constituintes (vitanolídeos) de *A. velutina*. Estes compostos confirmam a identidade quimiotaxonômica do gênero, incluída na subtribo Withaninae, juntamente com *Whitania*.

A. velutina (FIGURA 2, pag. 24), popularmente conhecida como baga-de-morcego, fruta-de-morcego ou jurubeba-de-morcego, é um arbusto ou arvoreta que frutifica entre os meses de janeiro a abril, sendo a única espécie com distribuição geográfica no estado do Ceará.

Figura 2 - Fotografias de *A. velutina* com destaque para folhas (**A**), frutos
(**B**) e flor (**C**).

Fonte: Edilberto Rocha Silveira

A Figura 3 abaixo, mostra a distribuição geográfica das espécies de *A. velutina*
proposta com base na localidade de coleta dos espécimes depositados nos herbários, sendo o
estado de Minas Gerais, o de maior concentração de indivíduos.

Figura 3 - Distribuição geográfica de *Ahenaea velutina*.
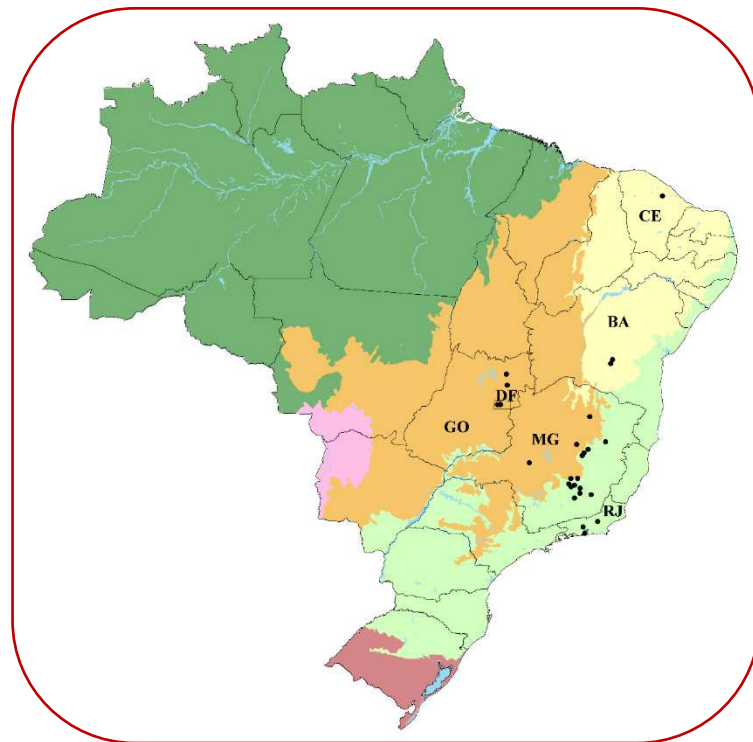
Fonte: ALMEIDA, A. A. (2019).

2.2 A química dos vitanolídeos

Os vitanolídeos são lactonas esteroidais com estrutura baseada no esqueleto ergostano C$_{28}$, no qual os carbonos 22 e 26 são oxidados para formar uma δ-lactona e menos comumente, com oxidação em C-23, para formar uma γ-lactona (LLANOS et al., 2017), como ilustrado na Figura 4. Outra variação, incluem os tipos δ e γ-lactóis, as formas reduzidas das carbonilas em C-26.

Figura 4 - Estruturas dos vitanolídeos δ e γ-lactonas.

δ-lactona γ-lactona
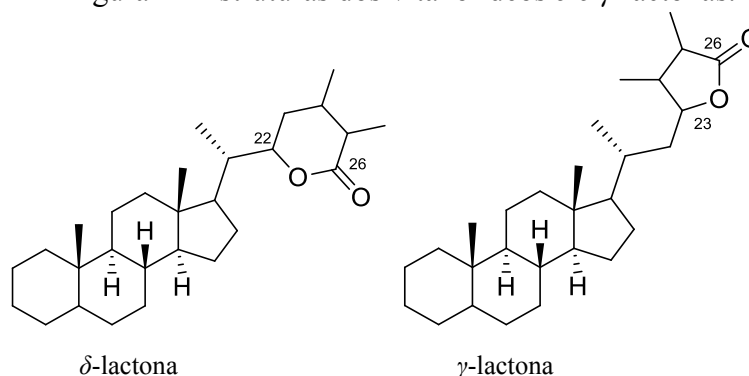
Os vitanolídeos apresentam a mesma estereoquímica em C-22, que corresponde configuração absoluta 22R, exceto quando os substituintes em C-23 ou C-22 alteram as prioridades relativas dos grupos em torno do centro assimétrico (MISICO et al., 2011).

A excessão foi verificada em daturacina, isolada de *Datura inoxia*, constituindo o primeiro Vitanolídeo com configuração absoluta 22S (configuração baseada no efeito Cotton negativo em 249,4 nm) (SIDDIQUI et al., 2005). No entanto, um vitanolídeo foi relatado com configuração 22S e necessita de revisão para mudança da estereoquímica (XIA et al., 2021).

As lactonas esteroidais C$_{28}$, do tipo δ-lactona, podem ser classificadas em dois subgrupos, ou seja, sem ou com modificações no esqueleto básico.

O esqueleto sem modificação é o mais abundante, sendo considerado um possível precursor dos outros vitanolídeos, representando aproximadamente 75 por cento de todos os tipos δ-lactona ou δ-lactol (XIA et al., 2021).

As várias possibilidades podem ser melhor compreendidas na Figura 5 (pag. 26) e incluem: 5β,6β-epóxidos (**a**), mais comuns, os quais normalmente trazem um grupo hidroxila em C-4 com orientação β; 5-eno (**b**), os que também são biossintetizados em número considerável; 6α,7α-epóxidos (**c**), que geralmente contém um grupo hidroxila em C-5 com configuração *alfa*. Os vitanolídeos 5α,6α-epóxidos (**d**) ocorrem em menor frequência, enquanto os 6β,7β-epóxidos (**e**) são bastante incomuns (CHEN; HE; QIU, 2011).

Figura 5 - Principais possibilidades de estruturas sem modificações no esqueleto.

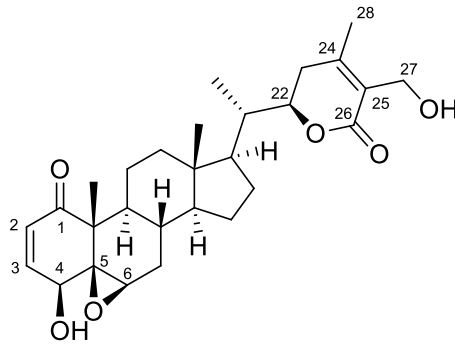(a)   (b)   (c)   (d)   (e)
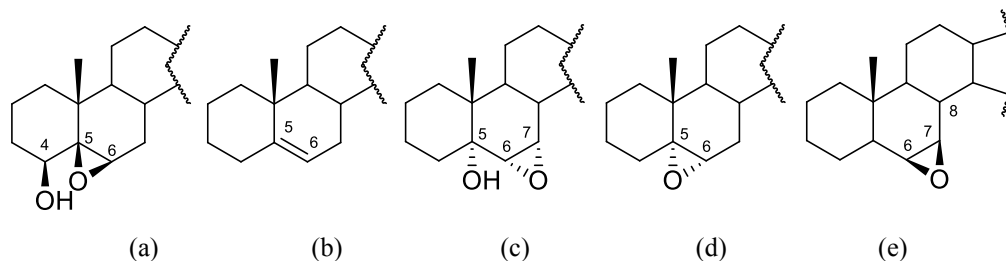
Os vitanolídeos também são facilmente oxidados na posição C-1, sendo mais de 90% desses compostos 1-oxosteroides (CHEN; HE; QIU, 2011). Com excessão do carbono quaternário (C-10), todos os átomos de carbono no esqueleto Vitanolídeo já foram encontrados em suas formas oxigenadas, tornando os grupos funcionais e os transformando em moléculas polioxigenadas (XIA et al., 2021).

Para esta grande família de lactonas esteroidais existem diversos tipos de estruturas, consequentemente, o elevado número de oxigenação produz inúmeras modificações do esqueleto, tanto no núcleo esteroide (C-14 a C-18) quanto na cadeia lateral (C-20, C-21, C-26 e C-27) (XU et al., 2016). Como resultado, os compostos são divididos em classes, como: vitafisalina, fisalina, neofisalina, acnistina, vitajardin, vitametelin, Vitanolídeo do tipo norbornano, sativolideo, δ-lactona espiranoide, δ-lactona subtriflora, $14\alpha, 20\alpha$-epóxido, anel A aromático, anel D aromático e δ-lactona taccalonolideo (CHEN; HE; QIU, 2011; MISICO, et al., 2011) representados no Quadro 1, pag. 28.
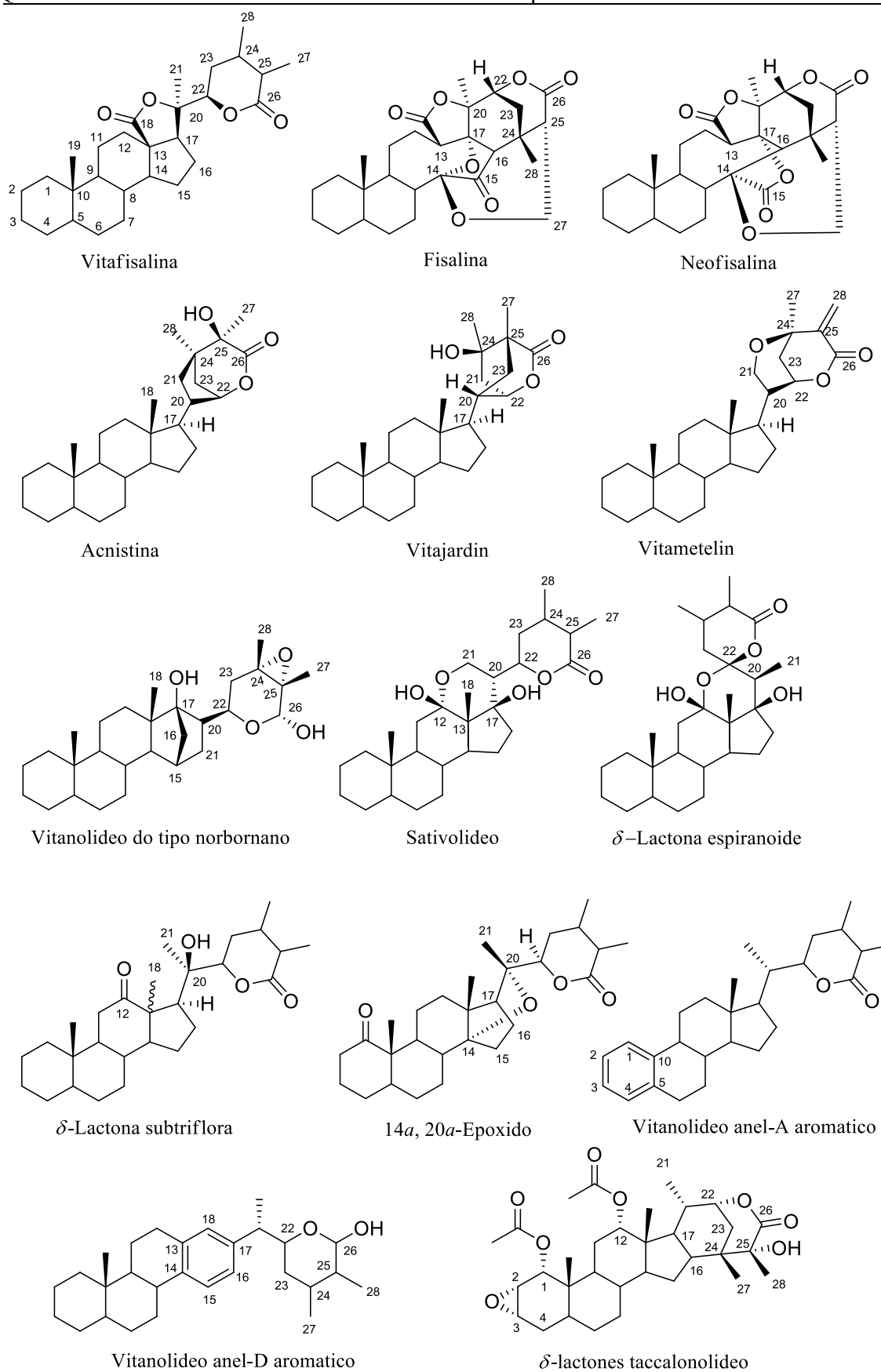
Dentre as diversas variações do esqueleto, para a estrutura da vitaferina A (FIGURA 6, pag. 27) foram relatadas inúmeras atividades biológicas/farmacológicas, atribuídas à presença do sistema $5\beta,6\beta$-epoxi-2-en-1-ona no anel A e B, bem como a insaturação no carbono C-24/C25 no anel E δ-lactona, enquanto a presença de outros substituintes contendo oxigênio é conhecida por modular essas atividades (XU et al., 2016).

A relação estrutura atividade dos vitanolídeos tem sido amplamente investigada, particularmente no que se refere à citotoxicidade sobre células tumorais. Independentemente do modelo estrutural, a presença do sistema α,β-conjugado no anel A, somado à presença da hidroxila em C-4 e do epóxido em C-5/C-6, ambos β-orientados, constituem as unidades farmacofóricas essenciais para a atividade (YONEYAMA et al., 2015; XU et al., 2015). Outro aspecto menos importante, embora relevante a ser mencionado, é a presença da dupla ligação em C-24/C-25, que ao sofrer epoxidação (XU et al., 2017) ou hidrogenação (KIM et al., 2019) tem sua atividade reduzida, bem como a hidroxilação em C-27 (XU et al., 2017).

Figura 6 - Estutura do Vitanolídeo vitaferina A.

Quadro 1 - Diferentes estruturas de vitanolídeos do tipo δ-lactona ou δ-lactol.

Vitafisalina

Fisalina

Neofisalina

Acnistina

Vitajardin

Vitametelin

Vitanolideo do tipo norbornano

Sativolideo

δ−Lactona espiranoide

δ-Lactona subtriflora

14a, 20a-Epoxido

Vitanolideo anel-A aromatico

Vitanolideo anel-D aromatico

δ-lactones taccalonolideo

Fonte: Adaptado de CHEN, HE, QIU, 2011; MISICO, et al., 2011.

2.3 A vitaferina A e suas atividades farmacológicas

Apesar das inúmeras atividades relatadas para os vitanolídeos, poucas plantas são produtoras destes compostos com aplicações etnofarmacológicas, como é o caso da *W. somnifera*, uma planta indiana cujas folhas e raízes são prescritas para a cura de tumores, inflamação e distúrbios relacionados (CHEN; HE; QIU, 2011), além de ser utilizada para fins terapêuticos como: sedativa, rejuvenecedora, afrodisíaca e intensificadora da saúde (YOUSEFIAN et al., 2018).

O uso tradicional de *W. somnifera* (Ashwagandha) está relacionado com o aumento da energia, vigor juvenil, força e resistência, além de aumentar os fluidos vitais, nutrir o corpo, sangue, produção das células e sêmen. Ajuda a combater a fadiga crônica, desidratação, fraqueza, impotência, tensão muscular, e atua no rejuvenescimento dos órgãos reprodutivos (KHANCHANDANI et al., 2019).

A Índia é o maior produtor de Ashwagandha, o mercardo de exportação internacional abrange mais de 3.000 milhões de dólares americanos (CHAUHAN et al., 2022).

Normalmente, a parte mais utilizada da planta é a raiz, facilmente encontrada em ervanários, lojas de produtos naturais, farmácias de manipulação, mercados e algumas feiras livres (KHANCHANDANI et al., 2019). Em sites de compras online o extrato na forma de cápsula é vendido pelos laboratórios Swanson®, OficialFarma® e Dehon®.

Devido ao enorme potencial etnofarmacológico de *W. somnifera*, em 1965 as pesquisas de Lavie, Glotter e Shvo resultaram no isolamento e caracterização do primeiro vitanolídeo, o qual foi denominado de vitaferina A, em alusão ao gênero. Este composto foi, posteriormente, comprovado ser o responsável pela atividade antitumoral, propriedade farmacológica de intensidade atribuída à planta (YOUSEFIAN et al., 2018; WIJERATNE et al., 2018).

Ao longo dos anos a vitaferina A foi objeto de uma grande variedade de estudos químicos e farmacológicos, sendo atualmente considerada como uma molécula altamente promissora na área oncológica (DOM; BERGHE; OSTADE, 2020).

Com isso, muitos estudos se concentraram na busca pelo isolamento e avaliação da atividade de compostos pertencentes a esta classe química.

Como consequência da diversidade estrutural, tem sido relatados uma variedade de atividades biológicas e farmacológicas, tais como: neuroprotetora (RABHI et al., 2019), leishmanicida (LIMA et al., 2018), antibacteriana (NICOLÁS et al., 2015), imunomoduladora (BHAT et al., 2005), antifúngica (ROUMY et al., 2010), antidiabética (LEE et al., 2016), anti-

inflamatória (DONG et al., 2019), e anticâncer, atividade de maior impacto para essa classe de compostos (MINGUZZI et al., 2002; ZHANG et al., 2011; TAO et al., 2015).

Adicionalmente, foi descrita pela primeira vez a atividade cardioprotetora em baixas concentrações da vitaferina A (GUO et al., 2019).

Ainda nesse contexto, os vitanolídeos têm sido investigados contra a COVID-19, um grande enredo na medicina com o recente surto da nova doença provocado pelo SARS-CoV2, gerando uma ameaça para toda a população humana por seu alto índice de contaminação e indisponibilidades de medicamentos específicos. Com isso, um elevado número de pesquisas concentraram seus esforços na busca pelo tratameno e cura desta doença. Em uma dessas pesquisas, realizadas por Chandel e colaboradoes (2020), foram selecionados 19 compostos antivirais e fitoquímicos ativos aprovados na biblioteca do FDA (*Food and Drug Administration*), cinco dos quais eram vitanolídeos, vitaferina A, Vitanolídeo D, 27-hidroxivitanolídeo, 17α-hidroxivitanolídeo e aswagandhanolídeo. Desses, a vitaferina A e o Vitanolídeo D mostraram-se potenciais inibidores contra a principal protease SARS-CoV2.

Outros estudos mostram que a vitaferina A é capaz de se ligar à proteína S de SARS-CoV-2, inibindo potencialmente a infecção e/ou disseminação da doença (STRAUGHN; KAKAR, 2020). Além disso, a vitaferina A pode ser usada com segurança em intervenções preventivas e terapêuticas para COVID-19 (CHAKRABORTY et al., 2022).

Recentemente, foi relatado que a vitaferina A aumenta a sensibilidade à leptina e previne a obesidade, uma vez que, pessoas obesas, em sua maioria, tornam-se resistentes à ação desse hormônio. O elevado nível de leptina no plasma coexiste com a adiposidade excessiva evidenciando uma resistência à leptina, impedindo sua aplicação clínica no tratamento da obesidade (GUO et al., 2022).

A vitaferina A ainda mostrou atividade de inibição da enzima acetilcolinesterase, com efeito neuroprotetor benéfico no tratamento do sistema colinérgico associado as doenças como a de Alzheimer. O estudo foi realizado para destacar os efeitos neuroprotetores da vitaferina A no comprometimento de memória induzida por escopolamina (BAKRIM et al., 2022).

Embora seja bastante explorado no campo oncológico, o mecanismo molecular de sua ação e vias de sinalização ainda não foram totalmente explorados. No entanto, uma triagem virtual identificou o potencial de interação em ambos os sítios catalíticos e alostéricos do ABL, sugerindo a vitaferina A, um inibidor da ABL e consequentemente da proliferação descontrolada e inibição da apoptose na Leucemia Mieloide Crônica, semelhante às drogas Imatinib e Asciminib (MALIK, et al., 2022).

3 METODOLOGIA

3.1 Materiais e métodos

3.1.1 Métodos cromatográficos

3.1.1.1 Cromatografia de adsorção

As separações cromatográficas foram realizadas por cromatografia de adsorção em coluna sobre sílica gel 60 com granulometria entre 0,063 e 0,200 mm da Merck e sílica para cromatografia gravitacional sob média pressão com granulometria entre 40 μm e 0,063 mm (cromatografia flash). O comprimento e o diâmetro das colunas variaram de acordo com as quantidades de adsorbato e de gel de sílica empregados. As colunas utilizadas na cromatografia de adsorção sob média pressão foram de vidro resistente à pressão e continham bulbos no ápice, para armazenamento de solvente. Foi empregada nesta técnica, bomba de ar comprimido modelo Inalar Compact N° 682403 de Ind. de aparelhos médicos Ltda.

As cromatografias em camada delgada foram efetuadas em placas pré-revestidas com 200 μm de espessura de sílica gel 60 F-254 (Silicycle). Os eluentes utilizados nos procedimentos cromatográficos foram: hexano, diclorometano, triclorometano, acetato de etila, acetona, isopropanol e metanol, puros ou em misturas binárias com proporções crescentes de polaridade ou não (isocrático) para a fase normal. A revelação das substâncias nas cromatoplacas analíticas foi realizada por exposição à radiação ultravioleta (UV) no equipamento Boitton modelo BOIT-LUB 01 em dois comprimentos de onda (254 e 365 nm) e/ou por aspersão com solução de sulfato de cério [Ce(SO$_4$)] seguido de aquecimento em chapa aquecedora a 100 °C por aproximadamente 1 minutos.

3.1.1.1 Cromatografia líquida de alta eficiência (CLAE)

A separação por CLAE foi realizada em aparelho da marca SHIMADZU®, modelo UFLC, equipado com sistema de bomba ternário modelo LC-20 AT, desgaseificador tipo DGU-20 AS, detector UV-Vis com arranjo de diodo, modelo SPD-M20A e um forno termostático para acomodar a coluna, modelo CTO-20 A. A separações foi realizada por coluna semi-preparativa de C18 (10 mm x 250 mm, 5 μm) da marca Phenomenex®, em temperatura mantida a 35°C. O metanol (solvente grau CLAE) foi filtrado em membranas de nylon com poros de

0,45 μm (Milipore). As amostras foram dissolvidas na mistura metanol e H_2O desionizada/TFA 0,1% e filtradas através de membranas de politetrafluoreltileno PTFE/B 0,22 μm da unichro.

3.1.2 Métodos espectroscópicos

3.1.2.1 Espectroscopia na região do infravermelho (IV)

Os espectros de absorção na região do infravermelho (IV) foram obtidos em espectrômetro Shimadzu IR-tracer-100, com transformada de Fourier. As amostras foram analizadas em pastilhas de KBr. Os dados por transmitância foram obtidos com 64 scans e resolução de 4 cm^{-1}.

3.1.2.2 Espectroscopia de ressonância magnética nuclear (RMN)

Os espectros de Ressonância magnética nuclear de prótio (RMN ^1H) e de carbono-13 (RMN ^{13}C) uni e bidimensionais, foram obtidos em espectrômetros Bruker, modelo AVANCE DPX-300, operando na frequência do hidrogênio a 300,13 MHz e na frequência do carbono a 75,48 MHz e AVANCE DRX-500, operando na frequência do hidrogênio a 500,13 MHz e na frequência do carbono a 175,48 MHz, pertencentes ao Centro Nordestino de Aplicação e Uso da Ressonância Magnética Nuclear, da Universidade Federal do Ceará (CENAUREMN-UFC). Os solventes deuterados utilizados na dissolução das amostras para obtenção dos espectros são comercializados pela Cambridge Isotope Laboratories Inc. Os deslocamentos químicos (δ) foram expressos em partes por milhão (ppm). Nos espectros de RMN ^1H as moléculas residuais não deuteradas dos solventes utilizados apresentaram sinais em δ_H 8,73, 7,59 e 7,22 para piridina e em δ_H 7,27 para o cloroformio. Nos espectros de RMN ^{13}C os resquícios de solventes não deuterados apresentaram deslocamentos químicos em δ_C 150.2; 136,0 e 123,9 para piridina e δ_C 77,7, 77,2 e 76,8 para o clorofórmio. A multiplicidade dos sinais de hidrogênio nos espectros de RMN ^1H foi indicada segundo a convenção: s (simpleto), d (dupleto), dd (dupleto de dupleto), dt (dupleto de tripleto), t (tripleto), td (tripleto de dupleto), m (multipleto). O padrão de hidrogenação dos carbonos foi determinado através da utilização da técnica BB e DEPT 135º (CH e CH_3 com amplitude em oposição ao CH_2).

3.1.2.1 Espectrometria de massa de alta resolução (EMAR)

Os espectros de massa de ionização por eletrospray de alta resolução (HRESIMS) foram obtidos em equipamento Acquity Xevo UPLC, acoplado a um sistema Quadrupolo/TOF, da Waters, pertencente à Empresa Brasileira de Pesquisa Agropecuária (EMBRAPA).

3.1.3 Métodos Físicos

3.1.3.1 Ponto de Fusão

Os pontos de fusão foram registrados em um aparelho digital MQAPF-302-Micro química Equipamento Ltda. Com temperatura inicial em 30 ºC e variação de 10 ºC/mim até 100 ºC e variação de 2 ºC/mim até a fusão.

3.1.3.2 Cristalografia de raios X

As medidas de difração de raios X de cristal único foram realizadas em um difratômetro Bruker D8 Venture equipado com fontes microfoco de Molibdênio ($\lambda K\alpha$ = 0,71073 Å) e Cobre ($\lambda K\alpha$ = 1,54178 Å) e um Detector CMOS Photon II. Os dados foram processados dentro da interface Bruker APEX e a estrutura determinada usando o pacote de programas Shelx.

3.2 Parte experimental

3.2.1 Coleta do material botânico

As folhas de *A. velutina* foram coletadas em Pico Alto, no municipio de Guaramiranga/Ceará, Brasil, em 14 de janeiro de 2019 (S 04º 12.590', W 38º 58.244') pelo Prof. Dr. Edilberto Rocha Silveira, do Departamento de Química Orgânica e Inorgânica da Universidade Federal do Ceará.

O material vegetal de *A. velutina* foi identificado pela botânica Profa. Drª Valéria Sampaio, do Departamento de Biologia da Universidade Federal do Ceará. A exsicata preparada foi depositada no Herbário Prisco Bezerra (EAC)/UFC, com o número de inscrição EAC45010. Amostra cadastrada no SisGen com número A5C2E09

3.2.2 Obtenção dos extratos das folhas de A. velutina: AVFH/A e AVFE

As folhas secas e pulverizadas de *A. velutina* (2,0 Kg) foram depositadas em frascos de Mariote para extração a frio com hexano/acetato de etila 1: 1 (10 L) à temperatura ambiente. Após 24 horas, o solvente foi evaporado sob pressão reduzida em evaporador rotativo, para a obtenção do extrato denominado AVFH/A. O mesmo procedimento de extração com solvente foi submetido com a torta mais duas vezes de 24 horas. Foi obtido nas três extrações um total de 95,0 g de AVFH/A, com rendimento de 4,7%. Uma segunda extração foi realizada com 10 L de etanol por 24 horas. Da mesma forma que à extração anterior, o solvente foi evaporado e a torta submetida à outra extração com etanol por 24 horas, obtendo um total de 104,0 g de extrato etanólico codificado AVFE, com rendimento de 5,2%.

3.2.3 Fracionamento Cromatográfico de AVFH/A

O extrato AVFH/A (90,0 g) foi adsorvido em 180,0 g de gel de sílica e fracionado em coluna cromatográfica de vidro (Øint= 7,3 cm) com 60,0 g de gel de sílica utilizando um sistema gradiente de eluição com hexano, hexano/AcOEt 2:1; hexano/AcOEt 1:1; AcOEt, AcOEt/MeOH 1:1 e MeOH 1:1 e MeOH. Foram obtidas 53 frações de 100 mL, que após análise comparativa em CCD, foram reunidas de acordo com suas semelhanças como pode ser observado na TABELA 3 abaixo.

Tabela 3 - Dados referentes ao fracionamento cromatográfico do extrato AVFH/A

Fração	Massa (g)
A (1)	3,6
B (2-9)	9,2
C (10-11)	20,1
D (12-13)	4,2
E (14-23)	8,3
F (24-27)	8,3
G (28-34)	7,1
H (35-42)	13,4
I (43-53)	8,8
	Massa total: 83,0 g
	Rendimento: 92,2%

Fonte: próprio autor

3.2.4 Coluna Cromatográfica da fração E (AVFH/A-E)

A fração E (8,3 g), eluída com hexano/AcOEt 2:1, foi adsorvida em 20,0 g de gel de sílica e acondicionada em uma coluna cromatográfica (Øint= 5,7 cm) contendo 100,0 g dessa

sílica. Em sistema gradiente de eluição com hexano/AcOEt 9:1, 7:3, 5:5, 4:6, 3:7, 8:2, AcOEt, e AcOEt/MeOH 1:1, foram obtidas 40 frações de 50 mL cada, reunidas após análise comparativa das frações nas cromatoplacas reveladas (TABELA 4, pag. 35).

Tabela 4 - Dados referentes ao fracionamento cromatográfico da fração AVFH/A-E

Subfração	Massa (mg)
EA (1-5)	245,0
EB (6-12)	846,3
EC (13-14)	956,0
ED (15-16)	1088,3
EE (18-20)	2240,7
EF (21-22)	1522,3
EG (23-25)	576,8
EH (26-28)	191,3
EI (29-40)	380,3
	Massa total: 8047,0 mg Rendimento: 97%

Fonte: próprio autor

Isolamento de AV1

A subfração EE (2240,7 mg), eluída com hexano/AcOEt 4:6, apresentou precipitado esverdeado após evaporação do solvente. O precipitado foi lavado com AcOEt obtendo-se 383,0 mg de cristais brancos (AV1).

3.2.5 Coluna cromatográfica fração Fp (AVFH/A-Fp)

A fração F (8,3 g), eluída com hexano/AcOEt 1:1, foi lavada com AcOEt obtendo 4,1 g de precipitado esverdeado. O precipitado (Fp) foi adsorvido em 8,5 g de gel de sílica e cromatografado (Øint= 4,6 cm) com 100,0 g dessa sílica em CH_2Cl_2/acetona 5% no modo isocrático, obtendo 57 frações de 25 mL cada. Após análise comparativa das cromatoplacas reveladas, as frações foram reunidas de acordo com suas semelhanças, como pode ser observado na Tabela 5 a seguir.

Tabela 5 - Dados referentes ao fracionamento cromatográfico de AVFH/A-Fp

Subfração	Massa (mg)
FpA (1-8)	22,6
FpB (9-13)	2239,0
FpC (14-27)	1138,0
FpD (28-37)	481,0
FpE (38-44)	76,2
FpF (45-47)	46,6
FpG (48-57)	39,6
	Massa total: 4043,0 mg Rendimento: 98,1%

Fonte: próprio autor

Isolamento de AV2

A subfração FpB (2239,0 mg) foi adsorvida em 4,0 g de gel de sílica e submetida em coluna cromatográfica (Øint= 3,3 cm) com 120,0 g dessa sílica. Sob média pressão, a fração foi eluída em sistema isocrático com CH_2Cl_2/acetona 5%. Foram obtidas 45 frações de 25 mL reunidas de acordo com suas semelhanças observadas em cromatoplacas da seguinte forma: 1-11 (FpBA-18,0 mg), 12-15 (FpBB-1490,0 mg)*, 16-21 (FpBC-156,9 mg), 22-33 (FpBD-436,0 mg)* e 34-45 (FpBE-14,5 mg) com rendimento de 94,5%. As subfrações FpBB e FpBD correspondem aos compostos AV1 e AV2 respectivamente.

Isolamento de AV3 e AV4

A subfração FpD (481,0 mg) foi adsorvida em 1,0 g de gel de sílica e submetida em coluna cromatográfica (Øint= 2,9 cm) acondicionada com 50,0 g de gel de sílica. Em sistema isocrático de eluição com CH_2Cl_2/acetona 3%, sob média pressão, foram obtidas 26 frações de 25 mL, as quais foram reunidas após análise comparativa por CCD da seguinte forma: 1-11 (FpDA-12,2 mg), 12-13 (FpDB-48,3 mg), 14-15 (FpDC-144,0 mg)*, 16-20 (FpDD-59,0 mg)* e 21-26 (FpDE-148,0 mg)* com rendimento de 85,6%. As subfrações FpDC, FpDD e FpDE precipitaram-se como sólidos cristalinos que correspondendo aos compostos AV2, AV3 e AV4 respectivamente.

3.2.6 Coluna cromatográfica fração Gp (AVFH/A-Gp) e G (AVFH/A-G)

A fração G (7,1), eluída com hexano/AcOEt 1:1, foi lavada com AcOEt obtendo 2,0 g de precipitado branco. O precipitado Gp (2,0 g) foi adsorvido em 4,0 g de gel de sílica e submetido em coluna cromatográfica (Øint= 4,6 cm) com 100,0 g de sílica. Através do sistema de eluição gradiente com CH_2Cl_2/acetona 9,5:0,5, 7:3, 5:5 e acetona, foram obtidos 54 subfrações de 25 mL reunidas após análise comparativa por CCD de acordo com a Tabela 6.

Tabela 6 - Dados referentes ao fracionamento cromatográfico de AVFH/A-Gp

Subfração	Massa (mg)
GpA (1-6)	25,1
GpB (7-11)	224,0
GpC (12-21)	630,0
GpD (22-23)	64,5
GpE (24-31)	629,8
GpF (32-36)	194,7
GpG (37-39)	30,1
GpH (40-45)	23,5
GpI (46-47)	6,0
GpJ (48-51)	43,1
GpK (52-54)	37,5
	Massa total: 1908,3 mg
	Rendimento: 95,4%

Fonte: próprio autor

Isolamento de AV5

As subfrações GpB, GpD e GpH precipitaram na forma de sólidos cristalinos correspondentes aos compostos AV2, AV4 e AV5 nesta ordem.

Isolamento de AV6, AV7, AV8, AV18 e A1

A fração G remanescente em AcOEt (5,1 g) foi adsorvida em 10,5 g de gel de sílica para o preparo do adsorbato, o qual foi submetido ao fracionamento em coluna cromatográfica (Øint= 5,5 cm) com 100,0 g de gel de sílica e eluído em sistema gradiente com hexano/AcOEt 10-80%, AcOEt e AcOEt/MeOH 1:1. Foram obtidas 47 subfrações de 50 mL cada, as quais foram analisadas e reunidas em acordo com suas semelhanças observadas em cromatoplacas (TABELA 7).

Tabela 7 - Dados referentes ao fracionamento cromatográfico de AVFH/A-G

Subfração	Massa (mg)
GA (1-14)	275,6
GB (15-23)	1181,9
GC (24-27)	481,4
GD (28-32)	944,5
GE (33-40)	37,9
GF (41-44)	684,2
GG (45-47)	498,2
	Massa total: 4103,7 mg
	Rendimento: 79,4%

Fonte: próprio autor

A subfração GD (944,5 mg), eluída com hexano/AcOEt 50%, foi adsorvida em 2,0 g de gel de sílica e fracionada em coluna cromatográfica em (Øint= 3,5 cm) com 30,0 g de gel de sílica, eluída em sistemas de gradiente com CH_2Cl_2/acetona 5%, 10%, 20% e 1:1, resultando em 38 subfrações de 20 mL cada, com rendimento de 86,8%. As subfrações foram analisadas e reunidas por suas semelhanças reveladas em cromatoplacas da seguinte forma: 1-5 (GDA-34,3 mg), 6-9 (GDB-234,6 mg), 10-12 (GDC-149,2 mg), 13-14 (GDD-103,3 mg)*, 15-24 (GDE-241,5 mg)*, 25-30 (GDF-26,5 mg) e 31-38 (GDG-30,4 mg).

A subfração GDD (103,3 mg), eluída com CH_2Cl_2/acetona 5%, foi adsorvida em 200,0 mg de gel de sílica, submetida ao fracionamento cromatográfico (Øint= 1,8 cm) em 20,0 g de gel de sílica e eluída em sistema isocrático com CH_2Cl_2/acetona 4%. Foram obtidas 40 frações de 10 mL cada, com rendimento de 76,4% e reunidas conforme suas semelhanças reveladas em cromatoplacas da seguinte forma: 1-14 (GDDA-14,4 mg), 15-25 (GDDB-23,1 mg)*, 26-36 (GDDC-8,0 mg), 37-38 (GDDD-10,4 mg), 39-40 (GDDE-22,8 mg)

A subfração GDDB (23,1 mg) foi submetida ao fracionamento por CLAE com injeção de 200 µL da amostra já dissolvida em 3 mL da mistura H_2O/ACN 60%. A separação foi realizada em coluna semipreparativa de C-18, usando como fase móvel H_2O(0,005%TFA)/ACN 65% em sistema isocrático, com um fluxo de 4,0 mL/min.

Foram coletados dois picos com tempo de retenção de 5,76 min (pico 1) e 8,71 min (pico 2), com tempo total de corrida de 10 minutos (Figura 7). O pico 2 forneceu 4,1 mg correspondente ao composto AV18

Figura 7 - Cromatograma da subfração GDDB observada na faixa de 210-400 nm.
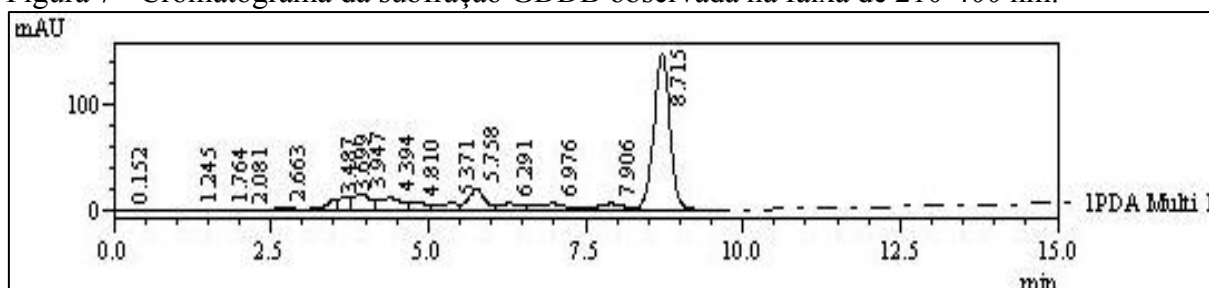
Fonte: Próprio autor

A subfração GDE (241,5 mg) um precipitado verde obtido da eluição com CH_2Cl_2/acetona 5 e 10%, foi lavado com AcOEt e obteve um precipitado branco com 99,5 mg resultando no composto AV7.

Enquanto isso, a subfração GDF (26,5 mg) foi adsorvida em 60 mg de gel de sílica e submetida em coluna cromatográfica (Øint= 3,5 cm) com gel de sílica (13,0 g), eluída com

CH$_2$Cl$_2$/acetona 10% resultando em 11 subfrações de 25 mL, com rendimento de 74,6%, as quais foram analisadas por CCD e reunidas por semelhanças da seguinte forma: 1-5 (GDFA- 7,5 mg), 6-9 (GDFB- 8,5 mg), 10-11 (GDFC- 3,7 mg)*. A subfração GDFB corresponde ao composto A1 (8,0 mg).

A subfração GF (684,2 mg) eluída com AcOEt, foi adsorvida em 1,40 g de gel de sílica e fracionada em coluna cromatográfica (Øint= 3,5 cm) empacotada com 30,0 g da mesma sílica. Utilizando o sistema de eluição gradiente com CH$_2$Cl$_2$/acetona 5%, 10%, 20% e 1:1, o fracionamento resultou em 29 subfrações de 25 mL, com rendimento de 86,2%, as quais foram analisadas por CCD e reunidas por semelhanças da seguinte forma: 1-5 (GFA-12,1 mg), 6-8 (GFB-88,5 mg), 9-11 (GFC-94,2 mg)*, 12-17 (GFD-96,3 mg), 15-24 (GFE-241,5 mg), 25-30 (GFF-26,5 mg) e 31-38 (GFG-30,4 mg).

A subfração GFC (94,2 mg), eluída com CH$_2$Cl$_2$/acetona 10%, foi adsorvida em 2,0 g de gel de sílica para preparo do adsorbato, o qual foi submetido ao fracionamento em coluna cromatográfica (Øint= 1,8 cm) empacotada com 30,0 g de sílica gel e eluído em sistema isocrático CH$_2$Cl$_2$/acetona 8%. Foram obtidas 18 subfrações de 25 mL cada, com rendimento de 92,0%. As fraçoes foram reunidas após análise comparativa por CCD da seguinte forma: 1-12 (GFCA-26,0 mg), 13-16 (GFCB-35,6 mg)* e 17-18 (GFCC-25,1 mg).

A subfração GFCB (35,6 mg) foi adsorvida em 70,0 mg de gel de sílica para preparo do adsorbato e submetida ao fracionamento cromatográfico (Øint= 1,4 cm) em 15,0 g de sílica gel e eluído em sistema isocrático CH$_2$Cl$_2$/isopropanol 2%. Foram obtidas 26 subfrações de 10 mL cada, com rendimento de 98,0%. As frações foram reunidas após análise comparativa por CCD da seguinte forma: 1-3 (GFCBA-3,2 mg), 4-5 (GFCBB-2,0 mg), 6-9 (GFCBC-6,0 mg)*, 10-11 (GFCBD-3,2 mg) e 12-26 (GFCBE-20,5 mg)*

As subfrações GFCBC e GFCBE correspondentem aos compostos AV6 e AV8 respectivamente.

3.2.7 Coluna cromatográfica fração H (AVFH/A-H)

A fração H (13,4 g) eluída com AcOEt, foi adsorvida em 27,0 g de gel de sílica. O adsorbato foi cromatografado (Øint= 5,5 cm) em 100,0 g dessa mesma sílica com eluição gradiente de CH$_2$Cl$_2$/AcOEt 8:2-5:5, 3:7, AcOEt, AcOEt/MeOH 9:1, 7:3 e 5:5. Foram obtidos 47 frações de 50 mL, analisadas e comparadas por suas semelhanças reveladas em cromatoplacas conforme mostra a Tabela 8 abaixo.

Tabela 8 - Dados referentes ao fracionamento cromatográfico de AVFH/A-H

Subfração	Massa (g)
HA (1-3)	0,1
HB (4-5)	0,6
HC (6-21)	**4,9**
HD (22-33)	**1,9**
HE (34-37)	1,1
HF (38-45)	1,7
HG (46-47)	1,4
	Massa total: 11,7 g
	Rendimento: 87,3%

Fonte: próprio autor

Isolamento de AV9, AV10, AV12 e A2

A subfração HC (4,9 g) eluída com CH_2Cl_2/AcOEt 20% foi adsorvida em 10,0 g de gel de sílica e adsorbato cromatografado em coluna (Øint= 5,7 cm) empacotada com de gel de sílica (120,0 g) e eluído em sistema isocrático com $CHCl_3$/MeOH 5%, resultando em 26 frações de 25 mL cada, com rendimento de 96,2%. As frações obtidas foram reunidas de acordo com suas semelhanças observadas em cromatoplacas da seguinte forma: 1-7 (HCA-153,5 mg), 8-10 (HCB-1227,4 mg) e 11-13 (HCC-1963,0 mg)*, 14-17 (HCD-1190,7 mg)*, 18-21 (HCE-113,9 mg) e 22-26 (HCF-76,8 mg).

A subfração HCD (1190,7 mg), um precipitado de verde, foi lavado com diclorometano até a obtenção de cristais brancos resultando no composto AV9 (208,0 mg).

A subfração HCC (1963,0 mg) foi adsorvida em 4,0 g de gel de sílica e submetida em coluna cromatográfica (Øint= 4,7 cm) empacotada com 80,0 g dessa mesma sílica, eluída com hexano/AcOEt/isopranol em sistema gradiente 6:3:1 - 4:5:1, resultando em 36 frações de 50 mL cada, com rendimento de 75,2%. Posteriormente, as frações foram reunidas de acordo com suas semelhanças observadas em cromatoplacas da seguinte forma: 1-12 (HCCA-332,6 mg)*, 13-15 (HCCB-299,5 mg) e 16-20 (HCCC-562,8 mg)* e 21-36 (HCCD-280,4 mg).

As subfrações HCCA (332,6 mg) e HCCC (562,8 mg) apresentaram um precipitado escuro que foi lavado com acetona até a obtenção de cristais brancos resultando na obtenção dos compostos AV12 (96,0 mg) e AV10 (353,8 mg) respectivamente

Isolamento de AV11, AV13, AV15 e AV16

A subfração HD (1,9 g) eluída com CH_2Cl_2/AcOEt 40% foi adsorvida em 4,0 g de gel de sílica e acondicionada em coluna (Øint = 4,6 cm) cromatográfica empacotada com 60,0 g de gel de sílica, eluída em sistema isocrático com CH_2Cl_2/isopropanol 5%, resultando em 28

frações de 30 mL cada, com rendimento de 81,3%. As frações obtidas foram reunidas de acordo com suas semelhanças observadas em cromatoplacas da seguinte forma: 1-7 (HDA-33,3 mg), 8-10 (HDB-328,1 mg)*, 11-16 (HDC-326,4 mg), 17-18 (HDD-663,2 mg)*, 19-22 (HDE-193,1 mg) e 22-28 (HDF-98.7 mg)*.

A subfração HDB (328,1 mg) foi adsorvida em 1,2 g de gel de sílica e submetida ao fracionamento cromatográfico (Øint= 3,5 cm) em 50,0 g dessa mesma sílica, eluída em um gradiente de hexano/AcOEt/isopranol 6:3:1- 4:5:1. Foram obtidas 33 frações de 25 mL cada, com rendimento de 93,5% e reunidas conforme suas semelhanças reveladas em cromatoplacas da seguinte forma: 1-15 (HDBA-67,7 mg), 16-20 (HDBB-138,1 mg), 21-23 (HDBC-50,0 mg)* e 24-33 (HDBD-51,7 mg). A subfração HDBC corresponde ao composto AV13.

A subfração HDD (663,2 mg) foi adsorvida em 1,5 g de gel de sílica e acondicionada em coluna cromatográfica (Øint= 4,6 cm) com 60,0 g dessa mesma sílica. Em sistema isocrático de eluição com $CHCl_3$/isopropanol 3%, foram obtidas 20 frações de 50 mL cada, com rendimento de 85,9%, reuídas após revelação em cromatoplacas da seguinte forma: 1-7 (HDDA-22,8 mg), 8-9 (HDDB-108,2 mg)*, 10-11 (HDDC-146,6 mg) e 12-20 (HDDD-292,0 mg)*. A subfração HDDD corresponde ao composto AV11.

A subfração HDDB (108,2 mg) foi adsorvida em 200,0 g de gel de sílica e submetida ao fracionamento cromatográfico (Øint= 1,4 cm) em 10,0 g de gel de sílica e eluição isocrática de CH_2Cl_2/ACN 7:3. Foram obtidas 28 frações de 10 mL cada, com rendimento de 85,4% e reunidas conforme suas semelhanças reveladas em cromatoplacas da seguinte forma: 1-11 (HDDBA-23,2 mg), 12-13 (HDDBB-6,1 mg)*, 14-21 (HDDBC-25,4 mg)* e 22-28 (HDDBD-37,7 mg). As subfrações HDDBB e HDDBC correspondem aos compostos AV16 e AV15 nessa ordem.

A subfração HDF (98,7 mg), um precipitado escuro, foi lavada com acetona até obter um pó verde claro, composto A2 (20,8 mg).

Isolamento de AV14 e AV17

A subfração HF (1,9 g) eluída com AcOEt e AcOEt/MeOH 9:1, foi adsorvida em 4,5 g de gel de sílica e submetida ao fracionamento cromatográfico (Øint= 1,7 cm) em gel de sílica (80,0 g) com eluição isocrática de CH_2Cl_2/ACN 7:3, resultando em 38 subfrações de 50 mL cada, com rendimento de 98,4%. As subfrações foram analisadas e reunidas por suas semelhanças reveladas em cromatoplacas da seguinte forma: 1-2 (HFA-85,5 mg), 3-4 (HFB-

335,3 mg), 5-7 (HFC-419,1 mg), 8-10 (HFD-349,0 mg), 11-14 (HFE-512,9 mg)* e 15-26 (HFF-167,7 mg)

A subfração HFE (512,9 mg) foi adsorvida em 1,0 g de gel de sílica e submetida ao fracionamento cromatográfico (Øint= 2,8 cm) em 40,0 g de gel de sílica, eluída em sistema isocrático com CH_2Cl_2/AcOEt/isopranol 8:1,5:0,5. Foram obtidas 23 frações de 20 mL cada, com rendimento de 76,4% e reunidas conforme suas semelhanças reveladas em cromatoplacas da seguinte forma: 1-10 (HFEA-52,6 mg), 11-12 (HFEB-24,6 mg), 13-15 (HFEC-112,9 mg)*, 16-18 (HFED-69,3 mg)* e 19-23 (HFEE-24,3 mg)

A subfração HFEC (112,9 mg) foi adsorvida em 200,0 mg de gel de sílica e submetida ao fracionamento cromatográfico (Øint= 2,3 cm) em 20,0 g de gel de sílica e eluição isocrática de CH_2Cl_2/ACN 7:3. Foram obtidas 28 frações de 10 mL cada, com rendimento de 95,1% e reunidas conforme suas semelhanças reveladas em cromatoplacas da seguinte forma: 1-14 (HFECA-22,9 mg), 15-18 (HFECB-12,2 mg), 19-21 (HFECC-42,0 mg)* e 22-26 (HFECD-30,3 mg)*. A subfração HFECC corresponde ao composto AV14.

A subfração HFED (69,3 mg) foi adsorvida em 140,0 mg de gel de sílica e submetida ao fracionamento cromatográfico (Øint= 1,4 cm) em gel de sílica (8,0 g) com eluição isocrática de CH_2Cl_2/ACN 7:3, resultando em 28 subfrações de 10 mL cada, com rendimento de 93,6%. As subfrações foram analisadas e reunidas por suas semelhanças reveladas em cromatoplacas da seguinte forma: 1-15 (HFEDA-8,8 mg), 16-18 (HFEDB-3,4 mg), 19-21 (HFEDC-14,6 mg) e 22-28 (HFEDD-38,1 mg)*

A subfração HFEDD (38,1 mg) foi submetida ao fracionamento por CLAE com injeção de 200 µL da amostra dissolvida em 3 mL da mistura H_2O/ACN 50%. A separação foi realizada em coluna semipreparativa de C18, usando como fase móvel H_2O (0,01%TFA)/ACN 50% em sistema isocrático, com um fluxo de 4,0 mL/min.

Foram coletados dois picos com tempo de retenção de 7,47 min (pico 1) e 8,65 min (pico 2), com tempo total de corrida de 10 minutos (Figura 8). O pico 1 forneceu 12,8 mg correspondente ao composto AV17

Figura 8 - Cromatograma da subfração HFEDD observada na faixa de 210-400 nm.
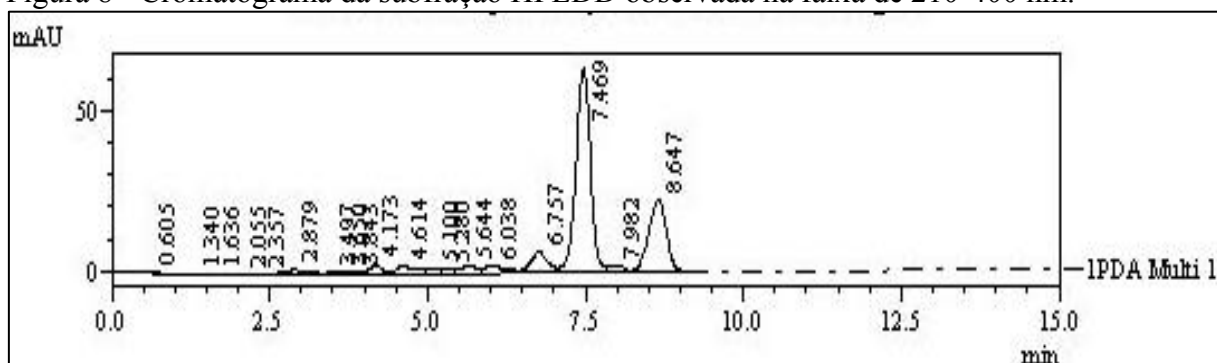
Fonte: Próprio autor

4 RESULTADOS E DISCUSSÃO

Este trabalho teve início com a investigação química do extrato hexano/AcOEt 1:1 das folhas de *A. velutina*. O isolamento das substâncias envolveu técnicas tradicionais de separação, como a cromatografia em coluna aberta e média pressão (*flash*), além da cromatografia líquida de alta eficiência (CLAE).

Através deste minucioso trabalho fitoquímico foram isolados dezoito vitanolídeos (FIGURA 10, pag.45), sendo treze novos, cujas estruturas foram determinadas por meio de técnicas espectroscópicas (IV, RMN 1D e 2D) e espectrométricas (EM), incluindo cristalografia de raios-X e cálculos teóricos como dicroismo circular (DC), certificando de forma inequívoca as determinações das configurações dos centros estereogênicos.

Aliado ao isolamento e caracterização dos compostos, foram realizados alguns testes farmacológicos. Além dos estudos *in vitro*, para a avaliar a atividade citotóxica e anti-inflamatória, foram realizados estudos *in silico* de modelagem molecular, visando a avaliação de possíveis inibidores, com destaque para a Protease Principal (Mpro), que desempenha papel essencial na tradução e transcrição do ciclo viral do SARS-CoV-2.

Os resultados obtidos nesta tese foram descritos em três capítulos, cada um constituindo um artigo, incluídos na seção de resultados e discussão.

Capítulo 1: Resultado da publicação de um artigo na revista *Phytochemistry* com título: "**Anti-inflammatory withajardins from the leaves of *Athenaea velutina***", *Phytochemistry*, 2022, 203, 113338. https://doi.org/10.1016/j.phytochem.2022.113338

Capítulo 2: Artigo publicado recentemente no *Journal of Biomolecular Structure and Dynamics* com título: "**Withanolides of *Athenaea velutina* with potential inhibitory**

properties against SARS coronavírus main protease (Mᵖʳᵒ): Molecular modeling studies", *J. Biomol. Struct. Dyn,* 2023, 1-9. https://doi.org/10.1080/07391102.2023.2167863

Capitulo 3: Trabalho intitulado "**Bioactive withanolides from the leaves of *Athenaea velutina* Sendt."**, que se encontra na forma de redação final artigo para submissão na *Phytochemistry*.

Ressalta-se que os vitanolídeos são uma grande classe de compostos naturais produzidos principalmente em plantas da família Solanaceae, restrito à subfamília Solanoideae, na qual incluem os gêneros da subtribo Withaninae, *Athenaea*, *Aureliana*, *Deprea*, *Tubocapsicum*, *Discopodium*, *Nothocestrum*, *Mellissia* e *Withania* (ZAMBERLAM, 2012).

Por conta da grande semelhança entre os gêneros *Withania* e *Athenaea*, a investigação química resultou no isolamento da vitaferina A, o primeiro vitanolídeo descrito na literatura em 1965 de *W. somnifera,* além de treze compostos com estruturas análogas.

Outros quatro vitanolídeos de estrutura modificada também foram isolados. Estes pertencem a um grupo especial de vitanolídeos, denominados vitajardins, encontrados anteriormente apenas nos gêneros *Deprea* (LUIS et al., 1994), *Nicandra* (NICOLÁS et al., 2015) e *Tubocapsicum* (KIYOTA et al., 2008; WANG et al., 2018; XIANG et al., 2021). Os vitajardins são caracterizados pela cadeia lateral bicíclica em C-17, formado pelo anel homocíclico de seis membros e um anel δ-lactona (ECHEVERRI et al., 1995).

Dentre as diversas variações no esqueleto dos vitanolídeos, é observado que a presença do sistema 5β,6β-epoxi-2-en-1-ona no anel A e B, bem como a insaturação no carbono C-24/C25 no anel E δ-lactona, constituem unidades farmacofóricas essenciais para muitas atividades (XU et al., 2016).

O fluxograma (FIGURA 9, pag. 44) representa uma forma resumida do fracionamento cromatográfico do extrato hexano/acetato de etila 1:1 das folhas de *A.velutina* até o isolamento dos vitanolídeos (AV1-AV18). A estrutura desses compostos, incluindo a ionona e o *N-trans-p*-coumaroiltiramina estão representados na Figura 10, pag. 45.

Figura 9 - Fluxograma do fracionamento cromatográfico do extrato de *A. velutina*.
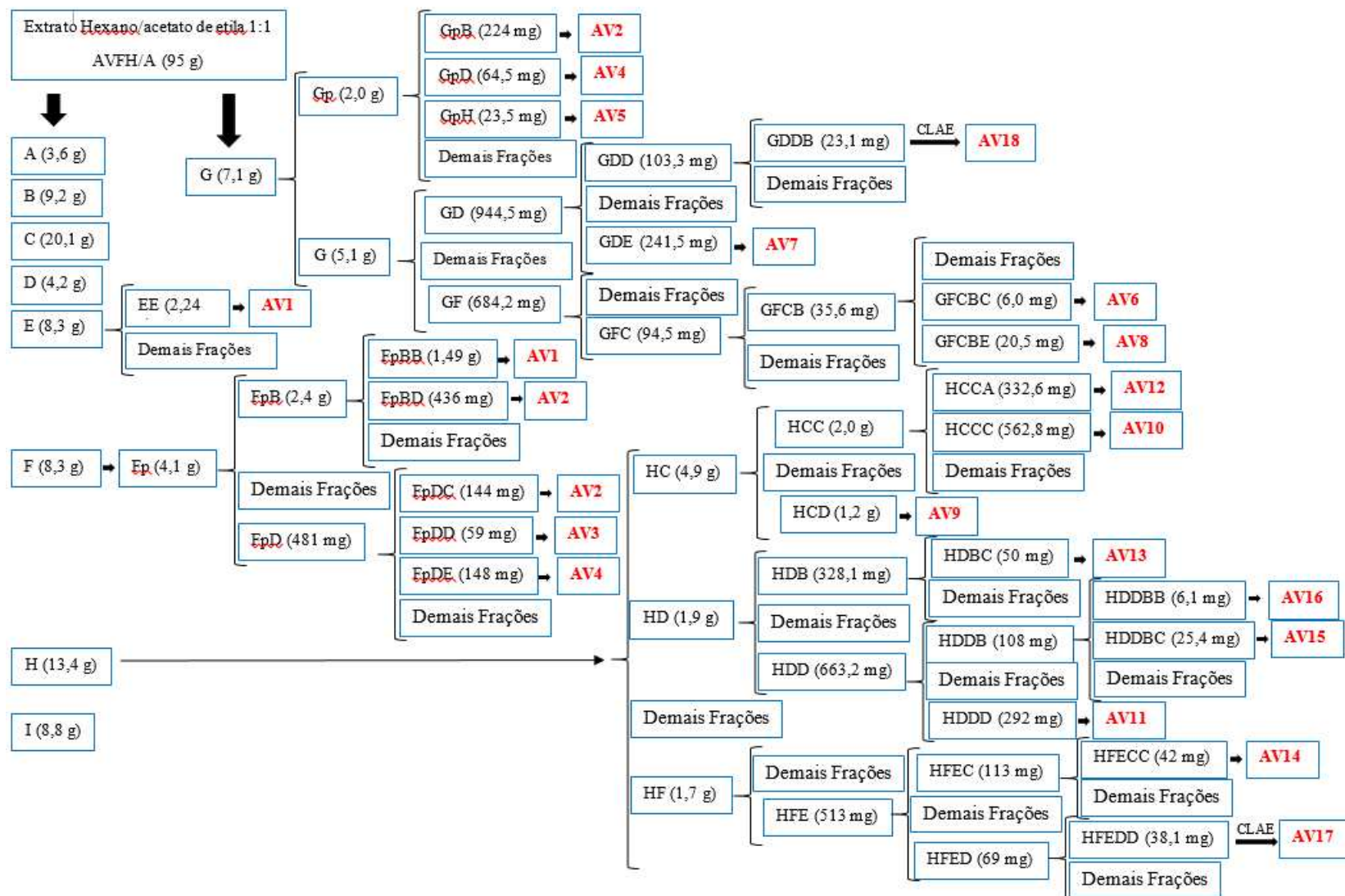
Figura 10 - Estrutura dos compostos isolados de *A. velutina*.
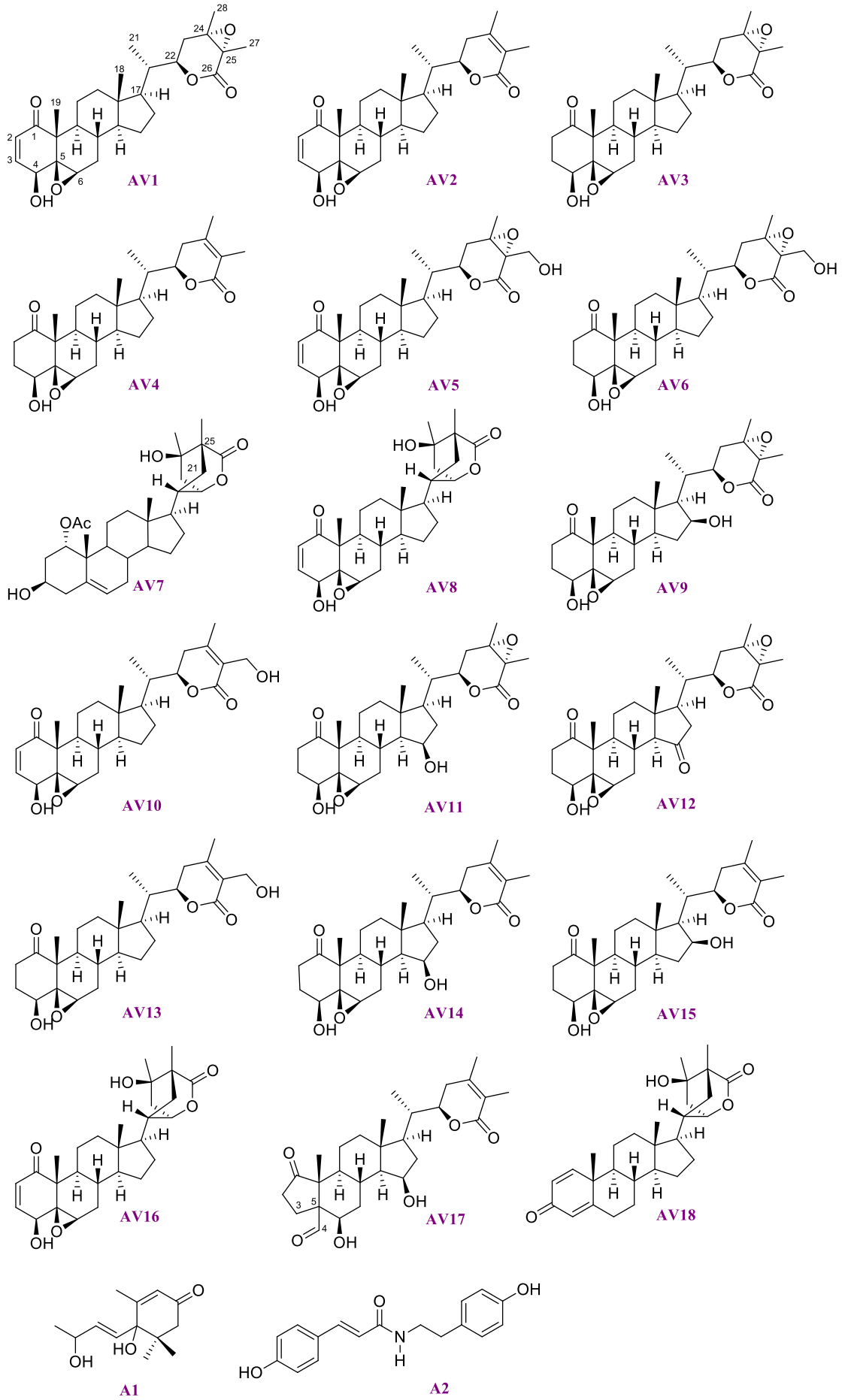
CAPÍTULO 1

Anti-inflammatory withajardins from the

leaves of *Athenaea velutina*
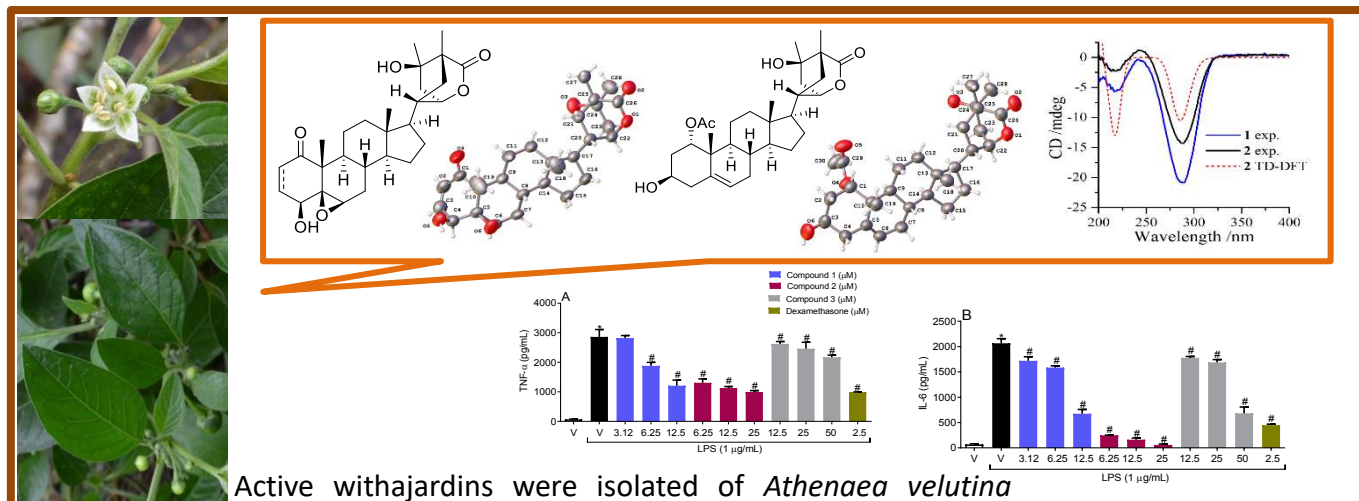
Active withajardins were isolated of *Athenaea velutina*

Anti-inflammatory withajardins from the leaves of *Athenaea velutina*

Késya Amanda Dantas Rocha[a], Tércio de Freitas Paulo[a], Alejandro Pedro Ayala[b], Valéria da Silva Sampaio[c], Paulo Iury Gomes Nunes[d], Flávia Almeida Santos[d], Kirley Marques Canuto[e], Edilberto Rocha Silveira[a], Otília Deusdenia Loiola Pessoa[a,*]

[a]*Departamento de Química Orgânica e Inorgânica, Centro de Ciências,Universidade Federal do Ceará, 60021-970, Fortaleza-CE, Brazil*

[b]*Departamento de Física, Centro de Ciências,Universidade Federal do Ceará, 60440-900, Fortaleza-CE, Brazil.*

[c]*Ciências Biológicas, Universidade Regional do Cariri, 63200-000, Missão Velha-CE, Brazil.*

[d]*Departamento de Fisiologia e Farmacologia, Faculdade de Medicina, Universidade Federal do Ceará, 60430-270, Fortaleza-CE, Brazil.*

[e]*Embrapa Agroindústria Tropical, 60511-110, Fortaleza-CE, Brazil*

* Corresponding author: opessoa@ufc.br

ABSTRACT

Withajardins, uncommon modified withanolide-type steroids, have been isolated exclusively from plants of the Solanaceaee family so far. Two undescribed withajardins and the known tuboanosigenin were isolated from the hexane/EtOAc 1:1 extract from *Athenaea velutina* leaves. Their structures were established by an extensive analysis of 1D- and 2D-NMR and HRMS data. The absolute configuration was determined by X-ray diffraction (withajardin L and tuboanosigenin) and circular dichroism (CD) analyses (withajardin M). The anti-inflammatory activity of compounds was evaluated through the inhibition of the lipopolysaccharide (LPS)-induced nitric oxide (NO), TNF-α, and IL-6 release in RAW264.7 cells. The cell viability effects to RAW 264.7 cells showed IC_{50} values of 74.4 to 354.4 µM. The compounds attenuated LPS-induced release of NO and decreased pro-inflammatory cytokines TNF-α and IL-6 in RAW264.7 cells.

Keywords: *Athenaea velutina*, Solanaceaee, Withanolides, Withajardins, Anti-inflammatory activity.

1. Introduction

The withanolides, also named withasteroids, constitute a large class of C_{28} steroidal lactones prevalent in some genera of the Solanaceae. Plants producing these specialised metabolites possess a piece of enzymatic machinery able to oxidize practically all the carbon atoms of both the steroidal nucleus and the side chain (Lima et al., 2018). It is worth noting that the alcohol, ketone, and epoxide groups are the reactive sites for many intramolecular bio-modifications yielding different scaffolds belonging to the withanolide family (Figure S1), such as withaphysalins, physalins, acnistins, neophysalins, withajardins, withametelins, norbornane-type withanolides, sativolides, spiranoid, subtriflora and taccalonolide δ-lactones, and $14\alpha,20\alpha$-epoxide, ring-D and ring-A aromatic withanolides (Chen et al., 2011; Misico et al., 2011). Withanolides display a broad spectrum of biological activities including leishmanicidal (Lima et al., 2018), neuroprotective (Rabhi et al., 2019; Crane et al., 2019), antibacterial (Nicolás et al., 2015), immunomodulatory (Bhat et al., 2005), antifungal (Roumy et al., 2010), antidiabetic (Lee et al., 2016), anti-inflammatory (Dong et al., 2019; Tan et al., 2020), and anticancer (Castro et al., 2019; Sun et al., 2020; Dom et al., 2020). These previous reports have encouraged the efforts to search for new botanical sources of these remarkable compounds at the "caatinga", the characteristic biome of the northeastern Brazil semiarid region.

Plants of *Athenaea* Sendtn. and *Aureliana* Sendtn. (subtribe Withaninae) have been described in the Notheast of Brazil, and according to the literature, they are producers of withanolides, compounds of our scientific interest. It is worth highlighting that these genera present high morphological similarity within the Solanaceae family (Sendtner, 1846; Hunziker and Barbosa 1990; Barboza et al., 2016). The recent botanical review performed by Rodrigues et al. (2019) based on calyx and pollen morphological aspects and phylogenetic studies based on DNA sequence reveals that *Athenaea* and *Aureliana* species are not distinct. Thus, all taxa recognized as *Aureliana* were transferred to *Athenaea* Sendtn. Currently, *Athenaea* is a small

and exclusively Neotropical genus with the highest species diversity in south-eastern Brazil, comprising 14 species of shrubs or small trees (Rodrigues et al., 2021).

Regarding the few studies reported to these genera so far, only the isolation of withanolides is described (Almeida-Lafetá et al., 2010; Silva et al., 2018). Recently, *in vitro* and pre-clinical studies of the extract on leaves of *Athenaea velutina* (Sendtn.) D'Arcy (Solanaceaee) exhibited potent antiproliferative, antimetastatic, and inducing apoptosis in murine B16F10 melanoma cells (Almeida et al., 2020; Almeida et al., 2021). In addition, the leaf extract of *A. velutina* also displayed antimicrobial activity on *S. aureus* (Rodrigues et al., 2020).

As part of our continuing interest in plants of the Solanaceaee family, particularly in withanolides, compounds of scientific interest to our research group (Batista et al., 2016; Carreiro et al., 2018; Wijeratne et al., 2018; Guerreiro et al., 2019), we have investigated the leaf extract of *A. velutina* from which we isolated three withajardins (Fig. 1), a small and interesting group of withanolides that have a specific and modified skeleton (Xu and Wang, 2020).

It is worth highlighting that withajardins have been found previously only in the genera *Deprea* (Luis et al., 1994), *Nicandra* (Nicolás et al., 2015), and *Tubocapsicum* (Kiyota et al., 2008; Wang et al., 2018; Xiang et al., 2021). *Tupocapsicum* plants also produce C_{28} steroidal glycosides as well as their aglycones which can be withajardins or acnistins. Withajardins are characterized by having a C-17 bicyclic side-chain possessing a six-membered homocyclic ring and a δ-lactone ring (Echeverri et al., 1995) while acnistins are characterized by having a similar C-17 bicyclic side-chain but possessing a five-membered homocyclic ring (Cardona et al., 2006). In contrast to the withanolides, there are few reports on the biological properties of the withajardins, among them antibacterial (Nicolás et al., 2015), cytotoxic (Wang et al., 2018), immunosuppressive (Echeverri et al., 1991) and leishmanicidal (Cardona et al., 2006) activities.
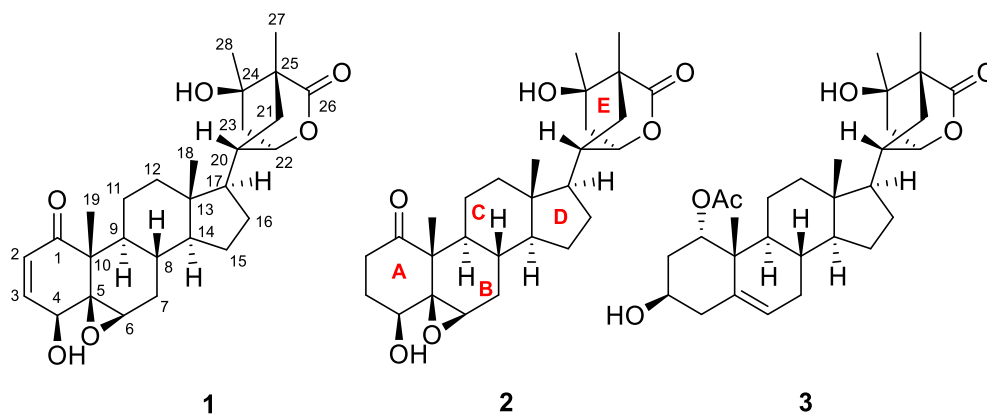
Fig. 1. Structures of withajardin L (**1**) and M (**2**), and tuboanosigenin (**3**).

2. Results and discussion

3.1 Structure elucidation

Withajardin L (**1**) had its molecular formula assigned by HRESIMS as $C_{28}H_{38}O_6$ (ten degrees of unsaturation) from the $[M + H]^+$ peak at *m/z* 471.2732. Its IR spectrum showed absorption bands to OH (3415 cm^{-1}), C=O of δ-lactone (1734 cm^{-1}), and α,β-unsaturated ketone (1672 cm^{-1}) functionalities. The combination of the ^{13}C NMR, DEPT 135º and HSQC spectra, characterized three oxy-methines protons at δ_H/δ_C 4.38/77.6 (C-22), 3.76/70.1 (C-4) and 3.23/62.7 (C-6), a vinyl unit at δ_H/δ_C 6.93/142.1 (C-3) and 6.20/132.4 (C-2), characteristic of an α,β-unsaturated carbon-carbon double bond conjugated to a carbonyl, along with five methines, seven methylenes, four methyls, and seven non-hydrogenated carbons, among which two carbonyls at δ_C 202.4 (C-1) and 177.5 (C-26) and two tertiary oxygenated δ_C 71.9 (C-24) and 64.1 (C-5), accounting for 28 carbon atoms indicating a withanolide like structure (Wijeratne et al., 2018). The 5,6-epoxy-4-hydroxy-α,β-unsaturated ketone moiety, commonly found in withanolides, was confirmed by the HMBC correlations of H$_2$-3 with C-1, C-4 and C-5 (δ_C 64.1), as well as for H$_2$-2 and H-6 with C-4. Additionally, key correlations of H-22 and H$_3$-27 (δ_H 1.12) with C-26, C-24 and C-21 (δ_C 31.1), and for Hα-21 (δ_H 2.14) with C-26, C-24, C-17 (δ_C 52.7) and C-25 (δ_C 47.5) showed that the methylene C-21 was directly bonded to the quaternary carbon (C-25), giving rise to a bicyclo[2,2,2] ring system bearing a δ-lactone (Fig.

2), characteristic of the withajardin-type withanolides (Echeverri et al., 1995). The β-orientation of HO-4 (δ_H 2.73) and the epoxy groups was determined by NOESY correlations of H-4 with H-6, OH-4 with H-8 (δ_H 1.51) as well as of H-8 with the β-positioned methyl (H-18, δ_H 0.66). The absolute configuration of the stereogenic centers of **1** w as deduced by single-crystal X-ray diffraction analysis (Fig. 3). Thus, the structure of **1** was established as (20*S*,22*R*,24*R*,25*R*)-5β,6β-epoxy-4β,24-dihydroxy-21,25-cycloergost-2-en-1-one, an analog of withajardins A - E previously isolated from *Deprea orinocensis* (Echeverri et al., 1995; Luiz et al., 1994), withajardins F to I from *Nicandra john-tyleriana* (Nicolás et al., 2015), and withajardins J, 17-*epi*-J, 'and K which were isolated from *Tubocapsicum anomalum* (Wang et al., 2018).

Withajardin M (**2**) had its molecular formula ($C_{28}H_{40}O_6$) deduced from the protonated molecule [M + H]$^+$ at *m/z* 473.2902 in the HRESIMS. Comparison of the ^{1}H and ^{13}C NMR data of **2** with those of withajardin L (**1**) revealed that **2** is the 2,3-dihydro derivative of **1**. This moiety was confirmed by the HMBC correlations of H$_2$-2 (δ_H 2.87/2.68) with C-1 (δ_C 211.5), C-4 (δ_C 73.3), C-10 (δ_C 51.2), and C-3 (δ_C 27.3). The NOESY spectrum displayed the correlations between H-4 (δ_H 3.77) and H-6 (δ_H 3.19) implying in a β-orientation for hydroxy at C-4 and epoxy functionalities (Fig. 2). Differently to compound **1**, the absolute configuration of **2** was determined by analysis of the experimental and TD-DFT calculated circular dichroism (CD) spectra. The experimental CD spectrum of **2** exhibited two negative bands at 217 and 287 nm, similar to that was observed for compound **1** (Fig. 4). This led us to realize that the differences in the A-ring of **1** and **2** do not affect significantly the Cotton effects. The TD-DFT calculated spectrum of **2** was found to be in good agreement with the experimental (Fig. 4). Therefore, compounds **1** and **2** were assigned to have identical absolute configurations establishing the structure of **2** as (20*S*,22*R*,24*R*,25*R*)-5β,6β-epoxy-4β,24-dihydroxy-21,25-cycloergostan-1-one.

Tuboanosigenin (**3**) presented a molecular formula of $C_{28}H_{40}O_6$, which was deduced by the protonated molecule [M + H]$^+$ at *m/z* 501.3214 in the HRESIMS. The ^{1}H and ^{13}C NMR,

including DEPT 135º and HSQC spectra displayed signals compatible with an 1-*O*-acetyl withajardin. Its ¹³C NMR data were identical to that reported for tuboanosigenin, a product obtained by an enzymatic hydrolysis reaction from the steroidal glycoside tuboanoside A, which was previously isolated from *Tubocapsicum anomalum* (Solanaceaee) (Kiyota et al., 2008). The still unreported absolute configuration of tuboanosigenin [(20*S*,22*R*,24*R*,25*R*)-1*α*-acetoxy-3*β*,24-dihydroxy-21,25-cycloergost-5-ene] was determined by single-crystal X-ray diffraction and CD analysis (Fig. 3).
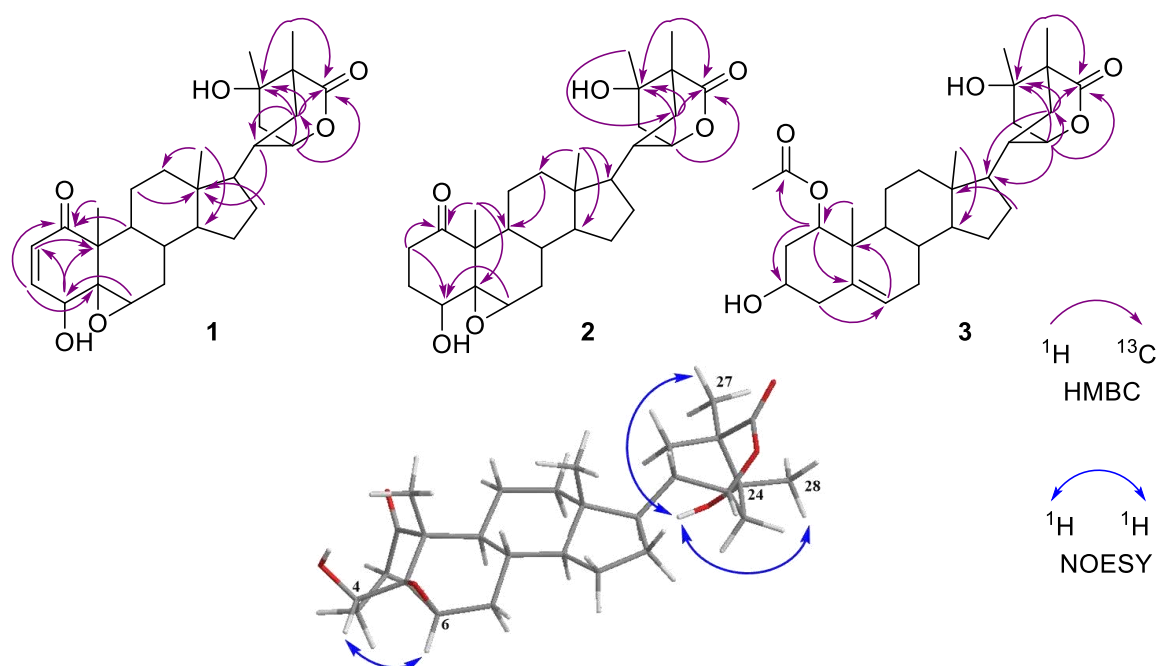
Fig. 2. Key HMBC for withajardin L (**1**) and M (**2**), and tuboanosigenin (**3**) and NOESY correlations for **2**.
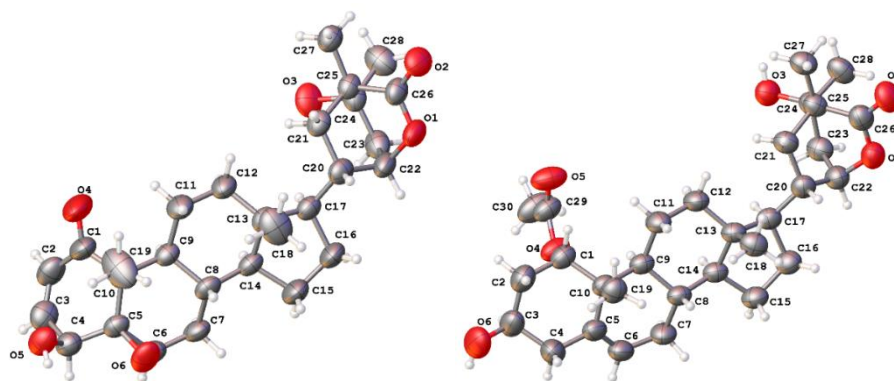
Fig. 3. X-ray ORTEP drawing of withajardin L (**1**) and tuboanosigenin (**3**).
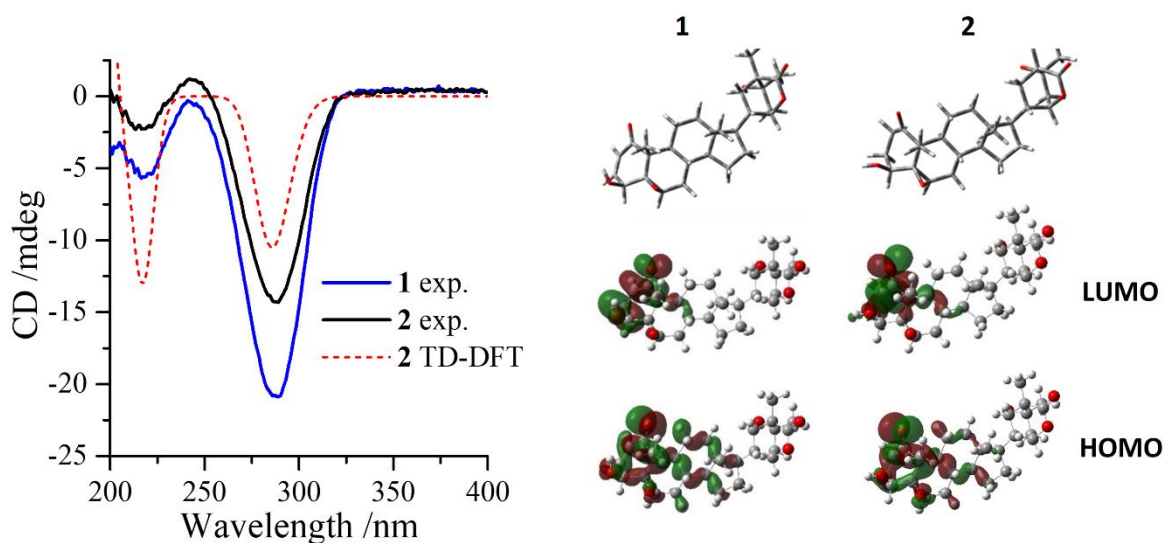
Fig. 4. Experimental CD spectra of **1** and **2** (in CH$_3$OH) and calculated CD spectrum of **2**. Optimized structures and calculated frontiers molecular orbitals (HOMO/LUMO) of **1** and **2**.

3.2 Biosynthetic proposal

Previous studies on withanolides biosynthesis suggested a terpenoid backbone generated by isoprenoid molecules from both mevalonate (MEV) and non-mevalonate (MEP) pathways, which share a common pathway from geranyl diphosphate to squalene that undergoes a well-known cyclization process to produce cycloartenol (Akhtar et al., 2013; Gupta et al., 2013). After several biochemical reactions, the latter one affords 24-methylene cholesterol, which is considered the precursor of the withanolides (Chaurasiya et al., 2012; Worland et al., 2020). This large class of compounds is recognized for their pharmacological and biological properties; however, little is known about their biosynthesis. Trying to understand the cyclization process from withanolides to withajardins, one can infer that the withajardins could easily be formed from the 24,25-epoxy withanolides. Further, an exhaustive literature survey looking at the 24,25-epoxy configuration, an *α*-orientation, i.e. 24*S* and 25*S*, was predominantly observed (White et al., 2016; Zhang and Tong, 2016; Xu and Wang, 2020), whereas the configuration of the C-24 and C-25 stereocenters of the previously isolated withajardins are both *R* (Luiz et al., 1994; Wang et al., 2018). Thus, supported on previous isolated withanolide

structures of *A. fasciculata* (Almeida-Lafetá et al., 2010), *A. martiana* (Silva et al., 2018), and *A. velutina* (Almeida et al, 2022) it was suggested a hypothetical biosynthetic pathway to the δ-lactone moiety of compounds **1** to **3** as well as to modified-withanolides, i.e. those bearing a δ-lactone bicycle like the withajardins (I), including the withametelins (II) and acnistins (III) (Fig. 5).
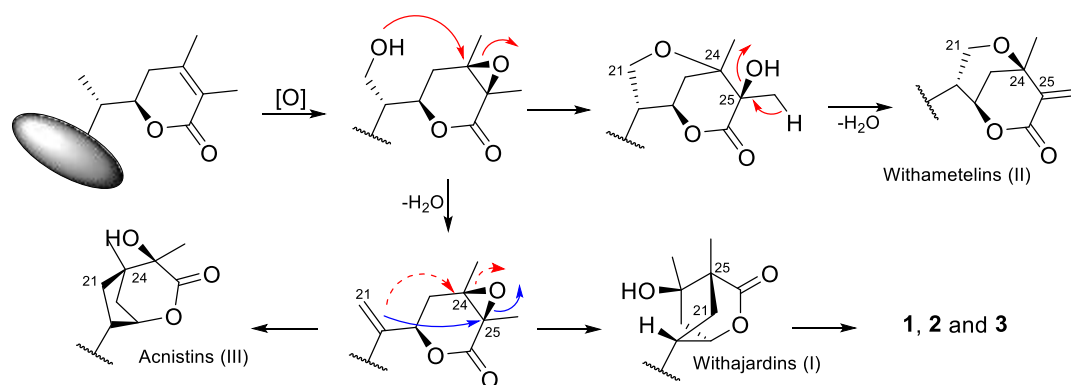
Fig. 5. Plausible biogenetic pathway to different bicycle δ-lactones: withajardins (I), withametelins (II), and acnistins (III).

3.3 Effect of compounds on NO, TNF-α and IL-6 release in LPS-stimulated RAW264.7 cells

Macrophages are cells with multiple functions and when induced by bacterial lipopolysaccharide (LPS) produce and secrete higher levels of pro-inflammatory mediators such as cytokines, including TNF-α, IL-1β, and IL-6, and NO (Fujiwara and Kobayashi, 2005; Bashir et al., 2016).

The MTT assay was carried out to evaluate the effects of all compounds on the viability of the RAW264.7 cells. As shown in Table 2, the compounds demonstrated a reduction of the cellular viability with half-maximal inhibitory concentration (IC$_{50}$) values between 74.43-354.40 μM.

To evaluate the effects of all compounds on the production of LPS-induced NO in RAW264.7 cells, the concentrations of nitrite in the culture medium were measured by Griess assay. NO levels in the culture supernatants from LPS-stimulated cells were significantly

reduced after treatment with the compounds. Compounds **1**, **2**, and **3** showed IC_{50} values of 1.41, 0.46, and 0.21 μM, respectively. Compound **3** had a lower IC_{50} value than dexamethasone, showing stronger activity compared to positive control.

The effects of the compounds on the production of pro-inflammatory cytokines TNF-α and IL-6 induced by LPS in RAW264.7 cells were measured by ELISA kits. LPS significantly elevated TNF-α and IL-6 levels in vehicle-treated cells. Compounds **1** − **3** were able to significantly reduce LPS-induced elevated levels of TNF-α and IL-6 in RAW264.7 cells (Fig. 6). However compound **2** caused a greater reduction of the IL-6 levels than dexamethasone, while the effect on the levels of TNF-α was similar to that of dexamethasone.
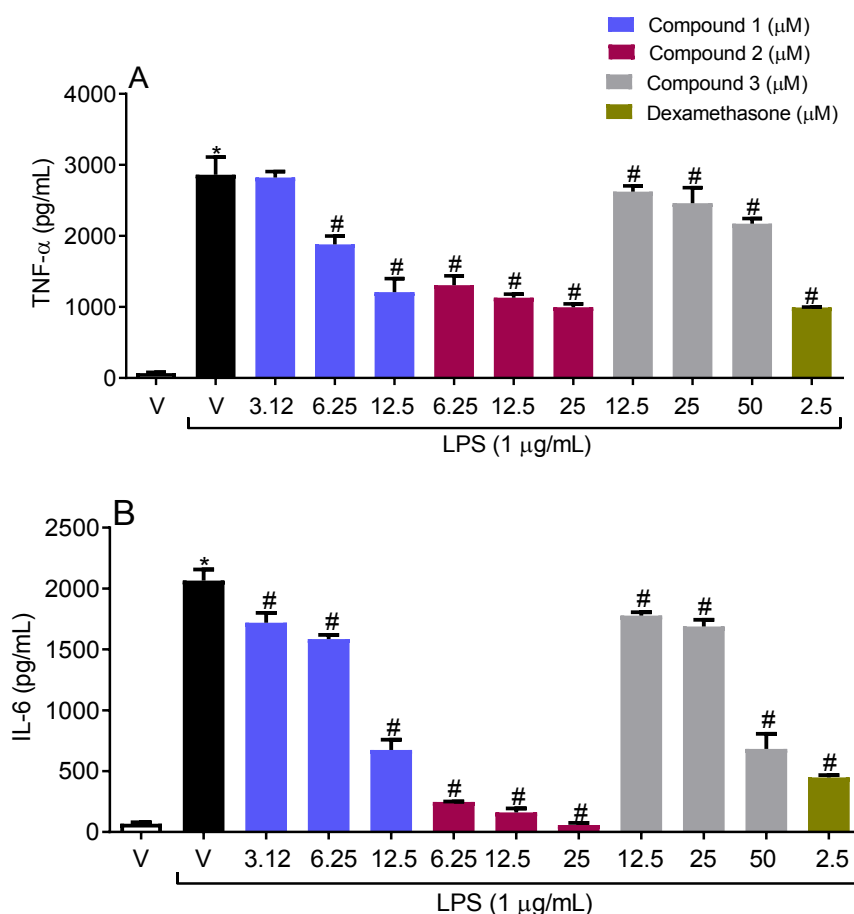
Fig. 6. Inhibitory effects of compounds **1** − **3** on the secretion of TNF-α (A) and IL-6 (B) in RAW264.7 cells stimulated with LPS (1 μg/mL). Dexamethasone (2,5 μM) was used as the positive control. DMSO was used as a solvent for both the test compounds and dexamethasone was added to the control vehicle (V) and non-stimulated cells (C). The results are expressed as mean ± S.D. for three independent experiments,

measured in triplicate. *$p < 0.05$ compared to non-stimulated cells (C); # $p < 0.05$ compared to control vehicle (V).

3. Conclusion

In this study, the hexane/EtOAc 1:1 extract from leaves of *A. velutina*, a plant species producing withanolides, was investigated. From this study, three modified withanolides bearing a [2,2,2-bicyclic] δ-lactone known as withajardins were isolated. Compounds **1 – 3** showed anti-inflammatory effects, however, while **3** showed better activity in inhibiting NO production, **2** was more effective in reducing the levels of pro-inflammatory cytokines (TNF-α and IL-6) in RAW264.7 macrophage cells. Indeed, comparatively with dexamethasone, compound **2** showed higher activity, therefore, being a very promising candidate to be further investigated regarding its anti-inflammatory potential.

4. Experimental

4.1. General Methods

Circular dichroism (CD) measurements were carried out on a Jasco J-815 spectropolarimeter (JASCO, Japan). CD spectra were acquired over a range of 210 to 400 nm in a quartz cuvette with a pathlength of 1 mm, at room temperature. The spectra were recorded with a scan speed of 100 nm/min and represented an average of 3 scans. Spectra were recorded in 1.0 nm increments. The samples were dissolved in methanol and all measurements were repeated at least 3 times. Melting points were recorded on a digital MQAPF-302. The Fourier transform infrared (FTIR) spectra were obtained on a Shimadzu IR-tracer-100. High-resolution mass spectra were recorded on a Waters Acquity UPLC system coupled to a quadrupole/time-of-flight (TOF) system (UPLC/Qtof MSE spectrometer) in the positive mode. The NMR spectra were performed either on a Bruker AVANCE DRX-500, operating at 500.13 MHz for ^{1}H, and 125.75 MHz for ^{13}C, or on a Bruker AVANCE DPX-300 operating at 300.13 MHz for ^{1}H and

75.48 MHz for ^{13}C. Chromatographic separations were performed by column chromatography on sílica gel 60 (0.063-0.200 mm - Merck) and/or flash sílica gel (40−75 μm - Merck) chromatography packing. Analytical TLC was carried out on precoated sílica gel 60 F−254 (200 μm) aluminum plates (Silicycle).

4.2. Plant material

The leaves of *Athenaea velutina* Sendtn. (Solanaceaee) were collected in Pico Alto, Guaramiranga/Ceará, Brazil (S 04º 12.590', W 38º 58.244'), in January 2019 at wet season, SisGen license number A5C2E09. The plant material was identified by Dr. Valéria S. Sampaio (Co-author) and a voucher specimen (EAC45010) has been deposited at the Herbarium Prisco Bezerra (EAC) of the Departmento de Biologia at the Universidade Federal do Ceará Federal.

4.3. Extraction and isolation

The dried and powdered leaves of *A. velutina* (2.0 Kg) were extracted with hexane/ EtOAc 1:1 (10 L, 3 x 24 h each). The solvent was removed by rotary evaporation under reduced pressure yielding 95.0 g of the crude extract. This extract was further fractionated using sílica gel column chromatography (60.0 g) by elution with hexane, hexane/EtOAc 2:1, 1:1, EtOAc, EtOAc/CH$_3$OH 1:1, and CH$_3$OH, to afford nine fractions (A-I). Fraction G (5.17 g) eluted with hexane/EtOAc 1:1, was subjected to sílica gel column chromatography (100.0 g) and, eluted with hexane/EtOAc 8:2, 7:3, 6:4, 5:5, 4:6, 7:3, 2:8, EtOAc, and EtOAc/CH$_3$OH 8:2, 7:3, 6:4 and 5:5, to yield seven subfractions (GA-GG). Afterward, subfraction GD (995 mg) eluted with hexane/EtOAc 5:5, was further fractionated by sílica gel column chromatography (30.0 g) and eluted with CH$_2$Cl$_2$/acetone 9:1, 8:2, 1:1, and acetone, yielding six subfractions (GDA-GDF). Next, the subfraction GDE (241 mg), a greenish precipitate, was crystallized from EtOAc, yielding compound **3** (99.5 mg). Meanwhile, the subfraction GF (684 mg) eluted with EtOAc, was separated into seven subfractions (GFA-GFG) through sílica gel column chromatography

(30.0 g) using CH_2Cl_2/acetone 9:1, 8:2, 2:1, 1:1, and acetone, as eluents. Later on, the subfraction GFC (94.2 mg) eluted with CH_2Cl_2/acetone 9:1, was further purified by sílica gel column chromatography (30.0 g) by elution with a CH_2Cl_2/acetone 9:1-5:5, gradient systems, yielding compound **1** (20.9 mg). The Fraction H (13.4 g), eluted with EtOAc, gave seven fractions (HA-HG) after being fractionated on sílica gel column (100.0 g) using the following eluents: CH_2Cl_2/EtOAc 8:2-2:8, EtOAc, EtOAc/CH_3OH 9:1-5:5. Next, the subfraction HD (1.9 g), eluted with CH_2Cl_2/EtOAc 6:4, was fractionated again by sílica gel column chromatography (60.0 g) by isocratic elution with CH_2Cl_2/isopropanol 5% to yield seven fractions (HDA-HDG). Posteriorly, the subfraction HDD (663 mg) was chromatographed twice over sílica gel (60.0 g) using CH_3Cl/isopropanol 3% as eluent to provide compound **2** (6.0 mg).

4.4. Spectroscopic data

4.4.1. Withajardin L [(20*S*,22*R*,24*R*,25*R*)-5β,6β-epoxy-4β,24-dihydroxy-21,25-cycloergost-2-en-1-one] (**1**)

$C_{28}H_{38}O_6$: Colourless crystals (acetone); mp 244-245 ºC; CD (CH_3OH) λ_{max} ($\Delta\varepsilon$) 217 (-5.7), 287 (-20.8) nm; IR (KBr) ν_{max} 3415, 1734, 1672, 1381, 1130, 1099 cm^{-1}; ^{1}H and ^{13}C NMR data, Table 1; HRESIMS *m/z* 471.2732 [M + H]$^+$ (calcd for $C_{28}H_{39}O_6$, 471.2747).

4.4.2. Withajardin M [(20*S*,22*R*,24*R*,25*R*)-5β,6β-epoxy-4β,24-dihydroxy-21,25-cycloergost-1-one] (**2**)

$C_{28}H_{40}O_6$: amorphous solid; CD (MeOH) λ_{max} ($\Delta\varepsilon$) 217 (-2.4), 287 (-14.3) nm; ^{1}H and ^{13}C NMR data, Table 1; HRESIMS *m/z* 473.2902 [M + H]$^+$ (calcd for $C_{28}H_{41}O_6$, 473.2903).

4.4.3. Tuboanosigenin [(20*S*,22*R*,24*R*,25*R*)-1α-acetoxy-3β,24-dihydroxy-21,25-cycloergost-5-ene] (**3**)

C$_{30}$H$_{44}$O$_6$: Colourless crystals (acetone); mp 218-220 ºC; CD (MeOH) λ$_{max}$ (Δε) 216 (-14.0) nm; IR (KBr) ν$_{max}$ 3481, 1743, 1714, 1375, 1053, 1026 (br), cm^{-1}; ^{1}H and ^{13}C NMR data, Table 1; HRESIMS m/z 501.3214 [M + H]$^+$ (calcd for C$_{30}$H$_{45}$O$_6$, 501.3216).

Table 1

^{13}C and ^{1}H NMR chemical shifts of compounds **1** − **3** (δ in ppm, J in Hz).

Position	1^a δ_C		δ_H	2^b δ_C		δ_H	3^a δ_C		δ_H
1	202.4	C		211.5	C		75.3	CH	5.06 t (3.0)
2	132.4	CH	6.20 d (9.9)	32.2	CH	2.87 m / 2.68 m	35.8	CH$_2$	2.08 m / 1.74 m
3	142.1	CH	6.93 dd (9.9, 5.8)	27.3	CH	2.19 m	66.8	H	3.86 sept (4.9)
4	70.1	CH	3.76 d (5.8)	73.3	CH	3.77 t (2.9)	41.6	CH$_2$	2.36 m
5	64.1	C		67.5	C		137.4	C	
6	62.7	CH	3.23 s	57.5	CH	3.19 s	124.3	CH	5.51 d (5.2)
7	31.4	CH$_2$	2.14 m / 1.27 m	32.1	CH$_2$	2.16 m / 1.38 m	31.8	CH$_2$	1.99 m / 1.60 m
8	30.0	CH	1.51 m	30.4	CH	1.39 m	32.0	CH	1.47 m
9	44.4	CH	1.02 m	43.7	CH	1.06 m	42.4	CH	1.31 m
10	47.9	C		51.2	C		40.5	C	
11	22.3	CH$_2$	1.85 m / 1.44 m	21.7	CH$_2$	1.39 m / 1.34 m	20.5	CH$_2$	1.40 m
12	39.3	CH$_2$	1.81 m / 1.24 m	39.2	CH$_2$	1.68 m / 1.01 m	39.6	CH$_2$	1.85 dt (12.2, 3.5) / 1.23 m
13	42.8	C		43.1	C		43.0	C	
14	55.7	CH	1.00 m	56.0	CH	0.77 td (11.7, 6.2)	56.0	CH	1.10 m
15	24.5	CH$_2$	1.65m / 1.16 m	24.7	CH$_2$	1.53 m / 0.97 m	24.5	CH$_2$	1.66 m / 1.16 m
16	26.8	CH$_2$	1.62 m / 1.35 m	27.0	CH$_2$	1.49 m / 1.16 m	26.9	CH$_2$	1.66 m / 1.34 m
17	52.7	CH	1.38 m	53.0	CH	1.49 m	52.8	CH	1.40 m
18	13.1	CH$_3$	0.66 s	12.9	CH$_3$	0.49 s	13.2	CH$_3$	0.67 s
19	17.6	CH$_3$	1.41 s	15.6	CH$_3$	1.64 s	19.7	CH$_3$	1.07 s
20	39.1	CH	2.00 m	39.8	CH	1.98 m	39.1	CH	2.04 m
21	31.1	CH$_2$	2.14 m / 1.28 m	31.8	CH$_2$	2.45 dd (13.1, 7.1) / 1.57 m	31.2	CH$_2$	2.16 m / 1.53 m
22	77.6	CH	4.38 t (3.4)	78.1	CH	4.48 t (3.8)	77.7	CH	4.39 t (3.6)
23	38.1	CH$_2$	1.97 m	39.6	CH$_2$	2.27 d (14.8) / 2.13 m	38.1	CH$_2$	1.99 m
24	71.9	C		71.3	C		72.0	C	
25	47.5	C		48.4	C		47.5	C	
26	177.5	C		178.3	C		177.6	C	
27	14.4	CH$_3$	1.12 s	15.4	CH$_3$	1.47 s	14.4	CH$_3$	1.12 s
28	29.3	CH$_3$	1.25 s	29.3	CH$_3$	1.46 s	29.2	CH$_3$	1.26 s
OAc-1							170.5 / 21.4	C / CH$_3$	2.04 s
OH-4			2.73 brs			7.40 brs			
OH-24						6.56 s			

The assignments were assigned based on HSQC, HMBC, and ^{1}H-^{1}H COSY spectra. ^{a} (CDCl$_3$, ^{13}C NMR 75.47 MHz and ^{1}H NMR 300.13 MHz).^{b} (C$_5$D$_5$N, ^{13}C NMR 125.77 and ^{1}H NMR 500.13 MHz).

Table 2
The cell viability and effect of compounds **1** − **3** on the production of nitric oxide (NO) in lipopolysaccharide (LPS)-induced RAW264.7 cells.

Compound	Cell viability IC$_{50}$ (mean ± SD, μM)	NO inhibition IC$_{50}$ (mean ± SD, μM)
1	74.4 ± 12.6	1.4 ± 0.2
2	95.0 ± 15.2	0.5 ± 0.1
3	354.4 ± 48.7	0.2 ± 0.0
Dexamethasone	-	0.6 ± 0.0

The values represent the means of the results from three independent experiments with similar patterns. Dexamethasone was used as the positive control.

4.5. X-ray crystallographic analyses of compounds 1 and 3

Single crystal X-ray diffraction data collection (ϕ scans and ω scans with κ and θ offsets) was recorded on a Bruker D8 Venture κ-geometry diffractometer equipped with a Photon II CPAD detector and a Cu Kα (λ = 1.54178 Å) IμS 3.0 Incoatec microfocus source. The APEX III software was used for the unit cell determination and data collection (Bruker, 2018a). The data reduction and global cell refinement were done using the Bruker SAINT (Bruker, 2018b). Data were corrected for absorption effects using the Multi-Scan method with SADABS (Krause et al., 2015; Sheldrick, 2015a). The structures were solved by intrinsic phasing using SHELXT (Sheldrick, 2015a) and refined with the ShelXL (Sheldrick, 2015b) refinement package using Least Squares minimization by using Olex^2 (Dolomanov et al., 2009) as a graphical interface. Non-hydrogen atoms were refined anisotropically. Hydrogen atoms were placed according to geometrical criteria and treated using the riding model. In the case of **3**, residual electron densities were observed in solvent-accessible voids associated with disordered water molecules and treated with the PLATON/SQUEEZE program (Spek, 2015).

Withajardin L (**1**): Colourless prism crystals (recrystallization solvent: acetone) C$_{28}$H$_{38}$O$_{6}$, M_{r} = 470.58 g mol^{-1}; size 0.066 × 0.125 × 0.275 mm; orthorhombic, space group $P2_12_12_1$, a = 7.6300(2) Å, b = 11.2782(3) Å, c = 29.0258(8) Å, V = 2497.75(12) Å^3, Z = 4, T = 298 K, μ(CuKα) = 0.699 mm^{-1}, numerical, $T_{\min}$ = 0.900, $T_{\max}$ = 0.955, $F(000)$ = 1016.0. The total number of reflections was 18664 (-9 ≤ h ≤9, -13 ≤ k ≤ 13, -34 ≤ l ≤ 34) measured in the range

$4.2° \leq \theta \leq 68.2°$, completeness θ_{max} = 99.9 %, 4573 unique (R_{int} = 0.0741) which were used in all calculations. Final indices: R_{1obs} = 0.0540, wR_{2obs} = 0.1364 [I ≥ 2σ(I)]; R_{1all} = 0.0713, wR_{2all} = 0.1476 [all data], GOOF = 1.033, largest difference peak and hole 0.29/-0.29 e Å^{-3}. Flack parameter:-0.1(2) Hooft parameter: -0.13(19)

Tuboanosigenin (**3**): Colourless prism crystals (recrystallization solvent: acetone), $C_{30}H_{44}O_6$, M_r = 500.65 g mol^{-1}; size 0.032 × 0.150 × 0.198 mm; monoclinic, space group *C2*, *a* = 27.9985(9) Å, *b* = 6.4010(2) Å, *c* = 20.5500(7) Å, β = 122.718(2)°, *V* = 3098.60(18) Å^3, *Z* = 4, *T* = 298 K, μ(CuKα) = 0.59 mm^{-1}, multi-scan, T_{min} = 0.669, T_{max} = 0.754, *F*(000) = 1088.0. The total number of reflections was 46931(-33 ≤ *h* ≤34, -7 ≤ *k* ≤ 7, -25 ≤ *l* ≤ 25) measured in the range $2.6° \leq \theta \leq 72.6°$, completeness θ_{max} = 99.8 %, 6083 unique (R_{int} = 0.0586) which were used in all calculations. Final indices: R_{1obs} = 0.0385, wR_{2obs} = 0.1099 [I ≥ 2σ(I)]; R_{1all} = 0.0416, wR_{2all} = 0.1125 [all data], GOOF = 1.072, largest difference peak and hole 0.29/-0.11 e Å^{-3}. Hooft parameter: 0.18(8).

Crystallographic data of **1** and **3** have been deposited at the Cambridge Crystallographic Data Center under codes 2049376 and 2049379, respectively. These data can be obtained free of charge via http://www.ccdc.cam.ac.uk/deposit, or from the CCDC, 12 Union Road, Cambridge CB2 1EZ, UK (fax: C44 1223 336 033; e-mail: deposit@ccdc.cam.ac.uk).

4.6. Computation details

The quantum chemical calculations were performed with the aid of the Gaussian 09 program package, Revision A.02 software for compounds (Frisch, et al., 2009). The ground state geometries were fully optimized by DFT with the B3LYP hybrid functional and with the 6-311++G(d,p) basis set starting from X-ray crystals (**1** and **3**) or NMR solution (2) structures. TD-DFT calculations were carried out with a polarizable continuum model using the integral equation formalism (IEFPCM) variant solvent model with methanol at the same level of the

theory above mentioned. The calculated electronic circular dichroism (CD) spectrum was extracted from output files by GaussSum 3.0 program (O'Boyle et al., 2008).

4.7. Cell culture and cell viability assay

The RAW 264.7 cells (ATCC® TIB-71™) were cultured in a Dulbecco's Modified Eagle Medium (DMEM), containing 10% fetal bovine serum, 100 units/mL of penicillin, and 100 μg/mL of streptomycin at 37 °C in an atmosphere containing 5% CO_2. Cell viability was evaluated using the MTT (3-[4,5-dimethylthiazol-2-yl]-2,5-diphenyl tetrazolium bromide) assay (Mosmann, 1983). The RAW 264.7 cells were seeded at a density of 1×10^5 cells/well in a 96-well plate and incubated for 24 h. The cells were treated with the test compounds **1**, **2**, and **3** (3.12 – 400 μM) for 24 h. MTT (1 mg/mL) was added to each cell well and incubated for 4 h at 37 °C. Then, the medium was removed and DMSO (100 μL) was added to each well. After 30 min incubation at 37 °C, the absorbance was measured at 570 nm using a microplate reader (Asys UVM 340, Biochrom, USA). The IC_{50} values were calculated from the concentration-response curves. Three independent experiments were carried out in triplicate.

4.8. LPS-induced NO, TNF-α, and IL-6 release in RAW264.7 cells

The concentration of NO, TNF-α, and IL-6 in the medium was measured as an indicator of anti-inflammatory activity. RAW 264.7 cells were seeded at a density of 5×10^5 cells/well in a 96-well plate and the cells were treated with compounds at different concentrations (1.56 – 50 μM) for 1 h, and then stimulated with LPS (1 μg/mL) at 37°C for 24 h. Dexamethasone (1.25 – 10 μM) was used as a positive control. For analysis, the culture supernatant was collected and mixed with an equal volume of Griess reagent (1% sulfanilamide, 0.1% N-[1-naphthyl]-ethylenediamine dihydrochloride, 5% phosphoric acid), and the absorbance measured at 540 nm. The amount of nitrite in the samples was calculated from a standard sodium nitrite curve

(Griess, 1959; Gasparrini et al., 2018). The concentrations of the secreted pro-inflammatory cytokines TNF-α and IL-6 were measured using TNF-α and IL-6 ELISA kit (Invitrogen, Massachusetts, EUA) according to the manufacturer's manual. Three independent experiments were carried out in triplicate.

4.9. Statistical analysis

The results were presented as mean $\pm$ standard deviation (SD) of three independent experiments. The statistical analysis was performed using GraphPad Prism version 5.01 (GraphPad Software, La Jolla, CA, USA). The differences between the groups were analyzed by one-way analysis of variance (ANOVA) followed by Tukey's multiple comparison test.

Acknowledgements

Declaration of competing interest

The corresponding authors declare that there is no potential competing or non-financial interest.

Appendix A. Supplementary data

Supplementary data associated with this article, including the IC$_{50}$ curves for the cell viability, IR, HRESIMS, 1D, and 2D NMR spectra for compounds **1** – **3**.

References

Akhtar, N., Gupta, P., Sangwan, N.S., Sangwan, R.S., Trivedi, P.K., 2013. Cloning and functional characterization of 3-hydroxy-3-methylglutaryl coenzyme A reductase gene from *Withania somnifera*: an important medicinal plant. Protoplasma 250, 613–622. https://doi.org/10.1007/s00709-012-0450-2.

Almeida, A.A., Lima, G.D.A., Simão, M.V.R.C., Moreira, G.A., Siqueira, R.P., Zanatta, A.C., Vilegas, W., Machado-Neves, M., Bressan, G.C., Leite, J.P.V., 2020. Screening of plants from the Brazilian Atlantic Forest led to the identification of *Athenaea velutina* (Solanaceae) as a novel source of antimetastatic agentes. Int. J. Exp. Path. 00, 1–16. https://doi.org/10.1111/iep.12351.

Almeida, A.A., Lima, G.D.A., Eiterer, M., Rodrigues, L.A., Vale, J.A., Zanatta, A.C., Bressan, G.C., Oliveira, L.L., Leite, J.P.V., 2021. A withanolide-rich fraction of *Athenaea velutina* induces apoptosis and cell cycle arrest in melanoma B16F10 cells. Planta Med. https://doi.org/10.1055/a-1395-9046.

Almeida, A.A., Cota, B.B., Rodrigues, L.M., Dutra, L.L. Kohlhoff, M., Bressan, G.C., Brandão,G.C., J.P.V., 2022. Withalutin, a new cytotoxic withanolide from *Athenaea velutina* (Sendtn.) D'Arcy. Nat. Prod. Res. https://doi.org/10.1080/14786419.2022.2039135

Almeida-Lafetá, R.C., Ferreira, M.J.P., Emerenciano, V.P., Kaplan, M.A.C., 2010. Withanolides from *Aureliana fasciculata* var. *fasciculata*. Helv. Chim. Acta 93, 2478–2487. https://doi.org/10.1002/hlca.201000126.

Barboza G.E, Hunziker A.T, Bernadello G., Cocucci A., Moscone A.E., García C.C., Anton A., 2016 Solanaceaee. In: Kadereit, J.W., Bittrich, V., Fuentes, V., Dillon, M.O., Bittrich, V., Cosa, M.T., Subils, R., Romanutti, A., Arroyo, S. (Eds), Flowering Plants. Eudicots. The families and genera of vascular plant. Springer International Publishing, Cham, Switzerland, pp. 295–357. https://doi.org/10.1007/978-3-319-28534-4_29.

Bashir, S., Sharma, Y., Elahi, A., Khan, F., 2016. Macrophage polarization: the link between inflammation and related diseases. Inflamm. Res. 65, 1–11. https://doi.org/10.1007/s00011-015-0874-1.

Batista, P.H.J., Lima, K.S.B., Pinto, F.C.L., Tavares, J.L., Uchoa, D.E.A., Costa-Lotufo, L.V., Rocha, D.D., Silveira, E.R., Bezerra, A.M.E., Canuto, K.M., Pessoa, O.D.L., 2016. Withanolides from leaves of cultivated *Acnistus arborescens*. Phytochemistry 130, 321–327. http://dx.doi.org/10.1016/j.phytochem.2016.07.003.

Bhat, B.A., Dhar, K.L., Puri, S.C., Qurishi, M.A., Khajuria, A., Guptac, A., Qazi, G.N., 2005. Isolation, characterization and biological evaluation of datura lactones as potential immunomodulators. Bioorg. Med. Chem. 13, 6672–6677. https://doi.org/10.1016/j.bmc.2005.07.040.

Bruker AXS Inc. 2018a. APEX3 Suite for Crystallographic Software - Single Crystal X-ray Diffraction, Madison, Wisconsin, USA (Version 2018.9).

Bruker AXS Inc. 2018b. SAINT Data Reduction Software + Integration Engine, Madison, Wisconsin, USA (Version 8.37A).

Cardona, D., Quinones, W., Torres, F., Robledo, S., Velez, I.D., Cruz, V., Notario, R., Echeverri, F., 2006. Leishmanicidal activity of withajardins and acnistins. An experimental and computational study. Tetrahedron 62, 6822–6829. https://doi.org/10.1016/j.tet.2006.04.101.

Carrero, D.A.S., Batista, P.H.J., Souza, L.G.S., Pinto, F.C.L., De Vasconcelos, M.A., Teixeira, E.H., Canuto, K.M., Santiago, G.M.P., Silveira, E.R., Pessoa, O.D.L., 2018. Withanolides from Leaves of *Nicandra physalodes*. J. Braz. Chem. Soc. 29, 11–16. http://dx.doi.org/10.21577/0103-5053.20170105.

Castro, S.J., Casero, C.N., Padrón, J.M., Nicotra, V.E.J., 2019. Selective antiproliferative withanolides from species in the genera *Eriolarynx* and *Deprea*. J. Nat. Prod. 82, 1338–1344. https://doi.org/10.1021/acs.jnatprod.9b00117.

Chaurasiya, N.D., Sangwan, N.S., Sabir, F., Misra, L., Sangwan, R.S., 2012. Withanolide biosynthesis recruits both mevalonate and DOXP pathways of isoprenogenesis in ashwagandha *Withania somnifera* L. (Dunal). Plant Cell Rep. 31, 1889–1897. https://doi.org/10.1007/s00299-012-1302-4.

Chen, L-X., He, H., Qiu, F., 2011. Natural withanolides: an overview. Nat. Prod. Rep. 28, 705–740. https://doi.org/10.1039/c0np00045k.

Crane, E.A., Heydenreuter, W., Beck, K.R., Strajhar, P., Vomacka, J., Smiesko, M., Mons, E., Barth, L., Neuburger, M., Vedani, A., Odermatt, A., Sieber, S.A., Gademann, K., 2019. Profiling withanolide A for therapeutic targets in neurodegenerative diseases. Bioorg. Med. Chem. 27, 2508–2520. https://doi.org/10.1016/j.bmc.2019.03.022.

Dolomanov, O.V., Bourhis, L.J., Gildea, R.J., Howard, J.A.K., Puschmann, H., 2009. OLEX2: a complete structure solution, refinement and analysis program. J. Appl. Crystallogr. 42, 339–341. https://doi.org/10.1107/S0021889808042726.

Dom, M., Berghe, W.V., Ostade, X.V., 2020. Broad-spectrum antitumor properties of withaferin A: a proteomic perspective. RSC Med. Chem. 11, 30–50. https://doi.org/10.1039/c9md00296k.

Dong, B., An, L., Yang, X., Zhang, X., Zhang, J., Tuerhong, M., Jin, D-Q., Ohizumi, Y., Lee, D., Xu, J., Guo, Y., 2019. Withanolides from *Physalis peruviana* showing nitric oxide inhibitory effects and affinities with iNOS. Bioorg. Chem. 87, 585–593. https://doi.org/10.1016/j.bioorg.2019.03.051.

Echeverri, F., Quiñones, W., Torres, F., Cardona, G., Archbold, R., 1995. Withajardin E, A withanolide from *Deprea orinocensis*. Phytochemistry 40, 923–925. https://doi.org/10.1016/0031-9422(95)00220-2.

Echeverri, F., Torres, F., Cardona, G., Lopez, J., Quinones, W., Gallego, L.H., Pelaez, C., Rojas, M., Garcia, F., Restrepo, L.M., 1991. Withajardins: structure and activity. Rev. Boliv. Quim. 10, 21–3.

Frisch, M.J., Trucks, G.W., Schlegel, H.B., Scuseria, G.E., Robb, M.A., Cheeseman, J.R., Scalmani, G., Barone, V., Petersson, G.A., Nakatsuji, H., Caricato, X.Li.M., Marenich, A., Bloino, J., Janesko, B.G., Gomperts, R., Mennucci, B., Hratchian, H.P., Ortiz, J.V., Izmaylov, A.F., Sonnenberg, J.L., Williams-Young, D., Ding, F., Lipparini, F., Egidi, F., Goings, J., Peng, B., Petrone, A., Henderson, T., Ranasinghe, D., Zakrzewski, V.G., Gao, J., Rega, N., Zheng, G., Liang, W., Hada, M., Ehara, M., Toyota, K., Fukuda, R., Hasegawa, J., Ishida, M., Nakajima, T., Honda, Y., Kitao, O., Nakai, H., Vreven, T., Throssell, K., Montgomery, J.A.Jr., Peralta, J.E., Ogliaro, F., Bearpark, M., Heyd, J.J., Brothers, E.,

Kudin, K.N., Staroverov, V.N., Keith, T., Kobayashi, R., Normand, J., Raghavachari, K., Rendell, A., Burant, J.C., Iyengar, S.S., Tomasi, J., Cossi, M., Millam, J.M., Klene, M., Adamo, C., Cammi, R., Ochterski, J.W., Martin, R.L., Morokuma, K., Farkas, O., Foresman, J.B., Gaussian D.J.F., 2009. Inc., Wallingford CT. Gaussian 09, Revision A.02.

Fujiwara, N., Kobayashi, K., 2005. Macrophages in inflammation. Inflamm. Allergy Drug Targets 4, 281–286. https://doi.org/10.2174/1568010054022024.

Gasparrini, M., Afrina, S., Forbes-Hernándeza, T.Y., Cianciosia, D., Reboredo-Rodrigueza, P., Amicia, A., Battinoa, M., Giampieri, F., 2018. Protective effects of Manuka honey on LPS-treated RAW 264.7 macrophages. Part 2: Control of oxidative stress induced damage, increase of antioxidant enzyme activities and attenuation of inflammation. Food Chem. Toxicol. 120, 578–587. https://doi.org/10.1016/j.fct.2018.08.001.

Griess, J.P., 1859. V. On new nitrogenous derivatives of the phenyl-and benzoyl-series. Proc. R. Soc. Lond. 9, 594–597. https://doi.org/10.1098/rspl.1857.0113.

Guerreiro, D.D., De Lima, L.F., De Sá, N.A.R., Tetaping, G.M., Alves, B.G., Lobo, C.H., Loiola, O.D., Smitz, J., De Figueiredo, J.R., Rodrigues, A.P.R., 2019. In vitro study of withanolide D toxicity on goat preantral follicles and its effects on the cell cycle. Reprod. Toxicol. 84, 18–25. https://doi.org/10.1016/j.reprotox.2018.12.007.

Gupta, P., Goel, R., Pathak, S., Srivastava, A., Singh, S.P., Sangwan, R.S., Asif, M.H., Trivedi, P.K., 2013. De novo assembly, functional annotation and comparative analysis of *Withania somnifera* leaf and root transcriptomes to identify putative genes involved in the withanolides biosynthesis. PLoS ONE 8 e62714. https://doi.org/10.1371/journal.pone.0062714.

Hunziker, A.T., Barboza, G.E., 1990. Estudios sobre Solanaceaee XXX. Revision de Aureliana. Darwiniana 30, 95–113. https://www.jstor.org/stable/23222520.

Kiyota, N., Shingu, K., Yamaguchi, K., Yoshitake, Y., Harano, K., Yoshimitsu, H., Miyashita, H., Ikeda, T., Tagawa, C., Nohara, T., 2008. New C_{28} steroidal glycosides from *Tubocapsicum anomalum*. Chem. Pharm. Bull. 56, 1038–1040. https://doi.org/10.1248/cpb.55.34.

Krause, L., Herbst-Irmer, R., Sheldrick, G.M., Stalke, D., 2015. Comparison of silver and molybdenum microfocus X-ray sources for single-crystal structure determination. J. Appl. Crystallogr. 48, 3–10. https://doi.org/10.1107/S1600576714022985.

Lee, J., Liu, J., Feng, X., Hernández, M.A.S., Mucka, P., Ibi, D., Choi, J.W., Ozcan, U., 2016. Withaferin A is a leptin sensitizer with strong antidiabetic properties in mice. Nat. Med. 22, 1023–1035. https://doi.org/10.1038/nm.4145.

Lima, S.C.M., Pacheco, J.S., Marques, A.M., Veltri, E.R.P., Almeida-Lafetá, R.C., Figueiredo, M.R., Kaplan, M.A. C., Torres-Santos, E.C., 2018. Leishmanicidal activity of withanolides from *Aureliana fasciculata* var. *fasciculata*. Molecules 23, 3160–3171. https://doi.org/10.3390/molecules23123160.

Luis, J.G., Echeverril, F., Quinones, W., González, A.G., 1994. Withajardins, withanolides with a new type of skeleton structure of withajardins A, B, C and D absolute configuration of withajardin C. Tetrahedron 50, 1217–1226. https://doi.org/10.1016/S0040-4020(01)80833-4.

Misico, R.I., Nicotra, V.E., Oberti, J.C., Barboza, G., Gil, R.R., Burton, G., Kinghorn, A.D., Falk, H., Kobayashi, J., 2011. Withanolides and related steroids, in: Kinghorn, A.D., Falk, H., Kobayashi, J. (Eds.), Progress in the Chemistry of Organic Natural Products. Springer, Berlin, pp. 127–229. https://doi.org/10.1007/978-3-7091-0748-5_3.

Mosmann, T., 1983. Rapid colorimetric assay for cellular growth and survival: application to proliferation and cytotoxicity assays. J. Immunol. Methods 65, 55–63. https://doi.org/10.1016/0022-1759(83)90303-4.

Nicolás, F.G., Reyes, G., Audisio, M.C., Uriburu, M.L., González, S.L., Barboza, G.E., Nicotra, V.E., 2015. Withanolides with antibacterial activity from *Nicandra john-tyleriana*. J. Nat. Prod. 78, 250–257. https://doi.org/10.1021/np500824f.

O'Boyle, N.M., Tenderholt, A.L., Langner. K.M., 2008. cclib: A library for package-independent computational chemistry algorithms. J. Comp. Chem., 29, 839–845. http://dx.doi.org/10.1002/jcc.20823.

Rabhi, C., Arcile, G., Goff, G.L., Noble, C.C., Ouazzani, J., 2019. Neuroprotective effect of CR-777, a glutathione derivative of withaferin A, obtained through the bioconversion of *Withania somnifera* (L.) Dunal extract by the fungus *Beauveria bassiana*. Molecules 24, 4599–4617. https://doi.org/10.3390/molecules24244599.

Rodrigues, I.M.C., Knapp, S., Stehmann, J.R., 2019. The nomenclatural re-establishment of *Athenaea* Sendtn. (Solanaceaee) with a nomenclatural synopsis of the genus. Taxon, 68, 839–846. https://doi.org/10.1002/tax.12089.

Rodrigues, I.M.C., Knapp, S., Stehmann, J.R., 2021. Two new species of *Athenaea* Sendtn. (Solanaceaee) from the Atlantic forests of south-eastern Brazil. PhytoKeys, 178, 1–15. https://doi.org/10.3897/phytokeys.178.6460.

Rodrigues, L.A., Almeida, A. das C., Gontijo, D.C.Salustiano, I.V., Almeida, A.A.,, Brandão, G.C., de Oliveira, A. Ribon, B., Leite, J.P.V., 2020. Antibacterial screening of plants from the Brazilian Atlantic Forest led to the identification of active compounds in *Miconia latecrenata* (DC.) Naudin. Nat. Prod. Res. 1–5. https://doi.org/10.1080/14786419.2020.1802271.

Roumy, V., Biabiany, M., Hennebelle, T., Aliouat, E.M., Pottier, M., Joseph, H., Joha, S., Quesnel, B., Alkhatib, R., Sahpaz, S., Bailleul, F.J., 2010. Antifungal and cytotoxic activity of withanolides from *Acnistus arborescens*. J. Nat. Prod. 73, 1313–1317. https://doi.org/10.1021/np100201p.

Sendtner, O., 1846. Solanaceae. in: Martius, C.F.P. (Ed.), Flora brasiliensis, Lipsiae [Leipzig], Monachii, Munich, pp. 5–228. https://doi.org/10.5962/bhl.title.454.

Sheldrick, G.M., 2015a SHELXT – Integrated space-group and crystal-structure determination. Acta Cryst. 71, 3–8. https://doi.org/10.1107/S2053273314026370.

Sheldrick, G.M., 2015b. Crystal structure refinement with SHELXL. Acta Cryst. 71, 3–8. https://doi.org/10.1107/S2053229614024218.

Silva, E.L., Almeida-Lafetá, R.C., Borges, R.M., Staerk, D., 2018. Athenolide A, a new steroidal lactone from the leaves of *Athenaea martiana* (Solanaceaee) determined by means of HPLC-HR-MS-SPENMR Analysis. Chem. Biodivers. 15, e1700455. https://doi.org/10.1002/cbdv.201700455.

Spek, A.L., 2015. PLATON SQUEEZE: a tool for the calculation of the disordered solvent contribution to the calculated structure factors. Acta Cryst. 71, 9–18. https://doi.org/10.1107/S2053229614024929

Sun, Y., Guo, T., Zhang, F., Wang, Y., Liu, Z., Guo, S., Li, L., 2020. Isolation and characterization of cytotoxic withanolides from the calyx of *Physalis alkekengi* L. var *franchetii*. Bioorg. Chem. 96, 103614. https://doi.org/10.1016/j.bioorg.2020.103614.

Tan, J., Liu, Y., Cheng, Y., Sun, Y., Pan, J., Guan, W., Li, X., Huang, J., Jiang, P., Guo, S., Kuang, H., Yang, B., 2020. New withanolides with anti-inflammatory activity from the leaves of *Datura metel* L. Bioorg. Chem. 95, 103541. https://doi.org/10.1016/j.bioorg.2019.103541.

Wang, S.-B., Dong-Rong Z., Biao, N., Jing, L., Ying-Jun, Z., Ling-Yi, K., Jian-Guang, L., 2018. Cytotoxic withanolides from the aerial parts of *Tubocapsicum anomalum*. Bioorg. Chem. 81, 396–404. https://doi.org/10.1016/j.bioorg.2018.08.034.

White, P.T., Subramanian, C., Motiwala, H.F., Cohen, M.S., 2016. Natural withanolides in the treatment of chronic diseases in: Gupta, S.C., Prasad, S., Aggarwal, B.B. (Eds.), Anti-inflammatory nutraceuticals and chronic diseases, advances in experimental medicine and biology. Springer, Berlin, pp. 329–373.

Wijeratne, E.M.K., Oliveira, M.C.F., Mafezoli, J., Xu, Y-M., Minguzzi, S., Batista, P.H.J., Pessoa, O.D.L., Whitesell, L., Gunatilaka, A.A.L., 2018. Withaferin A and withanolide D analogues with dual heat-shock-inducing and cytotoxic activities: semisynthesis and biological evaluation. J. Nat. Prod. 81, 825–837. https://doi.org/10.1021/acs.jnatprod.7b00918.

Worland, A.M., Czajka, J.J., Li, Y. Wang, Y. Tang, Y.J., Su, W.W., 2020. Biosynthesis of terpene compounds using the non-model yeast *Yarrowia lipolytica*: grand challenges and a few perspectives. Curr. Opin. Biotech. 64, 134–140. https://doi.org/10.1016/j.copbio.2020.02.020.

Xiang, K., Li, C., Li, M-X., Song, Z-R., Ma, X-X., Sun, D-J., Li, H., Chen, L-X., 2021. Withanolides isolated from *Tubocapsicum anomalum* and their antiproliferative activity. Bioorg. Chem. 110, 104809. https://doi.org/10.1016/j.bioorg.2021.104809.

Xu, Q-Q., Wang, K-W., 2020. Natural bioactive new withanolides. Mini-Rev. Med. Chem. 20, 1101–1117. https://doi.org/10.2174/1389557518666171129164056.

Zhang, W-N., Tong, W-Y., 2016. Chemical constituents and biological activities of plants from the genus *Physalis*. Chem. Biodiversity 13, 48–65. https://doi.org/10.1002/cbdv.201500435.

Supplementary Material

Contents

Figure S1. Structures of the different C₂₈ steroidal lactone/lactol skeletons.
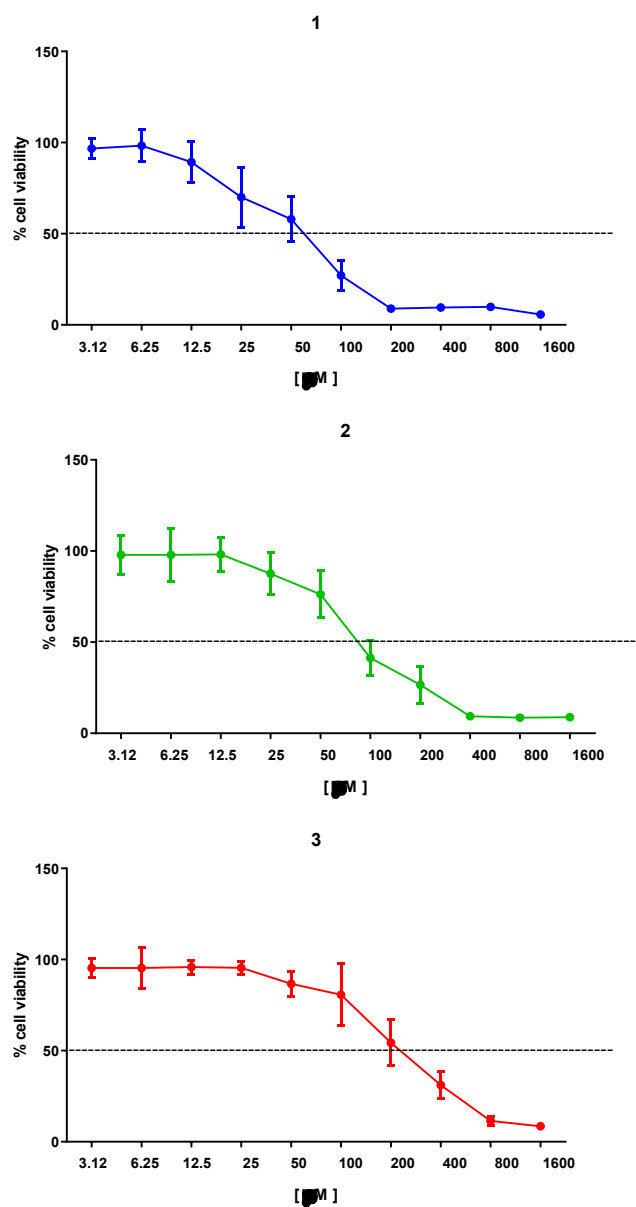
Figure S2. IC$_{50}$ curves for the cell viability of compounds 1 − 3
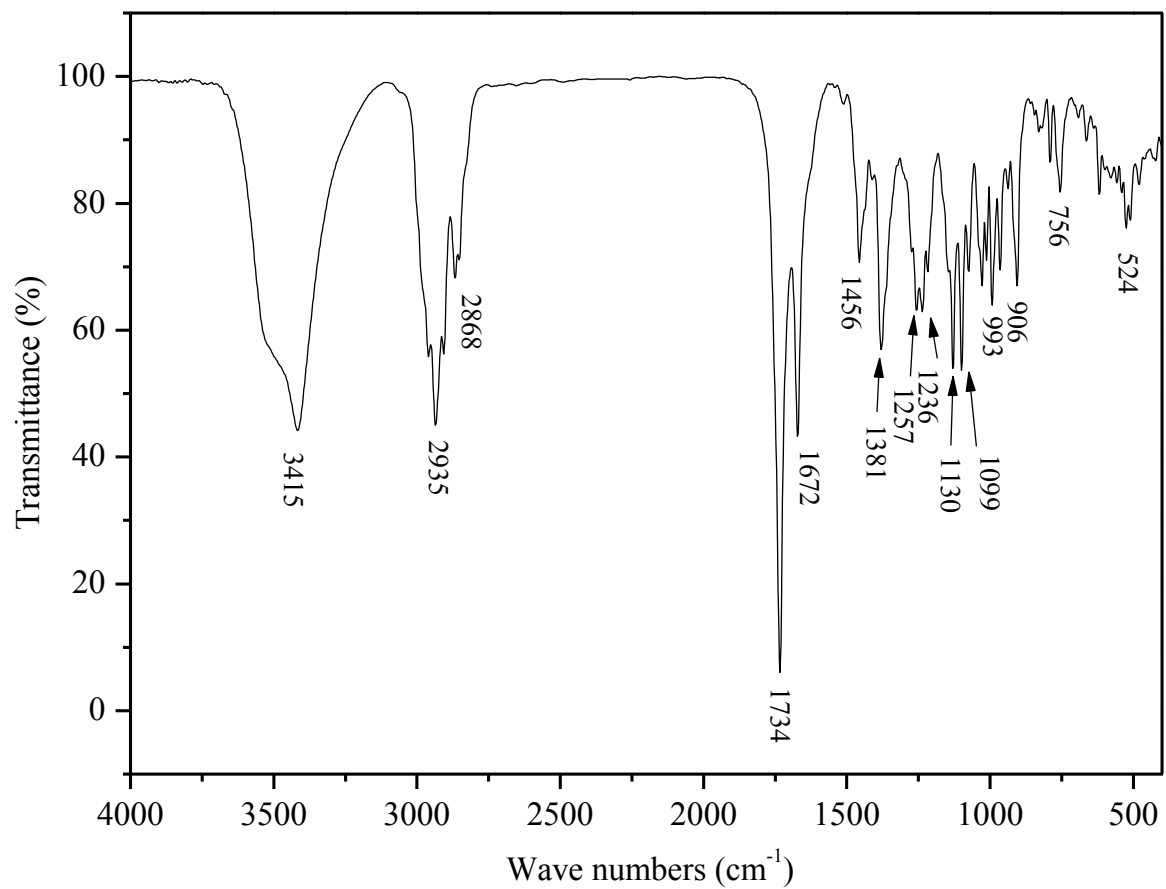
Figure S3. FTIR spectrum of 1.
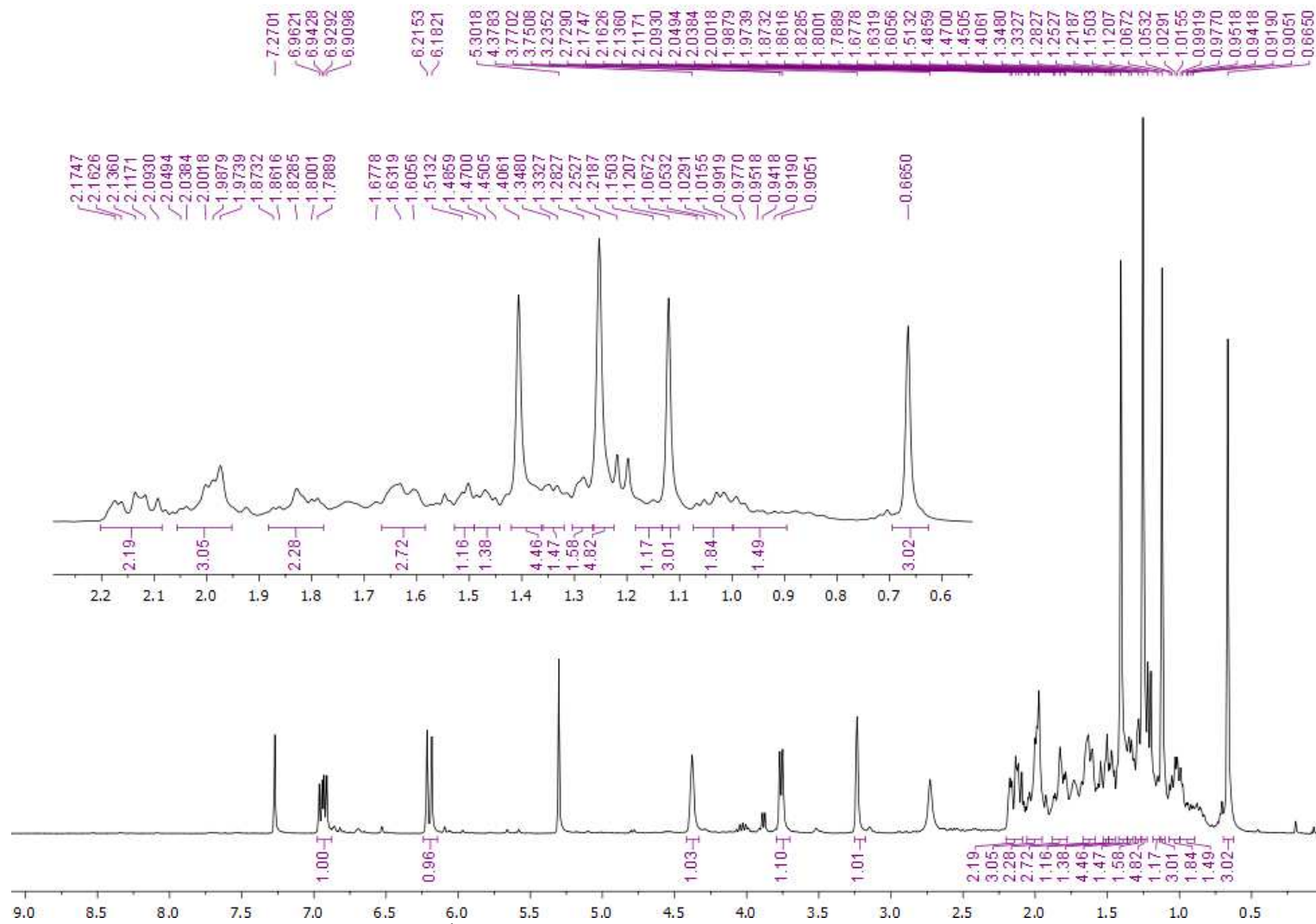
Figure S4. ¹H NMR (300.13 MHz) spectrum of 1, in CDCl₃.
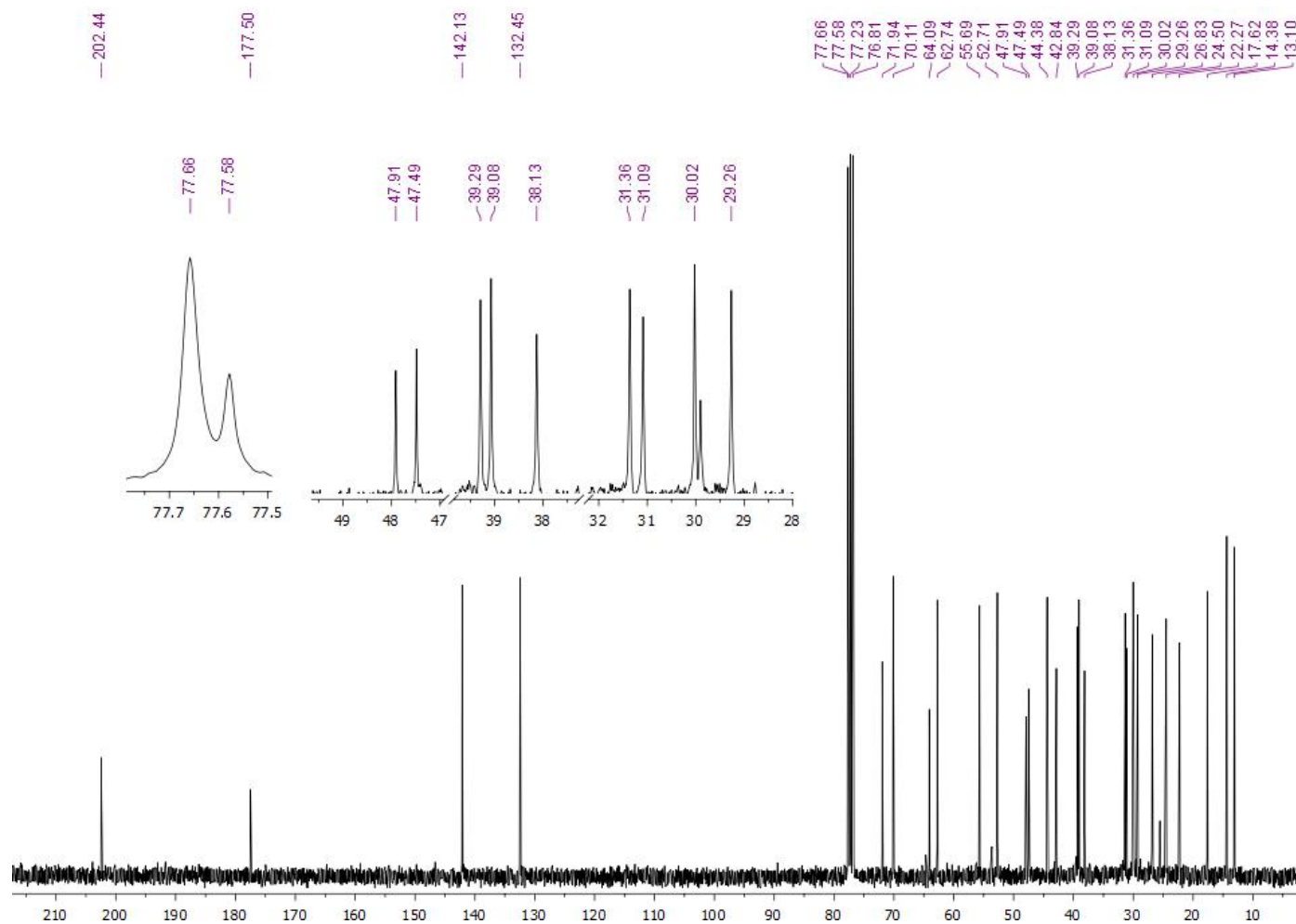
Figure S5. ^{13}C NMR (75.47 MHz) spectrum of 1, in CDCl$_3$.
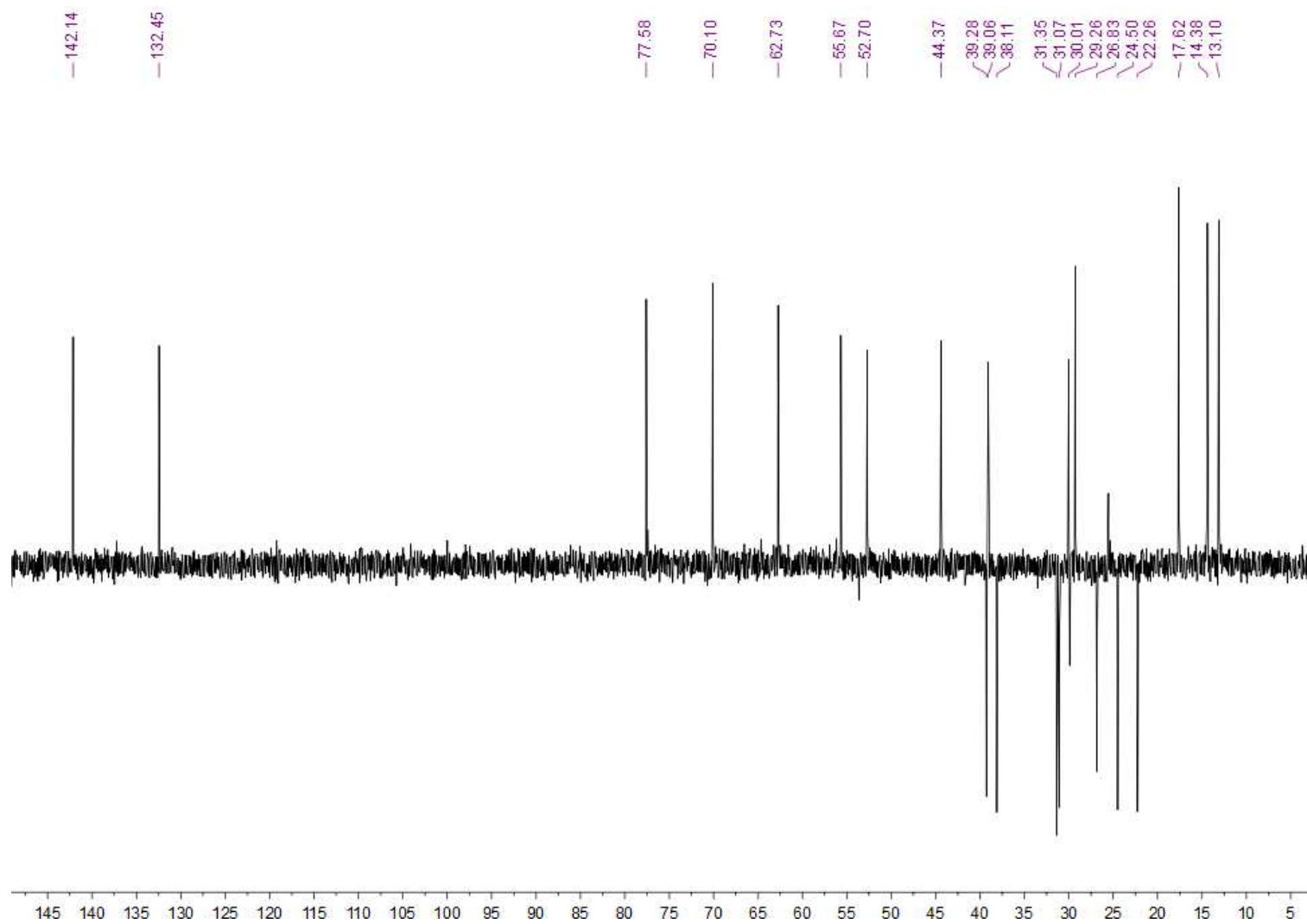
Figure S6. DEPT 135° NMR (75.47 MHz) spectrum of 1, in CDCl₃.
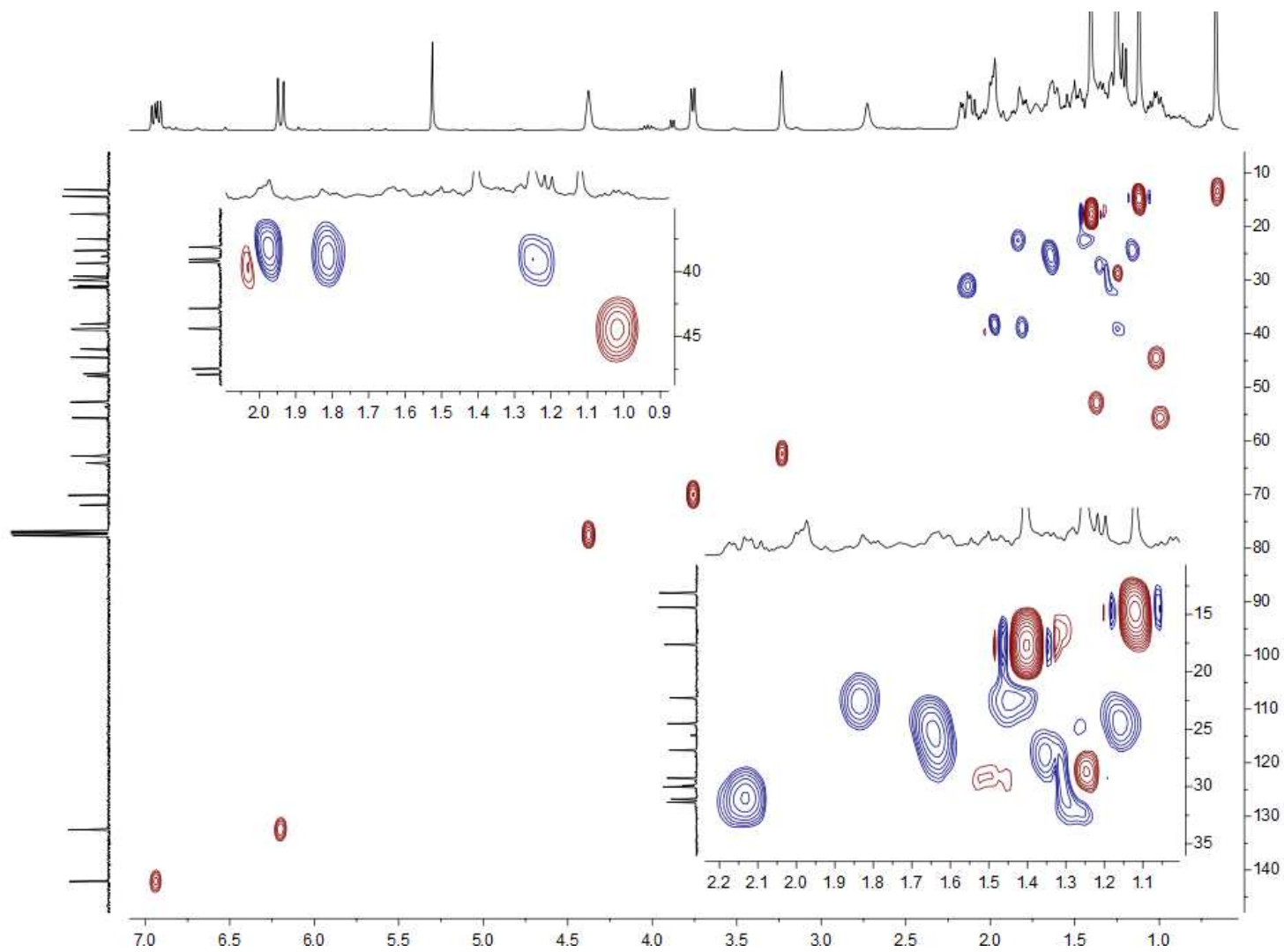
Figure S7. HSQC NMR spectrum of 1, in CDCl₃.
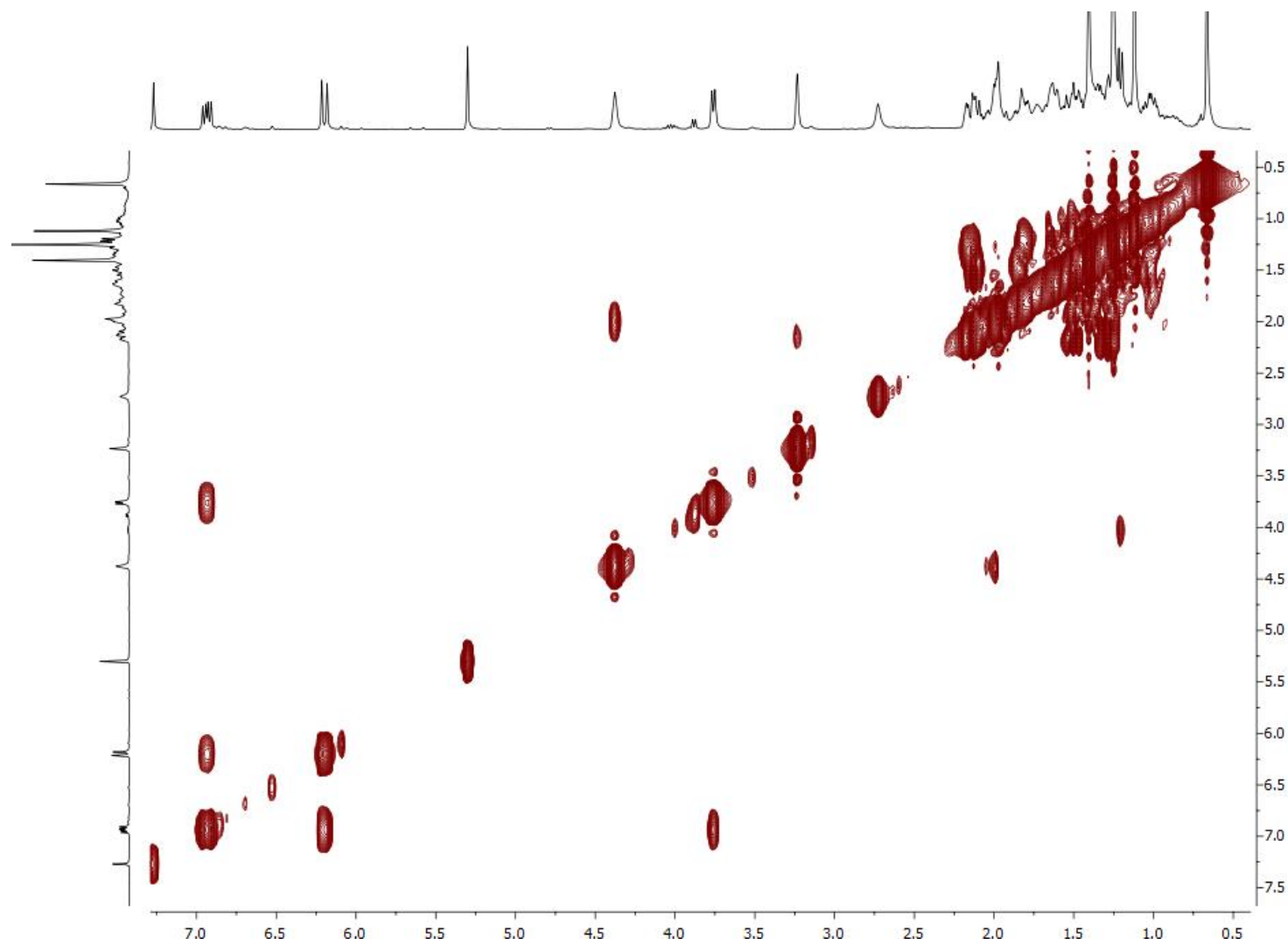
Figure S8. COSY NMR spectrum of 1, in CDCl₃.
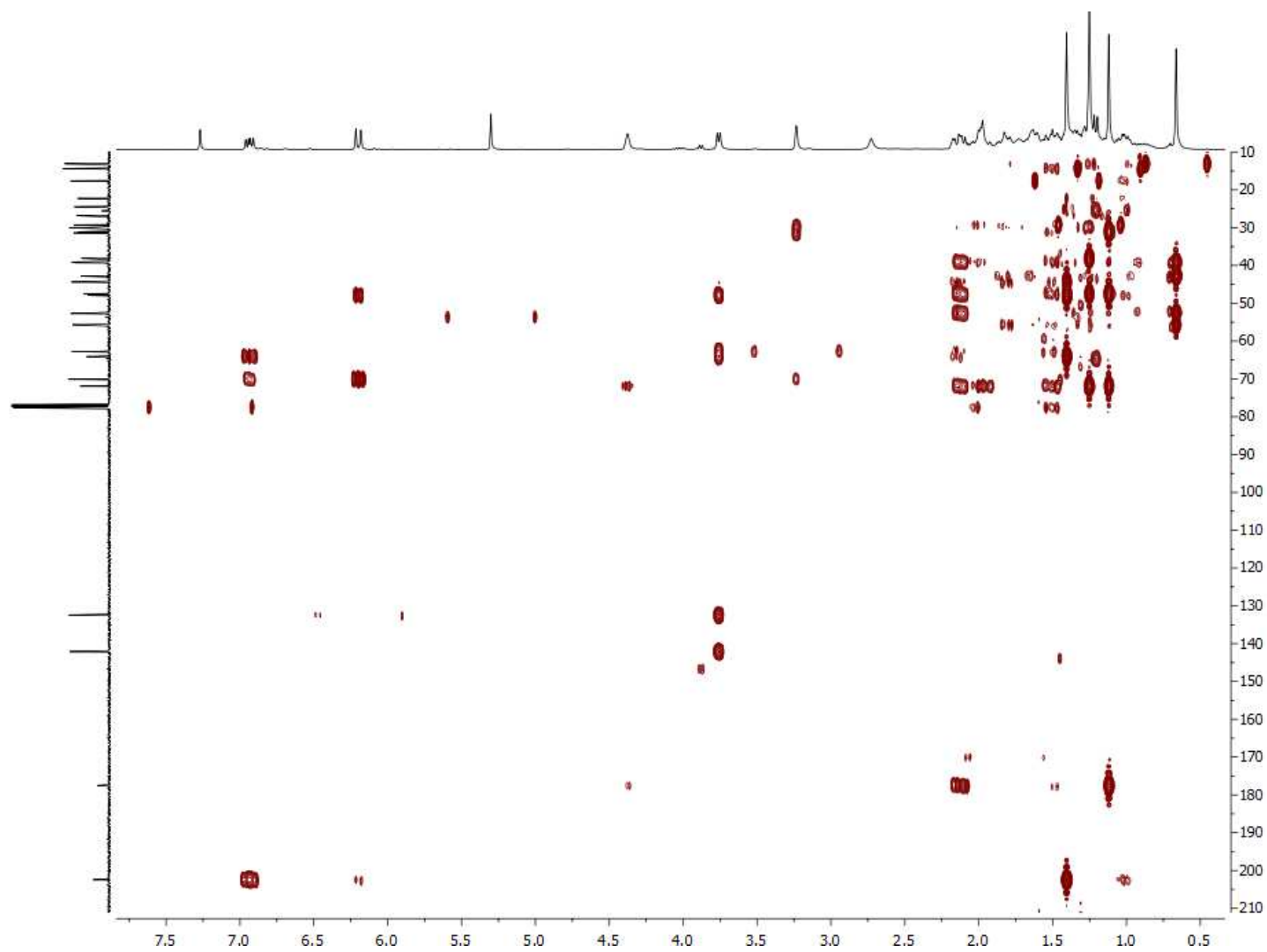
Figure S9. HMBC NMR spectrum of 1, in CDCl₃.
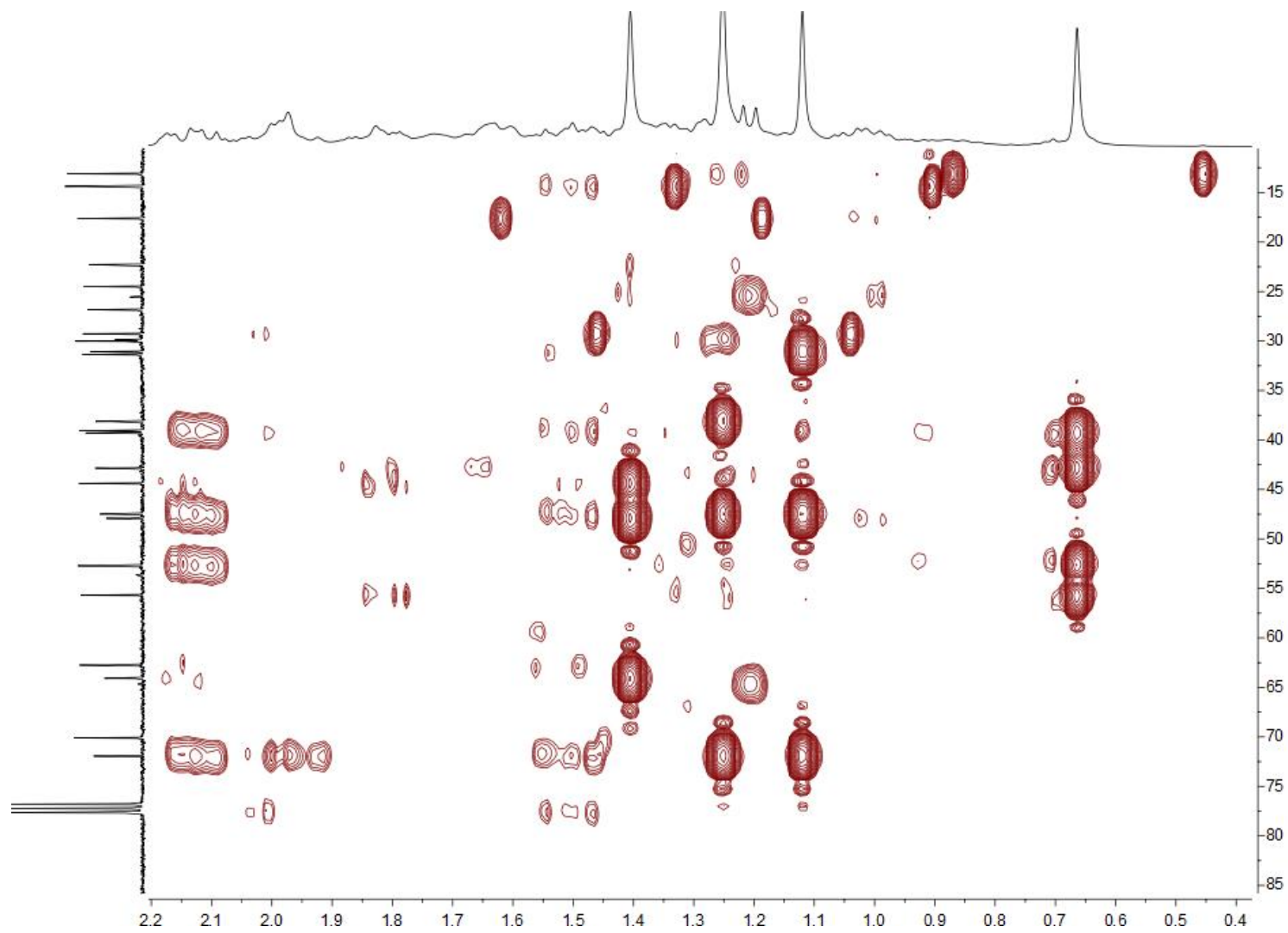
Figure S10. HMBC NMR spectrum of 1, in CDCl₃.
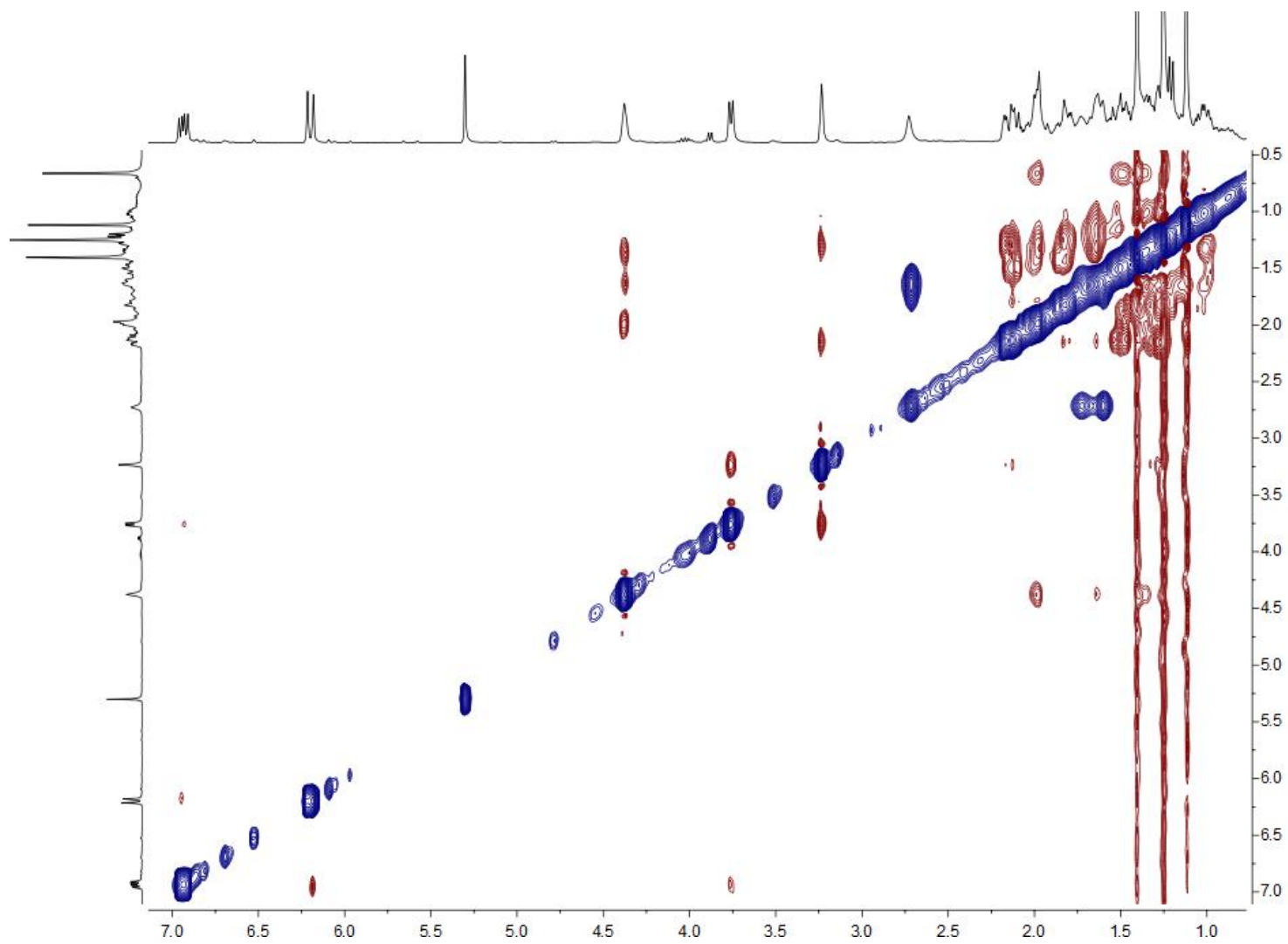
Figure S11. NOESY NMR spectrum of 1, in CDCl₃.
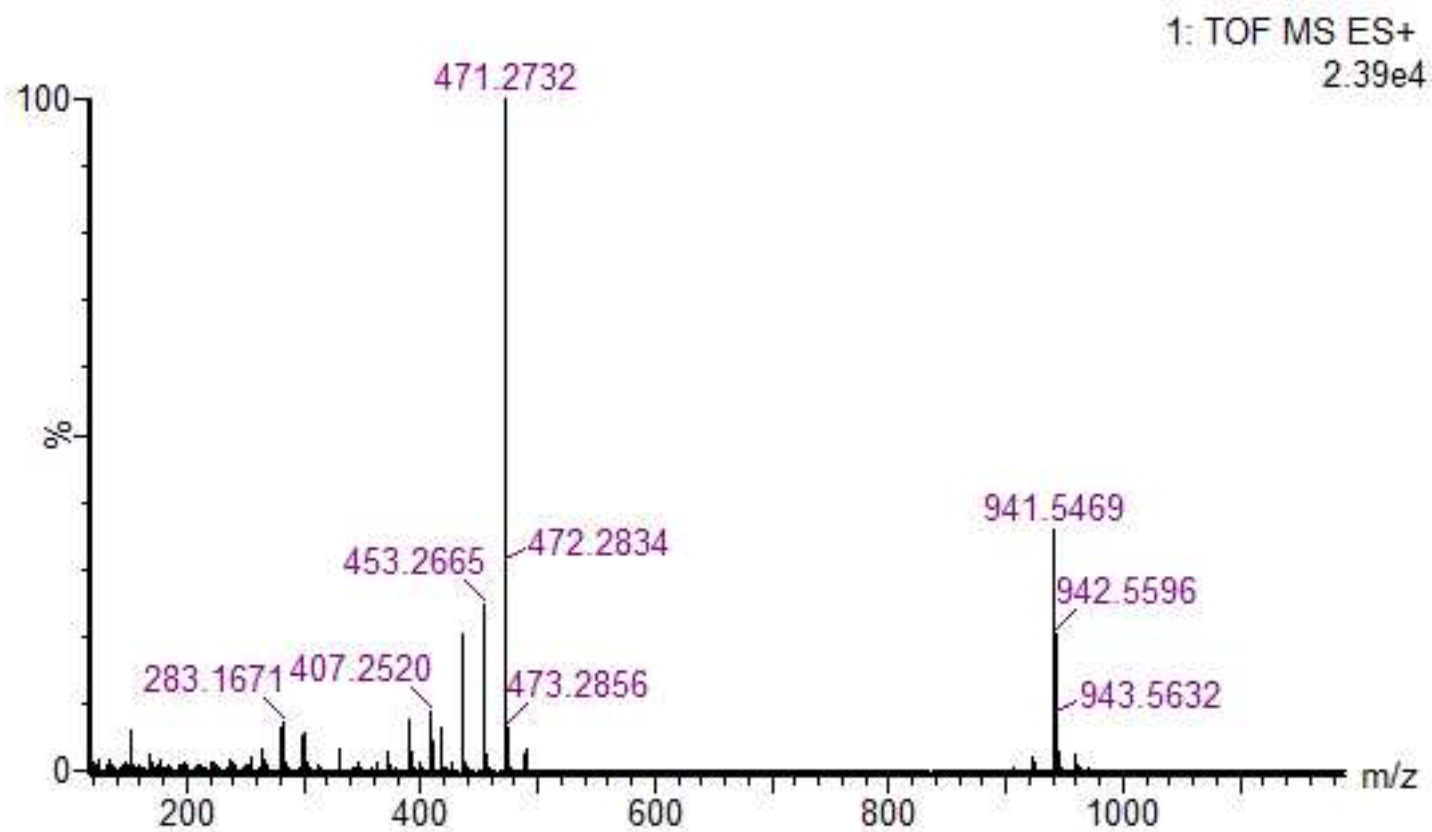
Figure S12. HRESIMS spectrum of 1.
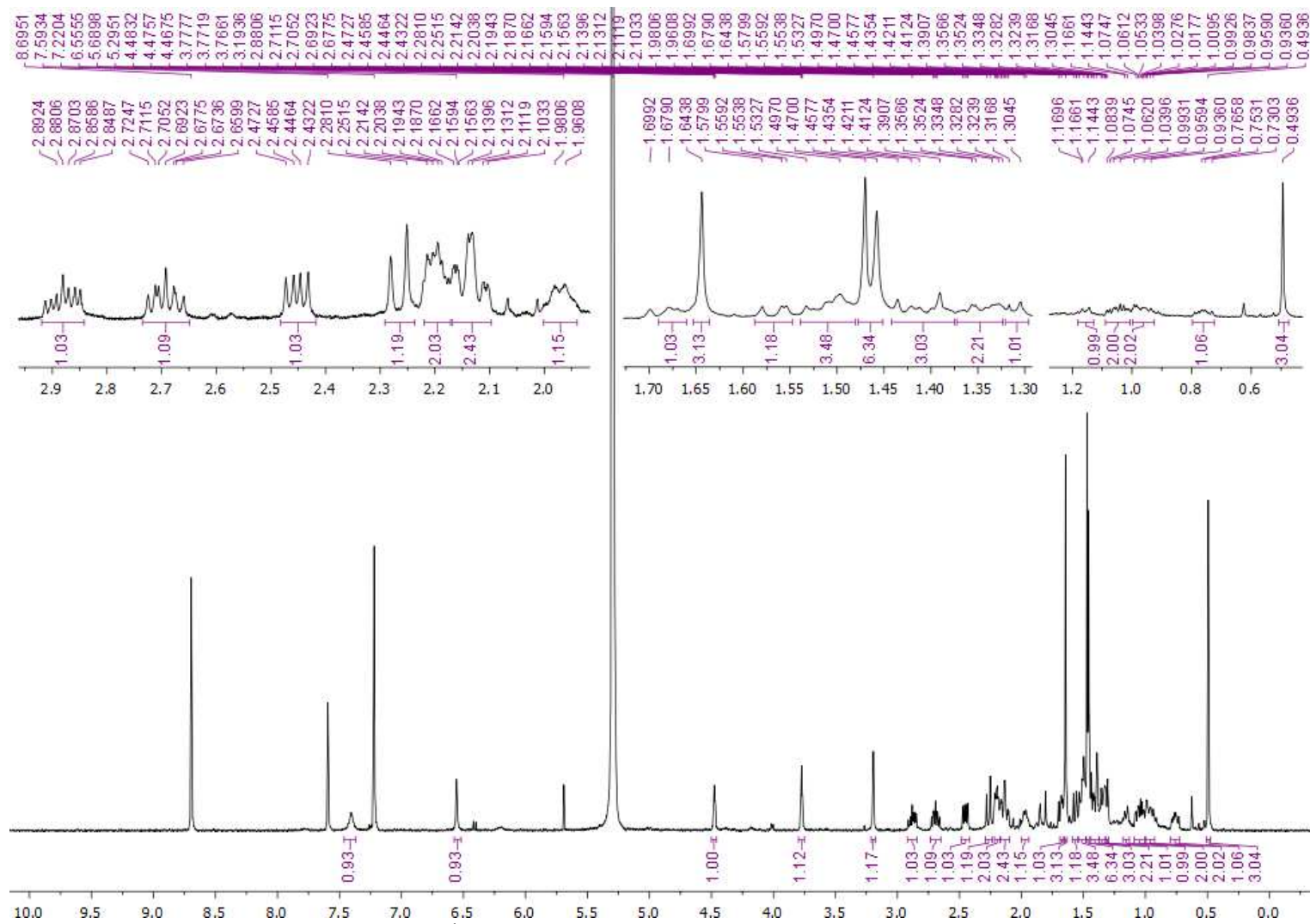
Figure S13. ^{1}H NMR (500.13 MHz) spectrum of 2, in C$_5$D$_5$N.

Figure S14. ^{13}C NMR (125.75 MHz) spectrum of **2**, in C$_5$D$_5$N.
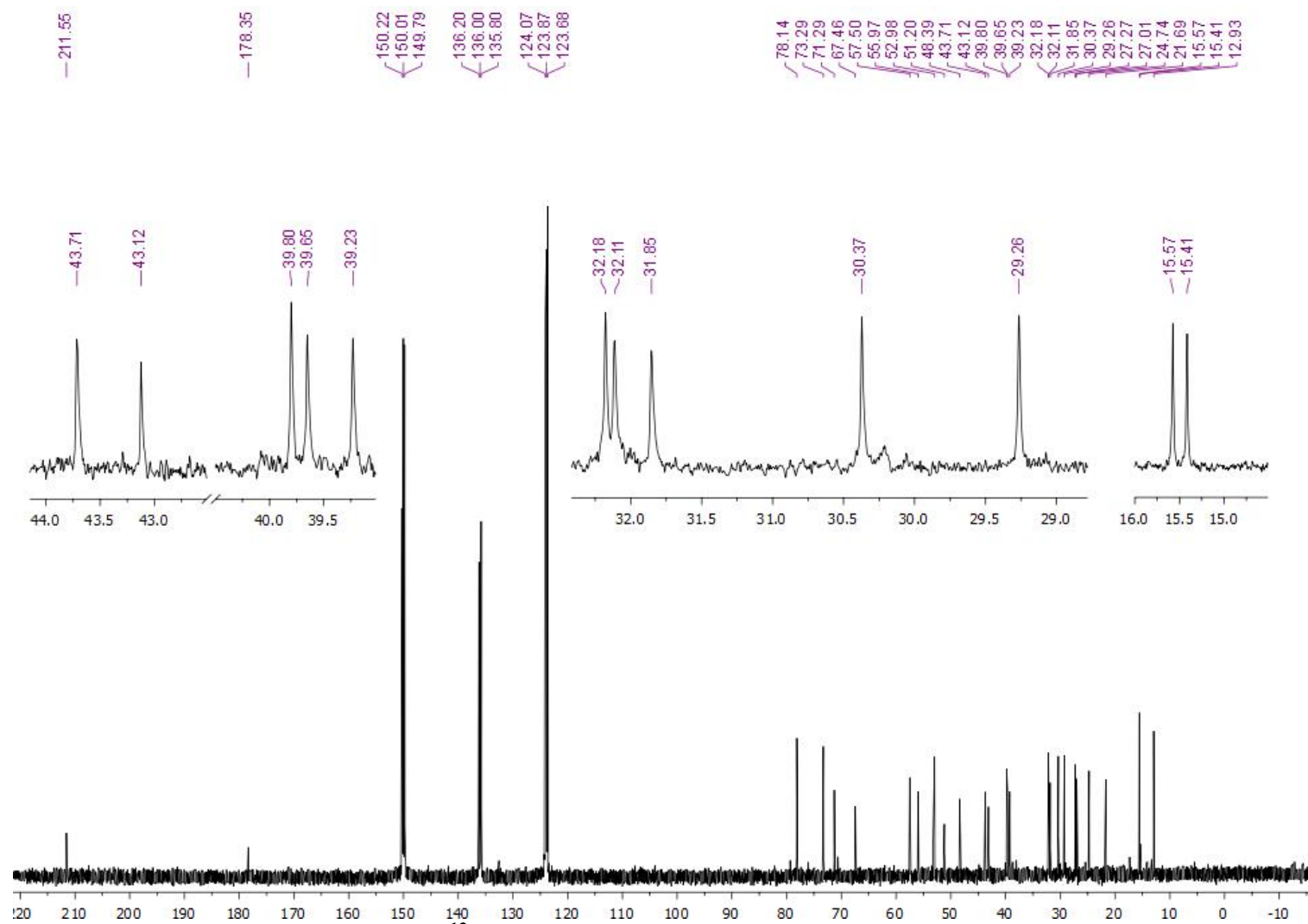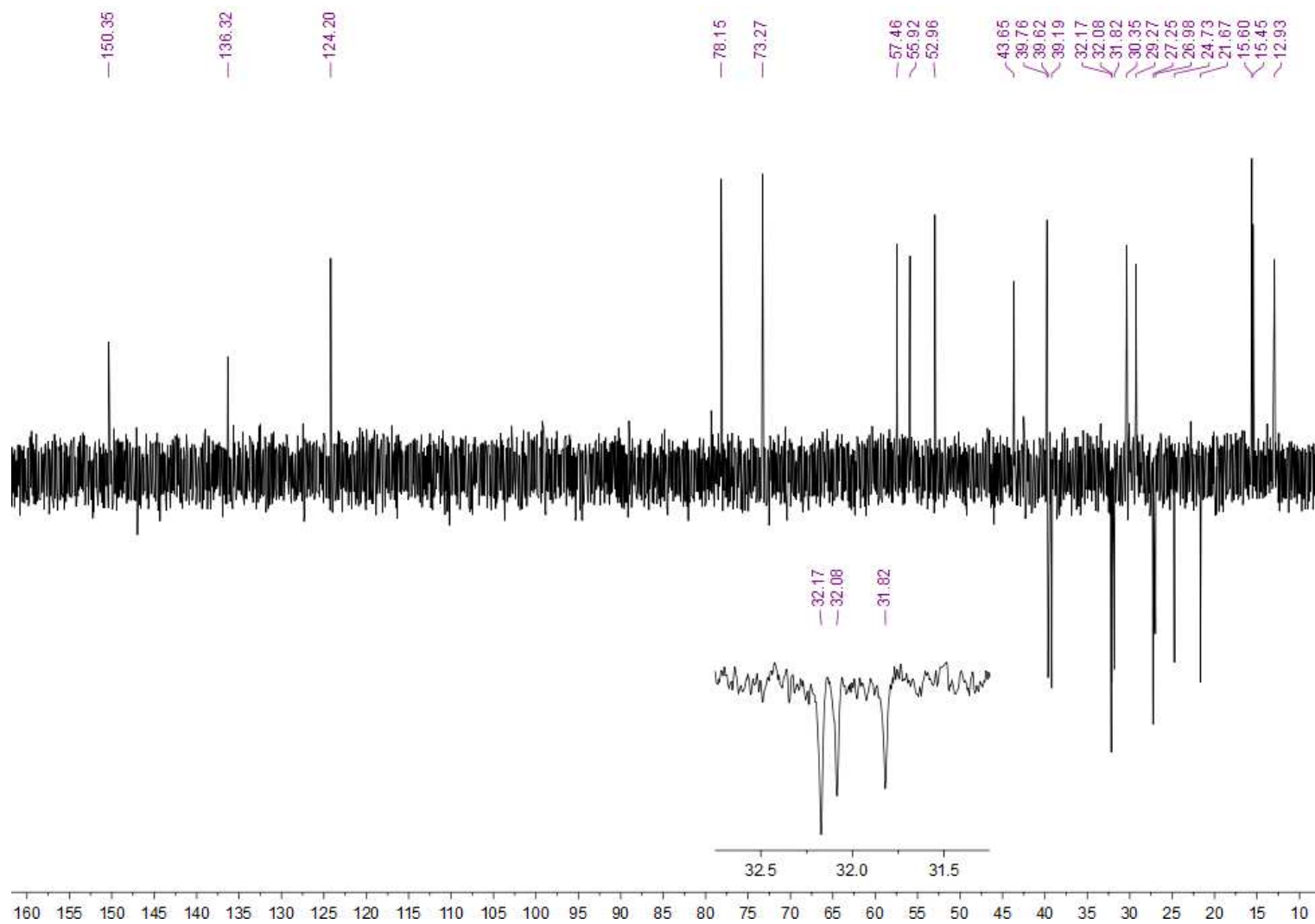
Figure S15. DEPT 135° NMR (125.75 MHz) spectrum of 2, in C₅D₅N.
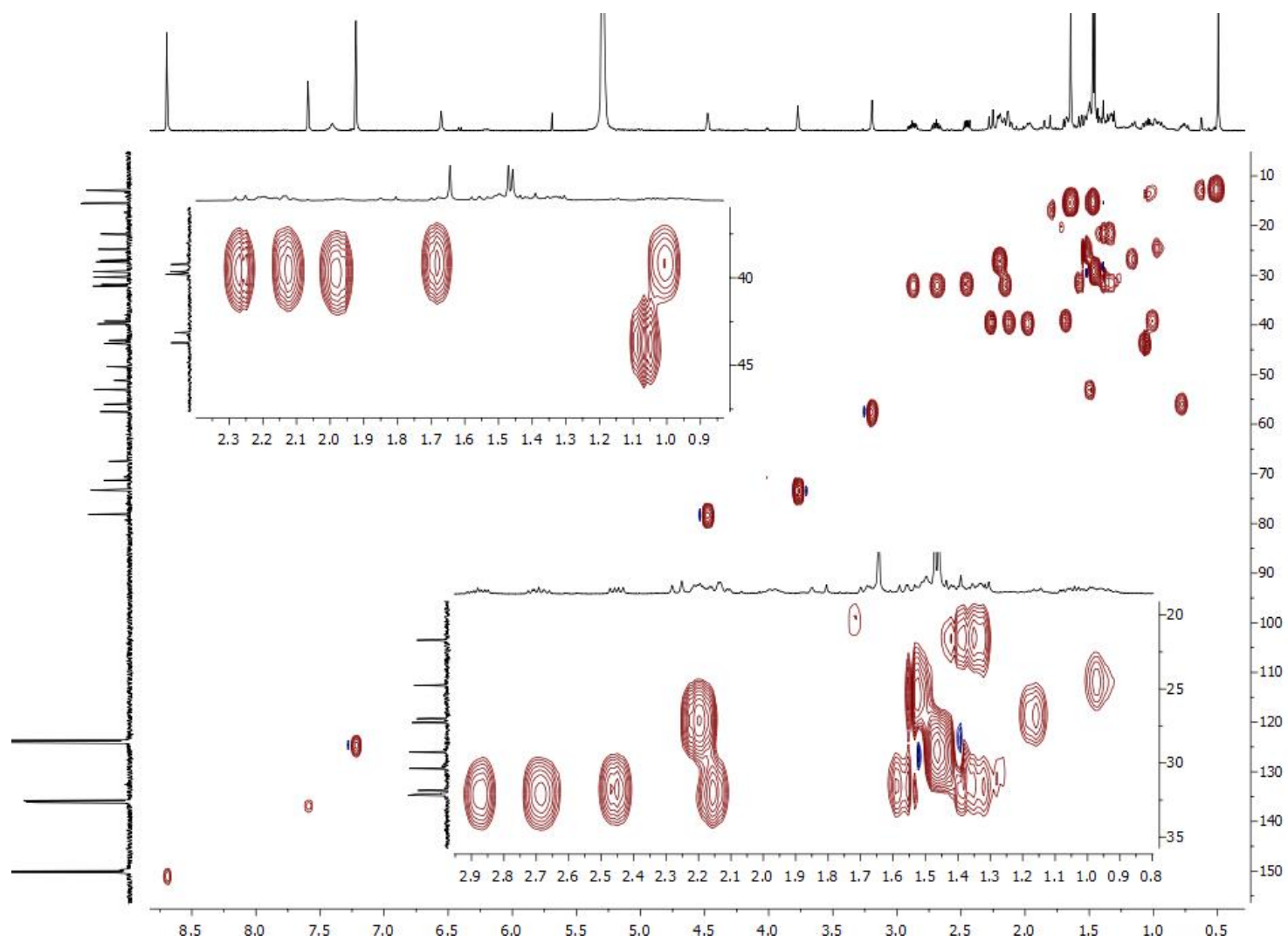
Figure S16. HSQC NMR spectrum of 2, in C₅D₅N.
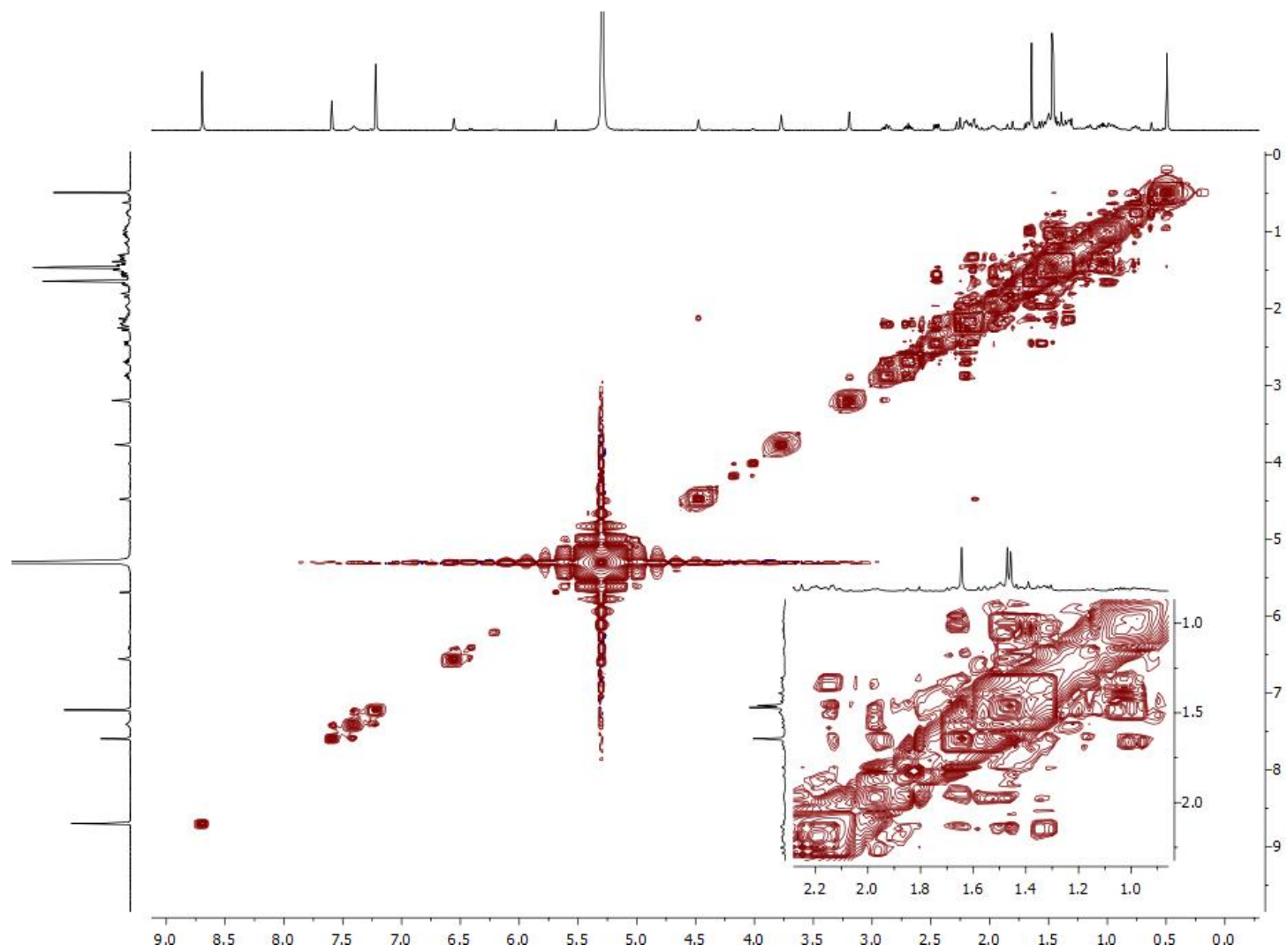
Figure S17. COSY NMR spectrum of 2, in C$_5$D$_5$N.
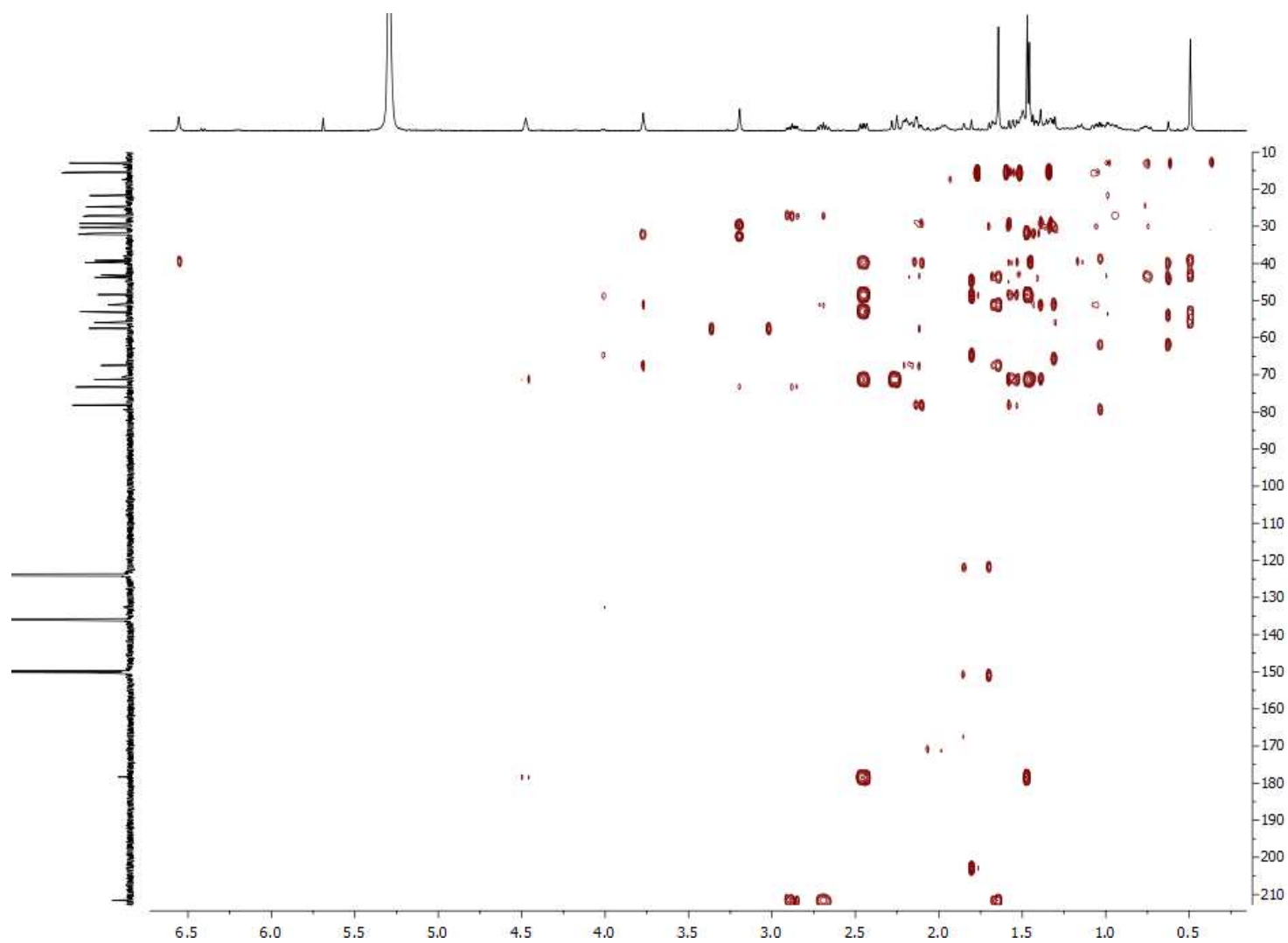
Figure S18. HMBC NMR spectrum of 2, in C₅D₅N.
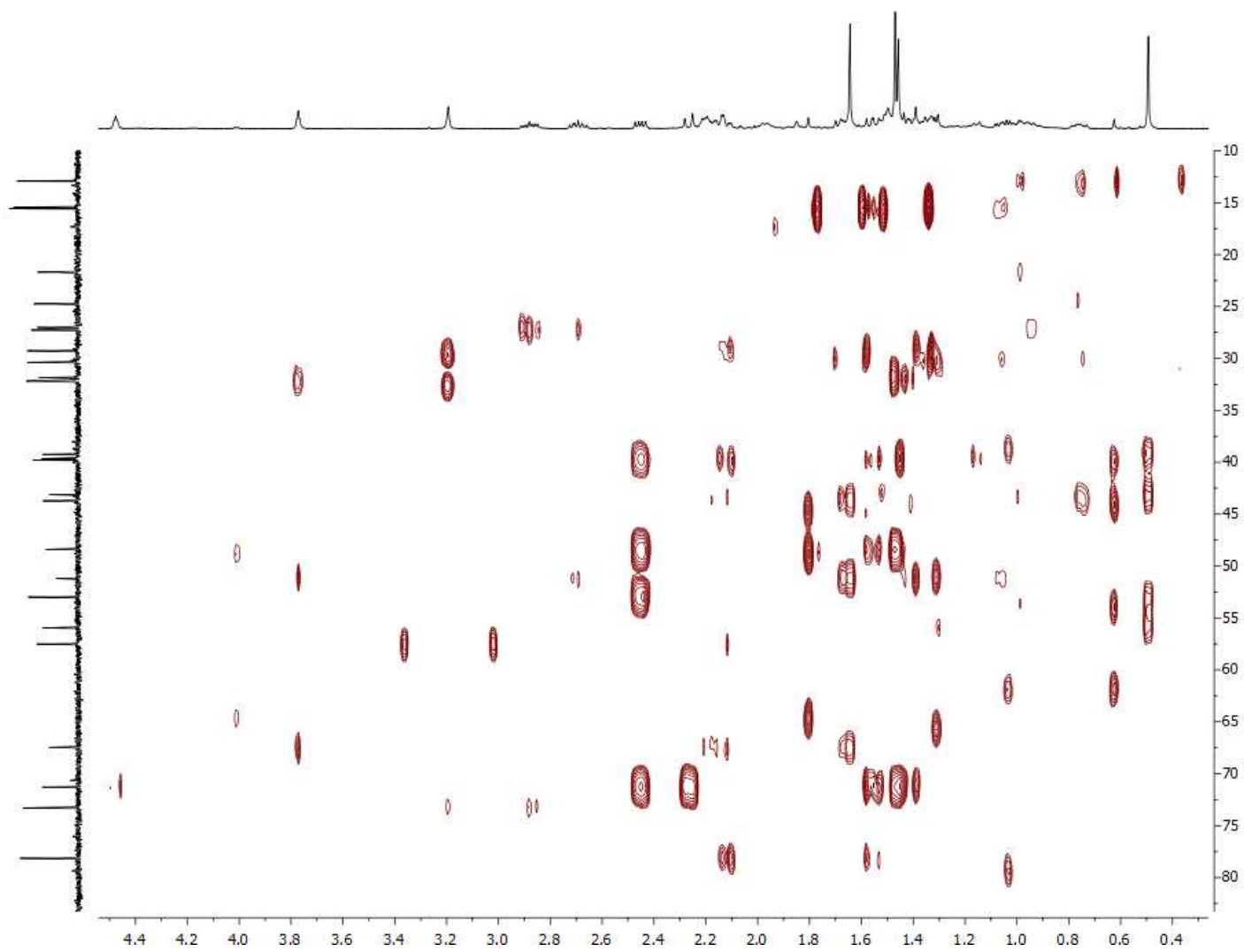
Figure S19. HMBC NMR spectrum of 2, in C₅D₅N.
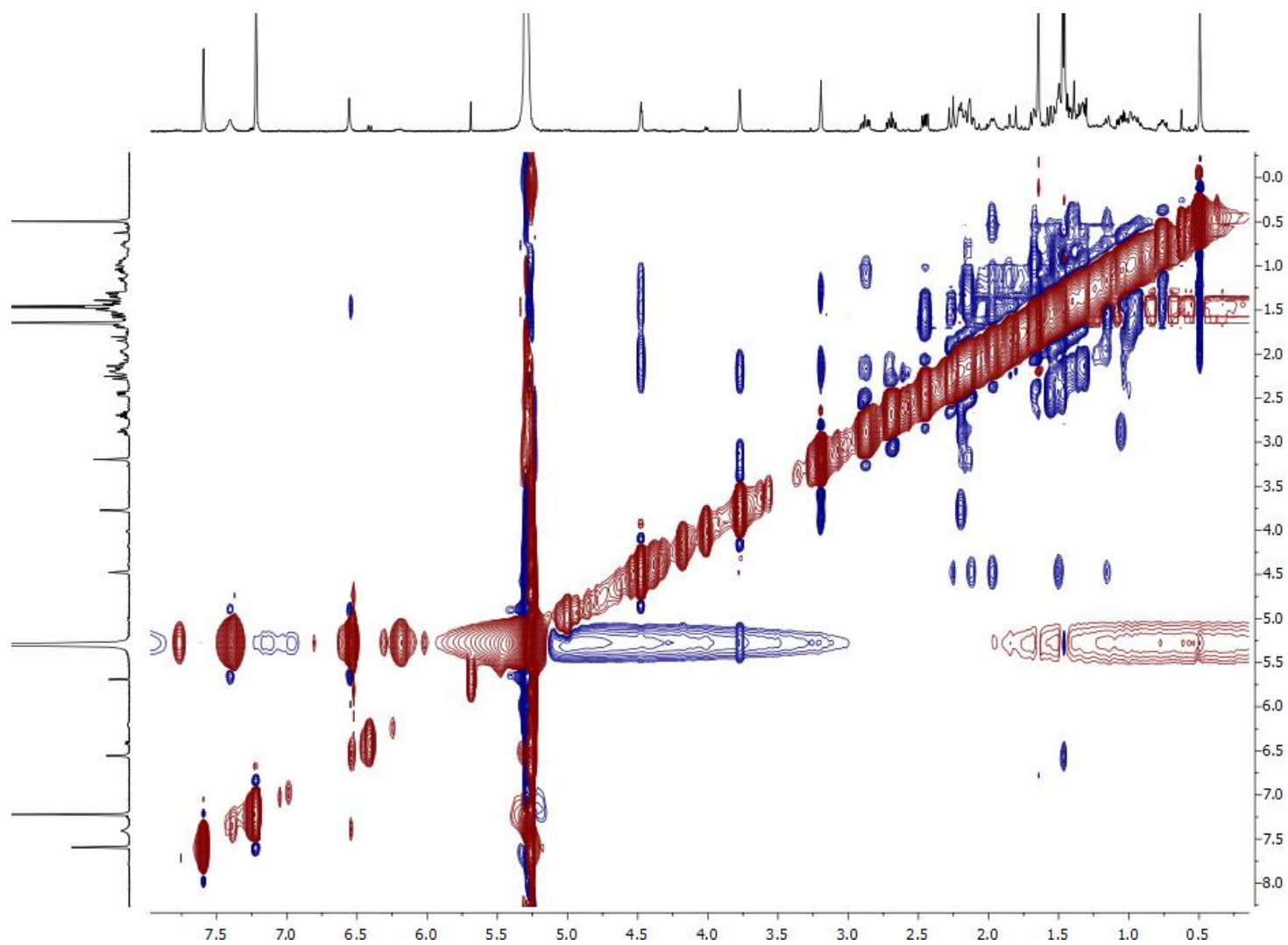
Figure S20. NOESY NMR spectrum of 2, in C$_5$D$_5$N.
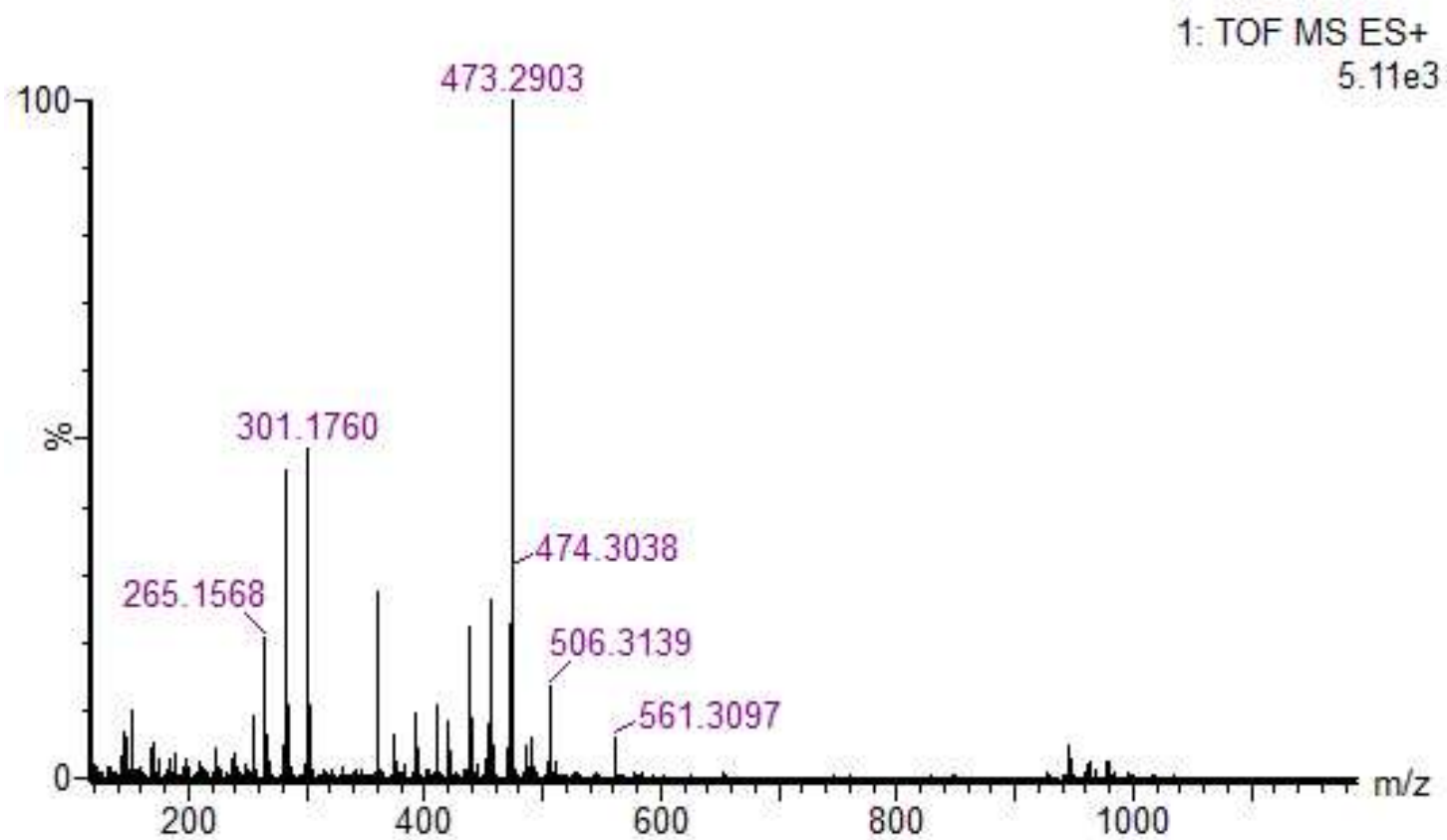
Figure S21. HRESIMS spectrum of 2.
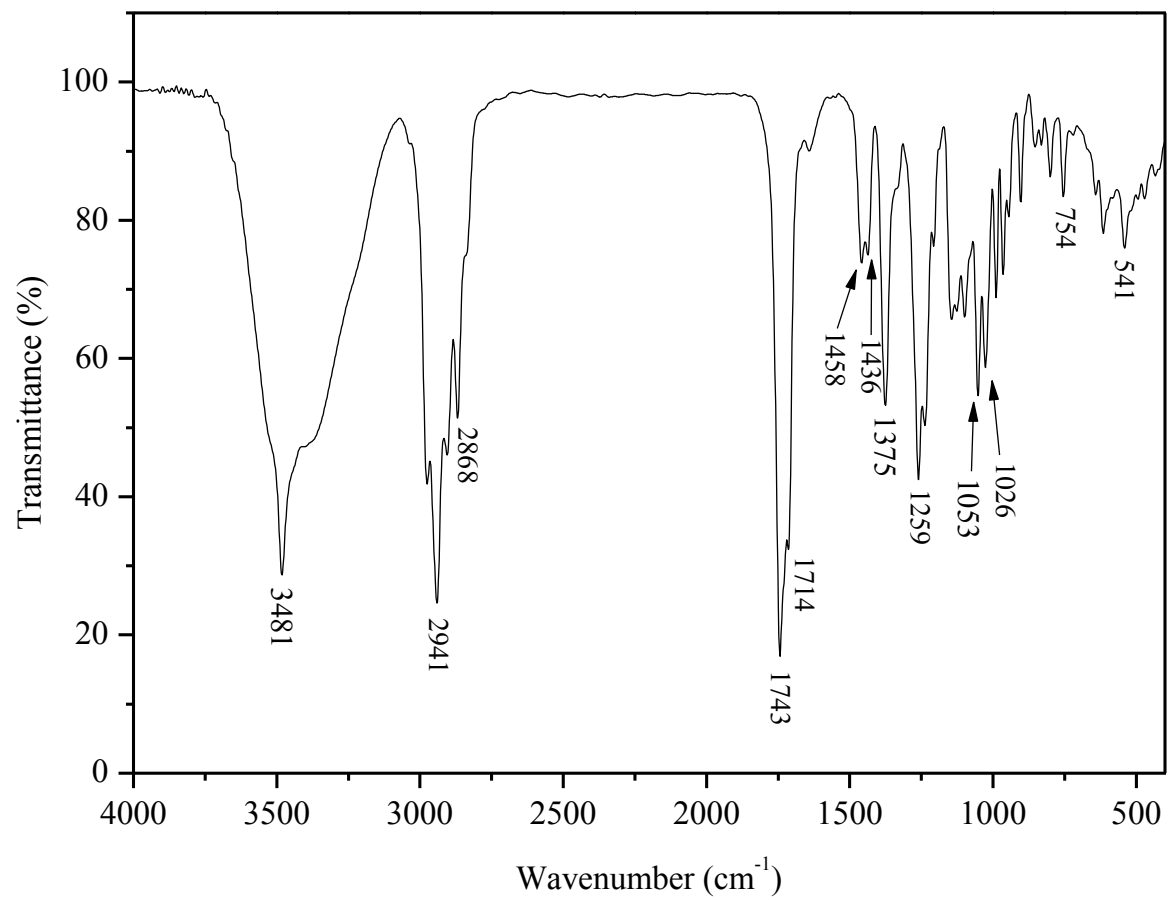
Figure S22. FTIR spectrum of 3.
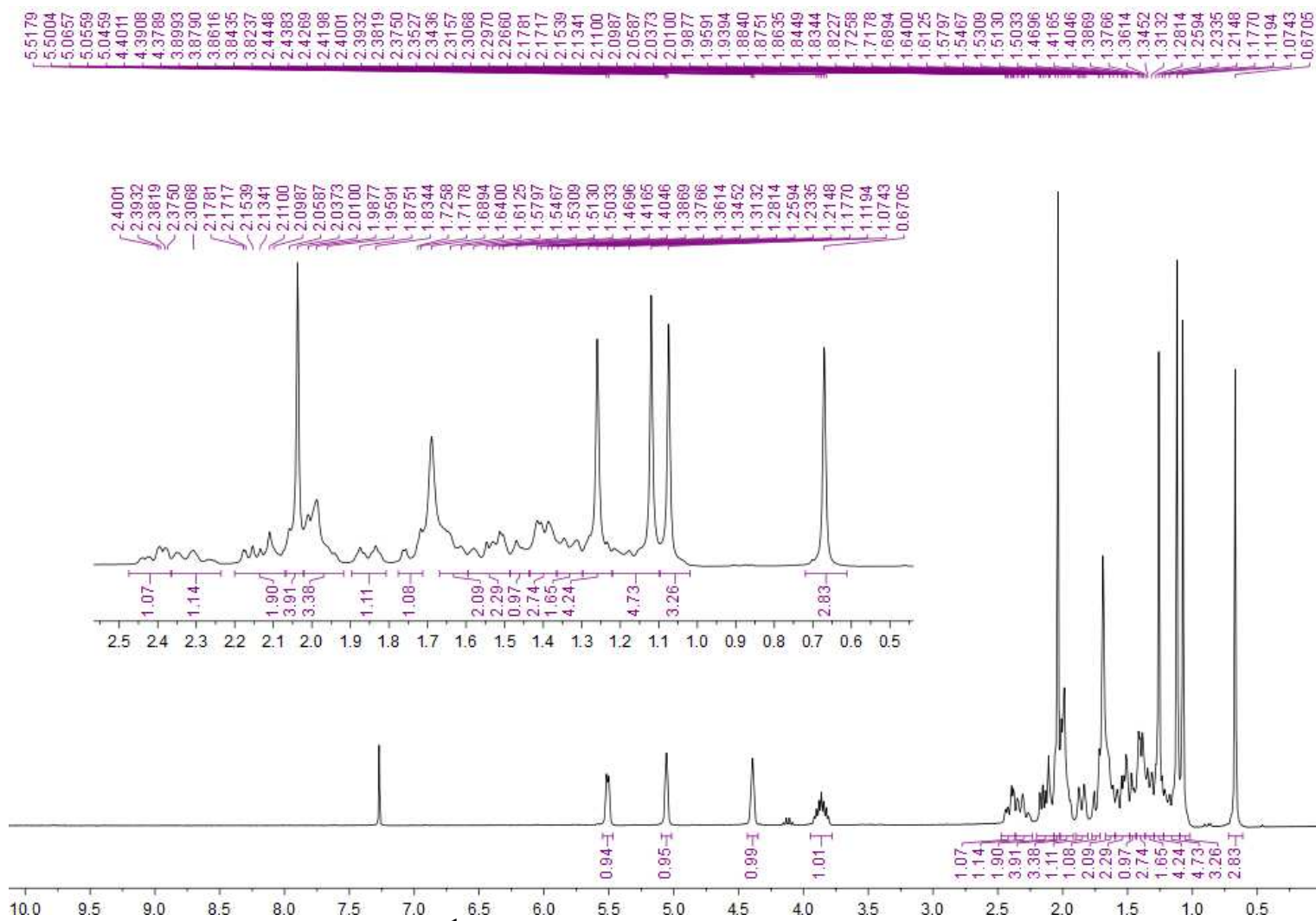
Figure S23. ¹H NMR (300.13 MHz) spectrum of 3, in CDCl₃.
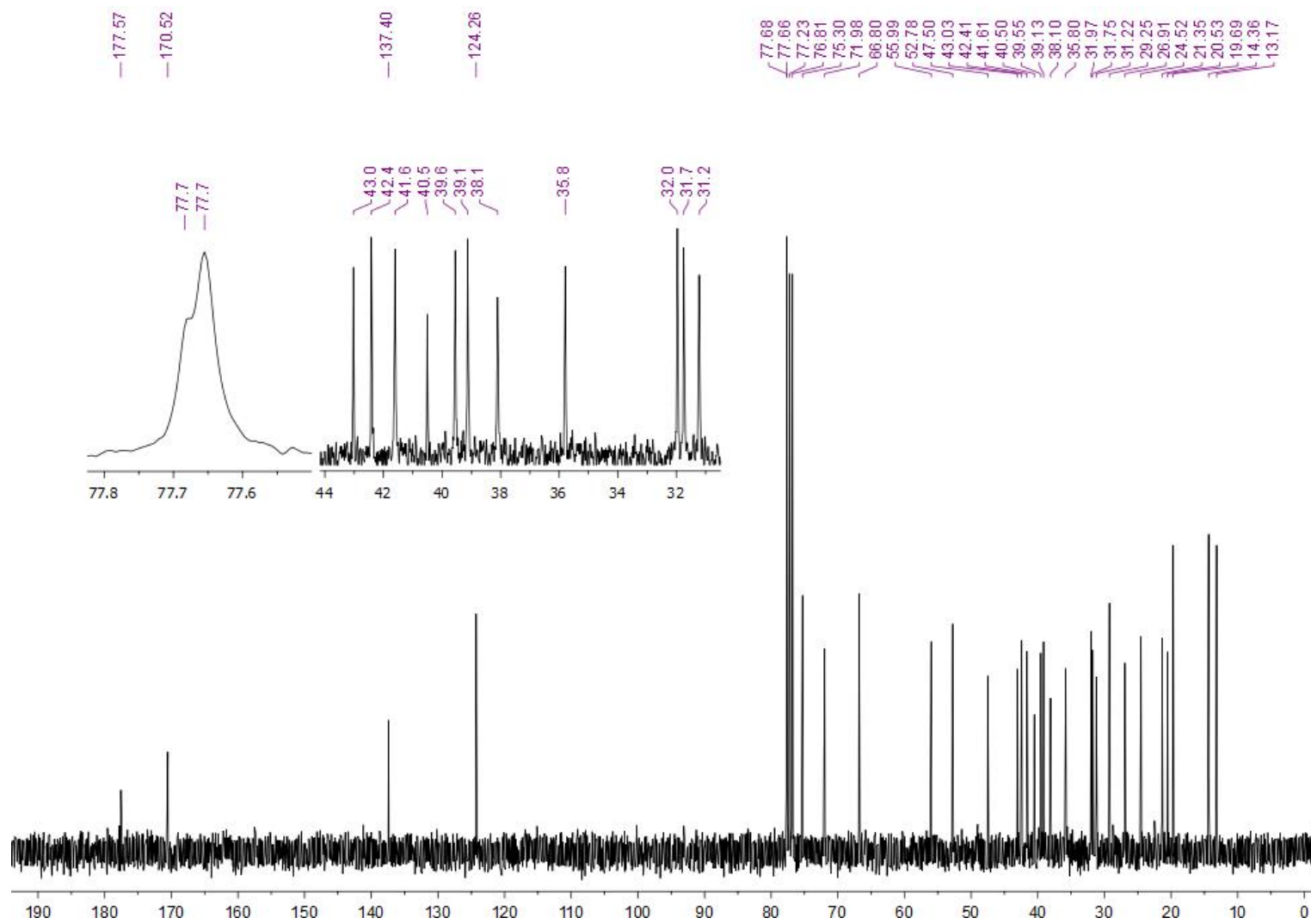
Figure S24. ^{13}C NMR (75.47 MHz) spectrum of **3**, in CDCl$_3$.
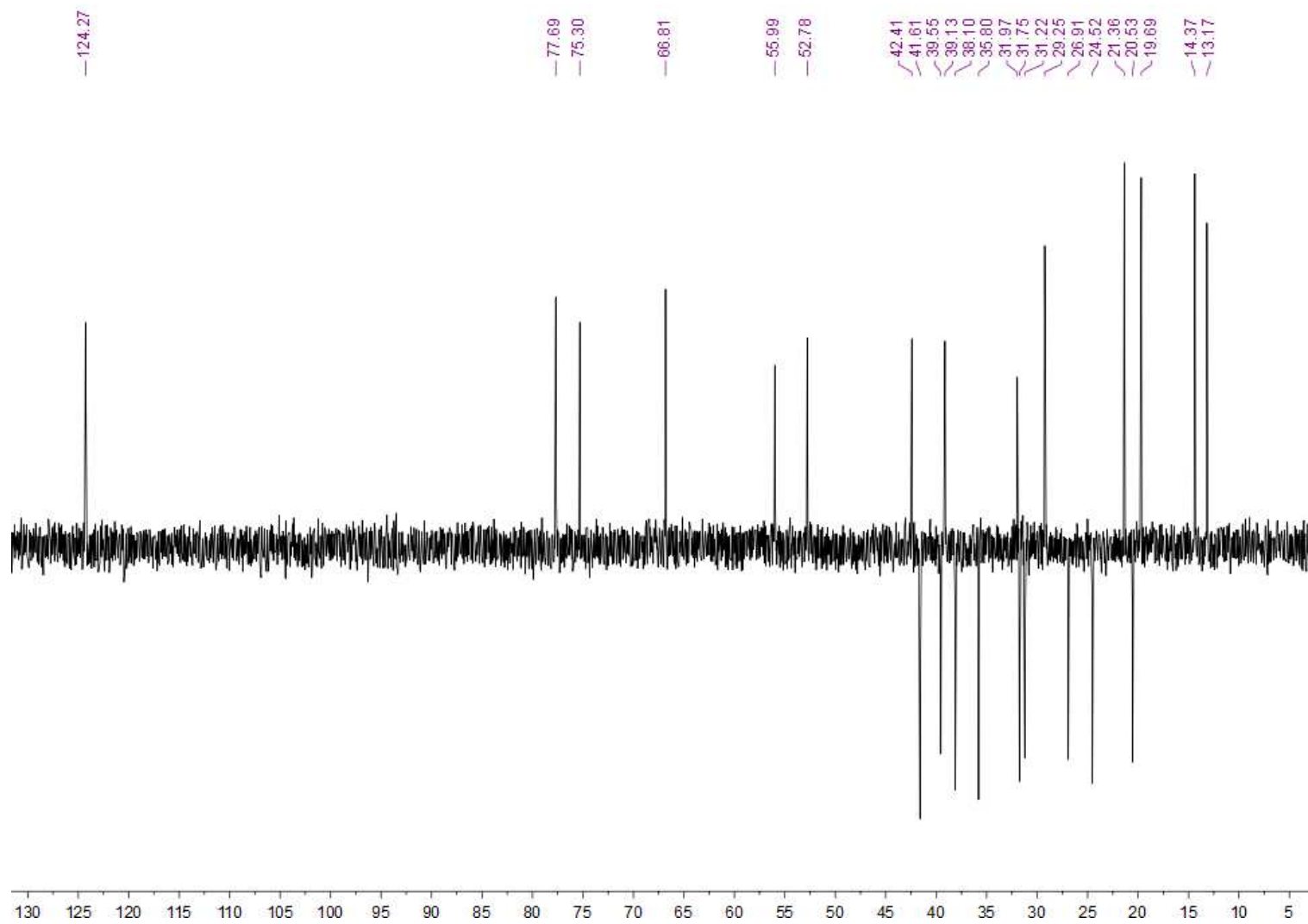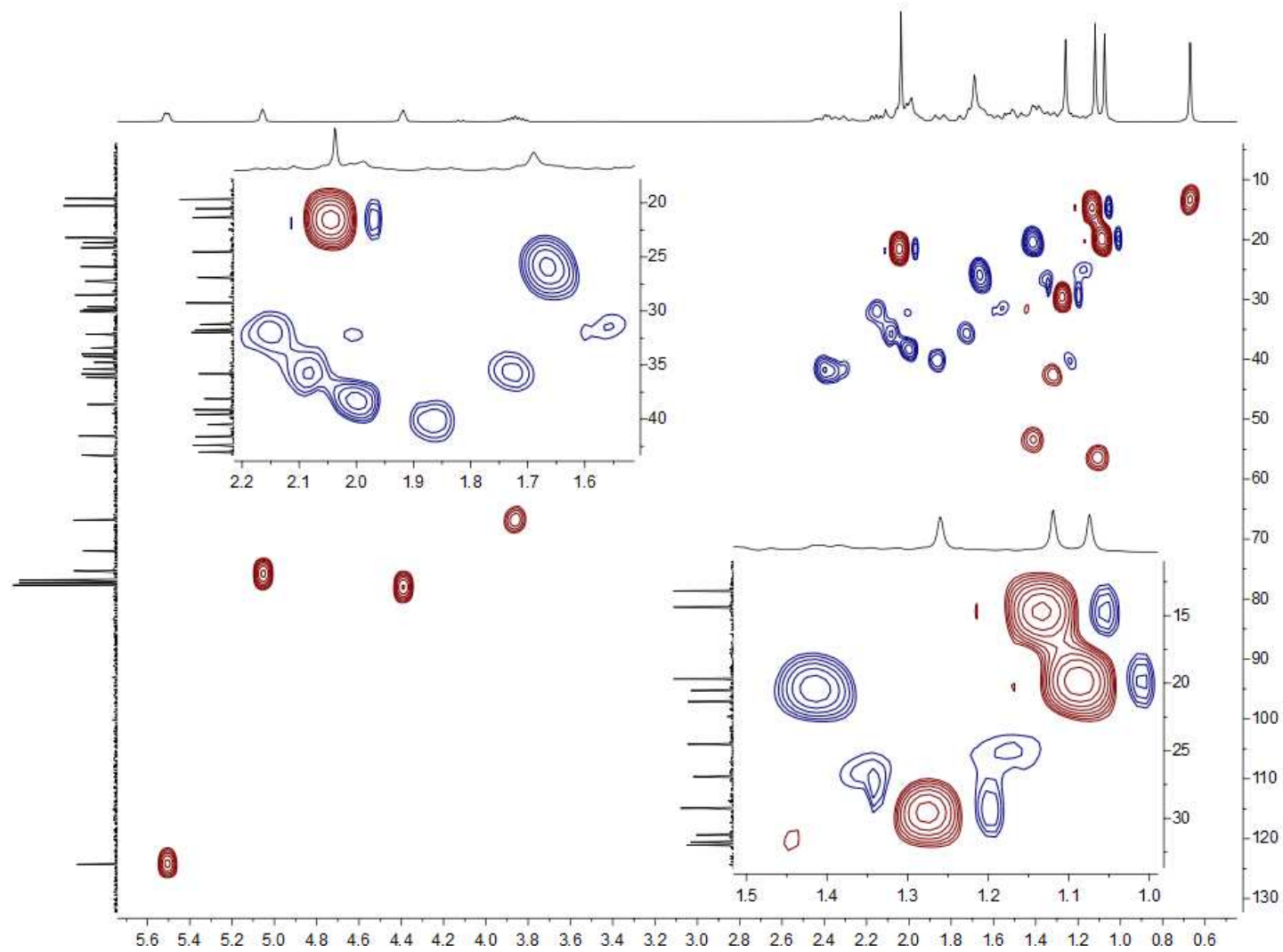
Figure S26. HSQC NMR spectrum of 3, in CDCl₃.
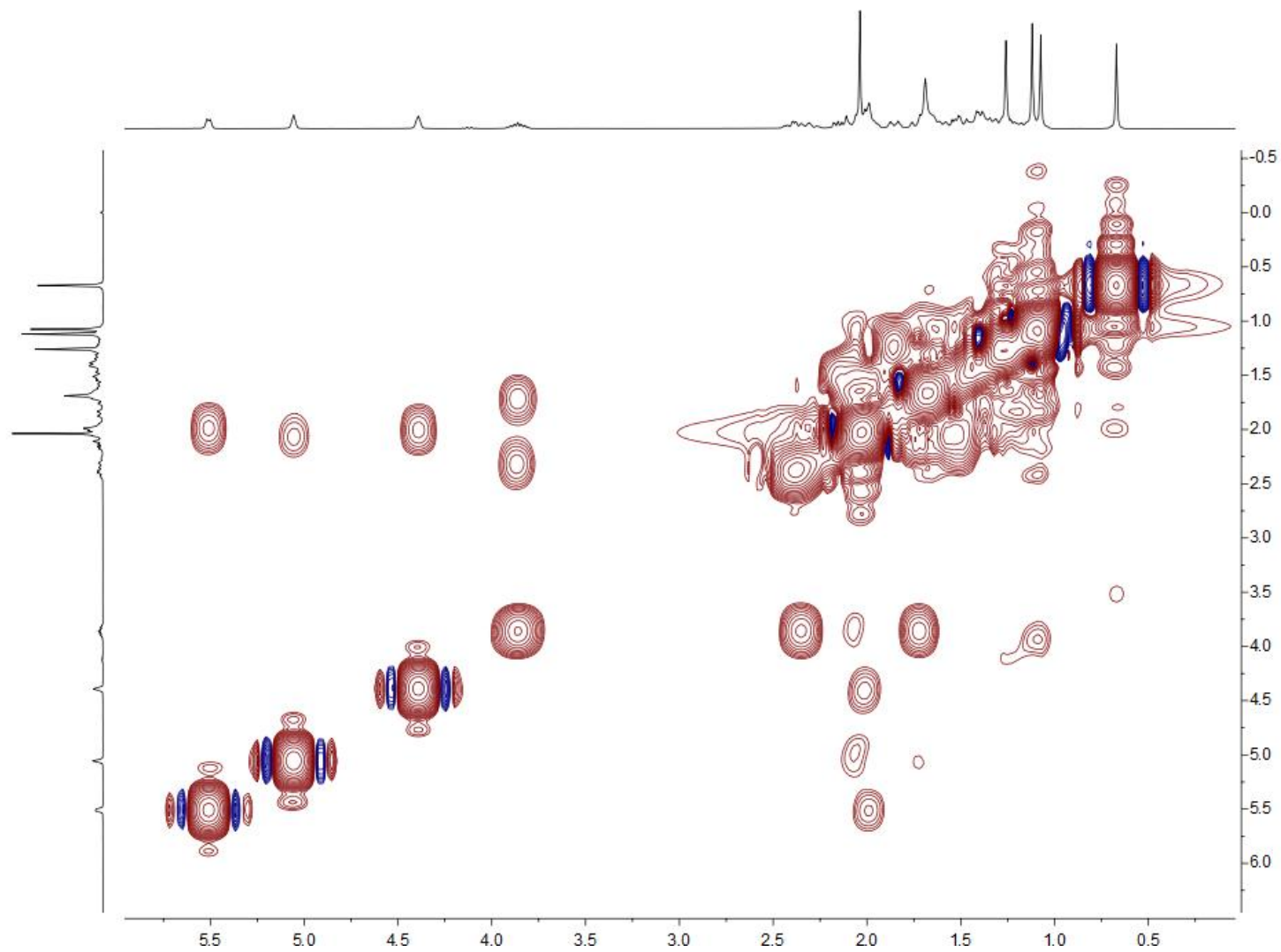
Figure S27. COSY NMR spectrum of 3, in CDCl₃.
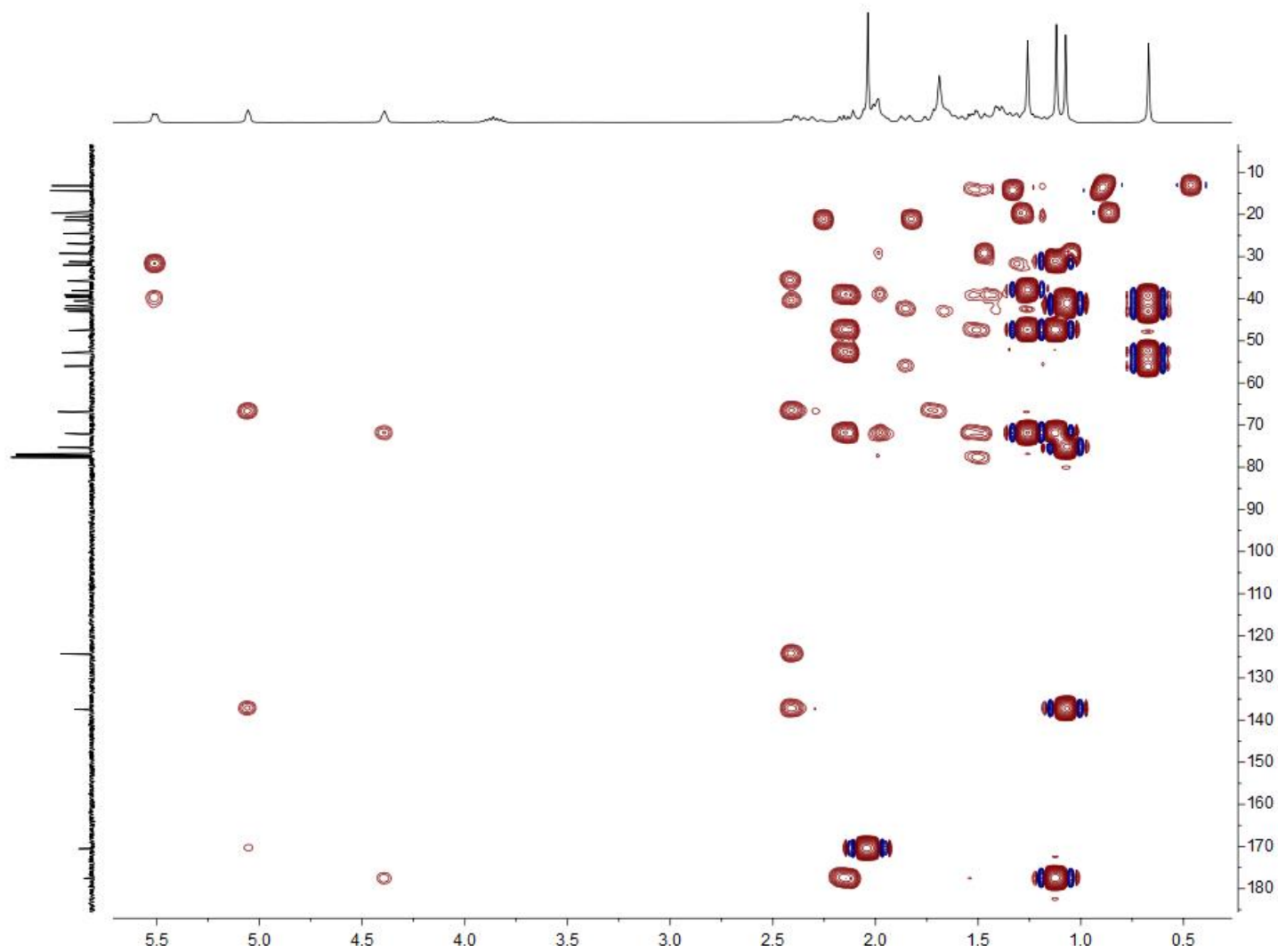
Figure S28. HMBC NMR spectrum of 3, in CDCl₃.
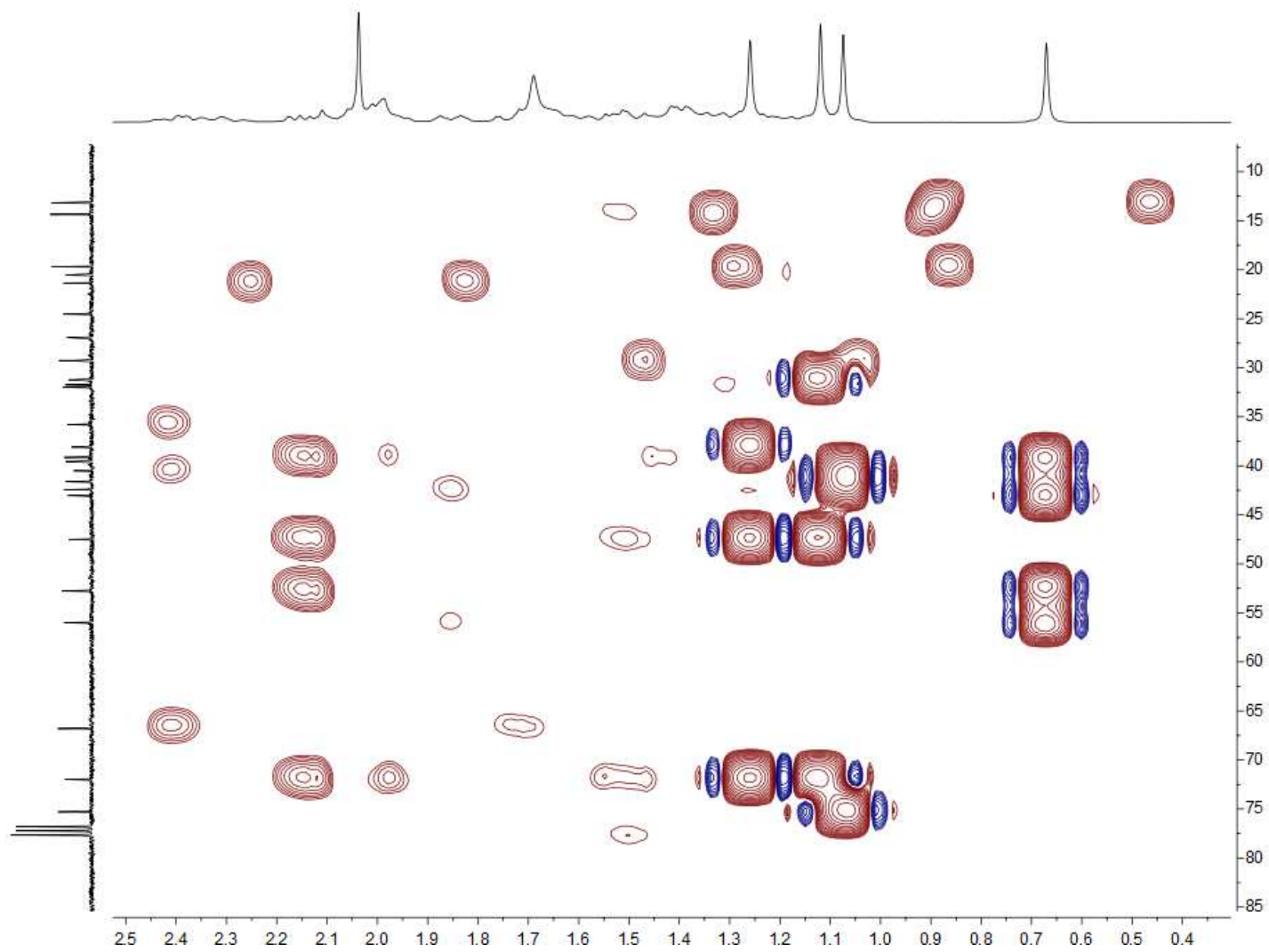
Figure S29. HMBC NMR spectrum of 3, in CDCl₃.
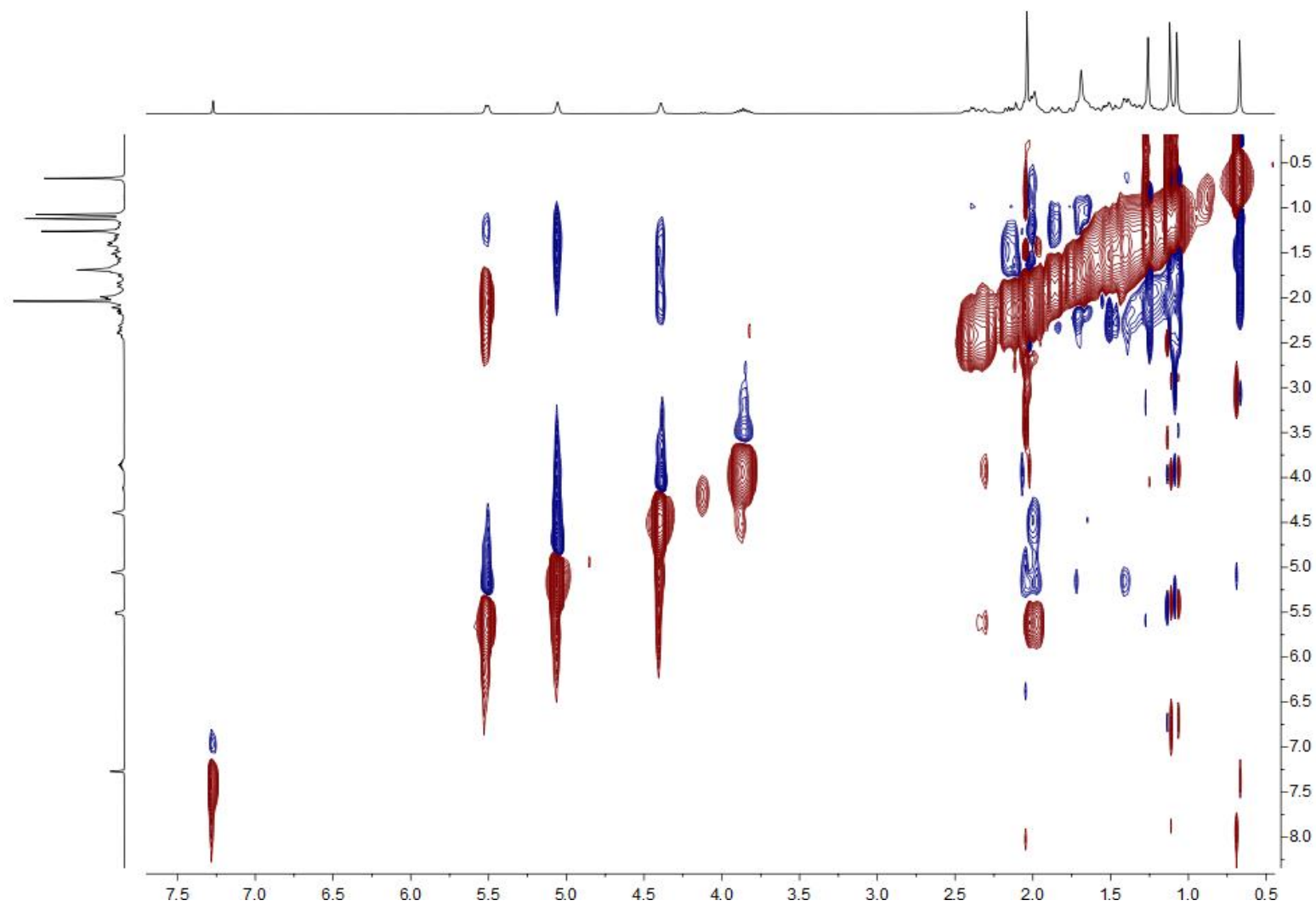
Figure S30. NOESY NMR spectrum of 3, in CDCl₃.
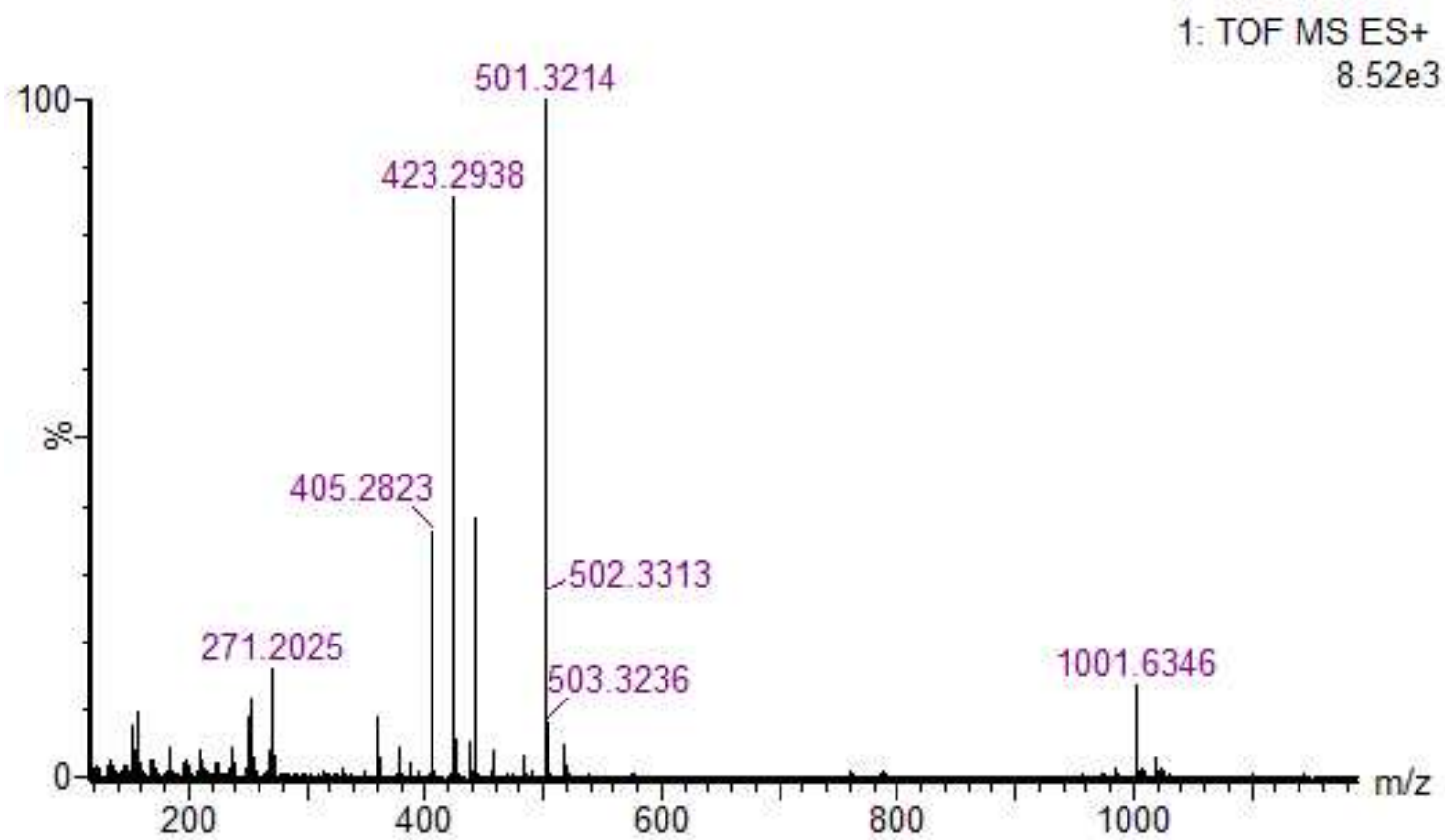
Figure S31. HRESIMS spectrum of 3.

CAPÍTULO 2

Withanolides of *Athenaea velutina* with

potential inhibitory properties against

SARS coronavírus main protease (M^{pro}):

Molecular modeling studies
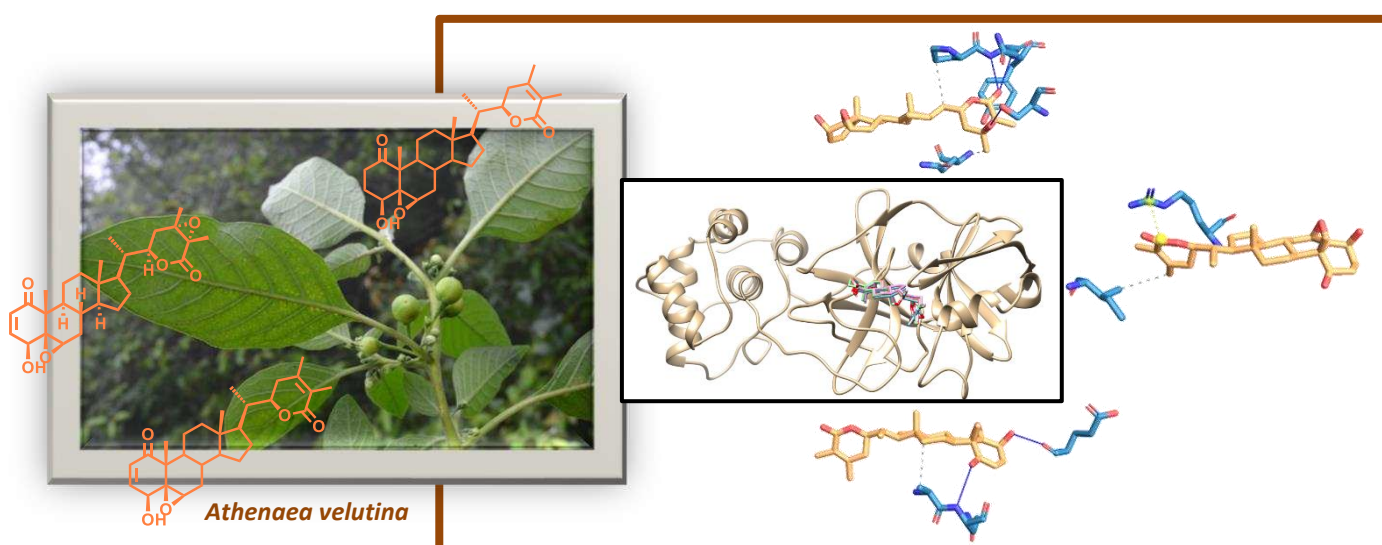
Athenaea velutina

Withanolides of *Athenaea velutina* with potential inhibitory properties against SARS coronavírus main protease (Mpro): Molecular modeling studies

Pabllo Abreu Alves,[a,b] Késya Amanda Dantas Rocha,[b] Lucas Lima Bezerra,[a] Alejandro Pedro Ayala,[c] Norberto de Kássio Vieira Monteiro,[a] Otília Deusdênia Loiola Pessoa[b]*

[a]*Departamento de Química Analítica e Físico Química, Centro de Ciências,Universidade Federal do Ceará, 60021-970, Fortaleza-CE, Brazil*

[b]*Departamento de Química Orgânica e Inorgânica, Centro de Ciências,Universidade Federal do Ceará, 60021-970, Fortaleza-CE, Brazil*

[c]*Departamento de Física, Centro de Ciências,Universidade Federal do Ceará, 60440-900, Fortaleza-CE, Brazil.*

* Corresponding author: opessoa@ufc.br

ABSTRACT

Since the global COVID-19 pandemic began, the scientific community has dedicated efforts to finding effective antiviral drugs to treat or minimize the effects caused by the SARS-CoV-2 coronavírus. Some targets can act as inhibitor substrates, highlighting the Main Protease (M^{pro}), which plays an essential role in the translation and transcription of the virus cycle. Withanolides, a class of natural C_{28} steroidal lactones, are compounds of interest as possible inhibitors of M^{pro} and other critical targets of the virus, such as papain-like protease. In this study, the isolation of a new withanolide (**1**), along with the known 27-deoxywithaferin A (**2**) and 2,3-dihydro-27-deoxywithaferin A (**3**), from the leaves of *Athenaea velutina* (Solanaceae) is described. Their structures were determined using spectroscopic and spectrometric methods (NMR, IR, HRESIMS). Moreover, the interaction and the stability of withanolides **1 – 3** and withanolide D (**4**), previously isolated of *Acnistus arborescens*, against the M^{pro} target through molecular docking, molecular dynamics, and binding free energy simulations were analyzed. The molecular dynamics results indicated that the complexes formed by the molecular docking simulations between the M^{pro} target with each of the withanolides **1 – 4** exhibited good stability during the simulations due to a slight change in the structure of complexes. The binding free energy results suggested that withanolide (**1**) can be a natural candidate against COVID-19 disease.

Keywords: *Athenaea velutina*, Molecular dynamics, Molecular docking, COVID-19, Withanolides, M^{pro}

1. Introduction

Since 2019, the world has been plagued by the highly contagious and deadly viral disease caused by severe acute respiratory syndrome coronavírus 2 (SARS-CoV-2), whose mortality rate has reached more than 4.5 million people (Troeger, 2022). Unfortunately, despite the efforts of scientists and researchers worldwide, even with vaccines, there is no effective drug available for the treatment of COVID-19 so far. Therefore, key strategies must be taken to find effective treatment routes or drugs against COVID-19, and for that, it is vital to look for targets, whether of the human cell or the viral structure.

So far, the most promising targets identified have been the spike protein, RNA-dependent RNA polymerase (RdRp), and the papain-like protease 3CL^{pro}, also known as the main protease (M^{pro}) (Houchi, 2022). The latter, together with the papain protease (PL^{pro}), produces viral components for transmission and infection of new cells (Arafet et al., 2020). Furthermore, the M^{pro} protease cleaves polyproteins at 11 sites resulting in the main NSP4-9 and NSP12-15 fragments, highlighting that NSPs from RNA complex are involved in many processes for the new virus in the host (Amporndanai et al., 2021).

Therefore, the search for new bioactive compounds against the M^{pro} target is urgent and primordial. Natural products have been unquestionable throughout research focused on drug development (Newman & Cragg, 2020a; Newman & Cragg, 2020b). Among the classes of natural products of importance medical, withanolides have attracted interest due to their versatile health benefits. Withanolides are a large group of C28 steroidal lactones based on the ergostane skeleton where the carbons 22, 23, and 26 can be oxidized to form a C22/C26 δ-lactone (Cao et al.,2015) or less commonly, to form a C23/C26 γ-lactone moiety (Xu et al., 2016; Llanos et al., 2017). These compounds have exhibited anti-inflammatory (Abdeljebbar et al., 2009), anxiolytic (Bhattacharya et al., 2000), cytotoxic (Budhiraja, Krishan, & Sudhir, 2000), immunomodulatory (Shohat & Joshua, 1971), anti-neurodegenerative (Baitharu et al.,

2014), antimicrobial (White, Subramanian, Motiwala, & Cohen, 2016), and anti-cancer properties (Yang et al., 2021; Ballesteros-Vivas et al., 2019). Furthermore, several studies have shown that withanolides could be indicated as good antiviral candidates against SARS-CoV-2 since several exhibited *in silico* activity against the new coronavírus main protease (Khanal et al., 2020; Patel et al., 2021).

The present study reports the analysis of the potential interaction of four withanolides (**1** – **4**, Figure 1) against the M^{pro} from SARS-CoV-2 through molecular docking, molecular dynamics, and binding free energy simulations. Withanolides **1** – **3** were isolated from the leaves of *Athenaea velutina*, while withanolide D (**4**), previously isolated from *Acnistus arborescens* (Batista et al., 2016), was used as a standard due to its relevance as an inhibitor of SARS-CoV-2.
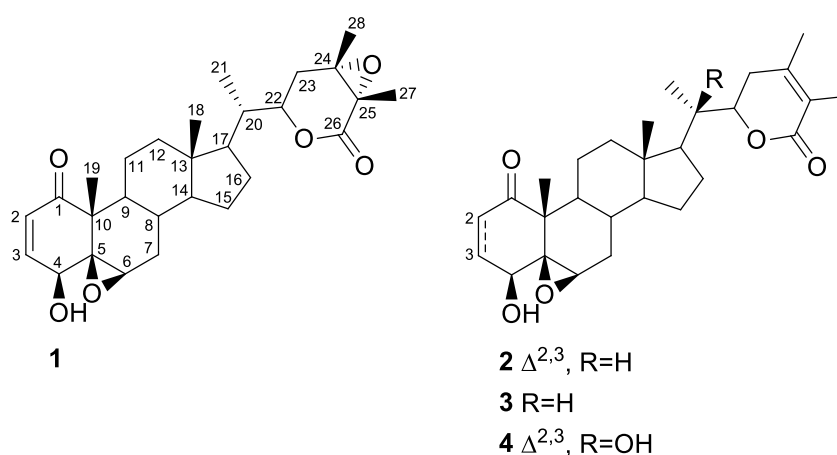
Fig. 1 Structures of the withanolides **1** – **4**

2. Experimental

2.1. General experimental procedures

Melting points were performed on a digital MQAPF-302 apparatus. IR spectra were recorded using a Shimadzu IR-tracer-100 spectrometer. NMR spectra were acquired on a Bruker AVANCE DPX-300 spectrometer operating at 300.13 MHz for ^{1}H and 75.48 MHz for ^{13}C.

High-resolution electrospray ionization mass spectra (HRESIMS) were acquired on an Acquity Xevo UPLC-QTOF-MS spectrometer from Waters. Chromatographic separations were performed on sílica gel 60 (0.063-0.200 mm and sílica gel 40 μm flash chromatography packing (Merck), while analytical TLC was performed on pre-coated 200 μm thick plates on sílica gel 60 with fluorescent indicator F-254 (Silicycle).

2.2. Plant material

The leaves of *Athenaea velutina* were collected in January 2019 (S 04º 12.590', W 38º 58.244') at Guaramiranga county, Ceará State-Brazil, under the license number A5C2E09. Drª Valéria Sampaio identified plant material, and a voucher specimen (EAC45010) is deposited at the Herbário Prisco Bezerra (EAC), Universidade Federal do Ceará (UFC).

2.3. Extraction and isolation

At room temperature, the dried and pulverized leaves of *A. velutina* (2.0 Kg) were extracted with hexane/EtOAc 1:1 (10 L, 3 x 24 h each). The solvent was removed by evaporation under reduced pressure yielding 95.0 g of crude extract. This extract (90.0 g) was fractionated on sílica gel (60.0 g) eluted with hexane, hexane/EtOAc 2:1 and 1:1, EtOAc, EtOAc/MeOH 1:1, and MeOH to afford nine fractions (A to I), after Thin Layer Chromatography (TLC) analysis. Fraction E (8.30 g) eluted by hexane/EtOAc 2:1 was subjected to further sílica gel column chromatography (100.0 g) eluting with the gradient solvent system of hexane/EtOAc 9:1, 7:3, 5:5, 4:6, 3:7, 8:2, EtOAc, and finally, EtOAc/MeOH 1:1 to yield nine subfractions (EA to EI). Subfraction EE (2.24 g), a greenish solid, was repeatedly recrystallized at EtOAc, to yield the pure compound **1** (383 mg). Fraction F (8.35 g), a dark precipitate, was initially washed with EtOAc, and the resulting material (Fp 4,12 g) was subjected to a sílica gel column chromatography eluted with CH₂Cl₂/acetone 5% to yield seven subfractions (FpA to FpG). Subfraction FpB (2.24 g) was subjected to a sílica gel flash column chromatography (120.0 g),

eluted with CH_2Cl_2/acetone 5% to afford compounds **1** (1.49 g) and **2** (436 mg). Subfraction FpD (481 mg) was also subjected to a sílica gel flash column chromatography (50.0 g, eluted with CH_2Cl_2/acetone 3% to yield compounds **2** (144 mg) and **3** (148 mg).

27-Deoxy-24,25-epoxywithaferin A (**1**): Colourless crystals (acetone); mp 212-214 °C; IR (KBr) v_{max} 3498, 1720, 1676, 1458, 1398, 1309, 1155, 1031 cm^{-1}; ^{1}H NMR (CDCl$_3$): 6.93 (1H, dd, *J*=9.9, 5.8 Hz, H-3), 6.20 (1H, d, *J*=9.9 Hz, H-2), 4.52 (1H, td, *J*=7.6, 3.5 Hz, H-22), 3.75 (1H, d, *J*=5.8, Hz, H-4), 3.22 (1H, s, H-6), 2,14 (2H, dt, *J*=14.8, 2.7 Hz, H-7), 1.94 (2H, m, H-12), 1.94 (2H, t, *J*=7.6 Hz, H-23), 1.89 (1H, m, H-20), 1.81 (2H, m, H-11), 1.71 (2H, m, H-16), 1.62 (2H, m, H-15), 1.55 (3H, s, H-27), 1.49 (1H, d, *J*=3.8 Hz, H-8), 1.47 (3H, s, H-28), 1.44 (2H, m, H-11), 1.39 (3H, s, H-19), 1.35 (2H, m, H-16), 1.29 (2H, m, H-7), 1.14 (2H, m, H-15), 1.09 (2H, m, H-12), 1.03 (1H, m, H-17), 0.99 (1H, m, H-9), 0.94 (1H, m, H-14), 0.89 (3H, d, *J*=6.6 Hz, H-21), 0.67 (3H, s, H-18); ^{13}C NMR (CDCl$_3$): 202.4, C (C-1), 170.2, C (C-26), 142.1, CH (C-3), 132.5, CH (C-2), 76.4, CH (C-22), 70.1, CH (C-4), 64.0, C (C-5), 62.8, C (C-24), 62.6, CH (C-6), 59.5, C (C-25), 56.3, CH (C-14), 52.2, CH (C-17), 47.9, C (C-10), 44.3, CH (C-9), 42.8, C (C-13), 39.5, CH$_2$ (C-12), 38.8, CH (C-20), 31.4, CH$_2$ (C-7), 30.0, CH (C-8), 29.0, CH$_2$ (C-23), 27.4, CH$_2$ (C-16), 24.4, CH$_2$ (C-15), 22.3, CH$_2$ (C-11), 18.1, CH$_3$ (C-28), 17.5, CH$_3$ (C-19), 13.8, CH$_3$ (C-27), 13.2, CH$_3$ (C-21), 11.8, CH$_3$ (C-18); HRESIMS *m/z* 493.2556 [M + Na]$^+$ (calcd for $C_{28}H_{38}NaO_6$, 493.2566).

27-Deoxywithaferin A (**2**): White crystals (acetone); mp 194-196 °C. IR (KBr) v_{max} 3394, 1683, 1458, 1396, 1134, 1039 cm^{-1}; ^{1}H and ^{13}C NMR spectra on SI.

27-Deoxy-2,3-dihydrowithaferin A (**3**): White crystals (acetone); mp 187-189 °C. IR (KBr) v_{max} 34048, 1707, 1687, 1450, 1396, 1315, 1134 cm^{-1}; ^{1}H and ^{13}C NMR spectra on SI.

2.4. X-ray crystallographic analyses of compounds 1 - 3

The data collection of single-crystal X-ray (φ scans and ω scans with κ and θ offsets) was recorded on a Bruker D8 Venture κ-geometry diffractometer equipped with a Photon II CPAD detector and a Cu Kα (λ = 1.54178 Å) IμS 3.0 Incoatec microfocus source. The APEX III software was used for the unit cell determination and data collection (Bruker AXS Inc, 2018a). The data reduction and global cell refinement were made using the Bruker SAINT (Bruker AXS Inc, 2018b). Data were corrected for absorption effects with SADABS (Sheldrick, 1996). The structures were solved by intrinsic phasing using SHELXT (Sheldrick, 2015b) and refined with the ShelXL (Sheldrick, 2015a) refinement package using Least Squares minimization using Olex as a graphical interface. Non-hydrogen atoms were refined anisotropically. Hydrogen atoms were placed according to geometrical criteria and treated using the riding model. Crystallographic data for the structures have been deposited with the Cambridge Crystallographic Data Centre. These data can be obtained free from The Cambridge Crystallographic Data Centre via www.ccdc.cam.ac.uk/structures.

X-ray Crystallography Analysis of 27-deoxy-24,25-epoxywithaferin A (**1**): Clear light colourless irregular crystals of compound **1** were obtained from acetone recrystallization. $C_{28}H_{38}O_6$, Mr = 470.58 g.mol^{-1}; size 0.214×0.283×0.764 mm. The crystalline system was orthorhombic, space group P2_1 2_1 2_1 and the final cell constants were a=9.5300(12) Å, b=10.0814(12) Å, c=26.783(3) Å, α=90°, β=90°, γ =90°; V = 2573.2(5) Å, Z = 4, ρcalc=1.215 g cm^{-3}, F (000) = 1016. Data were corrected for absorption effects using the numerical method. A total of 29015 reflections were collected in the range 9.85 to 140.37 (0.82 Å) (completeness = 97.6 %), with 4795 independent reflections (Rint = 0.0318, Rsigma = 0.0237) which were used in all calculations. Final indices: R1obs = 0.0350, ωR2obs = 0.0935 [I ≥ 2σ(I)]; R1all = 0.0359, ωR2all = 0.0974 [all data], goodness of fit on F2 was 1.042. The stereochemistry of the molecule was evidenced by the following parameters: Flack x = 0.07(4), Parsons z = 0.07(4),

Hooft y = 0.09(4). Crystallographic data for **1** have been deposited at the Cambridge Crystallographic Data Centre as deposit no CCDC 2084957.

X-ray Crystallography Analysis of 27-deoxywithaferin A (**2**): Clear light colourless plate crystals of compound **2** were obtained from acetone recrystallization. C28H38O5, Mr = 476.22 g.mol^{-1}; size 0.086×0.363×0.552 mm. The crystalline system was orthorhombic, space group P2_1 2_1 2_1 and the final cell constants were a=7.7019(2) Å, b=10.3098(3) Å, c=33.8786(7) Å, α=90°, β=90°, γ=90°; V = 2690.13(12) Å3, Z = 4, ρcalc=1.176 g.cm^{-3}, F (000) = 1027. Data were corrected for absorption effects using the numerical method. A total of 10613 reflections were collected in the range 12.63 to 140.10 (0.82 Å) (completeness = 97.9 %), with 4978 independent reflections (Rint = 0.0305, Rsigma = 0.0422) which were used in all calculations. Final indices: R1obs = 0.0599, ωR2obs = 0.1728 [I ≥ 2σ(I)]; R1all = 0.0624, ωR2all = 0.1758 [all data], goodness of fit on F2 was 1.049. The stereochemistry of the molecule was evidenced by the following parameters: Flack x = 0.01(10), Parsons z = -0.05(11), Hooft y = -0.02(11). Crystallographic data for **2** have been deposited at the Cambridge Crystallographic Data Centre as deposit no CCDC 2084958.

X-ray Crystallography Analysis of 27-deoxy-2,3-dihydrowithaferin A (**3**): Clear light colourless plate crystals of compound **3** were obtained from acetone recrystallization. C$_{28}$H$_{40}$O$_5$, Mr = 456.60 g.mol^{-1}; size 0.09×0.11×0.35 mm. The crystalline system was orthorhombic, space group P2_1 2_1 2_1 and the final cell constants were a=7.6790(2) Å, b=10.5223(3) Å, c=33.9196(8) Å, α=90°, β=90°, γ =90°; V = 2740.73(12) Å3, Z = 4, ρcalc=1.107 g cm^{-3}, F (000) = 992. Data were corrected for absorption effects using the numerical method. A total of 29350 reflections were collected in the range 9.89 to 140.37 (0.82 Å) (completeness = 98.8 %), with 5191 independent reflections (Rint = 0.0457, Rsigma = 0.0270) which were used in all calculations. Final indices: R1obs = 0.0397, ωR2obs = 0.1046 [I ≥ 2σ(I)]; R1all = 0.0493, ωR2all = 0.1153 [all data], goodness of fit on F2 was 1.023. The following parameters

evidenced the stereochemistry of the molecule: Flack x (Twin)= 0.4(3), Parsons z = 0.01(9), Hooft y = 0.04(8). Crystallographic data for **3** have been deposited at the Cambridge Crystallographic Data Centre as deposit no CCDC 2084959.

2.5. Computational section

2.5.1 Ligand preparation

The GaussianView 5.0 *software* was used to build the tridimensional structures of withanolides. Posteriorly, the Density Functional Theory (DFT) was employed in the gas phase to optimize these structures through the B3LYP hybrid functional (Becke, 1993; Lee, Yang, & Parr, 1988; Vosko, Wilk, & Nusair, 1980; Matos et al., 2022) with the 6-31 G (d,p) (Petersson et al., 1988) basis set implemented in Gaussian 09 package (Frisch et al., 2009). Posteriorly, the absence of negative frequencies was checked. Finally, these structures were used in the molecular docking simulations.

2.5.2 Molecular Docking

The M^{pro} target intituled as ''The crystal structure of COVID-19 main protease in complex with an inhibitor N3'' (PDB: ID 6LU7) (Khanal et al., 2020), was obtained by the Protein Data Bank (PDB) repository. This target was determined through the X-Ray Diffraction method, deposited with a resolution of 2.16 Å (R-Value Free: 0.235, R-Value Work: 0.202, and R-Value Observed: 0.204), and classified as Viral Protein. The target preparation consisted of the removal of water molecules and N-[(5-methylisoxazol-3-yl)carbonyl]ananyl-l-valyl-n-1-((1R,2Z)-4-(benzyloxy)-4-oxo-1-{[(3R)-2-oxopyrrolidin-3-yl]methyl}but-2-enyl)-l-leucinamide (N3) inhibitor, followed by the addition of hydrogens polar and Gasteiger charges through AutoDock Tools *software* (Morris et al., 2009). The grid box was defined in the active site with the following parameters: 40 Å × 40 Å × 40 Å and dimensions (x,y,z) = (-10.678,

27.322, and 66.294). The molecular docking was accomplished with the Autodock 1.5.6 (Holt, Chaires, & Trent, 2008) around atom 145 (oxygen atom, O145) of the Cys145 residue, which is included in the M^{pro} catalytic dyad, present in the P1 region (Gao et al., 2021). Autodock Vina 1.2 (Trott & Olson, 2009) *software* developed by Scripps Research Institute was employed for all the molecular docking simulations. The program used as the binding analysis *software* option was UCSF Chimera (version 1.14) (Pettersen et al., 2004). The used exhaustiveness was 16.

2.5.2 Molecular dynamics simulations

All the molecular dynamics simulations were performed in the Gromacs (Van Der Spoel et al., 2005) *software* implemented with the CHARMM27 (MacKerell et al., 2000) force field. The best pose from molecular docking simulations was utilized as the starting point for the molecular dynamics simulations. First, the SwissParam (Zoete, Cuendet, Grosdidier, & Michielin, 2011) server was utilized to obtain the withanolides **1** to **4** parameters. Next, the system was solvated through water molecules described by the TIP3P model, followed by additional counter ions to neutralize the system. The geometry of the system was performed by the steepest descent (Arfken, Weber, & Harris, 2013a; Arfken, Weber, & Harris, 2013b) and gradient conjugate (Shewchuk, 1994; Bezerra et al., 2022) algorithms, both with an energy tolerance of 10 kJ mol^{-1} nm^{-1} and 10^4 steps. Posteriorly, the equilibrium dynamics were simulated at 200 ps and divided into two steps. The first step was realized by the NVT ensemble using the V-rescale thermostat (Bussi et al., 2007) with a temperature of 310 K, followed by the NPT ensemble performed by the Parrinello-Rahman barostat (Nosé & Klein, 1983; Bezerra et al., 2022) with a pressure of 1.0 bar. Finally, the production step was simulated in 100 ns and three replicates using the Leap-Frog integrator. This step was performed using the same temperature and pressure as the equilibrium dynamics step.

2.6. Binding free energy simulations

The binding free energy (ΔG_{bind}) simulations were performed using the Molecular Mechanics Poisson-Boltzmann Surface Area (MM/PBSA) (Reddy et al., 2014) method by the g_mmpbsa tool (Kumari et al., 2014; Baker et al., 2001). The energy components for each complex analyzed were extracted at every 10 ps from the final 10 ns of simulation from the MD production step. Furthermore, the binding free energy simulations were performed in three replicates and may be summarized in the equations below:

$$\Delta G_{bind} = \Delta G_{complex} - (\Delta G_{receptor} + \Delta G_{ligand}) \tag{1}$$

$$\Delta G_{bind} = \Delta E_{MM} + \Delta G_{polar} + \Delta G_{non-polar} - TS \tag{2}$$

$$\Delta E_{MM} = \Delta E_{elect} + \Delta E_{vdw} \tag{3}$$

$$\Delta G_{non-polar} = \gamma SASA \tag{4}$$

ΔG_{bind} is the binding free energy, ΔE_{MM} is the molecular mechanics potential energy obtained by the summing between the electrostatic (ΔE_{elect}) and van der Waals (ΔE_{vdw}) energy terms. -TS term is the entropic contribution of the system. ΔG_{polar} represent the polar energy of solvation and $\Delta G_{non-polar}$ is the non-polar solvation energy using the Solvent Accessible Surface Area (SASA) non-polar model. The γ constant is in the value of 0.0226778 kJ mol^{-1}Å^{-2}.

3. Results and discussion

3.1. Structure elucidation

Three withanolides were isolated from the hexane/ethyl acetate 1:1 soluble fraction from leaves of *A. velutina*. Their structures were established using IR, ^{1}H/^{13}C NMR, HRMS, X-ray crystallographic techniques, and EDC calculations.

Withanolide **1** had its molecular formula assigned by HRMS as $C_{28}H_{38}O_6$ (ten degrees of unsaturation) from the $[M + Na]^+$ ion peak at *m/z* 493.2556. Its IR spectrum displayed absorption bands at 3498 cm^{-1} to hydroxyl and 1720 and 1676 cm^{-1} to unsaturated carbonyls of lactone and ketone, respectively. The ^{13}C NMR, DEPT 135º, and HSQC spectra showed signals to 28 carbon atoms ascribed to ten methines, including two olefinic at δ_H/δ_C 6.93/142.1 (C-3) and 6.20/132.5 (C-2) and three oxygenated at δ_H/δ_C 4.76.4 (C-22), 3.756/70.1 (C-4), and 3.22/62.6 (C-6); six methylenes, five methyls at δ_H/δ_C 1.47/18.1 (C-28), 1.39/17.5 (C-19), 1.55/13.8 (C-27), 0.89/13.2 (C-21) and 0.67/11.8 (C-18), and eight quaternary carbons, including two carbonyls at δ_C 202.4 (C-1) and 170.2 (C-26). Furthermore, the system 5,6-epoxy-4-hydroxy-α,β-unsaturated ketone was confirmed by the HMBC correlations for the proton at δ_H 6.93 (H-3) with the carbons at δ_C 202.4 (C-1) and 64.0 (C-5), for the protons at δ_H 6.20 (H-2) and 3.22 (H-6) with δ_C 70.1 (C-4), and δ_H 3.75 (H-4) with δ_C 132.5 (C-2) and 47.9 (C-10). Additionally, correlations of the oxymethine at δ_H 4.52 (H-22) with δ_C 62.8 (C-24) and 13.2 (C-21) and of the methyl at δ_H 1.12 (H-27) with δ_C 170.2 (C-26), 62.8 (C-24) and 59.5 (C-25) showed a 24,25-epoxy moiety in the δ-lactone withanolide. Based on the complete ^{1}H and ^{13}C NMR spectra (see SI, Figures S5 to S14) and single-crystal X-ray diffraction analysis (Figure 2), the structure of withanolide **1** was established as 5β,6β-epoxy-4β-hydroxy-1-oxowitha-2-enolide which was named 27-deoxy-24,25-epoxywithaferin A. In addition to **1**, the withanolides 27-deoxywithaferin A (**2**) and 2,3-dihydro-27-deoxywithaferin A (**3**) were also isolated (Nittala and Lavie, 1981), including their X-ray diffraction analysis (Figure 3).
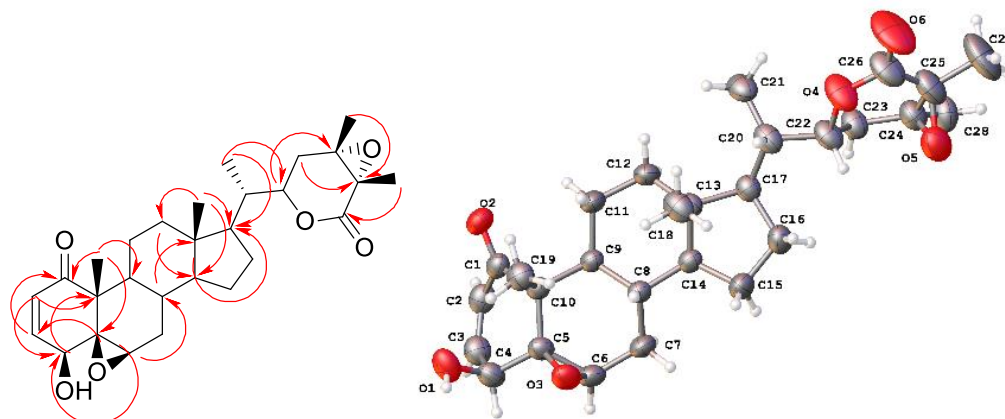
Fig. 2 Key HMBC and X-ray ORTEP drawing of withanolide **1**
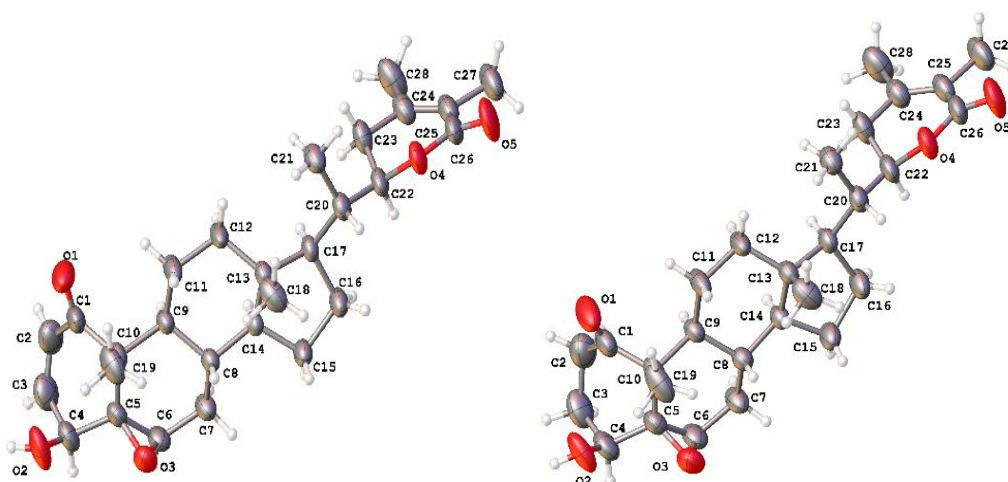
Fig. 3 X-ray ORTEP drawing of withanolides **2** and **3**

3.2 Molecular docking results

The molecular docking simulations were performed to obtain the complex between the M^{pro} target with the withanolide **1-4** ligands. Table 1 shows the binding energy and Root Mean Square Deviation (RMSD) values of the complexes. The M^{pro}-withanolide complexes **1** to **4** showed binding energy values of -8.3 kcal mol^{-1}, -7.9 kcal mol^{-1}, -7.9 kcal mol^{-1}, and -7.7 kcal mol^{-1}, respectively. Furthermore, these complexes registered the RMSDs values below 2.0 Å (Yusuf et al., 2008), validating the molecular docking simulations.

Table 1. Binding energy and RMSD values for the M^{pro} target with the withanolide molecules.

Complex	Binding energy (kcal mol^{-1})	RMSD (Å)
M^{pro}-withanolide **1**	-8.3	1.701
M^{pro}-withanolide **2**	-7.9	1.675
M^{pro}-withanolide **3**	-7.9	1.634
M^{pro}-withanolide **4**	-7.7	1.657

3.3 Molecular dynamics results

Molecular dynamics simulations are one of the best methods to analyze protein-ligand systems due to these simulations considering all the structures flexible in the box simulation and the presence of water molecules solvating the system, unlike molecular docking simulations. Furthermore, the behavior of the system can be analyzed as a function of time. For these reasons, molecular dynamics simulations were performed to analyze the stability of complexes formed by the molecular docking simulations. First, the RMSD of M^{pro}-withanolides complexes **1** to **4** (Figure 4a to 4d) were obtained using the C-α of the target as the reference. The average RMSD values for the M^{pro}-withanolide complexes **1** to **4** were 3.30, 3.62, 3.87, and 3.99 Å, respectively. Furthermore, the M^{pro}-withanolide complexes **1** to **4** reached the equilibrium from 60-100 ns. Therefore, the four complexes exhibited stability in the interactions between the ligands with the M^{pro} target, highlighted for the withanolide **1** due to the lowest RMSD values registered.
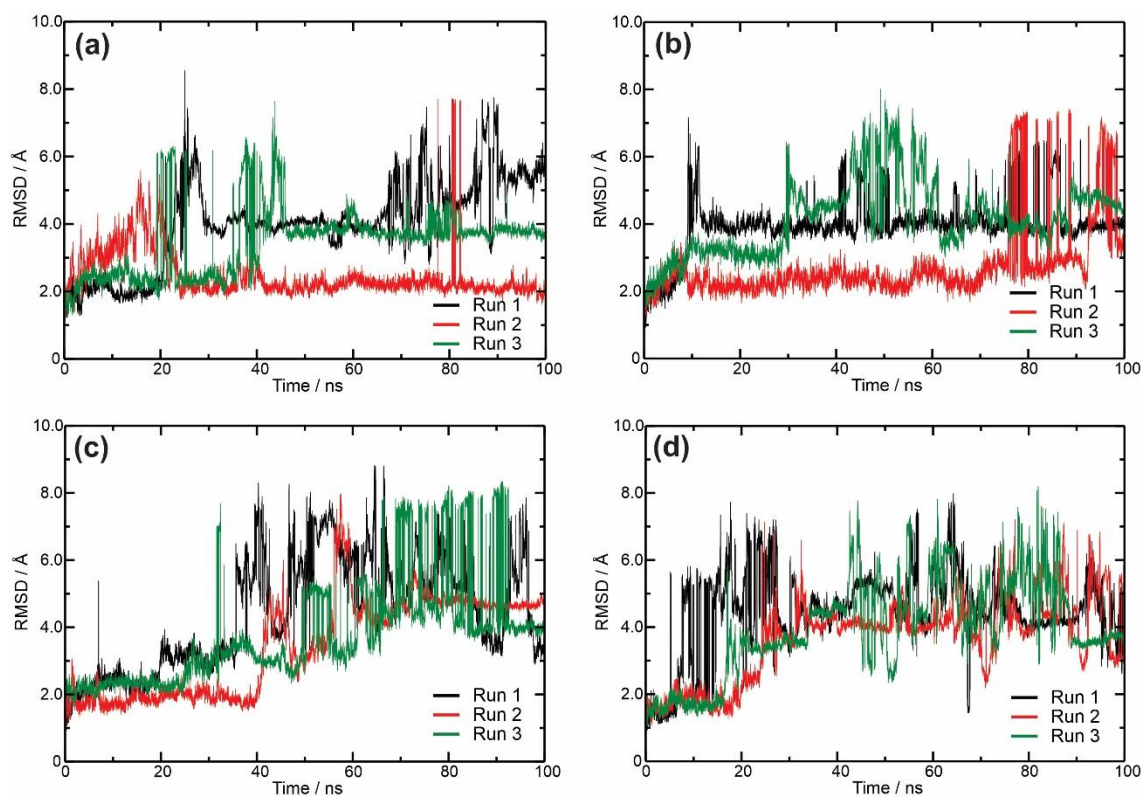
Fig. 4: Determination of RMSD for the M^{pro}-withanolides **1** (a), **2** (b), **3** (c), and **4** (d) complexes. The MD simulations were realized in three replicates (black, red, and green).

To evaluate the stability between the withanolides with the amino acid residues for the M^{pro} target, the Root Mean Square Fluctuation (RMSF) (Figure 5) was performed using the C-α of the target as reference. The M^{pro}-withanolide complex **1** registered fluctuation above 3.0 Å with the Ser 46, Glu 47, Asp 153, Tyr 154, Asp 155, Thr 190, Ala 191, Ala 194, Gly 195, Asn 277, and Gly 278 amino acid residues. On the other hand, the M^{pro}-withanolide complex **2** exhibited fluctuation only with the Asn 277 and Gly 278 residues. The M^{pro}-withanolide complex **3** registered fluctuation with the Arg 4, Lys 5, Met 6, Asp 153, Tyr 154, Ala 191, Gln 192, Asn 221, Arg 222, Phe 223, Thr 224, Gln 244, Asp 245, Gly 278, Arg 279, and Thr 280 residues. Finally, the M^{pro}-withanolide complex **4** registered fluctuation with the Ala 191, Gln 192, Ala 193, Arg 222, Phe 223, Asn 277, and Gly 278 residues. It is worth to mentioning that all the withanolides fluctuated with the 277 Asn and 278 Gly residues. Therefore, the presence of the withanolide molecules occasioned small changes in the M^{pro} target structure, particularly the withanolides **2** and **4**.
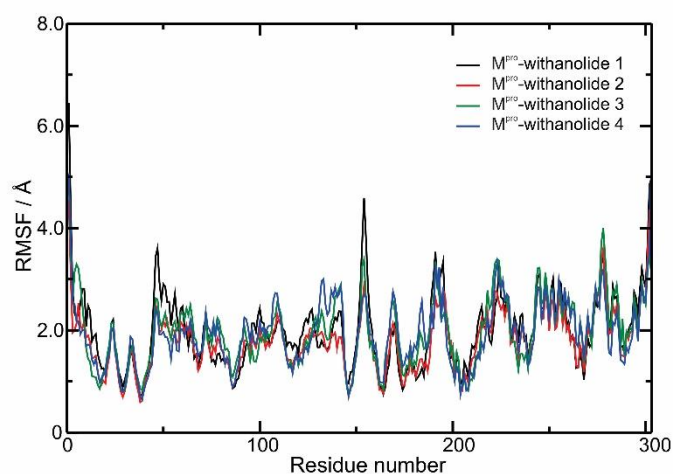
Fig. 5: Determination of RMSF for the M^{pro}-withanolides **1** (a), **2** (b), **3** (c), and **4** (d) complexes.

The binding free energy simulations, through MM/PBSA method, were utilized to mensurate the ΔG_{bind} value between the M^{pro} target and each of the withanolides (Table 2). The M^{pro}-withanolide complexes **1** to **4** registered the ΔG_{bind} values of -135.566 (±18.614) kJ mol^{-1}, -96.413 (±24.675) kJ mol^{-1}, -102.722 (±22.218) kJ mol^{-1}, and -91.033 (±20.028) kJ mol^{-1}, respectively. The difference in binding free energy values of complexes can be particularly explained by high contribution of van der Waals energy term of M^{pro}-withanolide complex **1** than concerning the other complexes. Therefore, the binding free energy results indicated that the withanolide **1** could be recommended against COVID-19 disease. Figure 6 shows the binding site of M^{pro}-withanolide complexes **1** to **4** in the last simulation frame (100000 ps).

Table 2 Binding free energy (kJ mol^{-1}) of M^{pro}-withanolide complexes **1−4** obtained by the MM/PBSA simulations, with standard deviation.

Energy (kJ mol^{-1})	M^{pro}-withanolide **1**	M^{pro}-withanolide **2**	M^{pro}-withanolide **3**	M^{pro}-withanolide **4**
van der Waals energy	-153.044	-121.164	-104.543	-123.873
(ΔE_{vdw})	(±13.194)	(±13.093)	(±17.607)	(±12.703)
Electrostatic energy	-75.002	-45.511	-57.186	-65.310
(ΔE_{elect})	(±22.496)	(±30.091)	(±16.293)	(±23.444)
Polar solvation energy	108.579	83.339	72.073	112.103
(ΔG_{polar})	(±12.904)	(±16.662)	(±23.150)	(±14.693)
SASA energy	-16.099	-13.077	-13.066	-13.952
($\Delta G_{non-polar}$)	(±1.056)	(±1.051)	(±1.740)	(±0.942)
Binding free energy	-135.566	-96.413	-102.722	-91.033
(ΔG_{bind})	(±18.614)	(±24.675)	(±22.218)	(±20.028)
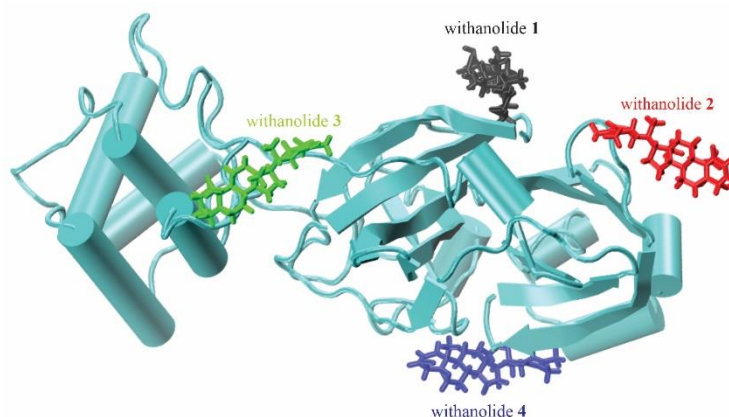
Fig. 6: Binding site for the M^{pro}-withanolides complexes **1-4**.

4. Conclusion

Since the new coronavírus pandemic, many studies involving natural products have been conducted to find possible anti-SARS-CoV-2 agents. In this context, the withanolides appear as promising inhibitors of the SARS-CoV-2 coronavírus. The molecular docking and molecular dynamics studies of three withanolides, not yet investigated against SARS-CoV-2 coronavírus, corroborate the antiviral potential of this large class of compounds. Furthermore, based on the

molecular dynamics and the binding free energy simulations, the withanolides evaluated in this work showed great stability and high interaction potential with the M^{pro} target, highlighted for the withanolide **1** that could be a promising anti-SARS-CoV-2 agent.

Ethical statement

This study does not require ethics approval.

Conflicts of interest

The authors declare no competing or financial interest.

ORCID
Pabllo Abreu Alves https://orcid.org/0000-0003-1137-377X
Késya Amanda Dantas Rocha https://orcid.org/0000-0001-7596-8700
Lucas Lima Bezerra https://orcid.org/0000-0002-6871-3045
Alejandro Pedro Ayala https://orcid.org/0000-0002-9247-6780
Norberto de Kássio Vieira Monteiro https://orcid.org/0000-0002-5847-5733
Otília Deusdênia Loiola Pessoa https://orcid.org/0000-0002-1617-7586

References

A Abdeljebbar, L. H., Benjouad, A., Morjani, H., Merghoub, N., Haddar, S. El, Humam, M., Hostettmann, K., & Amzazi, K. B. et S. (2009). Antiproliferative effects of withanolides from *Withania adpressa. Thérapie, 64*, 121–127. https://doi.org/10.2515/therapie/2009015

Amporndanai, K., Meng, X., Shang, W., Jin, Z., Rogers, M., Zhao, Y., Rhao, Z., Liu, Z., Yang, H., Zhang, L., O'neil, P.M., & Samar Hasnain, S. (2021). Inhibition mechanism of SARS-CoV-2 main protease by ebselen and its derivatives. *Nature Communications, 12*(1), 1–7. https://doi.org/10.1038/s41467-021-23313-7

Arafet, K., Aparicio, N., Lodola, A., Mulholland, A., González, F., Świderek, K., & Moliner, V. (2020). Mechanism of inhibition of SARS-CoV-2 M^pro by N3 peptidyl Michael Acceptor explained by QM/MM simulations and design of new derivatives with tunable chemical reactivity. *Chemical Science, 12*. https://doi.org/10.1039/D0SC06195F

Arfken, G. B., Weber, H. J., & Harris, F. E. (Eds.). (2013a). Front Matter. In *mathematical methods for physicists (Seventh Edition)* (Seventh Ed, p. iv). Boston: Academic Press. https://doi.org/https://doi.org/10.1016/B978-0-12-384654-9.00030-X

Arfken, G. B., Weber, H. J., & Harris, F. E. (Eds.). (2013b). Preface. In *mathematical methods for physicists (Seventh Edition)* (Seventh Ed, pp. xi–xiii). Boston: Academic Press. https://doi.org/https://doi.org/10.1016/B978-0-12-384654-9.00032-3

Baitharu, I., Jain, V., Deep, S. N., Shroff, S., Sahu, J. K., Naik, P. K., & Ilavazhagan, G. (2014). Withanolide a prevents neurodegeneration by modulating hippocampal glutathione biosynthesis during hypoxia. *PloS One, 9*(10), e105311. https://doi.org/10.1371/journal.pone.0105311

Baker, N. A., Sept, D., Joseph, S., Holst, M. J., & McCammon, J. A. (2001). Electrostatics of nanosystems: Application to microtubules and the ribosome. *Proceedings of the National Academy of Sciences of the United States of America, 98*(18), 10037–10041. https://doi.org/10.1073/pnas.181342398

Ballesteros-Vivas, D., Alvarez-Rivera, G., León, C., Morantes, S. J., Ibánez, E., Parada-Alfonso, F., Cifuentes, A., & Valdés, A. (2019). Anti-proliferative bioactivity against HT-29 colon cancer cells of a withanolides-rich extract from golden berry (*Physalis peruviana L.*) calyx investigated by Foodomics. *Journal of Functional Foods, 63*, 103567. https://doi.org/https://doi.org/10.1016/j.jff.2019.103567

Batista, P. H. J., de Lima, K. S. B., Pinto, F. C. L Tavares, J. L. Uchoa, D. E. A. Costa-Lotufo, L. V., Rocha, D. D., Silveira, E. R., Bezerra, A. M. E., Canuto, K. M., & Pessoa, O. D. L.(2016). Withanolides from leaves of cultivated *Acnistus arborescens. Phytochemistry 130* (2016) 321–327. http://dx.doi.org/10.1016/j.phytochem.2016.07.003

Becke, A. D. (1993). Density-functional thermochemistry. III. The role of exact exchange. *The Journal of Chemical Physics, 98*(7), 5648–5652. https://doi.org/10.1063/1.464913

Bezerra, L. L., Almeida-Neto, F. W. Q., Marinho, M. M., Santos Oliveira, L., Teixeira, A. M. R., Bandeira, P. N., dos Santos, H. S., Lima-Neto, P. de, & Marinho, E. S. (2022). Synthesis of aminochalcones and in silico evaluation of their antiparasitic potential against Leishmania. *Journal of Biomolecular Structure and Dynamics*, 1–8. https://doi.org/10.1080/07391102.2022.2103030

Bhattacharya, S. K., Bhattacharya, A., Sairam, K., & Ghosal, S. (2000). Anxiolytic-antidepressant activity of *Withania somnifera* glycowithanolides: an experimental study. *Phytomedicine : International Journal of Phytotherapy and Phytopharmacology, 7*(6), 463–469. https://doi.org/10.1016/S0944-7113(00)80030-6

Bruker AXS Inc. (2018a). APEX III. Madison, Wisconsin, USA. Retrieved from https://www.bruker.com/en/products-and-solutions/diffractometers-and-scattering-

systems/single-crystal-x-ray-diffractometers/sc-xrd-software/apex.html

Bruker AXS Inc. (2018b). Bruker SAINT. Madison, Wisconsin, USA.

Budhiraja, R., Krishan, P., & Sudhir, S. (2000). Biological activity of withanolides. *Journal of Scientific and Industrial Research (JSIR)*, *59*(11), 904–911.

Bussi, G., Donadio, D., & Parrinello, M. (2007). Canonical sampling through velocity rescaling. *The Journal of Chemical Physics*, *126*(1), 14101. https://doi.org/10.1063/1.2408420

Cao, C. M., Wu, X., Kindscher, K., Xu, L., & Timmermann, B. N. (2015). Withanolides and sucrose esters from *Physalis neomexicana*. *Journal of Natural Products*, *78*, 2488–2493. https://doi.org/10.1021/acs.jnatprod.5b00698

Carmo, B. A., Silva, A. D., Parente, A. M. S., Furtado, A. A., Carvalho, E., Oliveira, J. W. F., Santos, E.C.G., Silva, M.S., Silva, S.R.B., Júnior, A.A.S, & Monteiro, N. K. (2019). Potent and broad-spectrum antimicrobial activity of analogs from the scorpion peptide stigmurin. *International Journal of Molecular Sciences*, *20*, 623. Retrieved from https://doi.org/10.3390/ijms20030623.

Dhawan, M., Parmar, M., Sharun, K., Tiwari, R., Bilal, M., & Dhama, K. (2021). Medicinal and therapeutic potential of withanolides from *Withania somnifera* against COVID-19. *Journal of Applied Pharmaceutical Science*, *11*(4), 006–013. https://doi.org/10.7324/JAPS.2021.110402

Frisch, M. J., Trucks, G. W., Schlegel, H. B., Scuseria, G. E., Robb, M. A., Cheeseman, J. R., Scalmani, G., Barone, V., Mennucci, B., Petersson, G.A., Nakatsuji, H., Caricato, M., Li, X., Hratchian, H. P., Izmaylov, A. F., Bloino, J., Zheng, G., Sonnenberg, J. L., Hada, M., Ehara, M., Toyota, K., Fukuda, R., Hasegawa, J., Ishida, M., Nakajima, T., Honda, Y., Kitao, O., Nakai, H., Vreven, T., Montgomery Jr., J. A., Peralta, J. E., Ogliaro, F., Bearpark, M., Heyd, J. J., Brothers, E., Kudin, K. N., Staroverov, V. N., Kobayashi, R., Normand, J., Raghavachari, K., Rendell, A., Burant, J. C., Iyengar, S. S., Tomasi, J., Cossi, M., Rega, N., Millam, J. M., Klene, M., Knox, J. E., Cross, J. B., Bakken, V., Adamo, C., Jaramillo, J., Gomperts, R., Stratmann, R. E., Yazyev, O., Austin, A. J., Cammi, R., Pomelli, C., Ochterski, J. W., Martin, R. L., Morokuma, K., Zakrzewski, V. G., Voth, G. A., Salvador, P., Dannenberg, J. J., Dapprich, S., Daniels, A. D., Farkas, Ö., Foresman, J. B., Ortiz, J. V., Cioslowski, J., & Fox, D. J. (2009). Gaussian 9. Gaussian, Inc., Wallingford CT, 2016

Gao, K., Wang, R., Chen, J., Cheng, L., Frishcosy, J., Huzumi, Y., Qiu, Y., Schluckbier, T., & Wei, G.-W. (2021). Methodology-centered review of molecular modeling, simulation, and prediction of SARS-CoV-2. *Journal of Molecular Structures*, 1225.

Matos, G. C., da Silva, M., Almeida-Neto, W. Q. F., Marinho, M. E., de Menezes, R. R. P. P. B., Sampaio, T. L., da Rocha, M. N., Ribeiro, L. R., Magalhães, E. P., Teixeira, A. M. R., dos Santos, H. C., Marinho, E. S., de Lima-Neto, P., Martins, A. M. C., Monteiro, N. K. V., Marinho, M. M. (2022). Quantum mechanical, molecular docking, molecular dynamics, ADMET and antiproliferative activity on Trypanosoma cruzi (Y strain) of chalcone (E)-1-(2-hydroxy-3{,}4{,}6-trimethoxyphenyl)-3-(3-nitrophenyl)prop-2-en-1-one derived from a natural product. *Phys. Chem. Chem. Phys.*, *24*(8), 5052–5069. https://doi.org/10.1039/D1CP04992E

Gupta, G., & Rana, A. (2007). *Withania somnifera* (Ashwagandha): A Review. *Pharmacognosy Reviews*, *1*(1), 129–136.

Holt, P. A., Chaires, J. B., & Trent, J. O. (2008). Molecular docking of intercalators and groove-binders to nucleic acids using Autodock and Surflex. *Journal of Chemical Information and Modeling*, *48*(8), 1602–1615. https://doi.org/10.1021/ci800063v

Houchi, S., & Messasma, Z. (2022). Exploring the inhibitory potential of Saussurea costus and Saussurea involucrata phytoconstituents against the Spike glycoprotein receptor binding domain of SARS-CoV-2 Delta (B.1.617.2) variant and the main protease (M^{pro}) as therapeutic

candidates, using molecular docking, DFT, and ADME/Tox studies. *Journal of Molecular Structure*, *1263*, 133032. https://doi.org/10.1016/j.molstruc.2022.133032

Khanal, P., Chikhale, R., Dey, Y. N., Pasha, I., Chand, S., Gurav, N., Ayyanar, M., Patil, B.M., & Gurav, S. (2020). Withanolides from *Withania somnifera* as an immunity booster and their therapeutic options against COVID-19. *Journal of Biomolecular Structure and Dynamics*, *0*(0), 1–14. https://doi.org/10.1080/07391102.2020.1869588

Kirson, I., Glotter, E., Abraham, A., & Lavie, D. (1970). Constituents of *Withania somnifera* dun—XI: The structure of three new withanolides. *Tetrahedron*, *26*(9), 2209–2219. https://doi.org/https://doi.org/10.1016/S0040-4020(01)92800-5

Kumari, R., Kumar, R., & Lynn, A. (2014). g_mmpbsa—A GROMACS tool for high-throughput MM-PBSA calculations. *Journal of Chemical Information and Modeling*, *54*(7), 1951–1962. https://doi.org/10.1021/ci500020m

Lee, C., Yang, W., & Parr, R. G. (1988). Development of the Colle-Salvetti correlation-energy formula into a functional of the electron density. *Phys. Rev. B*, *37*(2), 785–789. https://doi.org/10.1103/PhysRevB.37.785

Llanos, G. G., Araujo, L. M., Jiménez, I. A., Moujir, L. M., Rodríguez, J., Jiménez, C., & Bazzocchi, I. L. (2017). Structure-based design, synthesis, and biological evaluation of withaferin A-analogues as potent apoptotic inducers. *Journal of Medicinal Chemistry*, *140*, 52–64. Retrieved from http://dx.doi.org/10.1016/j.ejmech.2017.09.004

Mark, P., & Nilsson, L. (2001). Structure and dynamics of the TIP3P, SPC, and SPC/E water models at 298 K. *The Journal of Physical Chemistry A*, *105*(43), 9954–9960. https://doi.org/10.1021/jp003020w

MacKerell Jr., A. D., Banavali, N., & Foloppe, N. (2000). Development and current status of the CHARMM force field for nucleic acids. *Biopolymers*, *56*(4), 257–265. https://doi.org/https://doi.org/10.1002/1097-0282(2000)56:4<257::AID-BIP10029>3.0.CO;2-W

Morris, G. M., Huey, R., Lindstrom, W., Sanner, M. F., Belew, R. K., Goodsell, D. S., & Olson, A. J. (2009). AutoDock4 and AutoDockTools4: Automated docking with selective receptor flexibility. *Journal of Computational Chemistry*, *30*(16), 2785–2791. https://doi.org/10.1002/jcc.21256

Newman, D. J., & Cragg, G. M. (2016). Natural products as sources of new drugs from 1981 to 2014. *Journal of Natural Products*, *79* (3), 629-661. https://doi.org/10.1021/acs.jnatprod.5b01055

Newman, D. J., & Cragg, G. M. (2020). Natural products as sources of new drugs over the nearly four decades from 01/1981 to 09/2019. *Journal of Natural Products*, *83*(3), 770–803. https://doi.org/10.1021/acs.jnatprod.9b01285

Nittala, S. S., & Lavie, D. (1981). Withanolides of *Acnistus breviflorus*. *Phytochemistry, 20*(12) 2735–2739.

Nosé, S., & Klein, M. L. (1983). Constant pressure molecular dynamics for molecular systems. *Molecular Physics*, *50*(5), 1055–1076. https://doi.org/10.1080/00268978300102851

Petersson, G.A., Bennett, A., Tensfeldt, T. G., Al-Laham, M. A., Shirley, W. A., & Mantzaris, J. (1988). A complete basis set model chemistry. I. The total energies of closed-shell atoms and hydrides of the first-row elements. *The Journal of Chemical Physics*, *89*(4), 2193–2218. https://doi.org/10.1063/1.455064

Reddy, M., Reddy, C., Rathore, R., Erion, M., Aparoy, P., Reddy, R., & Reddanna, P. (2014). Free energy calculations to estimate ligand-binding affinities in structure-based drug design. *Current Pharmaceutical Design*, *20*(20), 3323–3337. https://doi.org/10.2174/13816128113199990604

Sheldrick, G. M. (1996). SADABS. Program for empirical absorption correction for area detector data. University of Göttingen, Germany.

Sheldrick, G.M. (2008). A short history of SHELX. *Acta Crystallographica Section A: Foundations of Crystallography*, *64(1)*, pp.112–122.

Sheldrick, G.M. (2015) SHELXT-Integrated space-group and crystal-structure determination. *Acta Crystallographica Section A*, A71, 3-8. https://doi.org/10.1107/S2053273314026370

Shewchuk, J. R. (1994). An introduction to the conjugate gradient method without the agonizing pain. USA: Carnegie Mellon University. https://doi.org/https://doi.org/10.5555/865018

Troeger, C. (2022). Just how do deaths due to COVID-19 stack up? Think Global Health. Retrieved from https://www.thinkglobalhealth.org/article/just-how-do-deaths-due-covid-19-stack

Trott, O., & Olson, A. J. (2009). AutoDock Vina: Improving the speed and accuracy of docking with a new scoring function, efficient optimization, and multithreading. *Journal of Computational Chemistry*, *31*(2), NA-NA. https://doi.org/10.1002/jcc.21334

Van Der Spoel, D., Lindahl, E., Hess, B., Groenhof, G., Mark, A. E., & Berendsen, H. J. C. (2005). GROMACS: Fast, flexible, and free. *Journal of Computational Chemistry*, *26*(16), 1701–1718. https://doi.org/https://doi.org/10.1002/jcc.20291

Vosko, S.H., Wilk, L., & Nusair, M. (1980). Accurate spin-dependent electron liquid correlation energies for local spin density calculations: a critical analysis. *Canadian Journal of Physics*, *59*, 1200. https://doi.org/10.1139/p80-159

White, P. T., Subramanian, C., Motiwala, H. F., & Cohen, M. S. (2016). Natural withanolides in the treatment of chronic diseases. *Advances in Experimental Medicine and Biology*, *928*, 329–373. https://doi.org/10.1007/978-3-319-41334-1_14

Xu, Y., Bunting, D. P., Liu, M. X., Bandaranayake, H. A., & Gunatilaka, A. A. L. (2016). 17β-Hydroxy-18-acetoxywithanolides from aeroponically grown *Physalis crassifolia* and their potent and selective cytotoxicity for prostate cancer cells. *Journal of Natural Products*, *79*, 821–830. Retrieved from https://doi.org/10.1021/acs.jnatprod.5b00911

Yang, Y., Xiang, K., Sun, D., Zheng, M., Song, Z., Li, M., Wang, X., Li, H., & Chen, L. (2021). Withanolides from dietary tomatillo suppress HT1080 cancer cell growth by targeting mutant IDH1. *Bioorganic & Medicinal Chemistry*, *36*, 116095. https://doi.org/https://doi.org/10.1016/j.bmc.2021.116095

Yusuf, D., Davis, A. M., Kleywegt, G. J., & Schmitt, S. (2008). An alternative method for the evaluation of docking performance: RSR vs RMSD. *Journal of Chemical Information and Modeling*, *48*(7), 1411–1422. https://doi.org/10.1021/ci800084x

Supplementary Material
Contents

Figure S1. FTIR spectrum of 1.

Figure S2. ^{1}H NMR (300.13 MHz) spectrum of 1, in CDCl₃.

Figure S3. ^{13}C NMR (75.47 MHz) spectrum of **1**, in CDCl$_3$.

Figure S4. DEPT 135° NMR (75.47 MHz) spectrum of **1**, in CDCl₃.

Figure S5. HSQC NMR spectrum of 1, in CDCl₃.

Figure S6. COSY NMR spectrum of 1, in CDCl₃.
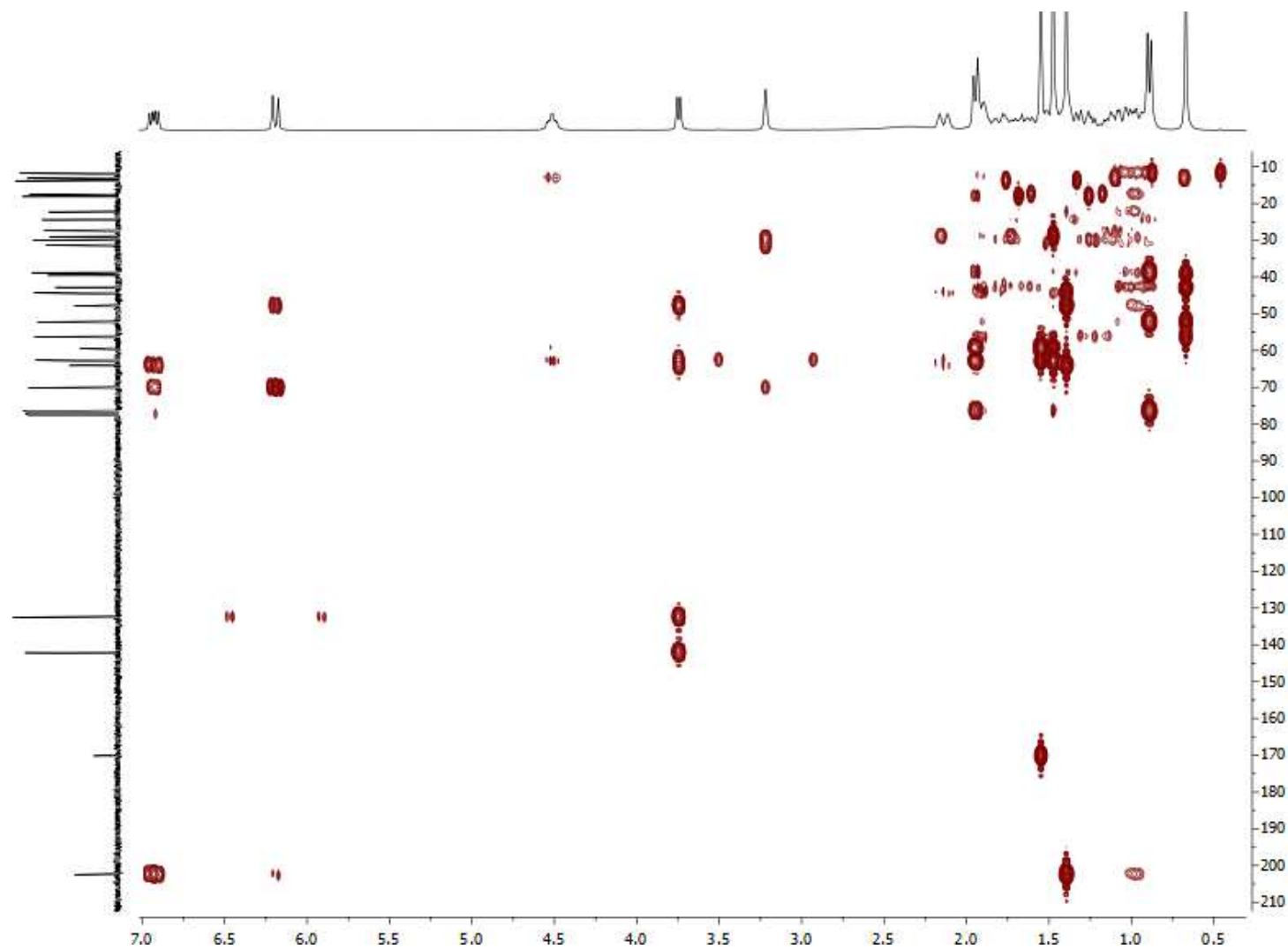
Figure S7. HMBC NMR spectrum of 1, in CDCl₃.
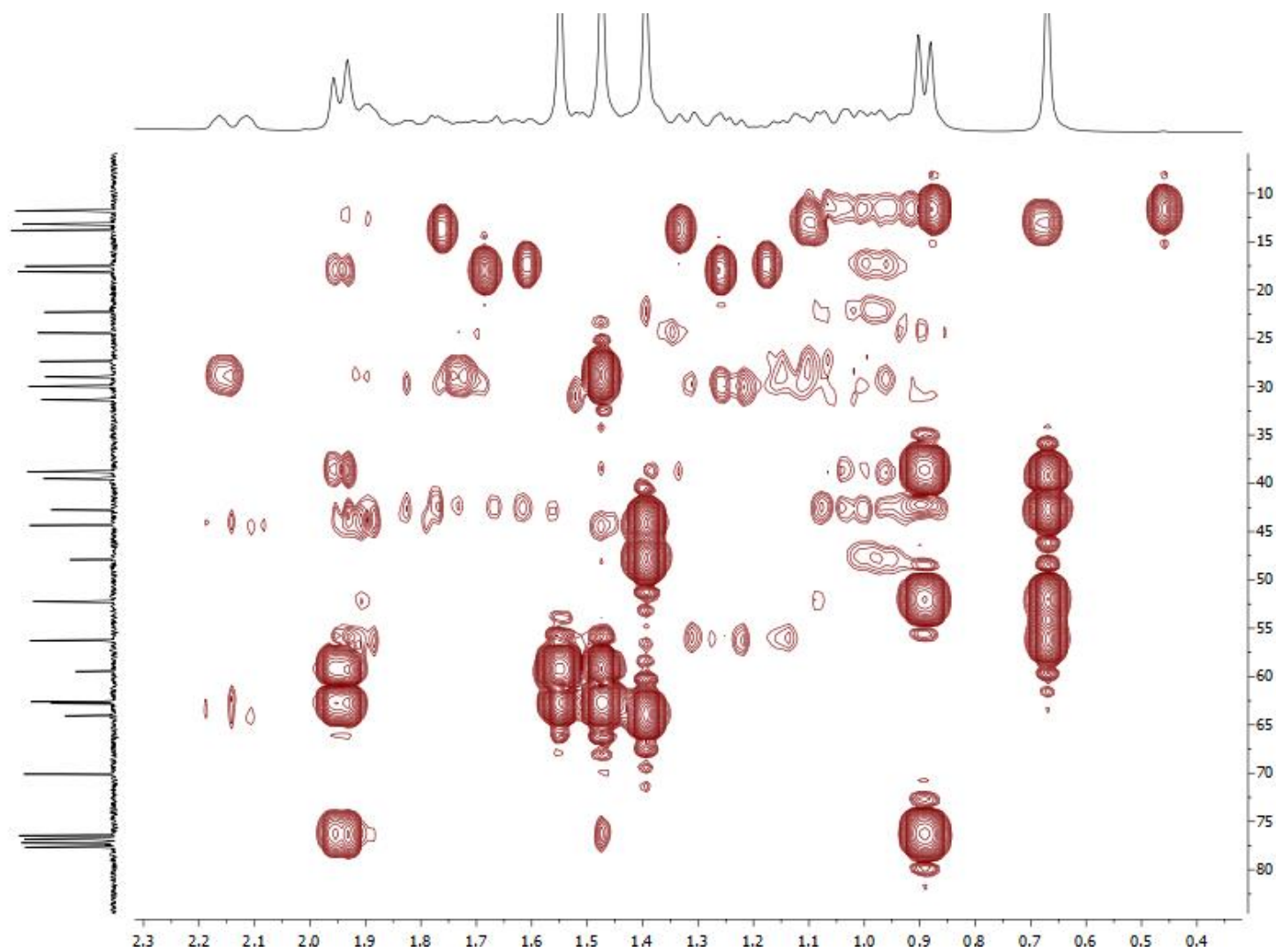
Figure S8. HMBC NMR spectrum of 1, in CDCl₃.
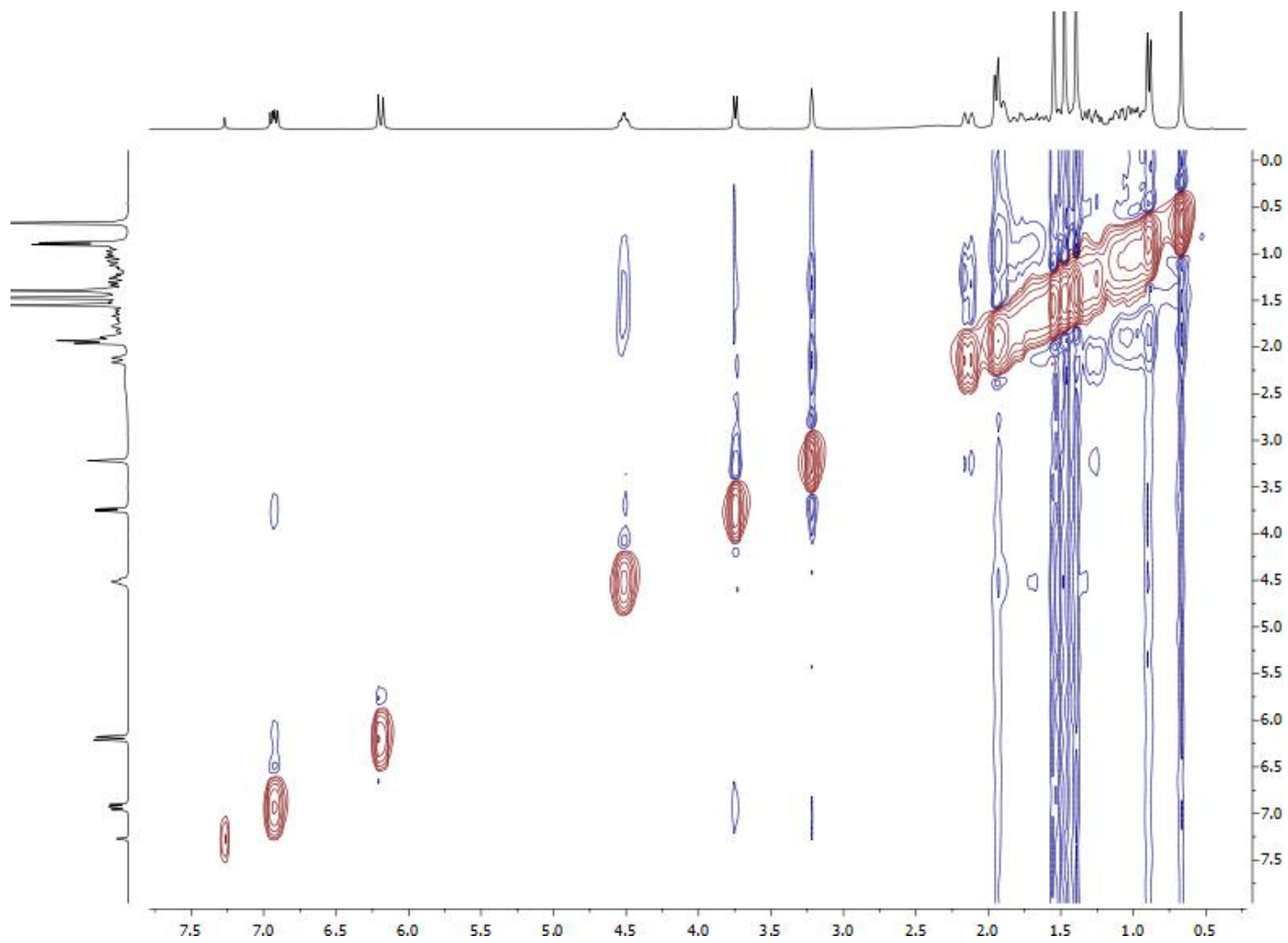
Figure S9. NOESY NMR spectrum of **1**, in CDCl₃.
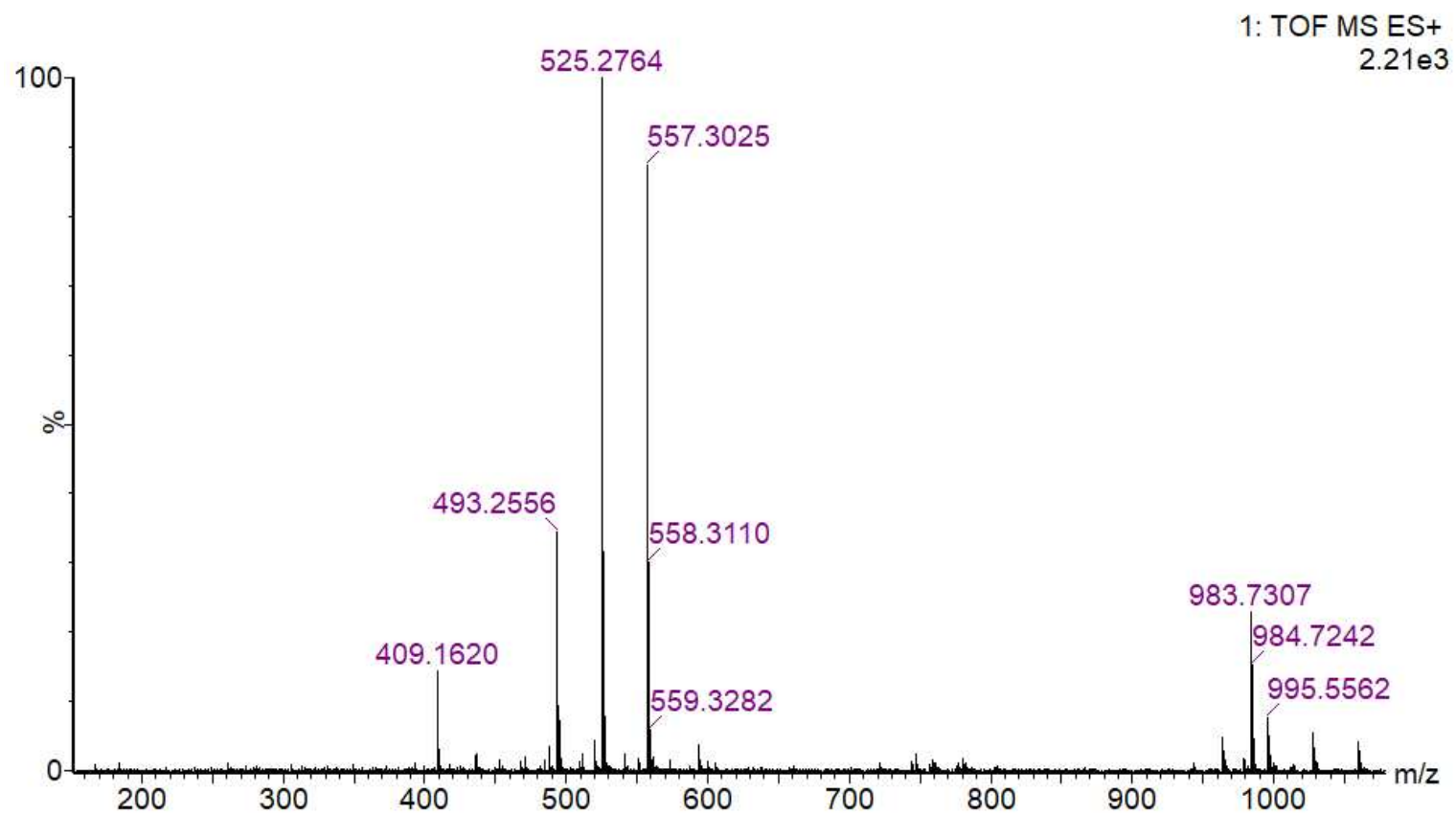
Figure S10. HRESIMS spectrum of **1**.
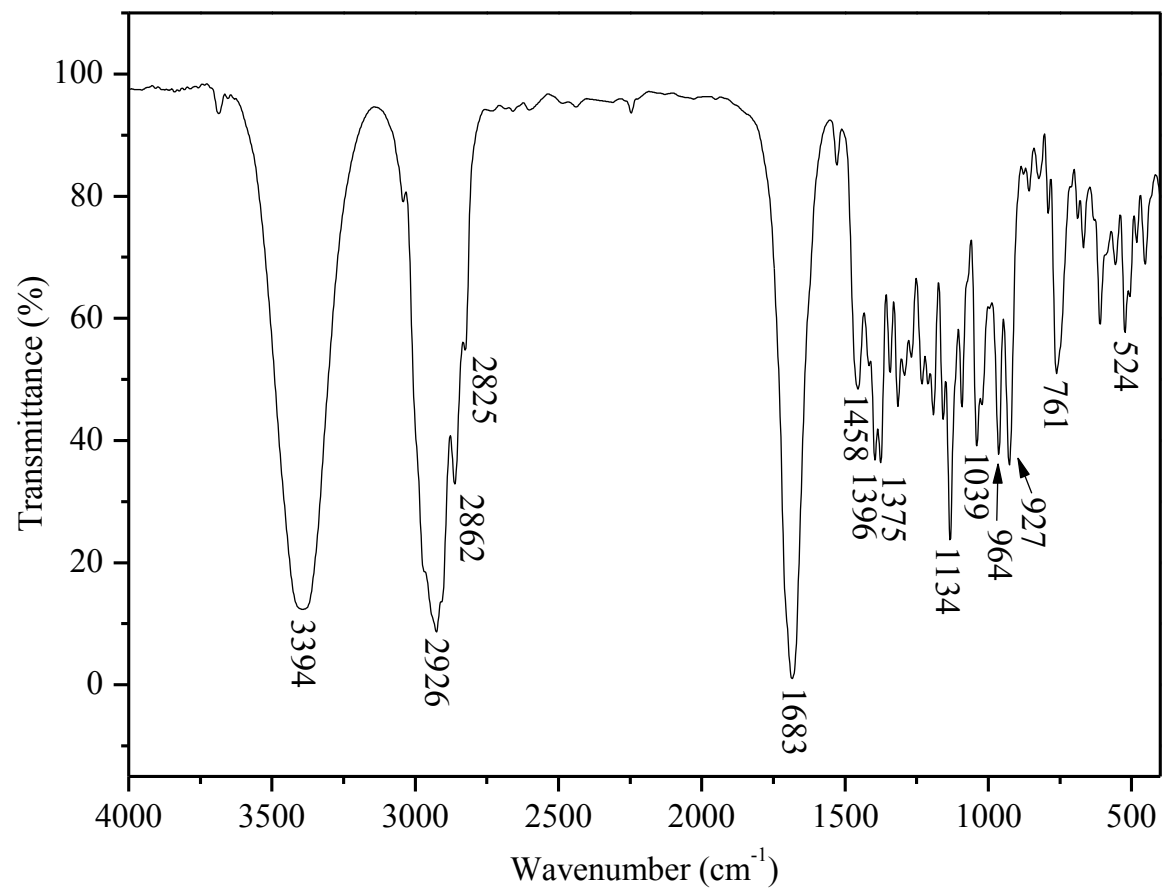
Figure S11. FTIR spectrum of 2.
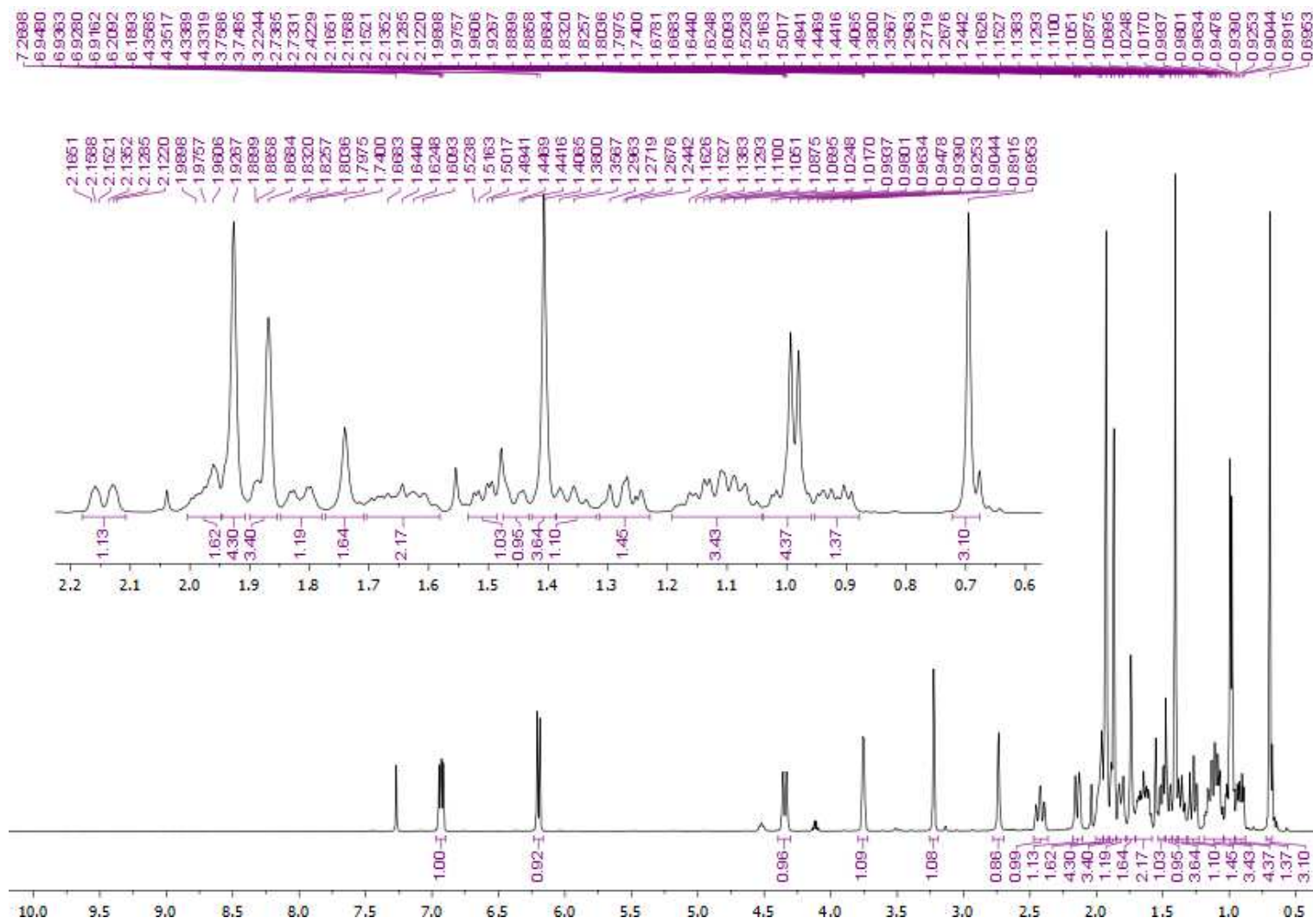
Figure S12. ¹H NMR (500.13 MHz) spectrum of 2, in CDCl₃.
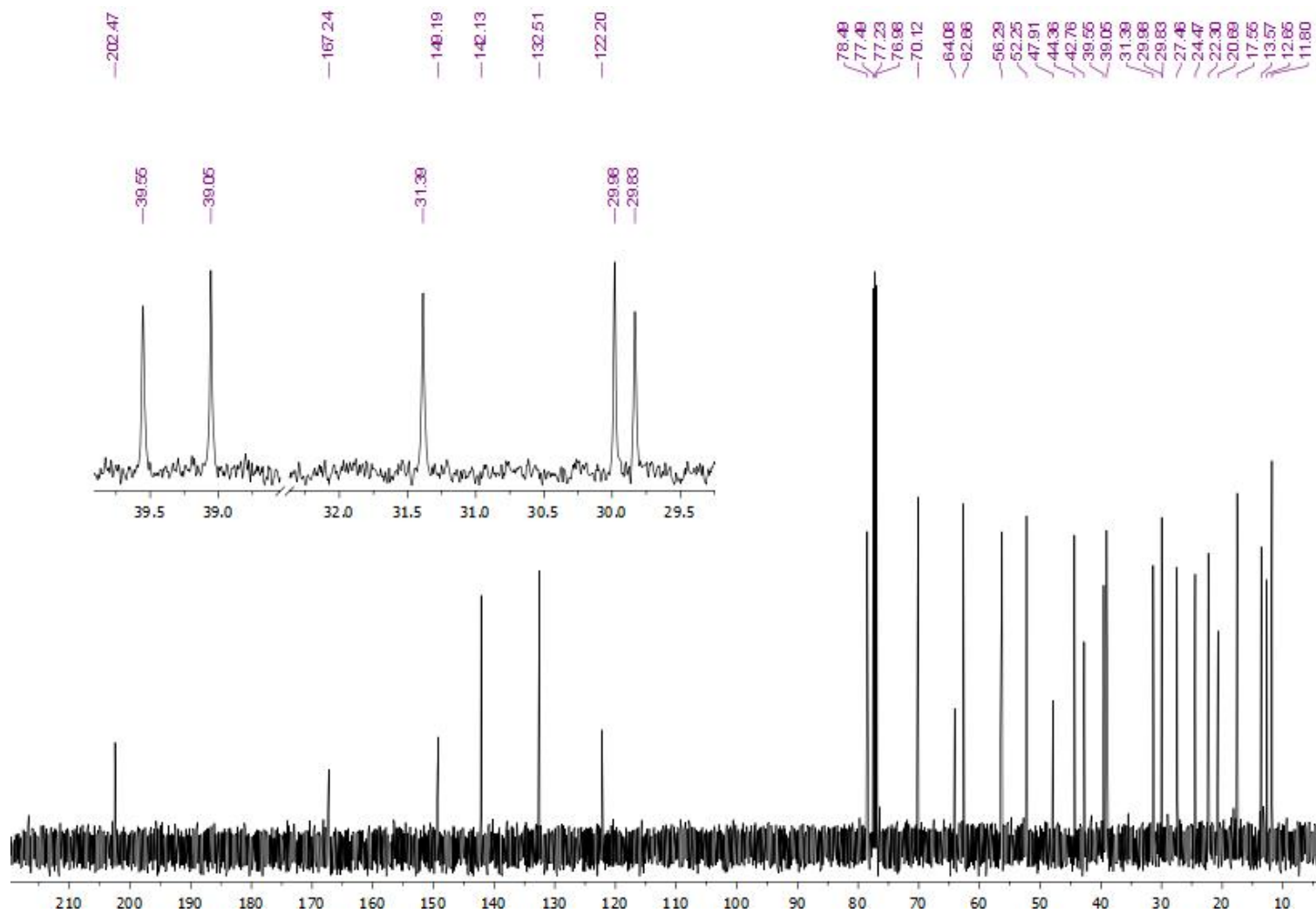
Figure S13. ^{13}C NMR (125.75 MHz) spectrum of 2, in CDCl$_3$.
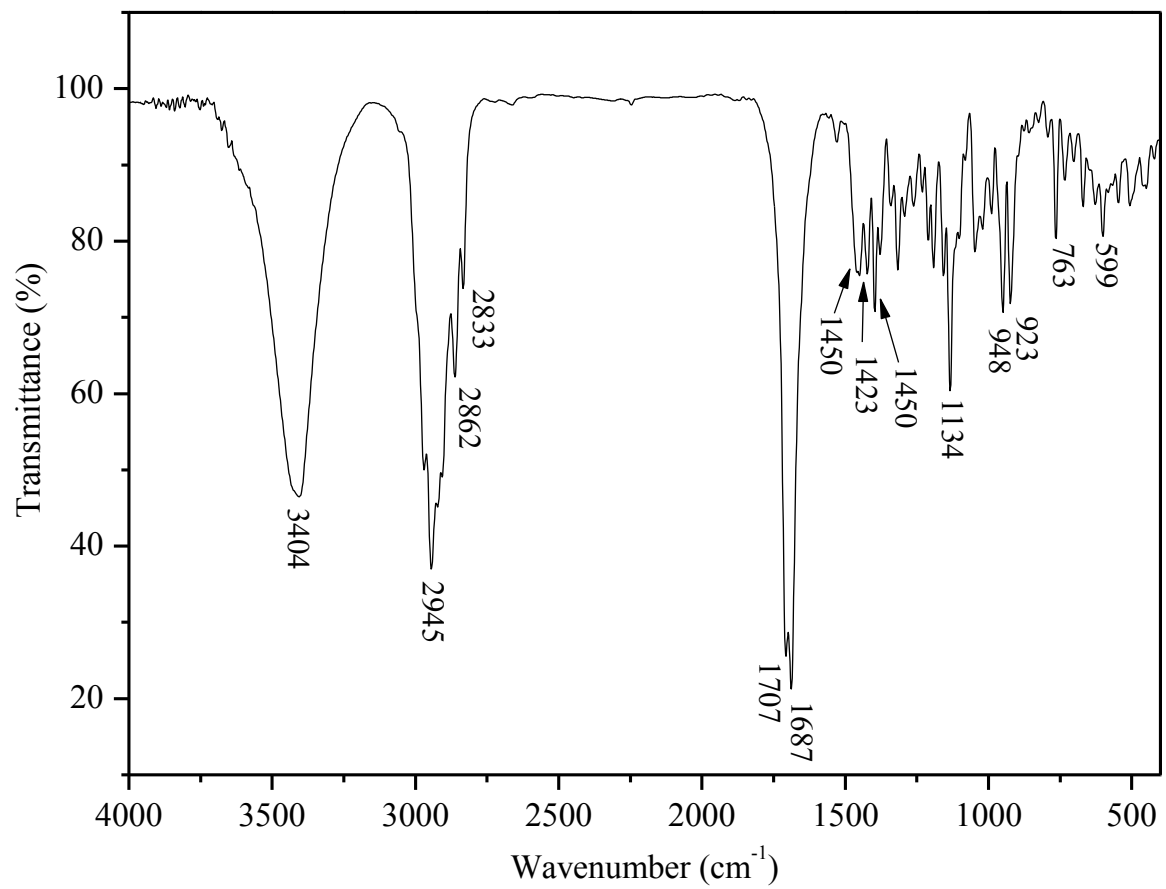
Figure S14. FTIR spectrum of **3**.
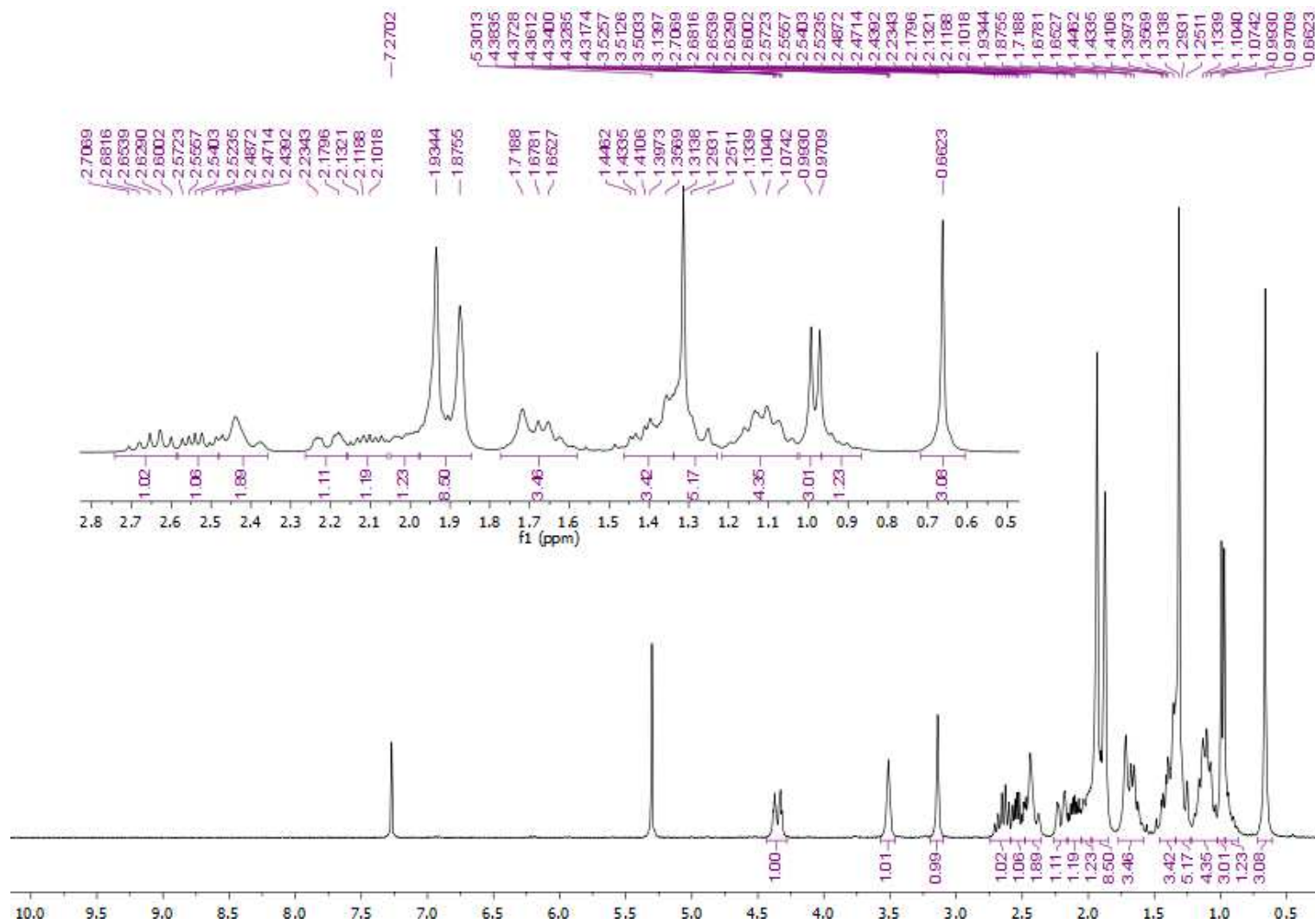
Figure S15. ¹H NMR (300.13 MHz) spectrum of **3**, in CDCl₃.
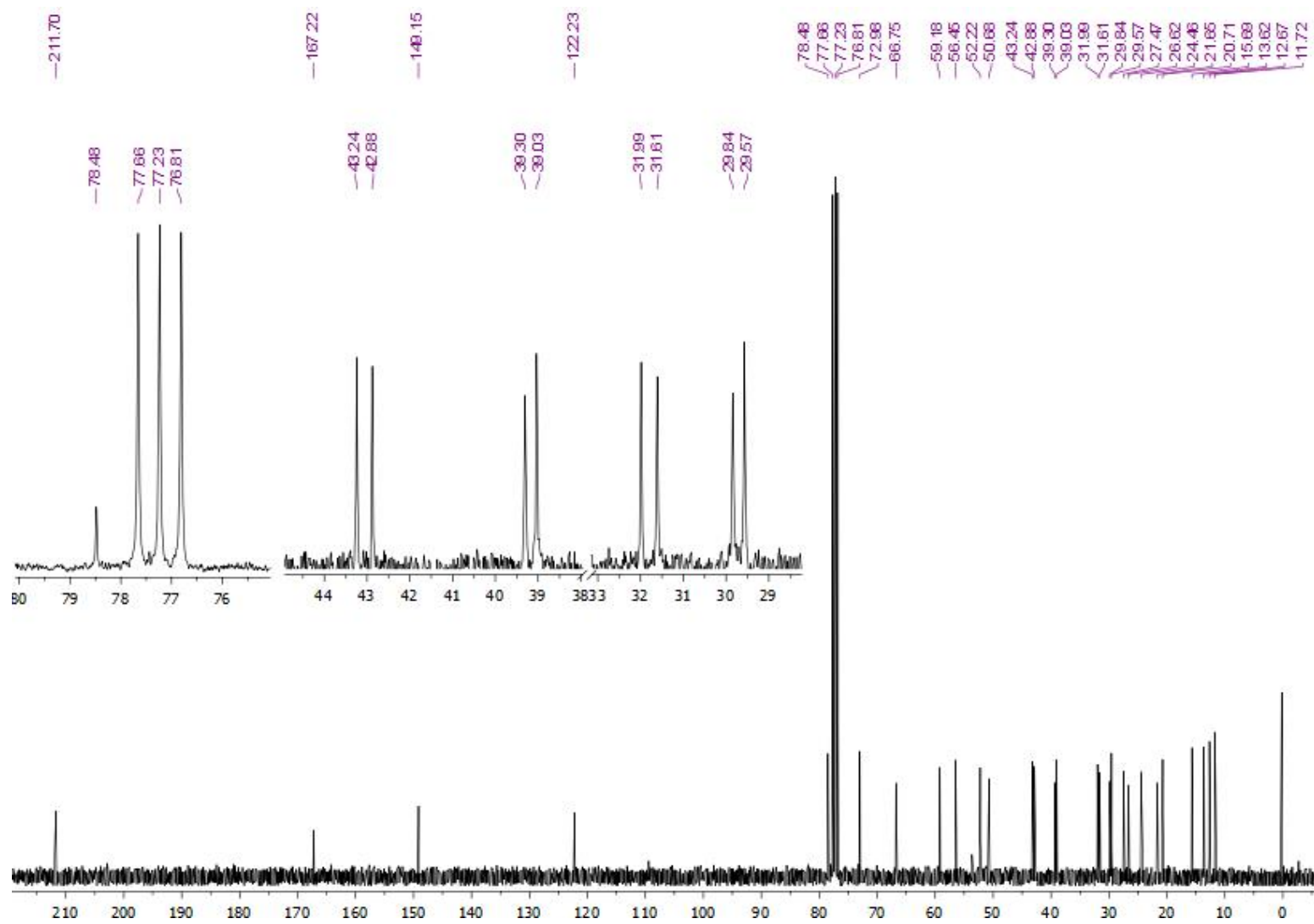
Figure S16. ^{13}C NMR (75.47 MHz) spectrum of **3**, in CDCl$_3$.

CAPÍTULO 3

Withanolides from the leaves of *Athenaea velutina* Sendt. with activity in different human cancer cell lines
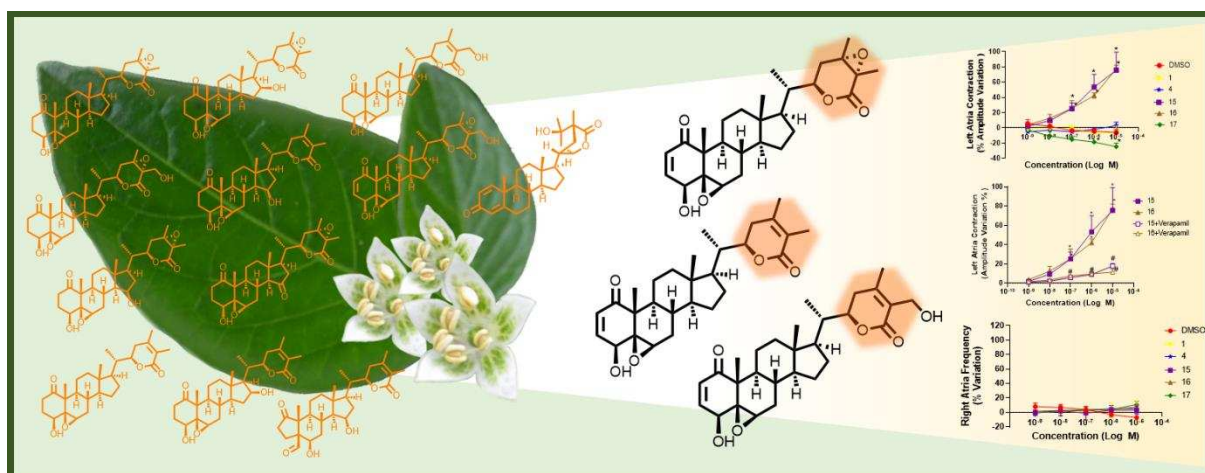
Bioactive withanolides from the leaves of *Athenaea velutina* Sendt.

Késya Amanda Dantas Rocha[a], Edilberto Rocha Silveira[a], Tércio de Freitas Paulo[a], Alejandro Pedro Ayala[b], Bruno Marques Soares[c], Sarah Sant'Anna Maranhão[c], Cláudia do Ó Pessoa[c], Iury Araújo Paz[d], Maria Lidia Barroso Rodrigues[d], Nilberto Robson Falcão do Nascimento[d], Kirley Marques Canuto[e], Otília Deusdenia Loiola Pessoa[a,*]

[a]Departamento de Química Orgânica e Inorgânica, Centro de Ciências, Universidade Federal do Ceará, 60021-970, Fortaleza-CE, Brazil

[b]Departamento de Física, Centro de Ciências, Universidade Federal do Ceará, 60440-900, Fortaleza-CE, Brazil.

[c]Núcleo de Pesquisa e Desenvolvimento de Medicamentos, Faculdade de Medicina, Universidade Federal do Ceará, 60430-270, Fortaleza-CE, Brazil.

[d]Instituto Superior de Ciências Biomédicas, Universidade Estadual do Ceará, 60714-903, Fortaleza, Ceará-Brazil.

[e]Embrapa Agroindústria Tropical, 60511-110, Fortaleza-CE, Brazil

* Corresponding author: opessoa@ufc.br

ABSTRACT

Withanolides are a substantial bio-diverse group of naturally occurring steroidal lactones. Herein, ten still undescribed withanolides (**1 - 10**), along with the knowns withaferin A (**11**), 2,3-dihidrowithaferin A (**12**), vomifoliol (**13**), and the *N-trans-p*-coumaroyltyramine were isolated from the hexane/EtOAc 1:1 leaf extract of *Athenaea velutina* (Solanaceaee). The structures of the withanolides were elucidated by an extensive analysis of their spectroscopic data: NMR, HRESIMS, single-crystal X-ray diffraction, and ECD calculations. The antiproliferative properties of the withanolides were evaluated against the human cancer cell lines: central nervous system (SNB-19), prostate (PC-3), colon (HCT-116), and leukemia (HL-60), and a *murine* fibroblast-like cell (L929). Withanolides **15** and **16** exhibited cytotoxic activity for all cancer cells, while **2** and **6** were selectively more cytotoxic to HL-60 cells. In addition, the withanolides were evaluated in guinea-pig cardiac tissues. Compounds **15** and **16** were shown to have cardiotonic activity devoid of a positive chronotropic effect which is a good pharmacological profile for an inotrope agent.

Keywords: *Athenaea velutina*, Solanaceaee, Withanolides, Withaferin, Cytotoxic activity, Cardiotonic Activity.

1. Introduction

Withanolides are an ancient class of steroidal lactones produced particularly by plants of the Solanaceaee family [1]. Despite the isolation of hundred of these compounds, the high degree of functions susceptible to oxidation, reduction, cyclization, rearrangement, and even Michael addition reactions can yield a larger number of new compounds with extraordinary structures [2]. In this regard, it is worth highlighting that the C-22 and C-26 carbon can be oxidized to form a δ-lactone, or less commonly, a γ-lactone with C-23 [3]. Following these biosynthetic pathways, several classes of these compounds such as withaphysalins, physalins, acnistins, neophysalins, withajardins, withametelins, norbornane-type withanolides, sativolides, spiranoid, subtriflora and taccalonolide δ-lactones, and $14\alpha,20\alpha$-epoxide, ring-D and ring-A aromatic withanolides are produced [4].

The first withanolide, withaferin A (WA), was isolated from *Withania somnifera* (Solanaceaee), an Indian medicinal plant popularly known as "Ashwagandha" or "Indian ginseng", commonly used in the Ayurvedic system for over 3,000 years [5,6]. Since its discovery (1965), WA has been the subject of numerous pharmacological studies and, currently, it is considered a highly promising molecule in the field of oncology [7]. Furthermore, *in vivo* studies showed that WA prevented high-fat diet-induced obesity [8], and improved memory deficits in the scopolamine-induced mice model of Alzheimer's disease [9]. Moreover, showed a high potential to treat or prevent the spread of COVID-19 [10,11].

The genus *Athenaea* (Sendtn.), also belonging to the Solanaceaee family, is represented by 14 exclusively neotropical species, which, almost entirely, are endemic to Brazil [12]. *Athenaea velutina* (Sendtn.) D'Arcy is a shrub with geographic distribution in the northeast, southeast, and midwest regions [13]. Recent studies report on the isolation of withanolides and their potential apoptosis-inducing activity in B16F10 murine melanoma cells, for a fraction enriched in these compounds, as well as antimicrobial activity for leaf extracts [14-16]. As part of our

interest in withanolide-producing plants we have investigated the hexane/EtOAc 1:1 leaf extract of *A. velutina* from which were isolated anti-inflammatory withajardins and withanolides with inhibitory properties against SARS-CoV-2 M^{pro} [4,17]. Herein, the isolation of twelve withanolides derivatives including ten new ones (**1** – **10**) is described (Fig. 1). Since WA exhibits prominent anticancer activity [7] and prevents myocardial ischemia [18]. The antiproliferative properties against cancer cell lines and the effects in guinea-pig cardiac tissues of the withanolides of *A. vetlutina* were evaluated.
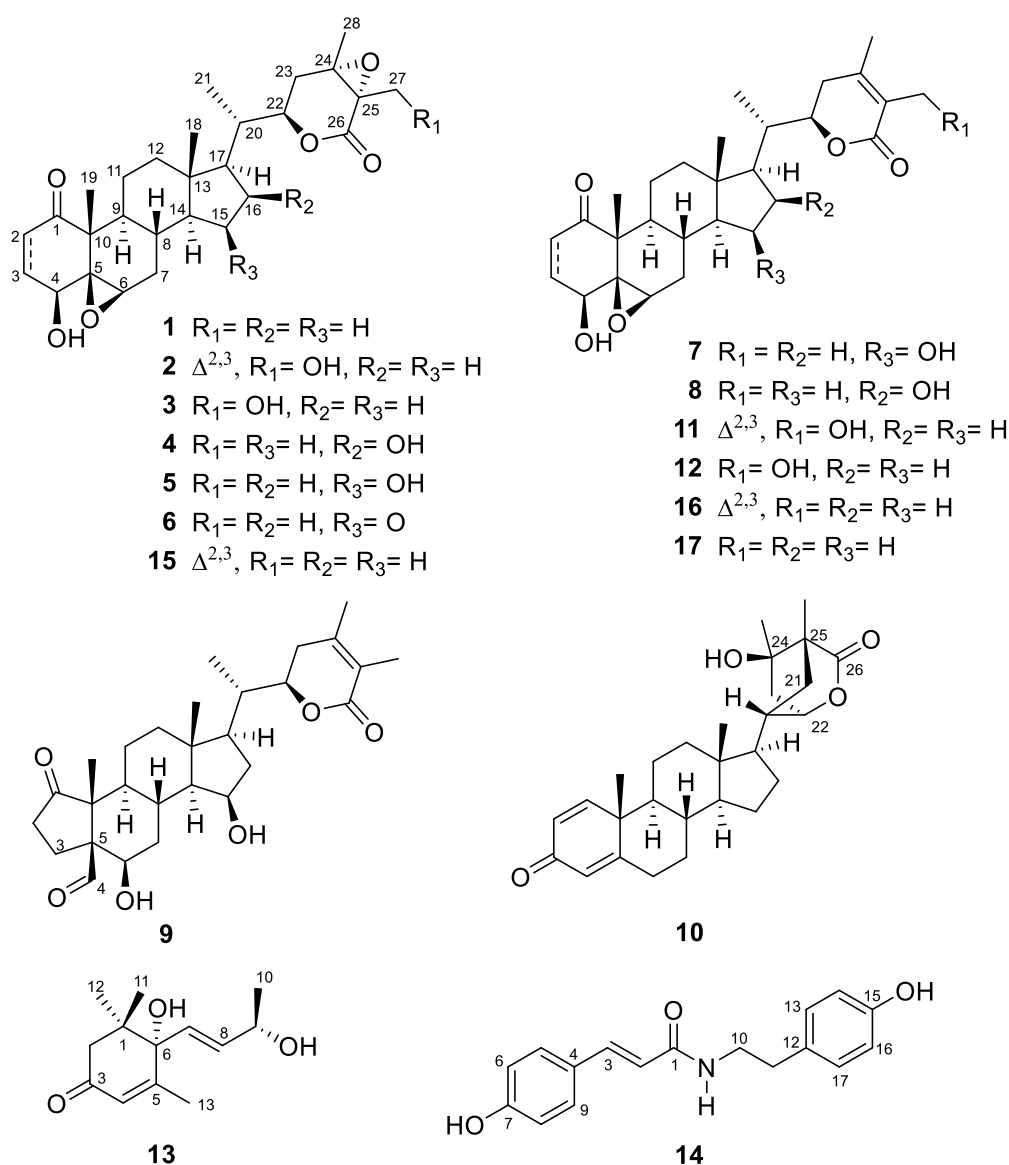
Fig. 1. Structures of all compounds isolated from *A. velutina* leaf extrac.

2. Results and discussion

The phytochemical investigation of the hexane/EtOAc 1:1 leaf extract of *A. vetutina* leads to the isolation of fourteen compounds. The structures of all compounds were elucidated by interpretation of their 1D and 2D NMR, infrared, and mass spectrometry data, while the absolute configuration was performed by X-ray diffraction and circular dichroism (CD) analyses. Thus, ten previously unreported withanolides (**1−10**) are being described, in addition to the known WA (**11**) [19], 2,3-dihydrowithaferin A (**12**) [19], vomifoliol (**13**) [20] and *N-trans-p*-coumaroyltyramine (**14**) [21] (Fig. 1).

Withanolide **1** was obtained as colorless prism crystals. Its molecular formula was assigned, by HRESIMS, as $C_{28}H_{40}O_6$ (nine indices of hydrogen deficiency) based on the sodium adduct $[M + Na]^+$ ion peak at *m/z* 495.2738. Its IR spectrum showed absorption bands for OH (3439 cm^{-1}) and C=O of non-conjugated lactone and ketone at 1730 and 1685 cm^{-1}, respectively. Analysis of the ^1H and ^{13}C, DEPT 135º, and HSQC NMR spectra (Tables 1 and 2) revealed signals for the ketone at δ_C 211.5 (C-1) and the lactone at δ_C 170.1 (C-26), corroborating with the IR spectrum, and indicating that the ring-A and the δ-lactone moiety of the withanolide **1** are not conjugated. The presence of six oxygenated carbon atoms distributed into three non-protonated carbons [δ_C 66.8 (C-5), 62.7 (C-24), and 59.3(C-25)] and three methines [δ_H/δ_C 4.53/76.3 (C-22), 3.52/72.8 (C-4), and 3.15/58.6 (C-6)] indicated a hydroxy at C-4 and two epoxy moieties at C-5/C-6 and C-24/C-25. HMBC correlations of H$_2$-2 (δ_H 2.67/2.54) with C-1, C-4, C-5, C-10 (δ_C 50.5), and C-3 (δ_C 26.3), as well as of H-4 with C-5, C-6 C-10 and C-2 (δ_C 31.6) what confirmed the 1-oxo-2,3-dihydro-4-hydroxy-5,6-epoxy moiety of the A/B rings. Likewise, the HMBC correlations of H-22 with C-24, H$_2$-23 (δ_H 2.00), H$_3$-27 (δ_H 1.56), and H$_3$-28 (δ_H 1.49) with both C-24 and C-25; and of H$_3$-27 with C-26 confirm a 24,25-dimethyl-24,25-epoxy-δ-lactone moiety (Fig. 2). Although these features are very common in withanolides, both moieties to the same molecule originate a new withanolide derivative whose absolute

configuration of their stereogenic centers was deduced by single-crystal X-ray diffraction analysis as shown in Fig. 3. Thus, the structure of **1** was established as (4*S*,5*R*,6*R*,8*S*,9*S*,10*R*,13*S*,14*S*,17*R*,20*S*,22*R*,24*S*,25*S*)-4*β*-hydroxy-5*β*,6*β*;24*α*,25*α*-diepoxy-1-oxowithanolide, that was simpleffied to 27-dehydroxy-2,3-dihydro-24,25-epoxywithaferin A.

Withanolide **2**, colorless crystals, had its molecular formula $C_{28}H_{38}O_7$ deduced from the [M + Na]$^+$ at *m/z* 509.2559 by HRESIMS. Analyses of the ^1H and ^{13}C NMR spectra indicated a similar structure to that of **1**. The proton signals at δ_H/δ_C 6.17/132.5 (C-2) and 6.92/142.3 (C-3), corresponding to a carbon-carbon double bond, and a shielded carbonyl carbon at δ_C 202.4 (C-1) indicated an *α,β*-unsaturated ketone system as confirmed by the HMBC correlation at H-3 and C-1. In the HSQC spectrum, the correlations of both diastereotopic protons δ_H 4.11 and 3.76 with δ_C 60.2 (C-27), as well as the HMBC correlations of these protons with the *δ*-lactone carboxyl at δ_C 170.2 (C-26) indicated the oxidation of the methyl group at C-25 to an oxymethylene (Fig. 2). The unequivocal structure of **2** was confirmed by single-crystal X-ray diffraction analysis (Fig. 3) and its structure was established as (4*S*,5*R*,6*R*,8*S*,9*S*,10*R*,13*S*,14*S*,17*R*,20*S*,22*R*,24*S*,25*S*)-4*β*,27-dihydroxy-5*β*,6*β*;24*α*,25*α*-diepoxy-1-oxowith-2-enolide, designated as 24,25-epoxywithaferin A.

The molecular formula $C_{28}H_{40}O_7$ of withanolide **3** was deduced based on the sodium adduct [M + Na]$^+$ at *m/z* 511.2654 having just one extra oxygen than **1**. Analyses of the ^1H and ^{13}C NMR spectra indicated that **3** was a 2,3-dihydro derivative of **2**, in agreement with the carbonyl group at the aliphatic ketone at δ_C 211.6 (C-1), like compound **1**, as confirmed by the HMBC correlations of the α-methylene H$_2$-2 (δ_H 2.63/2.54) with C-1 and C-4 (δ_C 72.9). The absolute configuration of **3** was suggested based on analysis of experimental and TD-DFT calculated circular dichroism (CD). The experimental CD spectrum exhibited a negative Cotton effect at 288 and 232 nm and is quite similar to that obtained for **1** (Fig. 4). Thus, the structure of **3** was

established as (4*S*,5*R*,6*R*,8*S*,9*S*,10*R*,13*S*,14*S*,17*R*,20*S*,22*R*,24*S*,25*S*)-4*β*,27-dihydroxy-5*β*,6*β*;24*α*,25*α*-diepoxy-1-oxowithanolide, desigated as 2,3-dihydro-24,25-epoxywithaferin A.

Withanolide **4** was isolated as colorless prism crystals. Its molecular formula $C_{28}H_{40}O_7$ was assigned from the sodium adduct [M + Na]$^+$ at *m/z* 511.2668 by HRESIMS. Comparison of its ^{1}H and ^{13}C NMR data with those of **1**, suggested the oxidation of one methylene carbon due to the appearance of an extra oxymethyne carbon at δ_C 70.4 correlated with the proton signal at δ_H 4.39 (brs). The unequivocal position of the hydroxy group at C-16 was assigned due to the correlation between δ_H 4.38 (H-16) with δ_H 2.32 (H-15) and 1.10 (H-17) in the COSY spectrum. Comparing the chemical shifts of compounds **1** and **4**, the deshielding of both C-15 ($\Delta\delta_C$ 11.4) and C-17 ($\Delta\delta_C$ 5.4) in **4** is in accordance with the hydroxy *β*-effect, while C-14 and C-20 are shielded due to the *γ*-effect of $\Delta\delta_C$ -1.2 and -4.4, respectively. In agreement with the works of Wijeratne (2018) [22] and Nicolás (2015) [23], the chemical shift value of C-16 varies according to the position of the -OH. For instance, when the HO-group is *β*-oriented, C-16 appears around δ_C 71.2 [22], while in an α orientation, it is shielded to about δ_C 76.5.[23] Therefore, the chemical shift at δ_C 70.4 to **4** supports a *β*-orientation to the 16-OH, also corroborated by the NOESY spectrum, through the dipole-dipole interactions of H-16 with H-22 (δ_H 5.49) and H-22 with H-17. The final structure of **4**, including its stereochemical features was depicted as the (4*S*,5*R*,6*R*,8*S*,9*S*,10*R*,13*S*,14*S*,16*S*,17*R*,20*S*,22*R*,24*S*,25*S*)-4*β*,16*β*-dihydroxy-5*β*,6*β*;24*α*,25*α*-diepoxy-1-oxowithanolide assigned by single-crystal X-ray diffraction analysis (Fig. 2) which was denominated 27-dehydroxy-2,3-dihydro-24,25-epoxy-16-hydroxywithaferin A.

Withanolide **5** was isolated as a colorless block crystal and its molecular formula $C_{28}H_{40}O_7$ was identical to that of **4**. A comparison of their NMR data showed differences in the chemical shift values for C-13 to C-17 [**4**: δ_C 70.4 (C-16), 57.4 (C-17), 55.0 (C-14), 43.1 (C-13) and 38.6 (C-15) and **5**: δ_C 69.8 (C-15), 60.9 (C-14), 52.4 (C-17), 42.5 (C-13), 39.9 (C-16)] suggesting a

change in the HO-position. In the COSY spectrum, the coupling of the oxymethine proton at δ_H 4.20 (H-15) with δ_H 2.26 (H-16) and 0.79 (H-14) indicates the hydroxyl group at C-15. Single-crystal X-ray diffraction analysis (Fig. 2) confirmed the structure of **5** as (4*S*,5*R*,6*R*,8*S*,9*S*,10*R*,13*S*,14*S*,15*R*,17*R*,20*S*,22*R*,24*S*,25*S*)-4β,15β-dihydroxy-5β,6β;24α,25α-diepoxy-1-oxowithanolide, denominated of 27-dehydroxy-2,3-dihydro-24,25-epoxy-15-hydroxywithaferin A

The molecular formula $C_{28}H_{38}O_7$ of withanolide **6** was deduced based on the $[M + Na]^+$ at *m/z* 509.2523 by HRESIMS. Analyses of the ^{13}C NMR spectra indicated this is an oxo derivative of **5**, in agreement with the extra carbonyl group at δ_C 213.2. The carbonyl position was confirmed by the HMBC correlations of H-14 (δ_H 1.61) and H$_2$-16 (δ_H 2.36/1.91) with C-15 (δ_C 213.2). The absolute configuration of **6** was suggested based on analysis of experimental and TD-DFT calculated circular dichroism (CD). Similar to **1** and **3**, the CD spectrum of **6** has exhibited a negative Cotton effect at 288 and 232 nm. (Fig. 4). Thus, the structure of **6** was established as (4*S*,5*R*,6*R*,8*S*,9*S*,10*R*,13*S*,14*S*,17*R*,20*S*,22*R*,24*S*,25*S*)-4β-hidroxy-5β,6β,24α,25α-diepoxy-1,15-dioxowithanolide, designated as 27-dehydroxy-2,3-dihydro-24,25-epoxy-15-oxowithaferin A.

Both withanolides **7** and **8** were obtained as colorless plate crystals with the molecular formulas assigned by HRESIMS as $C_{28}H_{40}O_6$. Their ^1H and ^{13}C NMR, DEPT 135° and HSQC spectra showed similar chemical shifts, but, were different from previously commented withanolides, exhibited the carbon signals of an unsaturated δ-lactone [**7**: δ_C 166.6 (C-26), 148.3 (C-24) and 122.7(C-25); **8**: 167.1 (C-26), 149.8 (C-24) and 122.2 (C-25)]. The difference between **7** and **8** was related to the position of the hydroxyl groups. To withanolide **7**, the hydroxyl group was positioned at C-15 (δ_H/δ_C 4.20/70.2) due to the vicinal coupling for the oxymethine H-15 with δ_H 2.26 (H-16) and 0.83 (H-14) through the COSY spectrum, whereas for **8**, the hydroxyl group was positioned at C-16 (δ_H/δ_C 4.45/70.7) based on the coupling of the

oxymethine proton H-16 with δ_H 2.37 (H-15) and 1.11 (H-17). The unequivocal structures of **7** and **8** were elucidated by analyses of the NMR and the single-crystal X-ray diffraction spectra (Fig. 2). Thus, withanolide **7** was designated as the (4*S*,5*R*,6*R*,8*S*,9*S*,10*R*,13*S*,14*S*,15*R*,17*R*,20*S*,22*R*)-4*β*,15*β*-dihydroxy-5*β*,6*β*-epoxy-1-oxowith-24-enolide named as 27-dehydroxy-2,3-dihydro-15-hydroxywithaferin A, while the structure of **8** was defined as the (4*S*,5*R*,6*R*,8*S*,9*S*,10*R*,13*S*,14*S*,16*S*,17*R*,20*S*,22*R*)-4*β*,16*β*-dihydroxy-5*β*,6*β*-epoxy-1-oxowith-24-enolide or 27-dehydroxy-2,3-dihydro-16-hydroxywithaferin A.

Withanolide **9** was determined to have the molecular formula $C_{28}H_{40}O_6$ based on the sodium adduct $[M + H - H_2CO]^+$ at *m/z* 443.2796 in the HRESIMS. A detailed analysis of the 1D and 2D NMR spectra revealed that **9** and **7** shared a partial structure, however, with significant differences related to the proton and carbon chemical shifts related to the A ring, like the signals for an aldehyde δ_H/δ_C 9.65/204.7 (C-4) and a more deshielded ketone carbonyl at δ_C 216.1 (C-1), in addition to a cyclopentanone bearing a formyl aldehyde moiety [δ_C 216.1 (C-1), 204.7 (C-4), 68.2 (C-6), 61.1 (C-5), 33.6 (C-2) and 22.8 (C-3)] that were supported by the HMBC proton correlations of the aldehyde (H-4), the diastereotopic *α*-methylene at δ_H 2.14; 1.52 (H$_2$-2) and the methyl at δ_H 1.19 (H$_3$-19) all with the quaternary C-5 (δ_C 61.1), indicating the ring A contraction of the withanolide skeleton [24]. The position of the hydroxy groups at C-6 and C-15 was assigned due to the spin-spin correlation of H-6 and H-7 (δ_H 2.49) and between H-16 (δ_H 2.27) and H-14 (0.92) with δ_H 4.26 (H-15) in the COSY spectrum. The dipolar coupling of H-4 with H$_3$-19 and H-6 observed in the NOESY spectrum, indicated the *β*-orientation of both 4-formyl and the 6-hydroxyl moieties. Furthermore, as in **7** and **8**, analysis of the experimental CD shows a negative Cotton effect at 289 nm, while a positive effect is observed at 252 and ca. 200 nm (Fig. 4). Consequently, the structure of **9** as the (5*R*,6*R*,8*S*,9*S*,10*R*,13*S*,15*R*,14*S*,17*R*,20*S*,22*R*)-4*β*-formyl-6*β*,15*β*-dihidroxy-1-oxowith-24-enolide named as withalutin B.

The molecular formula $C_{28}H_{38}O_4$ of the withanolide **10**, isolated as an amorphous solid, was defined based on the sodium adduct $[M + H]^+$ *m/z* 439.2843 in the HRESIMS. Analysis of ^{1}H and ^{13}C NMR data, including the DEPT and HSQC spectra revealed signals for a withanolide, but with different characteristics of the withanolides determined so far. The ^{1}H NMR spectrum exhibited signals for three olefinic protons at δ_H 7.06 (d, *J* = 10 Hz, H-1), 6.25 (d, *J* = 10 Hz, H-2), and 6.10 (s, H-4) which, in the HSQC spectrum, were correlated with the carbons δ_C 156.1 (C-1), 127.4 (C-2), and 124.1 (C-4), respectively. The *J* value of 10 Hz for H_1/H_2 suggested a *cis*-double bond. The ^{13}C NMR spectrum displayed seven non-protonated carbons, including signals of a conjugated ketone carbonyl δ_C 186.6 (C-3) and an olefinic carbon 169.5 (C-5). To attend to the proton and carbon chemical shift features, a cross-conjugated system involving the ketone carbonyl and both double bonds was assigned, which was corroborated by the HMBC correlations of H-1 with C-3, C-5, and C-10 (δ_C 43.8), of H-2 with C-4 and C-10, as well as of H-4 with C-2, C-10, and C-6 (δ_C 33.1) (Fig. 2). In addition, differently of compounds **1 – 9**, withanolide **10** did not show the methyl group C-21 attached to C-20 (δ_C 39.3), but a methylene group (δ_H/δ_C 2.13; 1.50/31.2) instead. Correlations of H_2-21 and H_3-27 (δ_H1.14) with C-26, C-24 (δ_C 72.0), and C-25 (δ_C 47.5) showed that the methylene group (C-21) is directly bonded to the quaternary carbon (C-25), forming a bicyclo ring system with the δ-lactone, what is characteristic of the withajardins.[4] The CD spectrum of **10** exhibited a negative Cotton effect at 260 and 204 nm and a positive one at 248 nm (Fig. 4). The structure of **10** as (17*R*,20*S*,22*R*,24*R*,25*R*)-24β-hydroxy-21,25-cycloergost-1,4-dien-3-one which was denominated withajardin N.

All the withanolides **1** to **12**, including **15**, **16**, and **17**, recently reported from the plant [16], were evaluated against the cell lines HL-60 (leukemia), HCT-116 (colon), PC-3 (prostate), SNB-19 (glioblastoma), and the non-tumorous murine cell line L929 (murine fibroblast) (Table

3). In addition, the carditonic activity of the major withanolides isolated was evaluated for their effects on the isolated cardiac tissue of the guinea pig.

Regarding to the cytotoxic activity, withanolides **15** and **16** showed potent antitumor action in all cancer cell lines, including for the non-tumor cell line L929, with IC_{50} values ranging from 0.24 to 2.10 µM. Thus, a non-selective cytotoxic activity is observed for these compounds. Whereas compounds **2** and **6** were particularly active only on HL-60 and HCT-116. On these two cells, the IC_{50} values for **2** were 0.94 and 1.93 µM, respectively, and an IC_{50} of 4.01 µM for L929, indicating that the compound is at least two times more selective for tumor cells than for non-tumor cells. However, **6** showed IC_{50} values of 0.45 and 2.01 µM without any cytotoxic activity against L929 showing even more selectivity for tumor cells. When comparing compounds **2**, **6**, and **15** that are from the same series, the presence of oxygen in R_3 position concerning **6**, and hydroxyl in R_1 position in **2** (Fig. 1)**,** give these two compounds more selectivity for tumor cells. Recent studies showed others three withanolides isolated from *Athenaea velutina* leaves exhibited reduced cancer cell viability with IC_{50} values ranging from 1.52 to 5.39 µM against B16F10 cells [16].

The other compounds exhibited low or no activity when compared to WA (**11**), which was used as a positive control. In view of the results, withanolide **6** is an interesting candidate for further studies related to its mechanism of action.

Withanolides **1**, **4**, **15**, **16**, and **17**, those isolated in major amounts, were evaluated for their potential inotropic activity in the electrically driven left atria of guinea pigs or potential chronotropic activity in the right atria (Fig. 5**A**, **B**, and **C**). Compounds **15** and **16** showed positive inotropic activity both increasing left atria force by 2-fold with EC_{50} of 0.8 (0.3-1.9 mM) and 1.3 (0.7-2.6 mM), respectively. In turn, compounds **1**, **4**, and **17** were devoid of positive inotropic activity. None of the compounds changed the frequency of spontaneous firing of the sinoatrial pacemaker and were therefore all devoid of chronotropic activity. A positive

inotropism that is not associated with increased cardiac frequency is a pharmacologically desired property because the increased tension is not associated with a great increase in oxygen demand. The inotropic activity induced by both withanolides **15** and **16** is likely dependent on increased calcium currents through L-type voltage-dependent calcium channels.
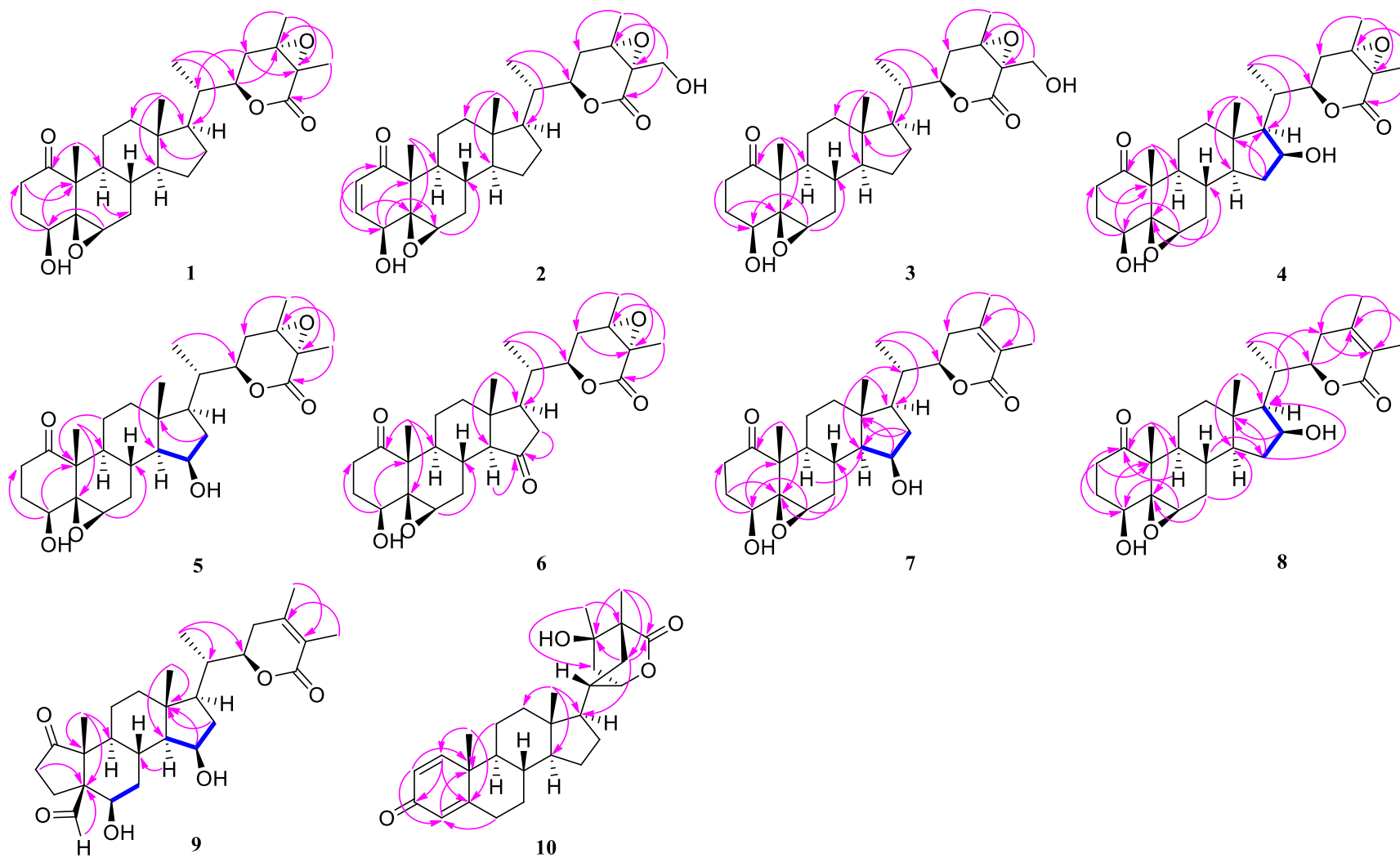
Fig. 2. HMBC ( ) and COSY ( ) the withanolides **1−10**.
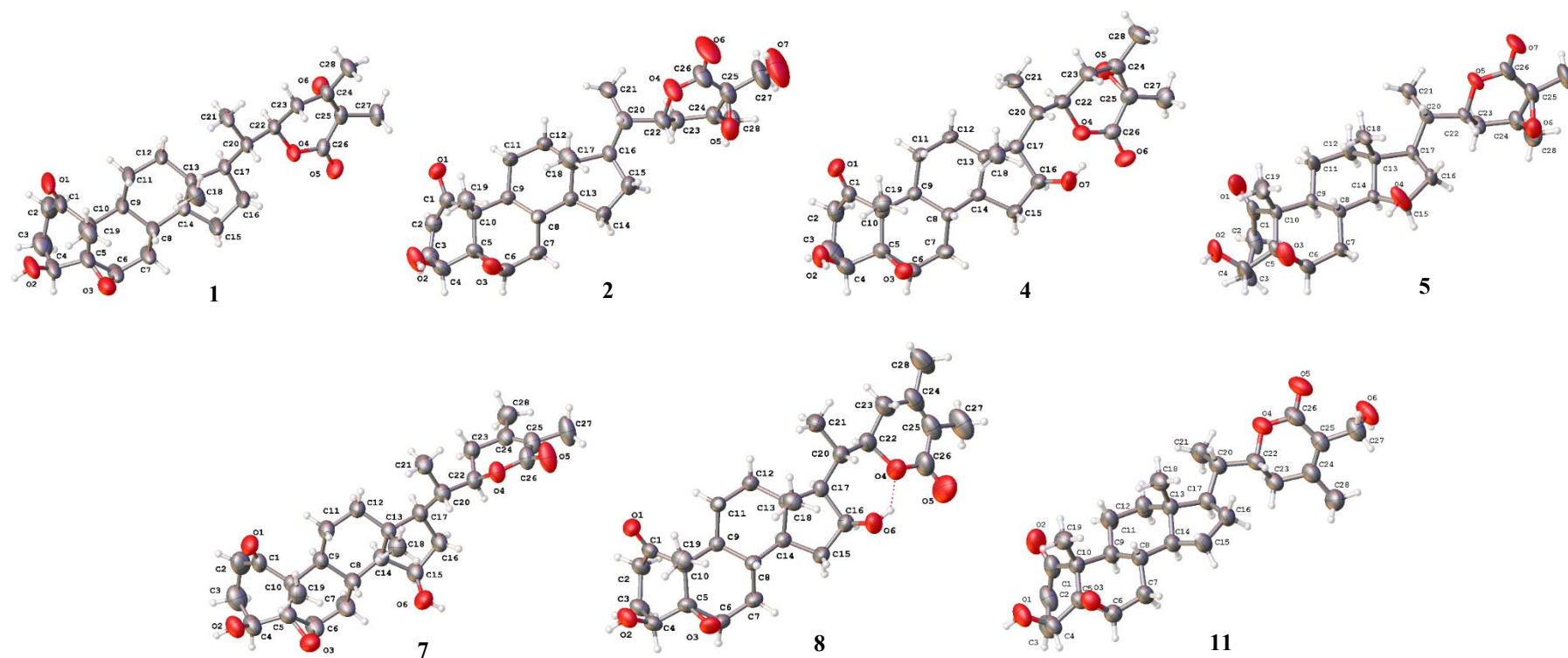
Fig. 3. X-ray ORTEP drawing of the withanolides **1-2**, **4-5**, **7-8** and **11**
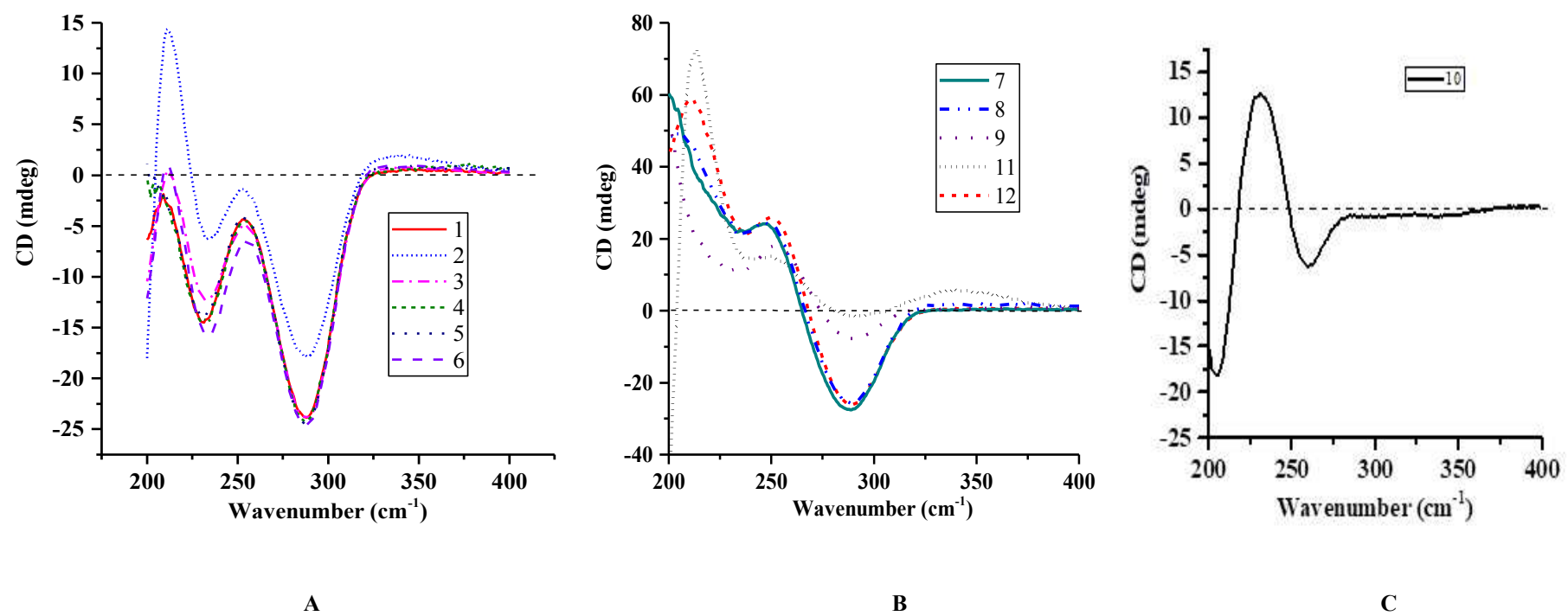
Fig. 4. Experimental CD spectra of **1-6** (**A**), **7-9**, **11**, and **12** (**B**) and of **10** (**C**), in CH₃O

3. Experimental section

General Experimental Procedures

Circular dichroism (CD) measurements were carried out on a Jasco J-815 spectropolarimeter (JASCO, Japan). CD spectra were acquired over a range of 200 to 400 nm in a quartz cuvette with a pathlength of 1 mm, at room temperature. The spectra were recorded with a scan speed of 100 nm/min, in 1.0 nm increments. The samples were dissolved in methanol and all measurements were repeated at least 3 times. Melting points were recorded on a digital MQAPF-302. The Fourier transform infrared (FTIR) spectra were obtained on a Shimadzu IR-tracer-100. High-resolution mass spectra were recorded on a Waters Acquity UPLC system coupled to a quadrupole/time-of-flight (TOF) system (UPLC/Qtof MSE spectrometer) in the positive mode. The NMR spectra were performed either on a Bruker AVANCE DRX-500, operating at 500.13 MHz for ^{1}H, and 125.75 MHz for ^{13}C, or on a Bruker AVANCE DPX-300 operating at 300.13 MHz for ^{1}H and 75.48 MHz for ^{13}C. Chromatographic separations were performed by column chromatography on sílica gel 60 (0.063-0.200 mm - Merck) and/or flash sílica gel (40−75 μm - Merck) chromatography. Analytical TLC was carried out on precoated sílica gel 60 F−254 (200 μm) aluminum plates (Silicycle).

Pant Material

The leaves of *Athenaea velutina* were collected in "Pico Alto", Guaramiranga/Ceará, Brazil (S 04º 12.590', W 38º 58.244'), in January 2019, SisGen license number A5C2E09. A voucher specimen (EAC45010) is deposited at the Herbário Prisco Bezerra (EAC), Universidade Federal do Ceará, Brazil. The plant material was identified by Dr. Valéria Sampaio.

Extraction and Isolation.

The dried and powdered leaves of *A. velutina* (2.0 Kg) were extracted with hexane/ethyl acetate 1:1 (10 L, 3 x 24 h each) at room temperature. The solvent was removed by rotatory evaporation under reduced pressure yielding 95.0 g of extract. This extract was further fractionated using sílica gel (60.0 g) column chromatography by elution with hexane, hexane/EtOAc 2:1-1:1, EtOAc, EtOAc/MeOH 1:1, and MeOH) to provide nine fractions (A-I). Fraction F (8.3 g), eluted with hexane/EtOAc 1:1, was washed with EtOAc and the precipitate obtained (Fp 4,1 g) was subjected to further sílica gel (100.0 g) column chromatography by elution with CH_2Cl_2/acetone 5% to provide seven combined subfractions (FpA-FpG). Subfraction FpD (481.0 mg) was also subjected to sílica gel flash (50.0 g) column chromatography by elution with CH_2Cl_2/acetone 3% to yield compound **1** (59.5 mg). Fraction G (7.1 g), eluted with hexane/EtOAc 1:1, was subjected to the same procedures as fraction F. The precipitate obtained (Gp 2.0 g) was fractioned by sílica gel (100.0 g) column chromatography by elution with CH_2Cl_2/acetone 9:0,5-5:5 and acetone resulting in compound **2** (23.5 mg). Fraction G (5.1 g) was subjected to sílica gel (100.0 g) column chromatography by elution with hexane/EtOAc 8:2-2:8, EtOAc, and EtOAc/CH_3OH 8:2-5:5, to yield seven subfractions (GA-GG). Afterward, subfraction GD (995.0 mg) eluted with hexane/EtOAc 5:5, was further fractionated by sílica gel (30.0 g) column chromatography by elution with CH_2Cl_2/acetone 9:1-8:2, 1:1, and acetone, yielding six subfractions (GDA-GDF). The subfração GDD (103.3 mg) eluted with CH_2Cl_2/acetone 5%, was further fractionated by sílica gel (200.0 mg) column chromatography by elution with CH_2Cl_2/acetone 4%, yielding five subfractions (GDDA-GDDE). Compound **10** (4.1 mg, tR = 8.74 min) was obtained from subfraction GDDB (23.1 mg) by C18 HPLC purification using H_2O(0,005%TFA)/ACN [35:65 (v/v) for 0−10 min] as the mobile phase. Meanwhile, the subfraction GDF (26.5 mg) was subjected to sílica gel (13.0 g) column chromatography, by elution with CH_2Cl_2/acetone 9:1,

resulting in compound **13** (8.5 mg). The subfraction GF (684.0 mg), eluted with EtOAc, was separated into seven subfractions (GFA-GFG) through sílica gel (30.0 g) column chromatography using CH_2Cl_2/acetone 9:1-8:2, 6:3, 5:5, and acetone, as eluents. Later on, the subfraction GFC (94.2 mg) by elution with CH_2Cl_2/acetone 9:1, was purified by sílica gel (30.0 g) column chromatography by elution with a CH_2Cl_2/acetone 8%, yielding three subfractions (GFCA-GFCC). The subfraction GFCB (35.6 mg) was subjected to sílica gel column chromatography (15.0 g), and eluted with CH_2Cl_2/isopropanol 2%, resulting in compound **3** (6.0 mg). The fraction H (13.4 g), eluted with EtOAc, gave seven subfractions (HA-HG) after being fractionated on a sílica gel column (100.0 g) using the following eluents: CH_2Cl_2/EtOAc 8:2-2:8, EtOAc, EtOAc/CH_3OH 9:1-5:5. Next, the subfraction HC (4.9 g) eluted with CH_2Cl_2/AcOEt 8:2, was further fractionated through sílica gel (120.0 g) column chromatography eluted with $CHCl_3$/MeOH 5% to yield six subfractions (HCA-HCF). The subfraction HCC (2.0 g) was further fractionated by sílica gel (80.0 g) column chromatography, eluting with hexane/EtOAc/isopropanol 6:3:1-4:5:1, yielding compounds **6** (96.0 mg) and **11** (240 mg). The subfraction HCD (1.2 g), a greenish precipitate, was washed with CH_2Cl_2 until colorless crystals of compound **4** (208.0 mg) were obtained. The subfraction HD (1.9 g), eluted with CH_2Cl_2/EtOAc 6:4, was once more fractionated again by sílica gel (60.0 g) column chromatography, eluted with CH_2Cl_2/isopropanol 5%, to yield six subfractions (HDA-HDF). The subfraction HDB (328.1 mg) was further fractionated by sílica gel (50.0 g) column chromatography, eluting with hexane/EtOAc/isopropanol 6:3:1-4:5:1, to yield compound **12** (50.0 mg). Posteriorly, the subfraction HDD (663.2 mg) was further fractionated by sílica gel (60.0 g) column chromatography, eluted with $CHCl_3$/isopropanol 3%, resulting in compound **5** (292.0 mg) and other three subfractions (HDDA-HDDC). The subfraction HDDB (108.2 mg) that was further fractionated by sílica gel (10.0 g) column chromatography, eluted with CH_2Cl_2/acetonitrile 7:3, yielded compound **8** (25.4 mg). The subfraction HDF (98.7 mg), a dark

precipitate, was washed with acetone until a light green powder, compound **14** (20.8 mg) was obtained. The Subfraction HF (2.2 g) eluted with EtOAc e EtOAc/MeOH 9:1, was further fractionated by sílica gel (80.0 g) column chromatography, eluted with CH_2Cl_2/acetonitrile 7:3, to yield six subfractions (HFA- HFF). The Subfraction HFE (512.9 mg) was further fractionated by sílica gel (40.0 g) column chromatography, eluted with CH_2Cl_2/EtOAc/isopropanol 8:1,5:0,5, to yield five subfractions (HFEA- HFEE). The Subfraction HFEC (112.9 mg) was further fractionated by sílica gel (20.0 g) column chromatography eluted with CH_2Cl_2/acetonitrile 7:3, to yield compound **7** (42.0 mg). Meanwhile, the subfraction HFED (69.3 mg) was separated into four subfractions (HFEDA-HFEDD) through sílica gel (8.0 g) column chromatography using CH_2Cl_2/acetonitrile 7:3 as eluent. Compound **9** (12.8 mg, tR = 7.48 min) was obtained from subfraction HFEDD (38.1 mg) after C18 HPLC purification using H_2O(0,005%TFA)/acetonitrile [50:50 (v/v) for 0−10 min] as the mobile phase.

27-Dehydroxy-2,3-dihydro-24,25-epoxywithaferin A (1): colorless crystals; mp 210-212 ºC; ECD (MeOH) λ_{ext} ($\Delta\varepsilon$) 288 (-24.3), 232 (-14.7); IR (KBr) ν_{max} 3439, 1730, 1685, 1456, 1388, 1305, 1166, 1136 cm^{-1}; ^1H and ^{13}C NMR data, Table 1 and 2; HRESIMS *m/z* 495.2738 [M + Na]$^+$ (calcd for $C_{28}H_{40}NaO_6$, 495.2723).

24,25-Epoxywithaferin A (2): colorless crystals; mp 228-230 ºC; ECD (MeOH) λ_{max} ($\Delta\varepsilon$) 288 (-17.8), 232 (-6.5), 211 (+14.1); IR (KBr) ν_{max} 3495, 1712, 1676, 1458, 1400, 1313, 1033 cm^{-1}; ^1H and ^{13}C NMR data, Table 1 and 2; HRESIMS *m/z* 509.2559 [M + Na]$^+$ (calcd for $C_{28}H_{38}NaO_7$, 509.2515).

2,3-Dehydroxy-24,25-epoxywithaferin A (3): colorless resin; ECD (MeOH) λ_{max} ($\Delta\varepsilon$) 288 (-24.3), 232 (-12.1); ^1H and ^{13}C NMR data, Table 1 and 2; HRESIMS *m/z* 511.2654 [M + Na]$^+$ (calcd for $C_{28}H_{40}NaO_7$, 511.2672).

27-Dehydroxy-2,3-dihydro-24,25-epoxy-16-hydroxywithaferin A (4): colorless crystals; mp 258-260 ºC; ECD (MeOH) λ_{max} ($\Delta\varepsilon$) 288 (-24.3), 232 (-14.3); IR (KBr) ν_{max} 3537, 3429, 1730,

1707, 1452, 1388, 1303, 1161, 1026 cm^{-1}; ^{1}H and ^{13}C NMR data, Table 1 and 2; HRESIMS m/z 511.2668 [M + Na]$^{+}$ (calcd for $C_{28}H_{40}NaO_7$, 511.2672).

27-Dehydroxy-2,3-dihydro-24,25-epoxy-15-hydroxywithaferin A (5): colorless crystals; mp 137 ºC; ECD (MeOH) λ_{max} ($\Delta\varepsilon$) 288 (-24.3), 232 (-13.9); IR (KBr) ν_{max} 3481, 1730, 1710, 1456. 1388, 1307, 1161, 1038, 1048 cm^{-1}; ^{1}H and ^{13}C NMR data, Table 1 and 2; HRESIMS m/z 511.2673 [M + Na]$^{+}$ (calcd for $C_{28}H_{40}NaO_7$, 511.2672).

27-Dehydroxy-2,3-dihydro-24,25-epoxy-15-oxowithaferin A (6): colorless crystals; mp 228 ºC; ECD (MeOH) λ_{max} ($\Delta\varepsilon$) 288 (-24.3), 232 (-15.9). IR (KBr) ν_{max} 3471, 1730, 1695, 1388, 1309, 1122 cm^{-1}; ^{1}H and ^{13}C NMR data, Table 1 and 2; HRESIMS m/z 509.2523 [M + Na]$^{+}$ (calcd for $C_{28}H_{38}NaO_7$, 509.2515).

27-Dehydroxy-2,3-dihydro-15-hydroxywithaferin A (7): colorless crystals; mp 187 ºC; ECD (MeOH) λ_{max} ($\Delta\varepsilon$) 289 (-27.3), 248 (+24.4), 201 (+60.9); IR (KBr) ν_{max} 3408, 1686, 1456, 1136 cm^{-1}; ^{1}H and ^{13}C NMR data, Table 1 and 2; HRESIMS m/z 495.2720 [M + Na]$^{+}$ (calcd for $C_{28}H_{40}NaO_6$, 495.2723).

27-Dehydroxy-2,3-dihydro-16-hydroxywithaferin A (8): colorless crystals; mp 196 ºC; ECD (MeOH) λ_{max} ($\Delta\varepsilon$) 288 (-25.3), 248 (+24.6), 204 (+45.6); IR (KBr) ν_{max} 3558, 3469, 1699, 1384, 1033 cm^{-1}; ^{1}H and ^{13}C NMR data, Table 1 and 2; HRESIMS m/z 495.2745 [M + Na]$^{+}$ (calcd for $C_{28}H_{40}NaO_6$, 495.2723).

Withalutin B (9): amorphous solid; ECD (MeOH) λ_{max} ($\Delta\varepsilon$) 289 (-6.0), 229 (+13.0), 205 (+51.4); ^{1}H and ^{13}C NMR data, Table 1 and 2; HRESIMS at m/z 443.2796 [M + H - H_2CO]$^{+}$ (calcd for $C_{27}H_{37}O_5$, 443.2797).

Withajardin N (10): amorphous solid; ECD (MeOH) λ_{max} ($\Delta\varepsilon$) 260. (-25.3), 248 (+24.6), 204 (-18.1). ^{1}H and ^{13}C NMR data, Table 1 and 2; HRESIMS m/z 439.2843 [M + H]$^{+}$ (calcd for $C_{28}H_{40}O_7$, 439.2848).

X-ray Crystallographic Analyses of Compounds 1, 2, 4, 5, 7, 8, and 11.

Single crystal X–ray diffraction data collection (ϕ scans and ω scans with κ and θ offsets) was recorded on a Bruker D8 Venture κ-geometry diffractometer equipped with a Photon II CPAD detector and a Cu Kα (λ = 1.54178 Å) IμS 3.0 Incoatec microfocus source. The sample temperature was controlled using an Oxford Cryostream cryostat (800 series Cryostream Plus) attached to the diffractometer. The APEX 4 software was used for the unit cell determination [25,26]. Data were corrected for absorption effects using SADABS [27,28] The structures were solved by intrinsic phasing using SHELXT [29] and refined with the ShelXL [30] refinement package using Least Squares minimization by using Olex^2 [31] as a graphical interface. Non-hydrogen atoms were refined anisotropically. Hydrogen atoms were placed according to geometrical criteria and treated using the riding model.

X-ray Crystallography Analysis of 27-Dehydroxy-2,3-dihydro-24,25-epoxywithaferin A (1): clear light colorless prism crystals of compound **1** were obtained from acetone. $C_{28}H_{40}O_6$, M_r = 472.60 g mol^{-1}; size 0.461×0.7×0.74 mm^3; monoclinic, $P2_1$ (4), a=10.7525(4) Å, b=7.5324(2) Å, c=31.5611(10) Å, a=90°, b=92.889(2)°, g=90°; V = 2552.95(14) Å^3, Z = 4, ρ_{calc}=1.230 g m^{-3}, μ (CuK_a) = 0.684 mm^{-1}, numerical, $F(000)$= 1024. The data were collected at 300.0 K. The total number of reflections was 66556 ($-12 \leq h \leq 12$, $-8 \leq k \leq 9$, $-38 \leq l \leq 38$) measured in the Θ range 5.61 to 136.70 (0.83 Å)°, completeness Θ$_{max}$ = 99.9 %, 9121 unique (R_{int} = 0.0605, R_{sigma} = 0.0351) which were used in all calculations; Final indices: R_{1obs} = 0.0409, wR_{2obs} = 0.1105 [I $\geq 2\sigma$(I)]; R_{1all} = 0.0467, wR_{2all} = [all data], GOOF = 1.016, Flack parameter = 0.05(7), Hooft parameter = 0.06(6), Parsons parameter = 0.06(7), largest difference peak and hole $-0.20/0.16$ e Å^{-3}.

X-ray Crystallography Analysis of 24,25-Epoxywithaferin A (2): clear light colorless plate crystals of compound **2** were obtained from acetone. $C_{28}H_{38}O_7$, M_r = 486.58 g mol^{-1}; size 0.152×0.312×0.433 mm^3; orthorhombic, $P2_12_12_1$ (19), a=9.3249(2) Å, b=10.0824(2) Å,

c=27.2584(5) Å, a=90°, b=90°, g=90°; V = 2562.76(9) Å^3, Z = 4, ρ_{calc}=1.261 g m^{-3}, μ (CuK_α) = 0.729 mm^{-1}, none, $F(000)$= 1048. The data were collected at 300 K. The total number of reflections was 27255 ($-11 \leq$ h ≤ 11, $-12 \leq$ k ≤ 11, $-33 \leq$ l ≤ 33) measured in the Θ range 9.35 to 144.41 (0.81 Å)°, completeness Θ_{max} = 99.8 %, 5053 unique (R_{int} = 0.0385, R_{sigma} = 0.0281) which were used in all calculations; Final indices: R_{1obs} = 0.0422, wR_{2obs} = 0.1191 [I $\geq 2\sigma$(I)]; R_{1all} = 0.0433, wR_{2all} = [all data], GOOF = 1.055, Flack parameter = -0.09(5), Hooft parameter =0.10(5), Parsons parameter = -0.09(5), largest difference peak and hole $-0.30/0.43$ e Å^{-3}.

X-ray Crystallography Analysis of 27-Dehydroxy-2,3-dihydro-24,25-epoxy-16-hydroxywithaferin A (4): clear light colorless prism crystals of compound **4** were obtained from dichloromethane. $C_{28}H_{40}O_7$, M_r = 488.60 g mol^{-1}; size 0.082×0.128×0.532 mm^3; orthorhombic, $P2_12_12_1$ (19), a=7.4373(2) Å, b=17.1310(6) Å, c=19.9880(6) Å, a=90°, b=90°, g=90°; V = 2546.64(14) Å^3, Z = 4, ρ_{calc}=1.274 g m^{-3}, μ (CuK_α) = 0.734 mm^{-1}, numerical, $F(000)$= 1056. The data were collected at 300 K. The total number of reflections was 21716 ($-8 \leq$ h ≤ 9, $-21 \leq$ k ≤ 21, $-24 \leq$ l ≤ 24) measured in the Θ range 6.80 to 144.42 (0.81 Å)°, completeness Θ_{max} = 99.9 %, 4980 unique (R_{int} = 0.0682, R_{sigma} = 0.0558) which were used in all calculations; Final indices: R_{1obs} = 0.0512, wR_{2obs} = 0.1255 [I $\geq 2\sigma$(I)]; R_{1all} = 0.0584, wR_{2all} = [all data], GOOF = 1.046, Flack parameter = 0.04(12), Hooft parameter = 0.01(11), Parsons parameter = 0.08(13), largest difference peak and hole $-0.26/0.20$ e Å^{-3}.

X-ray Crystallography Analysis of 27-Dehydroxy-2,3-dihydro-24,25-epoxy-15-hydroxywithaferin A (5): clear light colorless block crystals of compound **5** were obtained from acetone. $C_{28}H_{40}O_7$, M_r = 488.60 g mol^{-1}; size 0.3×0.4×0.6 mm^3; orthorhombic, $P2_12_12_1$ (19), a=11.2900(3) Å, b=12.5494(3) Å, c=18.6532(5) Å, a=90°, b=90°, g=90°; V = 2642.84(12) Å^3, Z = 4, ρ_{calc}=1.228 g m^{-3}, μ (CuK_α) = 0.707 mm^{-1}, none, $F(000)$= 1056. The data were collected at 302.00 K. The total number of reflections was 33632 ($-13 \leq$ h ≤ 13, $-15 \leq$ k ≤ 15, $-22 \leq$ l ≤ 23) measured in the Θ range 8.49 to 144.42 (0.81 Å)°, completeness Θ_{max} = 99.8 %, 5178

unique (R_{int} = 0.0370, R_{sigma} = 0.0289) which were used in all calculations; Final indices: R_{1obs} = 0.0416, wR_{2obs} = 0.1161 [I ≥ 2σ(I)]; R_{1all} = 0.0429, wR_{2all} = [all data], GOOF = 1.034, Flack parameter = 0.3(2), Hooft parameter = 0.19(5), Parsons parameter = 0.21(5) , largest difference peak and hole −0.16/0.25 e Å^{-3}.

X-ray Crystallography Analysis of 27-Dehydroxy-2,3-dihydro-15-hydroxywithaferin A (7): clear light colorless plate crystals of compound **7** were obtained from acetone. $C_{28}H_{40}O_6$, M_r = 472.60 g mol^{-1}; size 0.085×0.157×0.313 mm^3; monoclinic, $P2_1$ (4), a=6.2929(3) Å, b=21.0056(8) Å, c=10.3255(4) Å, a=90°, b=106.801(2)°, g=90°; V = 1306.63(10) Å^3, Z = 2, ρ_{calc}=1.201 g m^{-3}, μ (CuK_α) = 0.669 mm^{-1}, numerical, $F(000)$= 512. The data were collected at 300 K. The total number of reflections was 41463 (−7 ≤ h ≤ 7, −24 ≤ k ≤ 25, −12 ≤ l ≤ 12) measured in the Θ range 8.42 to 139.96 (0.82 Å)°, completeness Θ_{max} = 100.0 %, 4950 unique (R_{int} = 0.1020, R_{sigma} = 0.0515) which were used in all calculations; Final indices: R_{1obs} = 0.0475, wR_{2obs} = 0.1175 [I ≥ 2σ(I)]; R_{1all} = 0.0740, wR_{2all} = [all data], GOOF = 1.021, Flack parameter = -0.03(16), Hooft parameter = -0.10(13), Parsons parameter = -0.05(15), largest difference peak and hole −0.18/0.13 e Å^{-3}.

X-ray Crystallography Analysis of 27-Dehydroxy-2,3-dihydro-16-hydroxywithaferin A (8): clear light colorless plate crystals of compound **8** were obtained from acetone. $C_{28}H_{40}O_6$, M_r = 472.60 g mol^{-1}; size 0.054×0.302×0.321 mm^3; triclinic, $P1$ (1), a=6.5469(4) Å, b=6.5584(4) Å, c=30.811(2) Å, α=87.672(4)°, β=84.379(4)°, γ=69.066(4)°; V = 1229.67(14) Å^3, Z = 2, ρ_{calc}=1.276 g m^{-3}, μ (CuK_α) = 0.710 mm^{-1}, numerical, $F(000)$= 512. The data were collected at 300 K. The total number of reflections was 46870 (−7 ≤ h ≤ 7, −7 ≤ k ≤ 7, −37 ≤ l ≤ 37) measured in the Θ range 5.76 to 137.96 (0.83 Å)°, completeness Θ_{max} = 99.9 %, 8745 unique (R_{int} = 0.0608, R_{sigma} = 0.0449) which were used in all calculations; Final indices: R_{1obs} = 0.0503, wR_{2obs} = 0.1328 [I ≥ 2σ(I)]; R_{1all} = 0.0558, wR_{2all} = [all data], GOOF = 1.038, Flack parameter

= 0.07(9), Hooft parameter = 0.07(8), Parsons parameter = 0.10(8), largest difference peak and hole −0.22/0.19 e Å^{-3}.

X-ray Crystallography Analysis of Withaferin A (11): clear light colorless irregular crystals of compound **11** were obtained from acetone. $C_{28}H_{38}O_6$, M_r = 470.58 g mol^{-1}; size 0.114×0.211×0.362 mm^3; orthorhombic, $P2_12_12_1$ (19), a=10.7269(2) Å, b=12.3337(2) Å, c=18.7162(3) Å, α=90°, β=90°, γ=90°; V = 2476.20(7) Å^3, Z = 4, ρ_{calc}=1.262 g m^{-3}, μ (CuK_α) = 0.705 mm^{-1}, numerical, $F(000)$= 1016. The data were collected at 300 K. The total number of reflections was 31236 (−13 ≤ h ≤ 13, −15 ≤ k ≤ 15, −22 ≤ l ≤ 23) measured in the Θ range 8.59 to 144.19 (0.81 Å)°, completeness Θ_{max} = 100.0 %, 4882 unique (R_{int} = 0.0766, R_{sigma} = 0.0433) which were used in all calculations; Final indices: R_{1obs} = 0.0460, wR_{2obs} = 0.1151 [I ≥ 2σ(I)]; R_{1all} = 0.0726, wR_{2all} = [all data], GOOF = 1.013, Flack parameter = -0.02(13), Hooft parameter = -0.01(11), Parsons parameter = -0.03(14) , largest difference peak and hole −0.18/0.24 e Å^{-3}.

Crystallographic data of **1**, **2**, **4**, **5**, **7**, **8**, and **11** have been deposited at the Cambridge Crystallographic Data Center under codes 2234871 to 2234877, respectively. These data can be obtained free of charge via http://www.ccdc.cam.ac.uk/deposit, or from the CCDC, 12 Union Road, Cambridge CB2 1EZ, UK (fax: C44 1223 336 033; e-mail: deposit@ccdc.cam.ac.uk).

Cytotoxicity Tests.

Cytotoxicity was measured by the ability of living cells to reduce the yellow dye 3-(4,5-dimethyl-2-thiozolyl)-2,5-diphenyl-2H-tetrazolium bromide (MTT) to a purple formazan product [32]. The human cancer cell lines used in this work were all obtained from the National Cancer Institute (Bethesda, MD, USA). The cells were maintained in RPMI 1640 or DMEM medium supplemented with 10% fetal bovine serum, 2 mM glutamine, 100 U/mL penicillin, 100 µg/mL streptomycin at 37°C with 5% CO_2. For the experiments, cells were plated in 96-

well plates (0.7×10^5 cells/well for HCT-116 and 0.1×10^6 cells/mL PC-3, SNB-19, and L929

cell lines, 0.3×10^6 cells/well for HL-60 cell line). The compounds were dissolved in DMSO

(0.1%), after a serial dilution were incubated for 72 h. DMSO (0.1%) and Withaferin A were

used as negative and positive controls, respectively. Thereafter, the plates were centrifuged and

then the medium was replaced by fresh medium containing 0.5 mg/mL MTT. Three hours later,

the MTT formazan product was dissolved in DMSO, and absorbance was measured using a

microplate reader (Spectra Count, Packard, Ontario, Canada). The compound effect was

quantified as the percentage of control absorbance of the reduced dye at 595 nm.

Cardiac tissues bioassay

To evaluate the effect of the withanolides from *A. velutina* on cardiac mechanical properties

such as inotropism and chronotropism the guinea pig model was used. Therefore, male guinea

pigs were sacrificed under isoflurane anesthesia (5% isoflurane and 2 L/min oxygen) followed

by exsanguination. Thereafter, the left atrium or right atrium was removed and rapidly mounted

in 10 mL organ baths filled with Krebs-Henseleit solution kept at 37°C, pH 7.4, and gassed

with 5% CO_2 in 95% O_2. The modified Krebs-Henseleit solution had the following composition

(mmol): NaCl 124; KCl 4.75; $MgCl_2$ 1.3; $CaCl_2$ 2.25; $NaHCO_3$ 25; NaH_2PO_4 0.6; Glucose 10.

Tissues were attached to the isometric force transducers model TRI201 (Panlab, Barcelona,

Spain) connected to PowerLab computerized data acquisition system (ADInstruments, Sydney,

Australia). The tissues were mounted under a 1 g tension. The right atria were used for

recordings of the spontaneous contractions generated by the sinoatrial pacemaker. The left atria

were electrically stimulated using square wave pulses 50% above the threshold, 10 ms duration,

and 2 Hz frequency using platinum electrodes attached to an S88 Grass stimulator (West

Warwick, Rhode Island, USA). After a 30-min stabilization period, withanolides **1**, **4**, **15**, **16**,

and **17** were added to the organ bath chamber in cumulative concentrations from 10-9 to 10-5

M and the effect of each concentration was recorded for 5 minutes before the addition of the

next concentration. To check the involvement of voltage-dependent calcium channels in the cardiotonic effect the concentration-response curves obtained for the withanolides in the left atria were repeated in both the presence or absence of verapamil a calcium channel blocker. Verapamil was added to the bath 15 minutes before the cumulative concentration curve for **15** or **16** was initiated.

Table 1. ¹H NMR Data of Compounds 1-10 (δ in ppm).

No.	1ª	2ª	3ª	4ᵇ	5ª	6ª	7ª	8ᵇ	9ª	10ª
1										7.06 d (10.0)
2	2.67 m 2.54 m	6.17 d (9.9)	2.63 m 2.54 m	2.79 m 2.68 m	2.58 m 2.54 m	2.73 t (7.7) 2.47 m	2.70 m 2.53 m	2.83 m 2.68 m	2.14 m 1.52 m	6.25 d (10.0)
3	2.11 m	92 dd (9.9, 5.9)	2.11 m 2.03 m	2.13 m	2.08 m 2.01 m	2.13 m 1.99 m	2.15 m 2.02 m	2.15 m	1.80 m	
4	3.52 t (3.5)	3.72 d (5.9)	3.5 t (3.5)	3.78 s	3.47 brs	3.51 t (3.2)	3.53 t (3.6)	3.78 t (3.0)	9.66 s	6.10 s
6	3.15 s	3.20 s	3.13 s	3.21 s	3.16 s	3.16 s	3.20 s	3.21 s	4.32 s	dt (14.0, 6.3) 2.37 m
7	2.24 m 1.38 m	2.13 m 1.48 m	2.18 m	2.23 m 1.36 m	43 d (14.3) 1.36 m	1.99 m	2.45 m 1.42 m	25 dd (15.2, 4.6) 1.43 m	2.49 m 2.27 m	1.95 m 1.04 m
8	1.44 d (4.6)	1.45 m	1.40 m	1.68 d (4.8)	1.83 m	76 dd (10.9, 3.3)	83 dd (11.5; 4.5)	56 dd (11.2, 4.6)	2.14 m	1.64 m
9	1.05 m	0.97 m	1.10 m	1.25 m	1.13 m	1.18 m	1.22 m	27 dt (11.2, 4.6)	1.05 m	1.40 m
11	1.34 m	1.79 m 1.43 m	1.33 ovl.	1.49 ovl.	1.27 ovl.	1.44 m 1.33 overlap	1.39 m	1.57 m 1.48 m	1.46 m 1.27 m	1.72 m
12	1.05 m	1.91 m 1.07 m	1.90 m 1.07 m	1.89 d (12.6)	1.85 m 0.98 m	1.99 m	1.89 m 1.08 m	1.93 d (12.3) 1.09 m	⁴4 overlap	1.89 m 1.23 m
14	0.94 m	0.92 m	0.95 m	0.90 m	0.79 m	1.61 d (10.8)	83 dd (11.0, 4.8)	0.92 m	0.92 m	1.04 m
15	1.75 m 1.41 m	1.75 m 1.32 m	1.71 m 1.33 ovl.	2.32 m 1.42 m	.20, t (5.6)		4.22 t (4.5)	2.37 m 1.48 m	4.26 s	1.65 m 1.20 m
16	1.64 m 1.15 m	1.64 m 1.14 m	1.65 m 1.14 m	4.39 brs	2.26 m 1.38 m	36 dd (18.9, 8.5) 1.91 m	2.26 m 1.44 m	4.45 brs	2.27 m 1.50 m	1.66 m 1.35 m
17	1.02 m	1.02 m	1.00 m	1.10 m	0.96 m	1.53 m	1.06 m	1.11 m	1.10 m	1.06 m
18	0.65 s	0.65 s	0.65 s	1.04 s	0.88 s	0.74 s	0.94 s	1.05 s	1.00 s	0.75 s
19	1.35 s	1.37 s	1.25 s	1.72 s	1.30 s	1.33 s	1.37 s	1.72 s	1.19 s	1.24 s
20	1.90 m	1.96 m	1.90 m	2.83 m	2.01 m	2.05 m	2.12 m	2.90 m	2.11 m	1.98 m
21	0.90 d (6.5)	0,88 d (6.5)	0.90 d (6.0)	1.03 d (5.4)	0.88 ovl.	0.98 d (6.5)	1.01 d (6.5)	1.12 d (6.8)	.00 ovl.	dd (13.0, 7.3) 1.50 m
22	53 td (7.7, 3.5)	4.52 d (11.2)	56 td (9.8, 5.6)	19 dt (12.0, 3.4)	5.50 brs	43 dt (11.3, 3.3)	35 dt (13.2; 3.6)	.22 dt (6.9, 3.4)	4.35 s	4.40 s
23	2.00 t (7.6)	1.99 m	2.00 m	2.23 m	1.92 m	1.99 m 1.25 m	2.42 m 1.90 m	2.42 m 2.12 m	2.42 m 1.92 m	2.02 m
27	1.56 s	4.11 d (12.6)	4.13 d (12.5)	1.63 s	1.53 s	1.56 s	1.89 s	1.86 s	1.87 s	1.14 s

		3.76 (12.6)	3.78 d (12.5)							
28	1.49 s	1.54 s	1.56 s	1.49 s	1.46 s	1.50 s	1.94 s	1.77s	1.94 s	1.27 s
OH-4		2.75 brs								
OH-16				6.35 brs						

[a] Coupling constants (Hz) are in parentheses. The assignments were based on HSQC, HMBC, and ^{1}H-^{1}H COSY experiments. [b] (CDCl$_3$). [c] (C$_5$D$_5$N).

Table 2. ¹³C NMR Data of Compounds 1-10 (δ in ppm)

No.	1ᵃ	2ᵃ	3ᵃ	4ᵇ	5ᵃ	6ᵃ	7ᵃ	8ᵇ	9ᵃ	10ᵃ
1	211.6, C	202.4, C	211.6, C	211.3, C	211.7, C	211.8, C	211.0, C	211.3, C	216.7, C	156.1, CH
2	31.6, CH₂	132.5, CH	31.9, CH₂	32.3, CH₂	31.8, CH₂	32.1, CH₂	32.2, CH₂	32.2, CH₂	33.6, CH₂	127.4, CH
3	26.3, CH₂	142.3, CH	26.6, CH₂	27.3, CH	26.4, CH₂	26.8, CH₂	27.0, CH₂	27.3, CH₂	22.8, CH₂	186.6, C
4	72.8, CH	70.0, CH	72.9, CH	73.3, CH	72.8, CH	72.7, CH	73.0, CH	73.3, CH	204.7, CH	124.1, CH
5	66.8, C	64.0, C	66.7, C	67.6, C	67.0, C	66.1, C	66.8, C	67.6, C	61.1, C	169.5, C
6	58.6, CH	62.2, CH	59.1, CH	57.5, CH	58.9, CH	59.4, CH	59.3, CH	57.5, CH	68.2, CH	33.1, CH₂
7	31.4, CH₂	31.3, CH₂	31.6, CH₂	32.2, CH₂	30.9, CH₂	30.1, CH₂	31.2, CH₂	32.4, CH₂	32.7, CH₂	33.9, CH₂
8	29.5, CH	29.9, CH	29.6, CH	30.3, CH	25.4, CH	26.1, CH	25.8, CH	30.3, CH	25.6, CH	35.9, CH
9	43.1, CH	44.2, CH	43.2, CH	43.8, CH	43.5, CH	42.6, CH	44.0, CH	43.9, CH	42.9, CH	52.8, CH
10	50.5, C	47.8, C	50.6, C	51.3, C	50.8, C	50.6, C	51.0, C	51.3, C	53.0, C	43.8, C
11	21.3, CH₂	22.0, CH₂	21.6, CH₂	21.7, CH₂	21.4, CH₂	21.6, CH₂	21.8, CH₂	21.7, CH₂	20.9, CH₂	23.0, CH₂
12	39.1, CH₂	39.4, CH₂	39.3, CH₂	40.0, CH₂	40.5, CH₂	39.3, CH₂	41.0, CH₂	40.1, CH₂	41.0, CH₂	39.5, CH₂
13	42.7, C	42.7, C	42.9, C	43.1, C	42.5, C	42.5, C	42.8, C	43.1, C	43.2, C	43.4, C
14	56.2, CH	56.1, CH	56.4, CH	55.0, CH	60.9, CH	65.7, CH	61.3, CH	55.0, CH	60.5, CH	54.9, CH
15	27.2, CH₂	27.3, CH₂	27.4, CH₂	38.6, CH₂	69.8, CH	213.2, C	70.2, CH	38.5, CH₂	70.1, CH	24.7, CH₂
16	24.3, CH₂	24.3, CH₂	24.4, CH₂	70.4, CH	39.9, CH₂	40.8, CH₂	40.7, CH₂	70.7, CH	40.3, CH	26.9, CH₂
17	52.0, CH	52.1, CH	52.2, CH	57.4, CH	52.4, CH	47.6, CH	53.0, CH	57.5, CH	57.4, CH₂	52.7, CH
18	11.5, CH₃	11.7, CH₃	11.5, CH₃	13.2, CH₃	13.2 CH₃	12.6, CH₃	14.5 CH₃	13.2 CH₃	14.8, CH₃	13.4, CH₃
19	15.2, CH₃	17.3, CH₃	15.6, CH₃	15.7, CH₃	15.5, CH₃	15.9, CH₃	15.6, CH₃	15.7, CH₃	13.1, CH₃	18.9, CH₃
20	38.6, CH	38.6, CH	38.7, CH	34.0, CH	38.5, CH	38.6, CH	39.1, CH	34.3, CH	38.9, CH	39.3, CH
21	13.1, CH₃	13.1, CH₃	13.2, CH₃	13.2, CH₃	14.3, CH₃	13.8, CH₃	13.8, CH₃	13.6, CH₃	14.0, CH₃	31.2, CH₂
22	76.3, CH	76.5, CH	76.9, CH	76.6, CH	76.9, CH	75.9, CH	78.6, CH	78.3, CH	78.8, CH	77.5, CH
23	28.8, CH₂	29.4, CH₂	29.4, CH₂	29.6, CH₂	29.4, CH₂	29.4, CH₂	30.6, CH₂	30.6, CH₂	30.4, CH₂	38.3, CH₂
24	62.7, C	63.4, C	63.4, C	63.7, C	62.7, C	62.6, C	148.3, C	149.8, C	149.5, C	72.0, C
25	59.3, C	60.7, C	60.8, C	60.1, C	59.4, C	59.5, C	122.7, C	122.2, C	122.4, C	47.5, C
26	170.1, C	170.2, C	170.2, C	170.5, C	170.1, C	169.8, C	166.6, C	167.1, C	167.5, C	177.3, C
27	13.7, CH₃	60.2, CH₃	60.4, CH₂	14.3CH₃	13.7, CH₃	13.8, CH₃	12.5, CH₃	13.0, CH₃	12.6, CH₃	14.4 CH₃
28	18.0, CH₃	17.5, CH₃	17.6, CH₃	18.2, CH₃	18.0, CH₃	18.1, CH₃	20.4, CH₃	20.4, CH₃	20.7, CH₃	29.3, CH₃

ᵃ (CDCl₃,).ᵇ (C₅D₅N).

Table 3. Cytotoxic activity (IC$_{50}$[a], µM) of compounds 1-12 evaluated by MTT assay against four human tumor cell lines and a non-tumor cell line.

Compounds	Cell lines[b]				
	HL-60	HCT116	SNB-19	PC-3	L-929
1	12.54 (9.42 to 16.76)	> 20	> 20	> 20	> 20
2	0.94 (0.86 to 1.01)	1.93 (1.52 to 2,49)	5.01 (4.19 to 6.00)	6.23 (5.30 to 7.27)	4.01 (3.53 to 4.52)
3	10.54 (9.82 to 11,34)	6.84 (5.32 to 8.80)	10.93 (9.41 to 12.73)	14.69 (12.77 to 16.90)	> 20
4	11.85 (9.11 to 14.45)	>20	>20	5.16 (4.36 to 6.06)	>20
5	>20	>20	>20	>20	>20
6	0.45 (0.41 to 0.49)	2.01 (1.77 to 2.32)	5.69 (2.10 to 6.55)	2.18 (1.89 to 2.53)	>20
7	>20	>20	>20	>20	>20
8	8.97 (7.41 to 10.88)	18.96 (17.43 to 20.63)	>20	>20	>20
9	*ND	>20	>20	>20	>20
10	*ND	>20	>20	>20	>20
11[c]	0.39 (0.35 to 0.43)	1.72 (1.59 to 1.84)	3.77 (3.36 to 4.24)	1.80 (1.60 to 2.03)	1.89 (0.94 to 2.55)
12	*ND	>20	>20	>20	>20
15	0.46 (0.40 to 0.53)	1.50 (1.23 a 1.82)	2.10 (1.63 to 2.68)	0.94 (0.84 to 1.06)	1.21 (1.13 to 1,30)
16	0.33 (0.28 to 0.37)	1.19 (0.99 to 1.43)	1.74 (1.45 to 2.04)	0.66 (0.55 to 0.81)	0.24 (0.17 to 0.31)
17	12.85 (11.20 to 14.74)	> 20	> 20	> 20	> 20

[a] IC$_{50}$: Half maximal inhibitory concentration; >20: is the highest concentration tested (20 µM), inhibition of 50% of cell viability was not verified and hence IC50 is above that value.*ND: Not determined.

[b] Cell lines: HL-60 (Acute promyelocytic leukemia); HCT-116 (Colorectal carcinoma); SNB-19(astrocytoma CNS); PC-3 (Prostate adenocarcinoma); L929 (Murine fibroblast).

[c] Withaferin A (positive control)
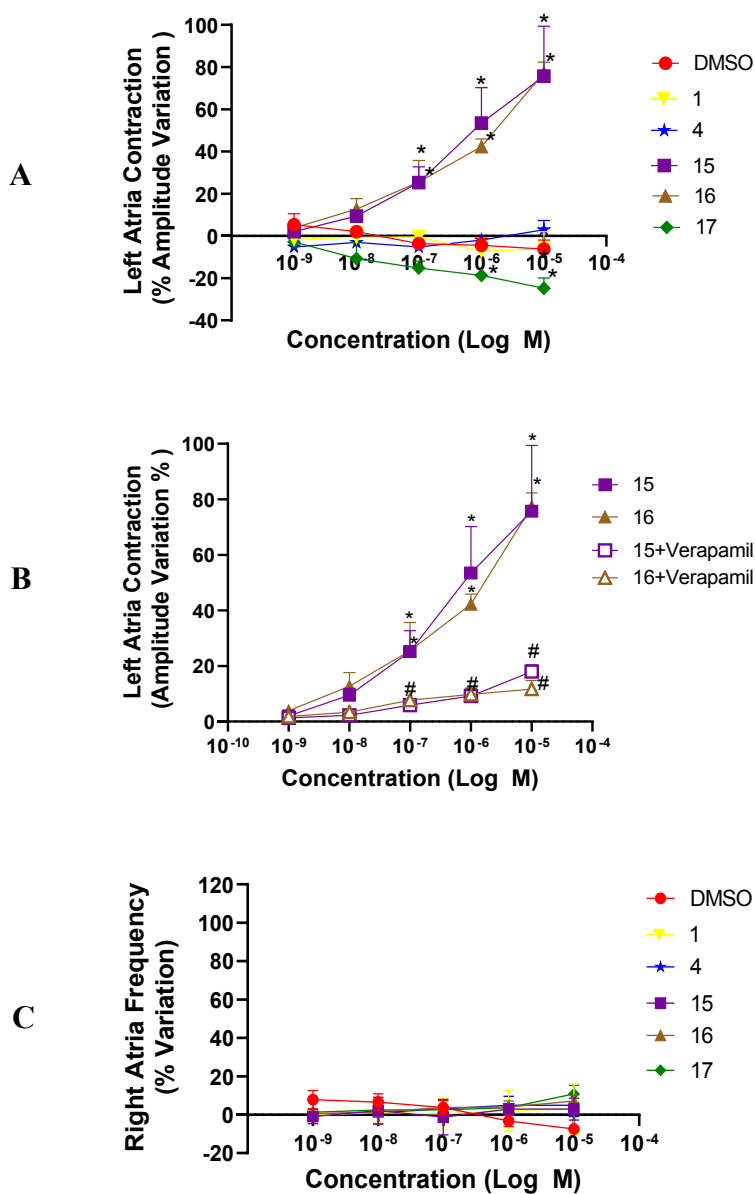
Fig. 5. Panel **A** depicts that **15 and 16** have cardiotonic effect while **1**, **4** and **17** are devoid of such effect. Panel **B** shows that verapamil, a calcium channel blocker, can impair the cardiotonic effect induced by both **15** and **16**. Panel **C** shows that none of the compounds affects the sinoatrial pacemaker frequency. *$p < 0.05$ vs. internal control basal values; #$p < 0.05$ vs. **15** or **16** in the absence of verapamil.

ASSOCIATED CONTENT

Supporting Information

IR, HRESIMS, NMR, and CD data of compounds **1**–**10**.

X-ray crystallographic files of compounds **1-2**, **4-5**, **7-8**, **11** (CIF).

AUTHOR INFORMATION

Corresponding Author

*Phone: +55-85-33669441. E-mail: opessoa@ufc.br

Authors-ORCID

Késya Amanda Dantas Rocha: 0000-0001-7596-8700

Edilberto Rocha Silveira: 0000-0003-4178-0296

Tércio de Freitas Paulo: 0000-0001-6815-7547

Alejandro Pedro Ayala: 0000-0002-9247-6780

Bruno Marques Soares: 0000-0003-3650-9653

Sarah Sant'Anna Maranhão: 0000-0002-5379-2780

Cláudia do Ó Pessoa: 0000-0002-4344-4336

Iury Araújo Paz: 0000-0001-8678-3664

Maria Lidia Barroso Rodrigues: 0000-0003-4645-4932

Nilberto Robson Falcão do Nascimento: 0000-0001-6156-5927

Kirley Marques Canuto: 0000-0003-3194-6125

Otília Deusdenia L. Pessoa: 0000-0002-1617-7586

Notes

The authors declare no competing financial interest.

ACKNOWLEDGMENTS

REFERENCES

[1] M. Zhang, B. Zhang, C. Guang, B. Jiang, X. He, S. Cao, L. Ding, N. Kang, L. Chen, F. Qiu, RSC Adv. 10 (2020) 22819. https://doi.org/10.1039/d0ra04106h

[2] S.J. Castro, C.N. Casero, J.M. Padrón, V.E.J. Nicotra, Nat. Prod. 82 (2019) 1338–1344. https://doi.org/10.1021/acs.jnatprod.9b00117

[3] G.G. Llanos, L.M. Araujo, I.A. Jimenez, L.M. Moujir, J. Rodríguez, C. Jimenez, I.L. Bazzocchi, Eur. J. Med. Chem. 140 (2017) 52–64. http://dx.doi.org/10.1016/j.ejmech.2017.09.004

[4] K.A.D. Rocha, T.F. Paulo, A.P. Ayala, V.S. Sampaio, P.I.G. Nunes, F.A. Santos, K.M. Canuto, E.R. Silveira, O.D.L. Pessoa, Phytochemistry 203 (2022) 113338. https://doi.org/10.1016/j.phytochem.2022.113338

[5] R.I. Misico, V.E. Nicotra, J.C. Oberti, G. Barboza, R.R. Gil, G. Burton, Withanolides and related steroids, in: A.D. Kinghorn, H. Falk, J. Kobayashi (Eds.), Progress in the Chemistry of Organic Natural Products, v. 94, Springer-Verlag/Wien, New York, 2011, pp. 128–229. https://doi.org/10.1007/978-3-7091-0748-5_3

[6] S. Kim, J.S. Yu, J.Y. Lee, S.U. Choi, J. Lee, K.H. Kim, J. Nat. Prod. 82 (2019) 765–773. https://doi.org/10.1021/acs.jnatprod.8b00665

[7] M. Dom, W.V. Berghe, X.V. Ostade, RSC Med. Chem. 11 (2020) 30–50. https://doi.org/10.1039/c9md00296k

[8] B. Guo, J. Liu, B. Wang, C. Zhang, Z. Su, M. Zhao, L. Qin, W. Zhang, R. Zheng, Diabetes 71 (2022) 249–263. https://doi.org/10.2337/db21-0470

[9] W.B. Bakrim, L. Bouzidi, H. Manouze, J. Hafsa, M. Sobeh, S. Ba-M'hamed, K. Bekkouche, L. Kouisni, Arab. J. Chem. 15 (2022) 103529. https://doi.org/10.1016/j.arabjc.2021.103529

[10] A.R. Straughn, S.S.J. Kakar, Ovar. Res. 13 (2020). https://doi.org/10.1186/s13048-020-00684-x

[11] S. Chakraborty, D. Mallick, M. Goswami, F.P. Guengerich, A. Chakrabarty, G.J. Chowdhury, Nat. Prod. 85 (2022) 2340−2350. https://doi.org/10.1021/acs.jnatprod.2c00521

[12] I.M.C. Rodrigues, S. Knapp, J.R. Stehmann, PhytoKeys 178 (2021) 1–15. https://doi.org/10.3897/phytokeys.178.6460

[13] I. M.C. Rodrigues, S. Knapp, J.R. Stehmann, Taxon 68 (2019) 839-846. https://doi.org/10.1002/tax.12089

[14] L.A. Rodrigues, A. das C. Almeida, D.C. Gontijo, I.V. Salustiano, A.A. Almeida, G.C. Brandão, A. de Oliveira, B. Ribon, J.P.V. Leite, Nat. Prod. Res. (2020) 1-5. https://doi.org/10.1080/14786419.2020.1802271

[15] A.A. Almeida, G.D.A. Lima, M. Eiterer, L.A. Rodrigues, J.A. Vale, A.C. Zanatta, G.C. Bressan, L.L. Oliveira, J.P.V. Leite, Planta Med. 88 (2022) 429-439. https://doi.org/10.1055/a-1395-9046

[16] A.A. Almeida, B.B. Cota, L.A. Rodrigues, L.L. Dutra, M. Kohlhoff, G.C. Bressan, G.C. Brandão, J.P.V. Leite, Nat. Prod. Res. 36 (2022) 6304–6311. https://doi.org/1080/14786419.2022.2039135

[17] P.A. Alves, K.A.D. Rocha, L.L. Bezerra, A.P. Ayala, N.K.V. Monteiro, O.D.L. Pessoa, J. Biomol. Struct. Dyn. (2023) 1-9. https://doi.org/10.1080/07391102.2023.2167863

[18] R. Guo, L. Gan, W.B. Lau, Z. Yan, D. Xie, E. Gao, T.A. Christopher, B.L. Lopez, X. Ma, Y. Wang, Circ. J. 83 (2019) 1726–1736. https://doi.org/10.1253/circj.CJ-18-1391

[19] H. Zhang, A.K. Samadi, R.J. Gallagher, J.J. Araya, X. Tong, V.W. Day, M.S. Cohen, K. Kindscher, R. Gollapudi, B.N.J. Timmermann, Nat. Prod. 74 (2011) 2532–2544. https://dx.doi.org/10.1021/np200635r

[20] X. Zhang, G. Li, Q. Deng, Z. Xu, J. Cen, J. Xu, Bioorg. Med. Chem. Lett. 48 (2021) 128235. https://doi.org/10.1016/j.bmcl.2021.128235

[21] A. Wongsakul, N. Lertnitikul, R. Suttisri, S. Jianmongkol, Anticancer Res. 42 (2022) 1833–1844. https://doi.org/10.21873/anticanres.15659

[22] E.M.K. Wijeratne, M.C.F. Oliveira, J. Mafezoli, Y-M. Xu, S. Minguzzi, P.H.J. Batista, O.D.L. Pessoa, L. Whitesell, A.A.L. Gunatilaka, J. Nat. Prod. 81 (2018) 825−837. https://doi.org/10.1021/acs.jnatprod.7b00918

[23] F.G. Nicolás, G. Reyes, M.C. Audisio, M.L. Uriburu, S.L. González, G.E. Barboza, V.E.J. Nicotra, Nat. Prod. 78 (2015) 250−257. https://doi.org/10.1021/np500824f

[24] G.G. LLanos, L.M. Araujo, I.A. Jiménez, L.M. Moujir, I.L. Bazzocchi, Eur. J. Med. Chem. 54 (2012) 499–511. https://doi:10.1016/j.ejmech.2012.05.032

[25] Bruker AXS Inc. (2021). APEX4 Data Collection software (Version 2021.4-0), Madison, Wisconsin, USA.

[26] Bruker AXS Inc. (2019). SAINT Data Reduction Software (Version 8.40b), Madison, Wisconsin, USA.

[27] G.M. Sheldrick, (1996). SADABS. Program for Empirical Absorption Correction. University of Gottingen, Germany.

[28] L. Krause, R. Herbst-Irmer, G.M. Sheldrick, D. Stalke, J. Appl. Crystallogr. 48 (2015) 3–10. https://doi.org/10.1107/S1600576714022985

[29] G.M. Sheldrick, SHELXT – Integrated space-group and crystal-structure determination. Acta Crystallogr. A: Found. Adv. 71 (2015a) 3–8. https://doi.org/10.1107/S2053273314026370

[30] G.M. Sheldrick, Crystal structure refinement with SHELXL. Acta Crystallogr. C Struct. Chem. 71 (2015b) 3–8. https://doi.org/10.1107/S2053229614024218

[31] O.V. Dolomanov, L.J. Bourhis, R.J. Gildea, J.A.K. Howard, H. Puschmann, J. Appl. Crystallogr. 42 (2009) 339–341. https://doi.org/10.1107/S0021889808042726

[32] T. Mosman, J. Immunol. Methods 65 (1983) 55–63.

Supporting information

CONTENTS

Figure S 1. FTIR spectrum of **1**.

Figure S 2. ^{1}H NMR (300.13 MHz) spectrum of 1, in CDCl$_3$.

Figure S 3. ^{13}C NMR (75.47 MHz) spectrum of **1**, in CDCl$_3$.
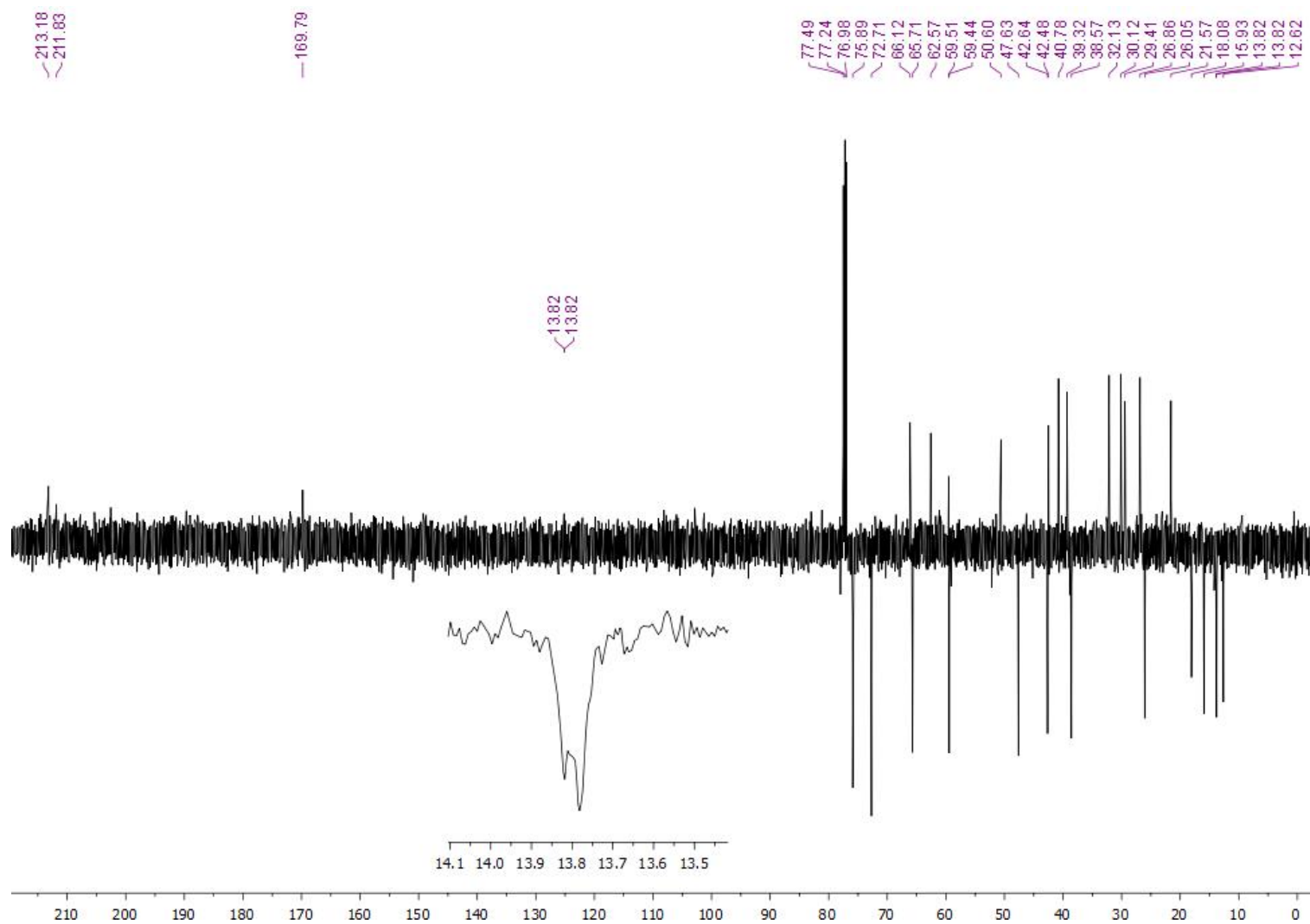
Figure S 4. DEPT 135° NMR (75.47 MHz) spectrum of 1, in CDCl₃.

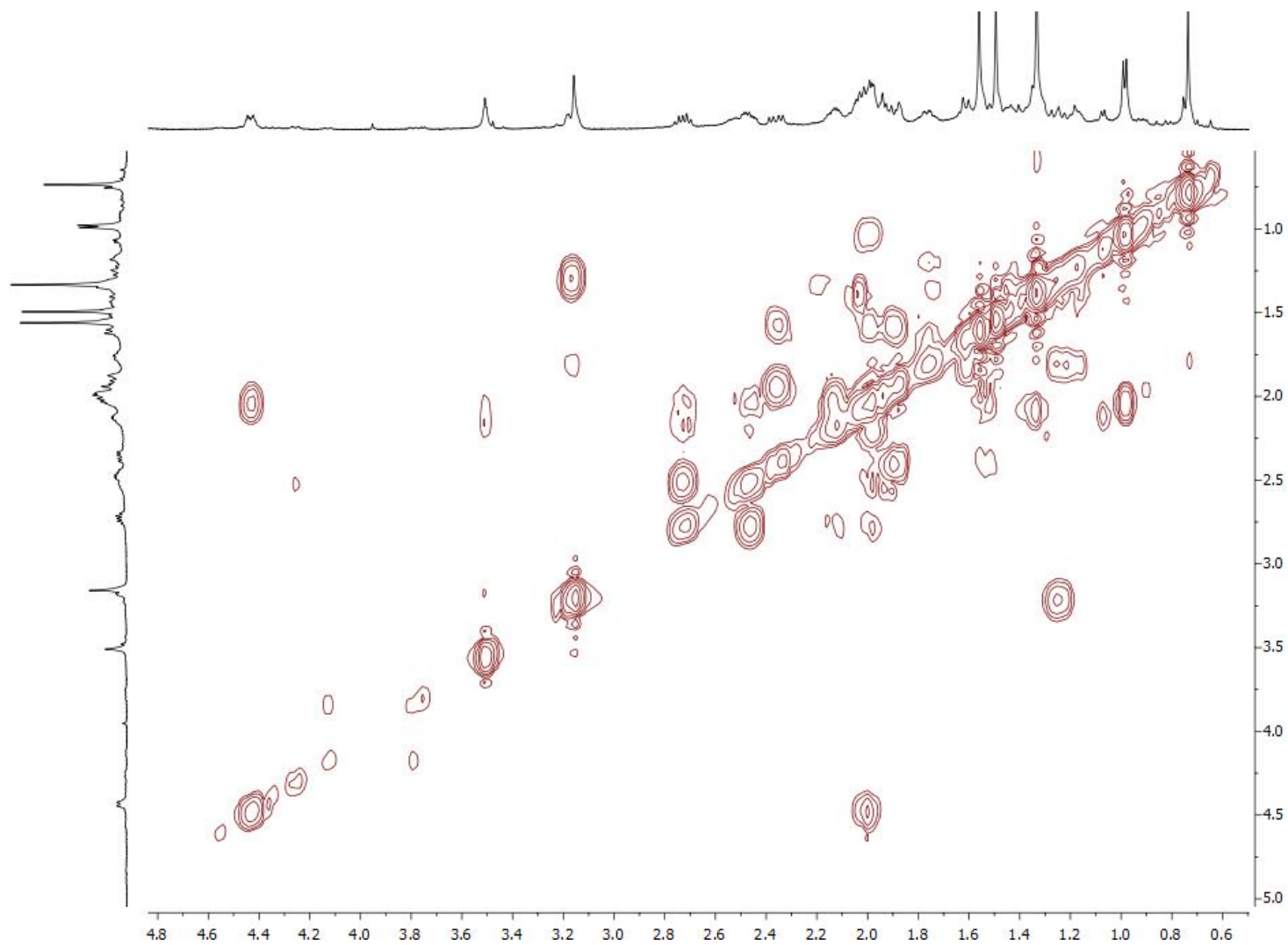**Figure S 5. HSQC NMR spectrum of 1, in CDCl₃.**
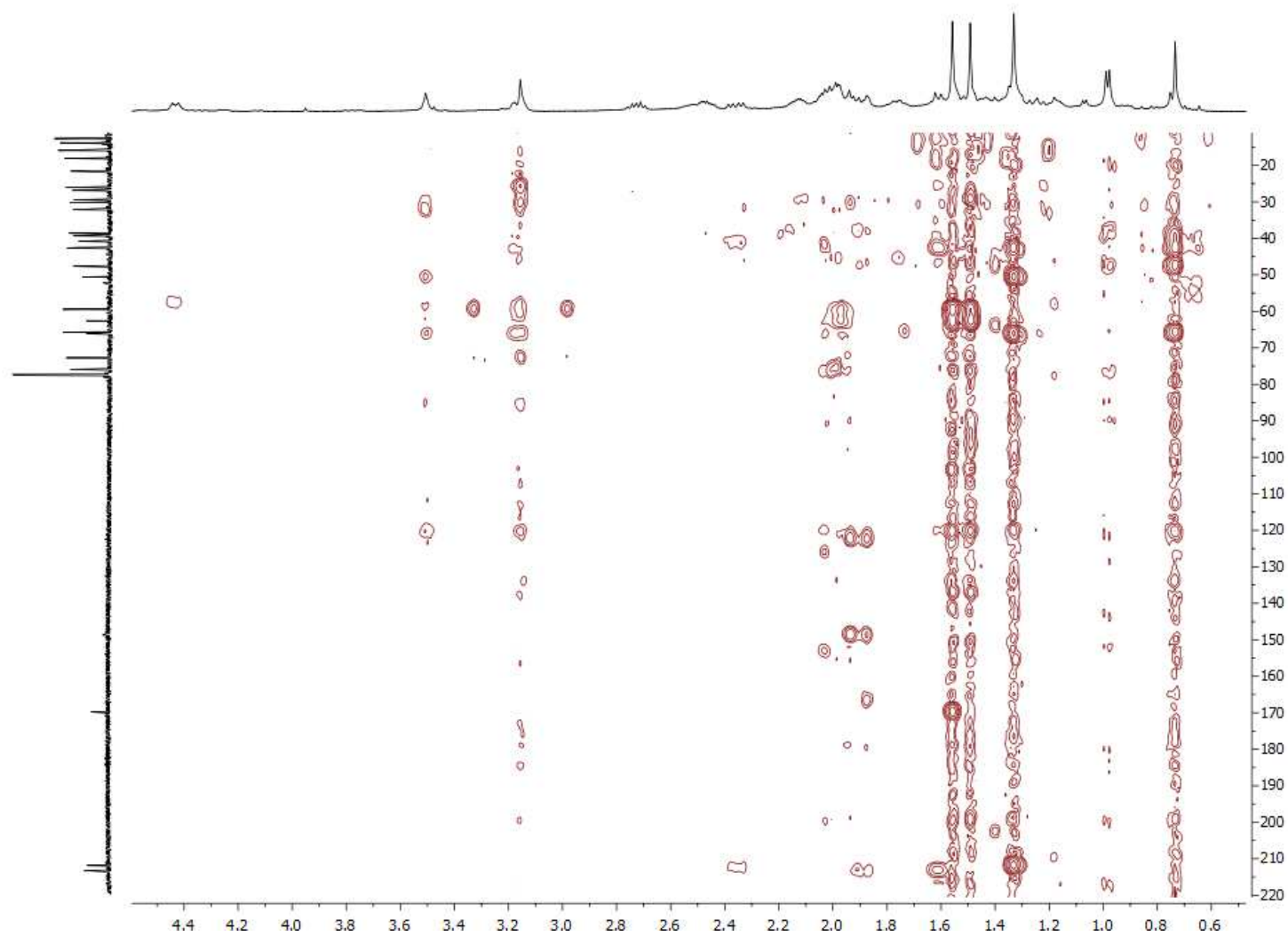
Figure S 6. HMBC NMR spectrum of 1, in CDCl₃.

Figure S 7. HMBC expansion of 1, in CDCl₃.
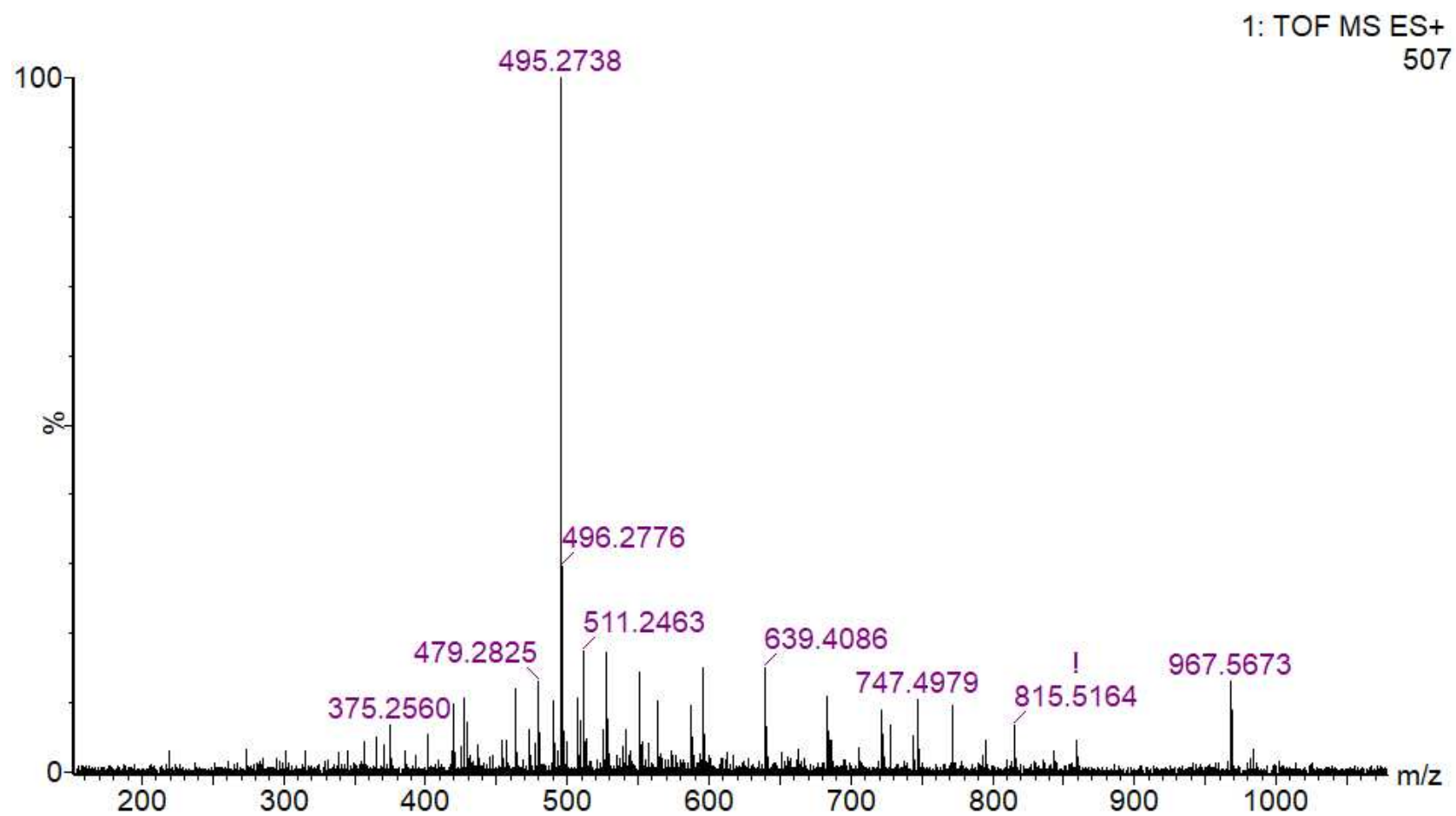
Figure S 8. HRESIMS spectrum of 1.
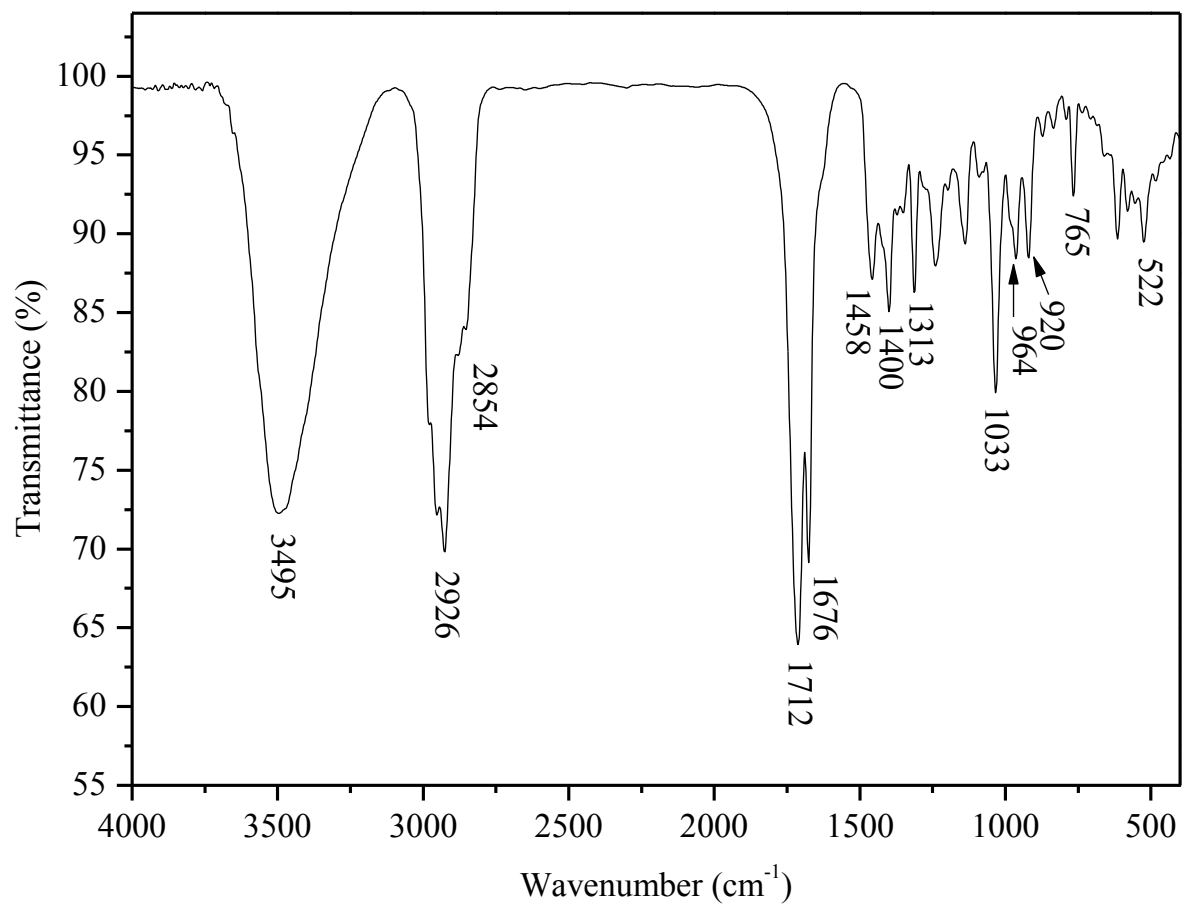
Figure S 9. FTIR spectrum of 2.
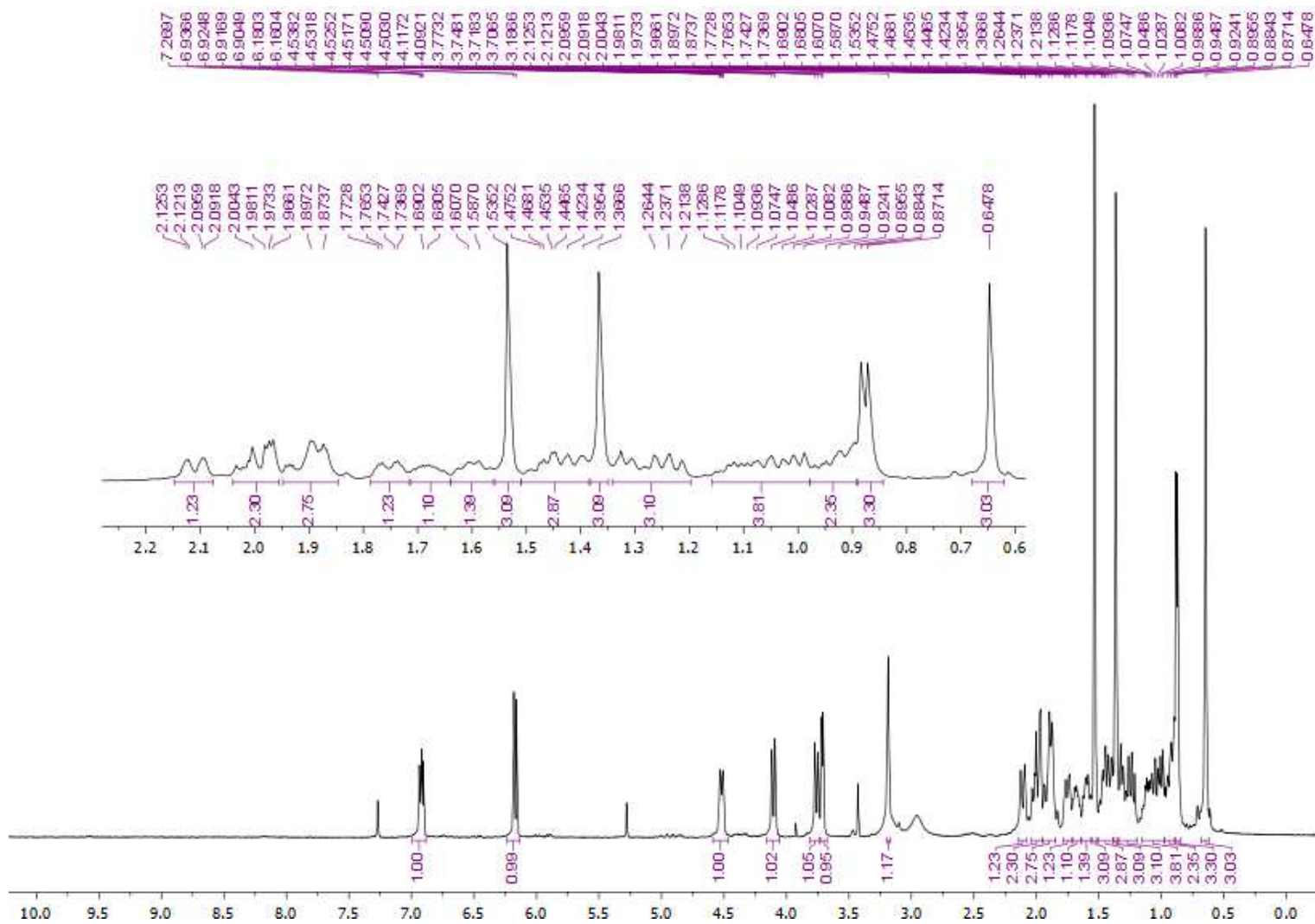
Figure S 10. ^{1}H NMR (500.13 MHz) spectrum of 2, in CDCl$_3$.
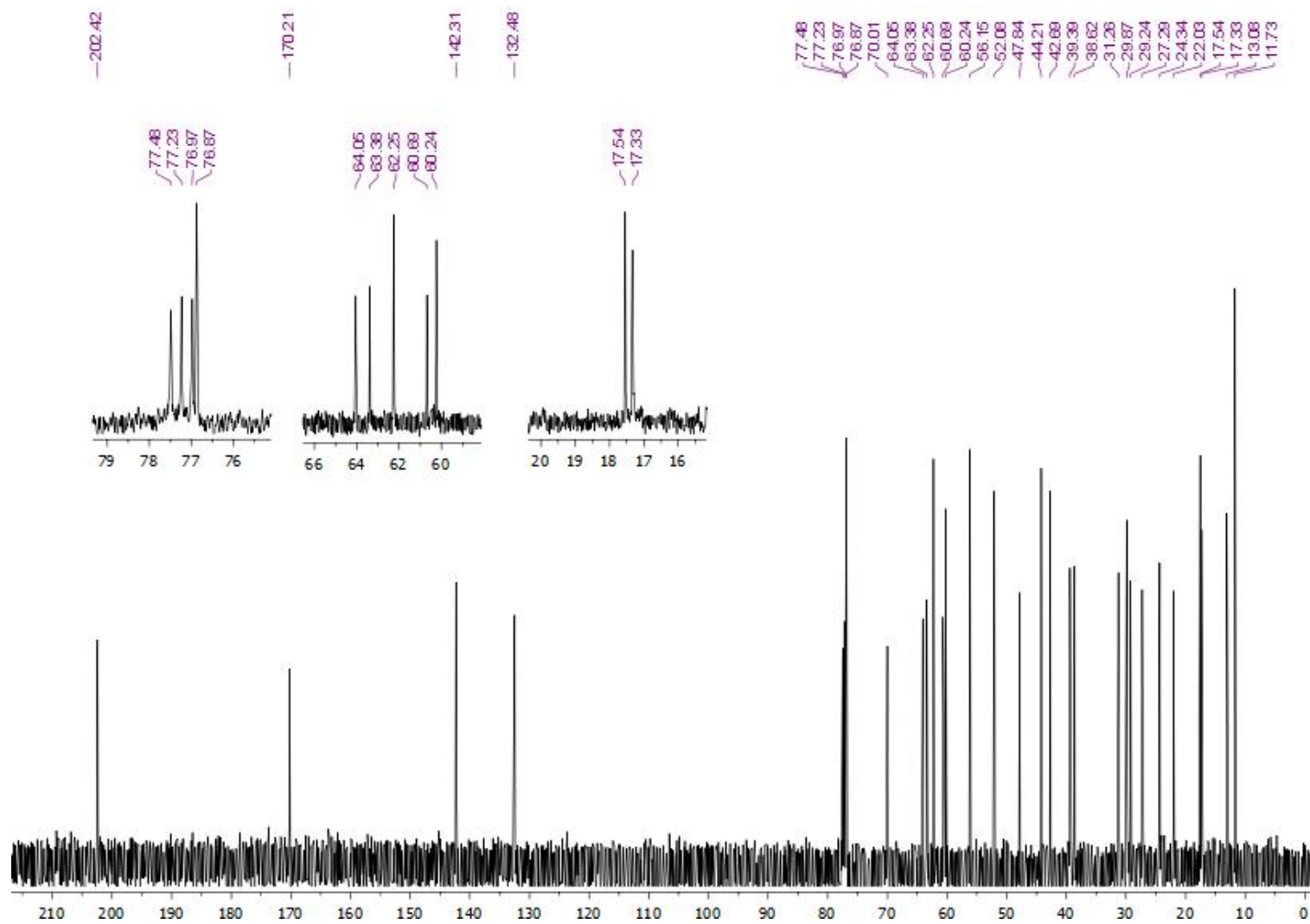
Figure S 11. ^{13}C NMR (125.75 MHz) spectrum of **2**, in CDCl₃.
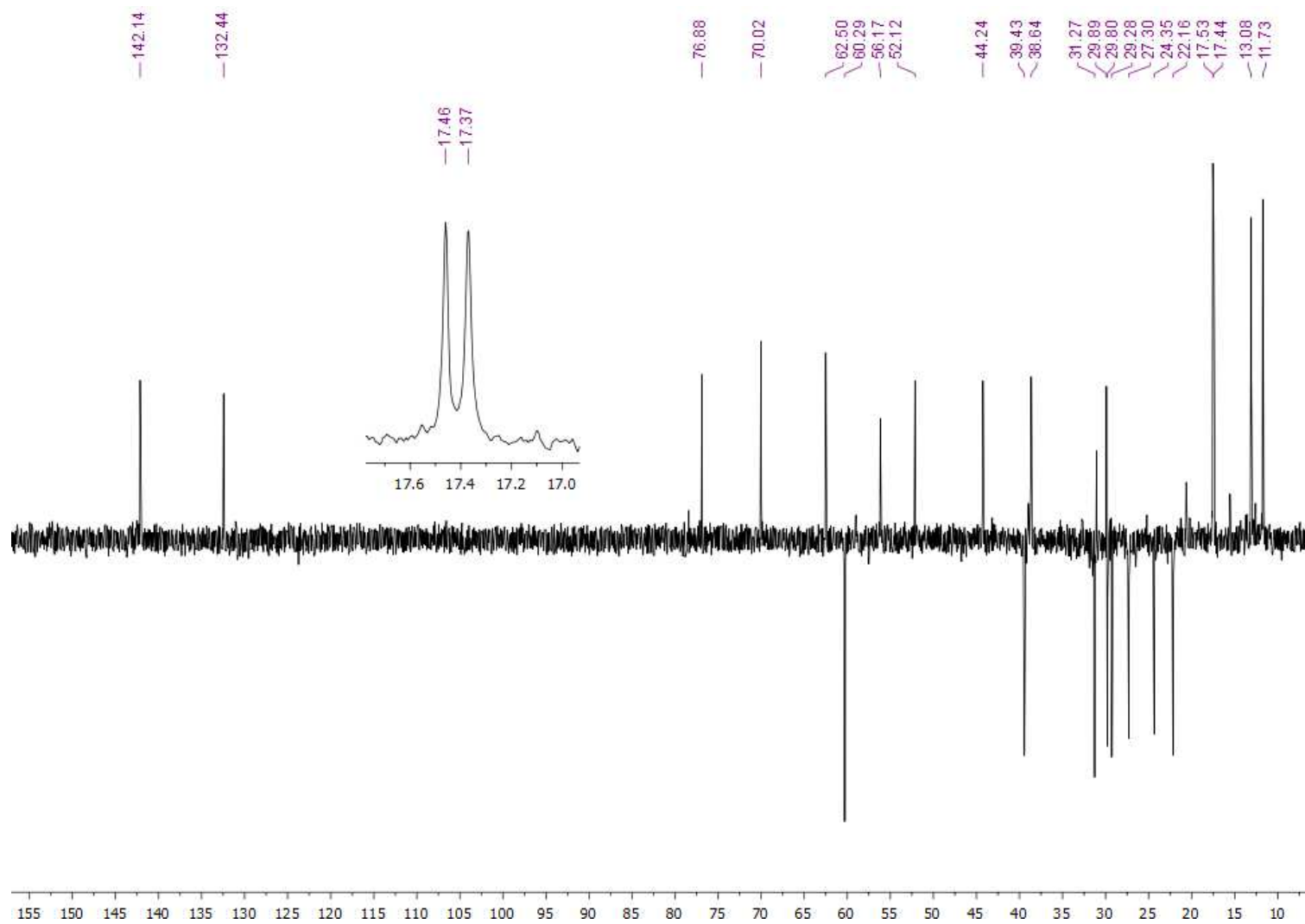
Figure S 12. DEPT 135° NMR (125.75 MHz) spectrum of 2, in CDCl₃.
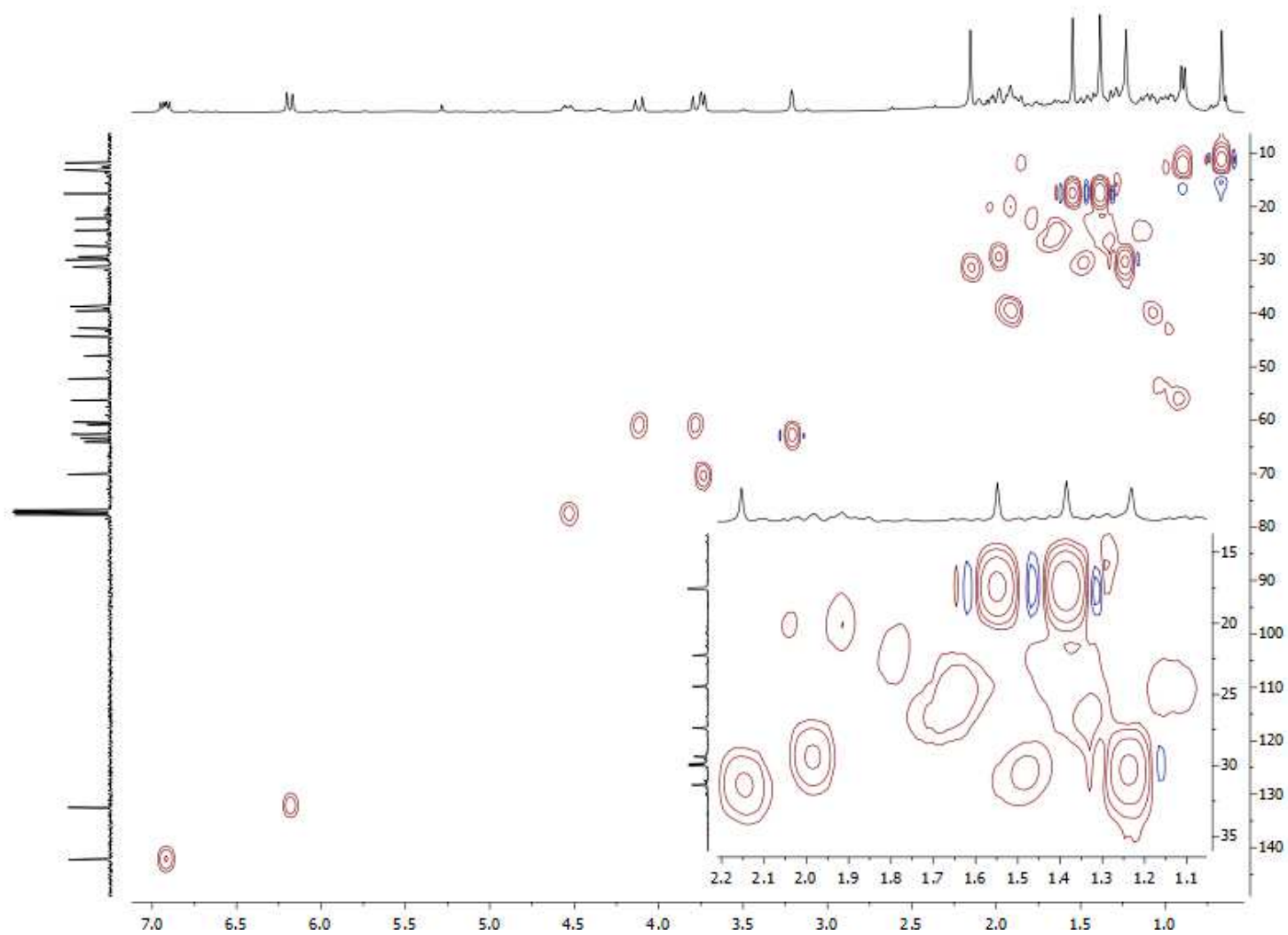
Figure S 13. HSQC NMR spectrum of 2, in CDCl₃.
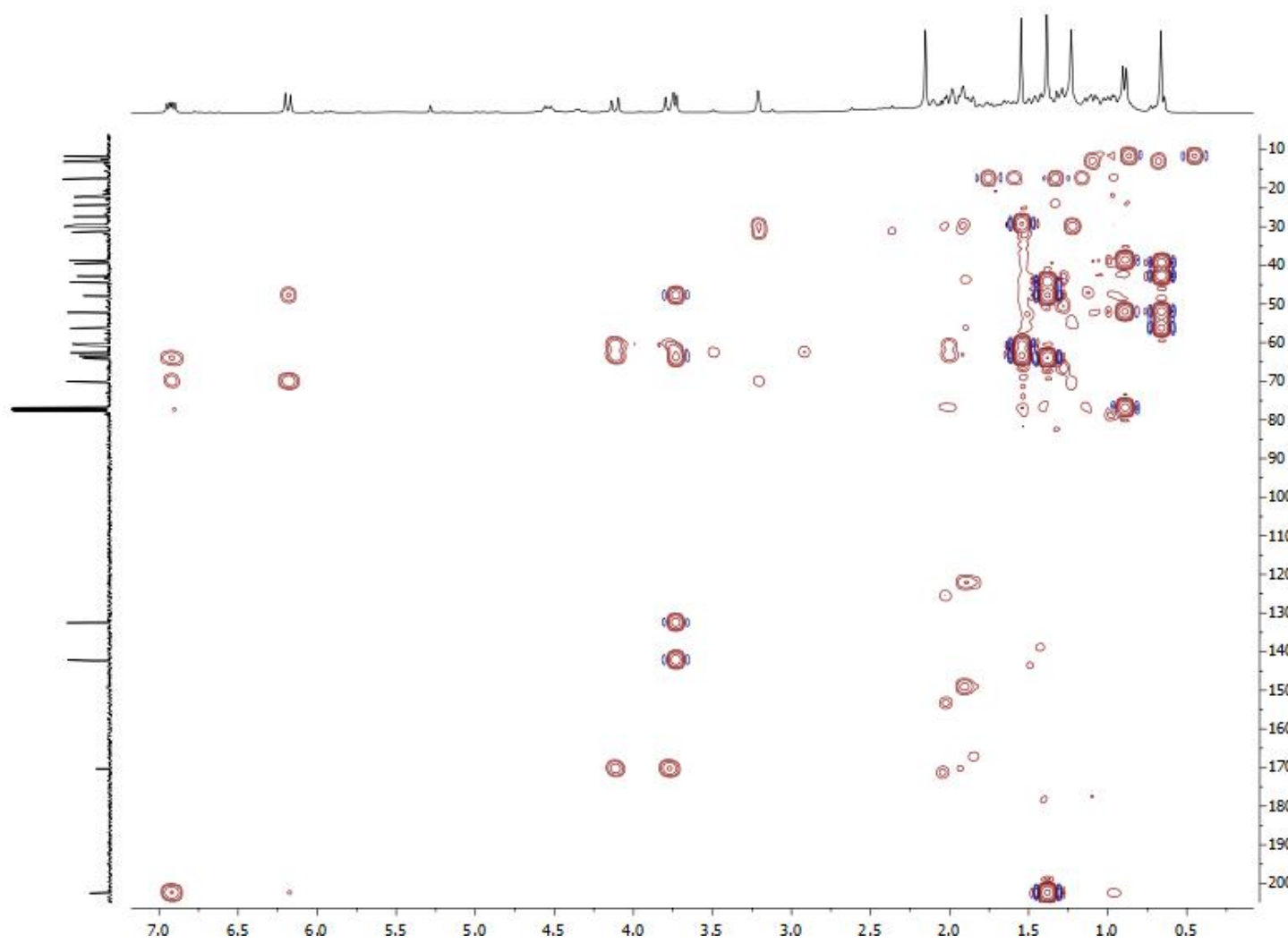
Figure S 14. HMBC NMR spectrum of 2, in CDCl₃.
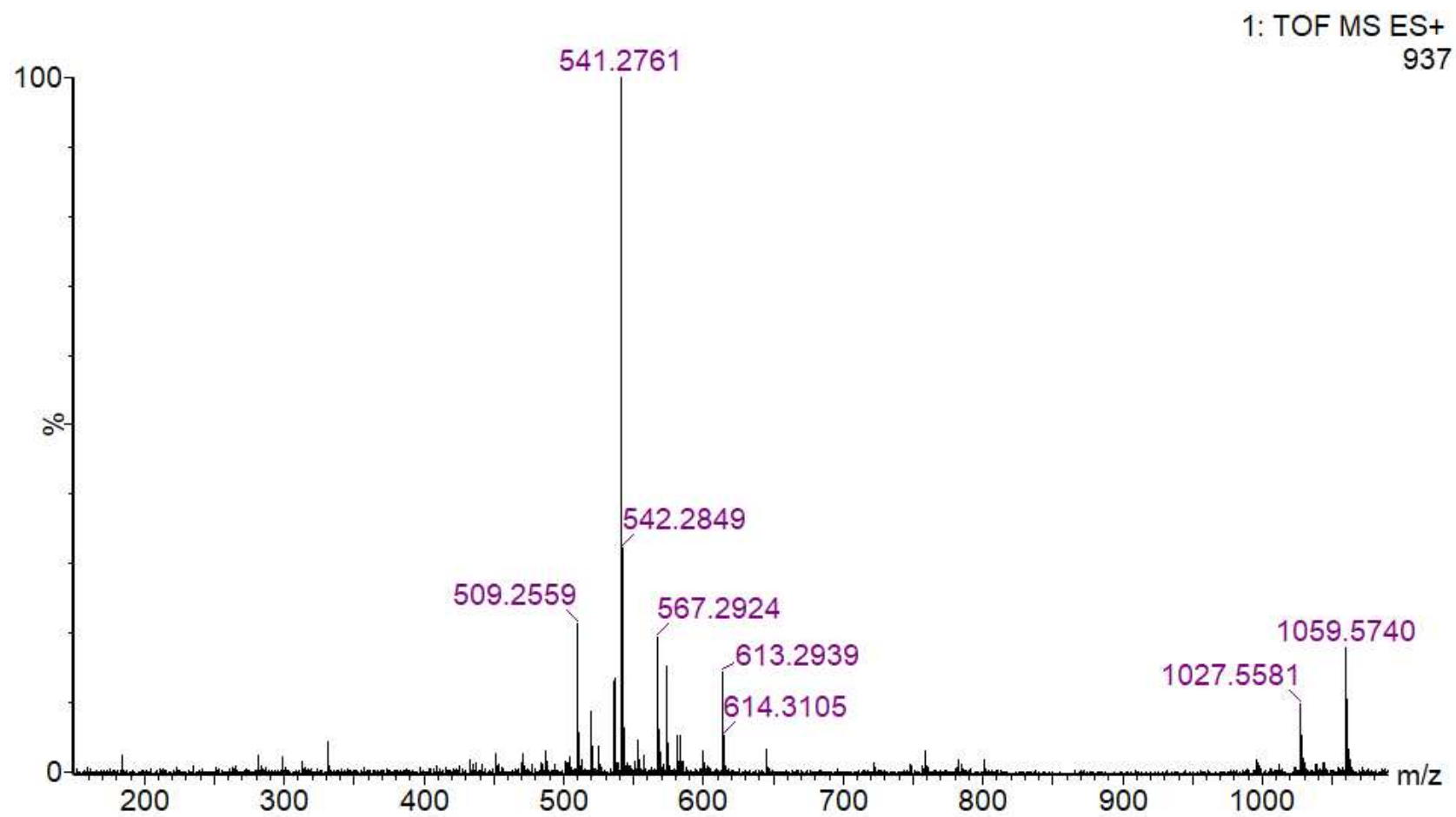
Figure S 15. HRESIMS spectrum of 2.
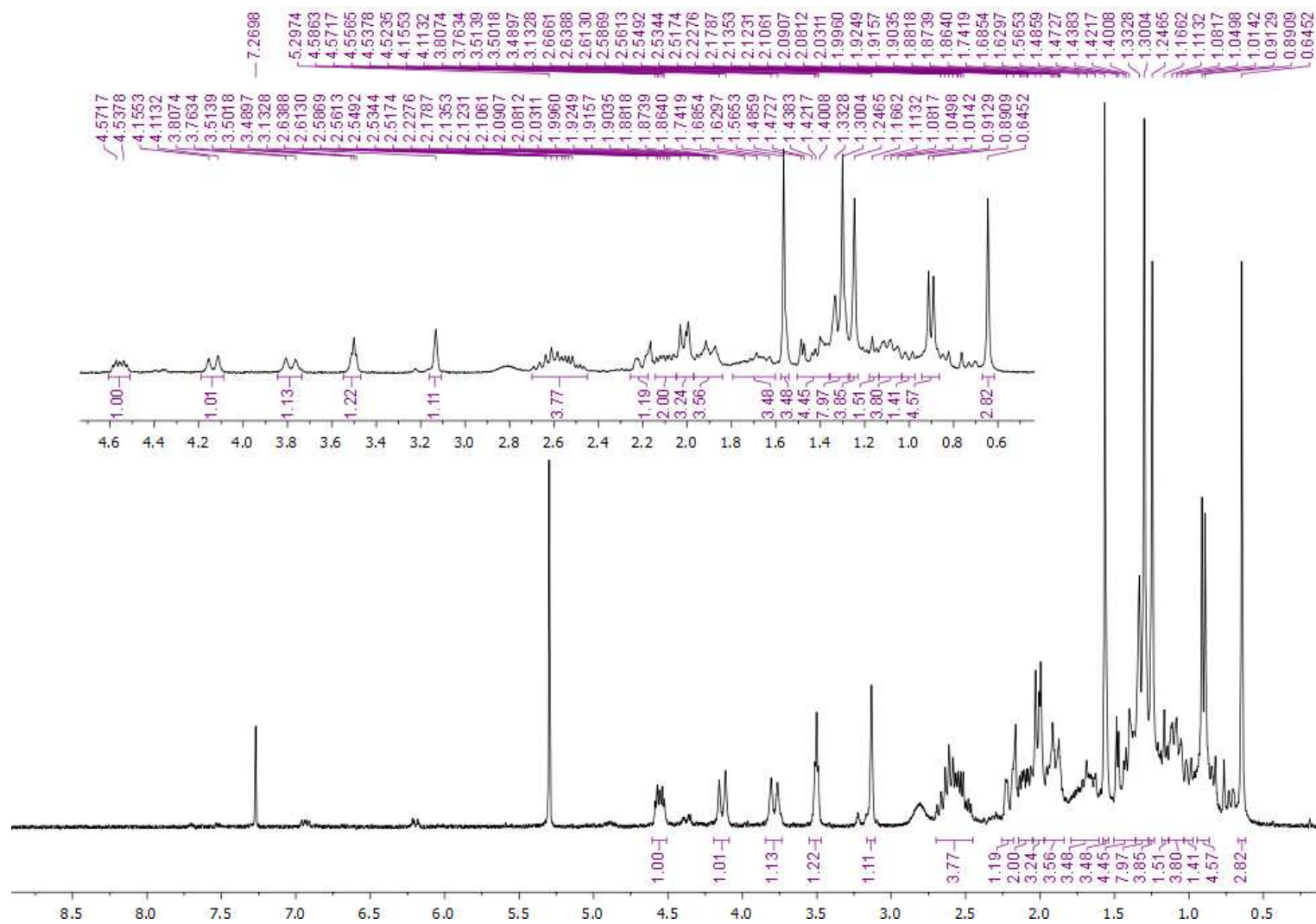
Figure S 16. ¹H NMR (300.13 MHz) spectrum of 3, in CDCl₃.
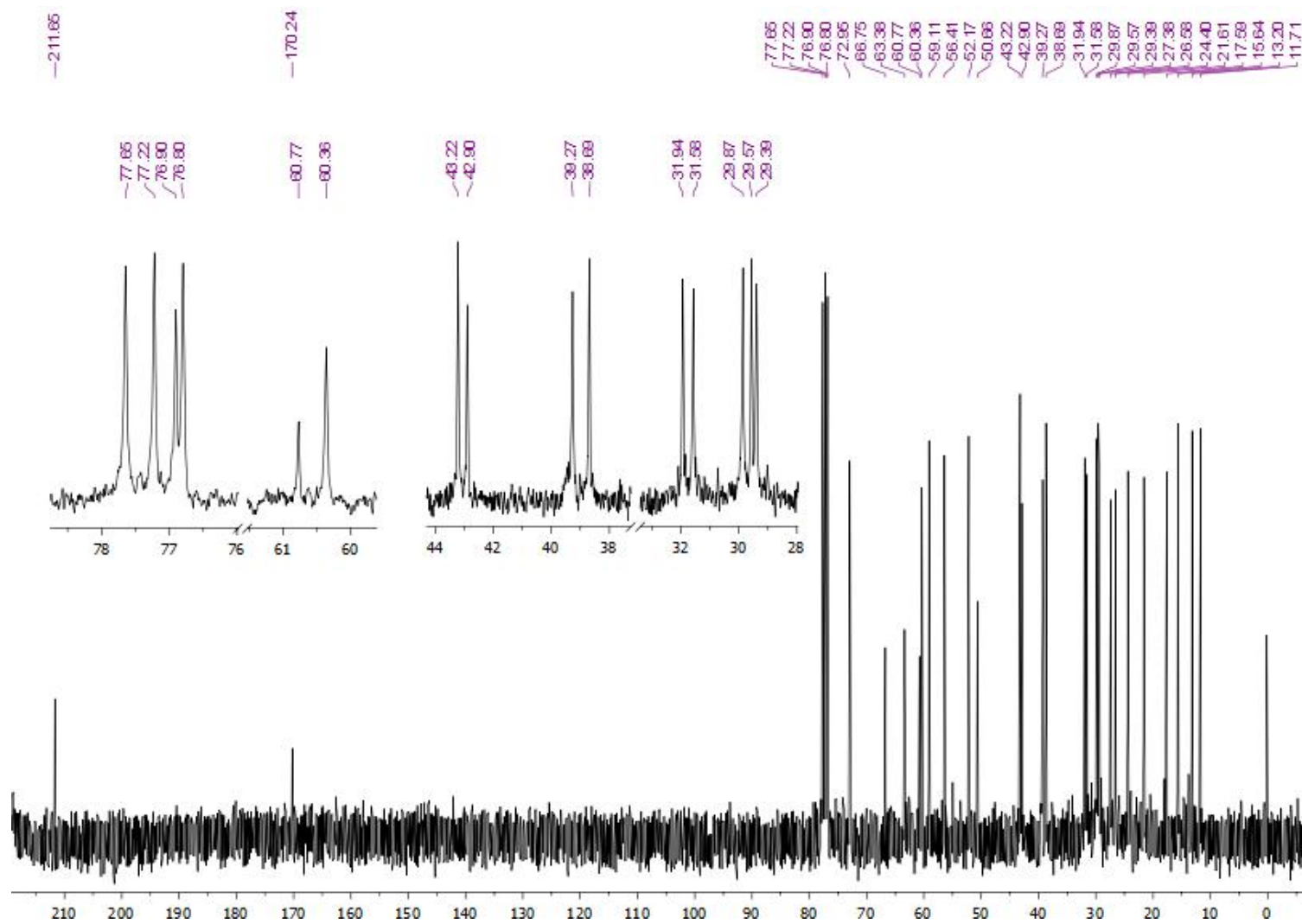
Figure S 17. ^{13}C NMR (75.47 MHz) spectrum of **3**, in CDCl$_3$.
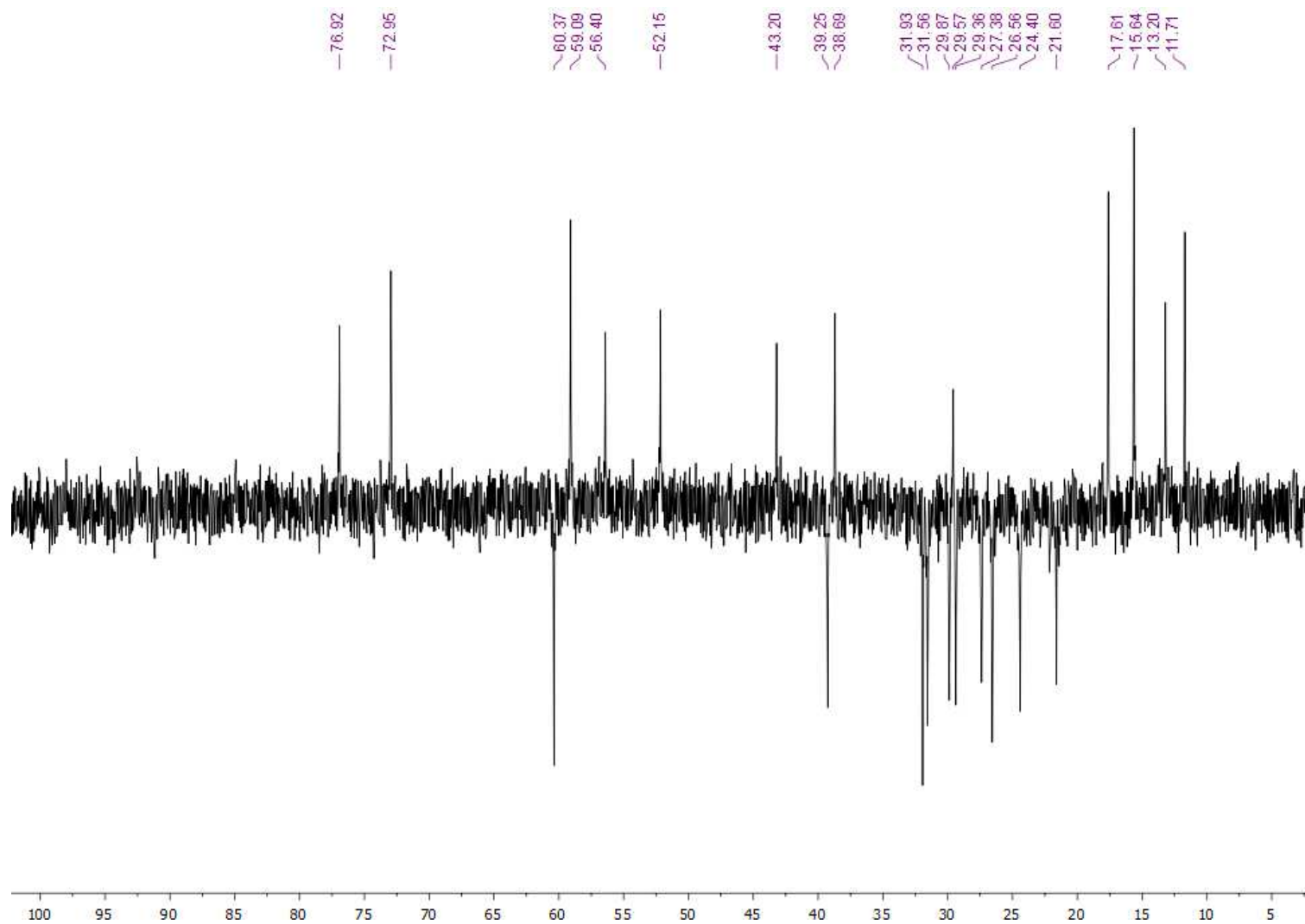
Figure S 18. DEPT 135° NMR (75.47 MHz) spectrum of 3, in CDCl₃.
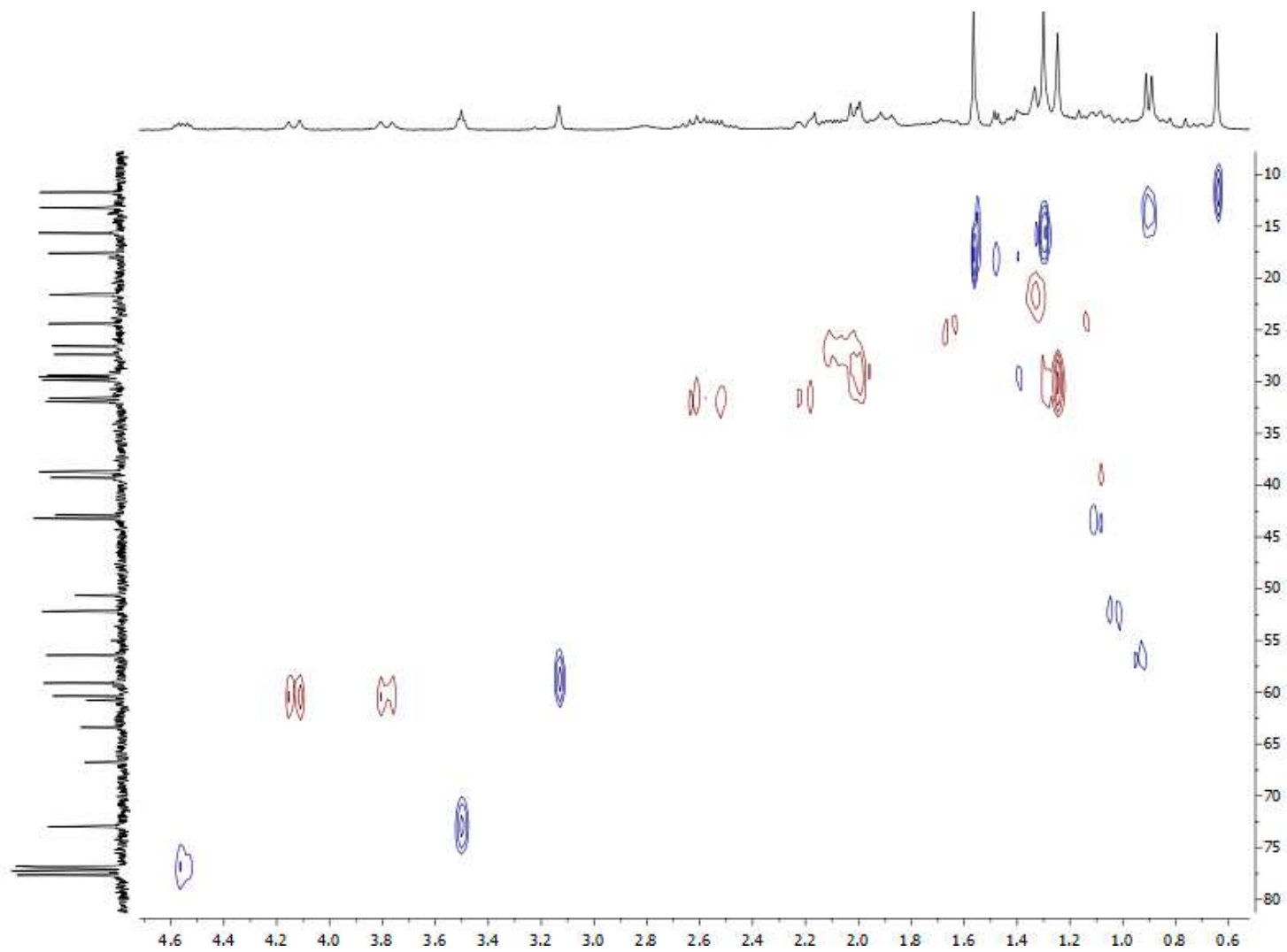
Figure S 19. HSQC NMR spectrum of 3, in CDCl₃.
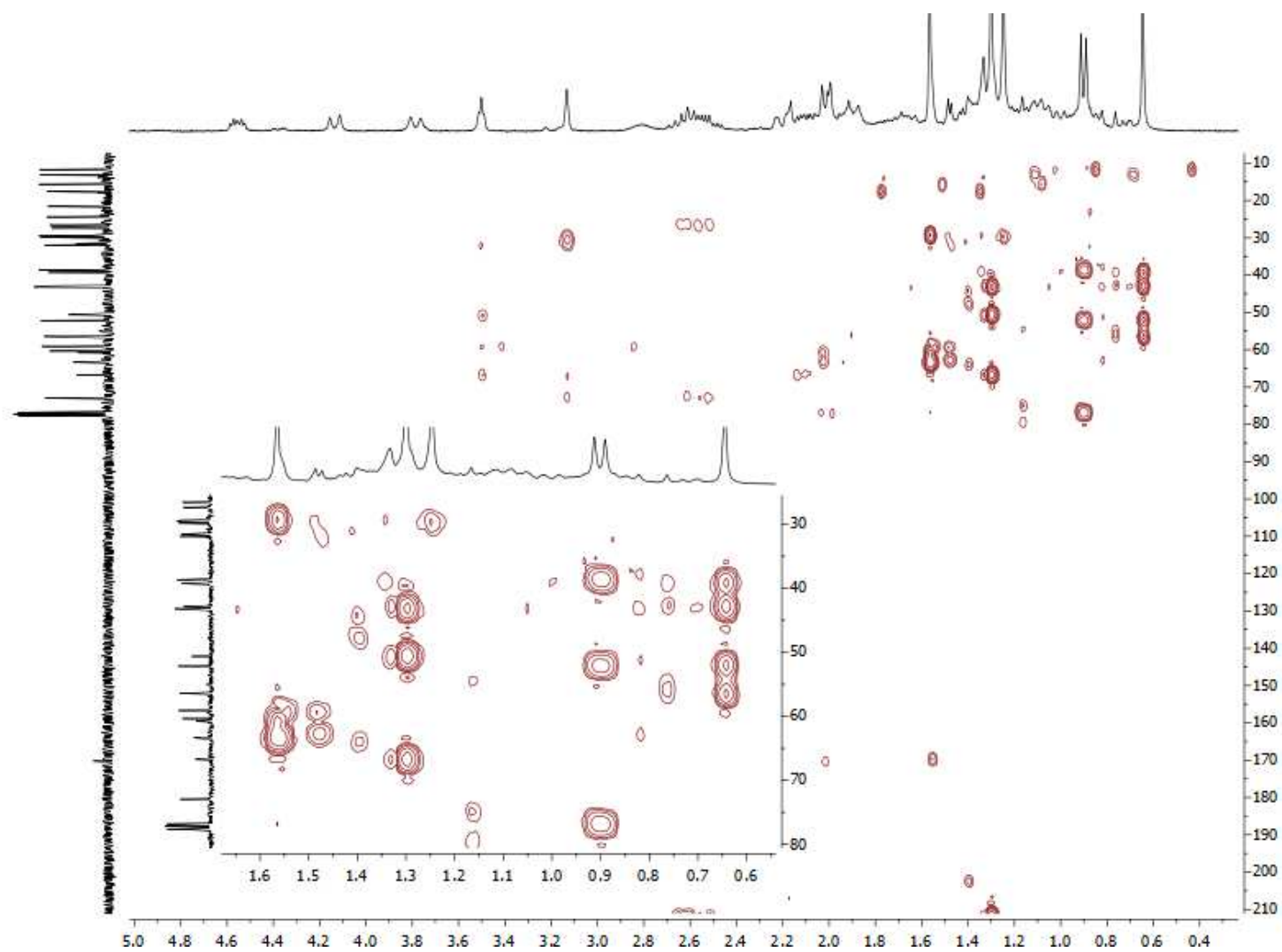
Figure S 20. HMBC NMR spectrum of 3, in CDCl₃.
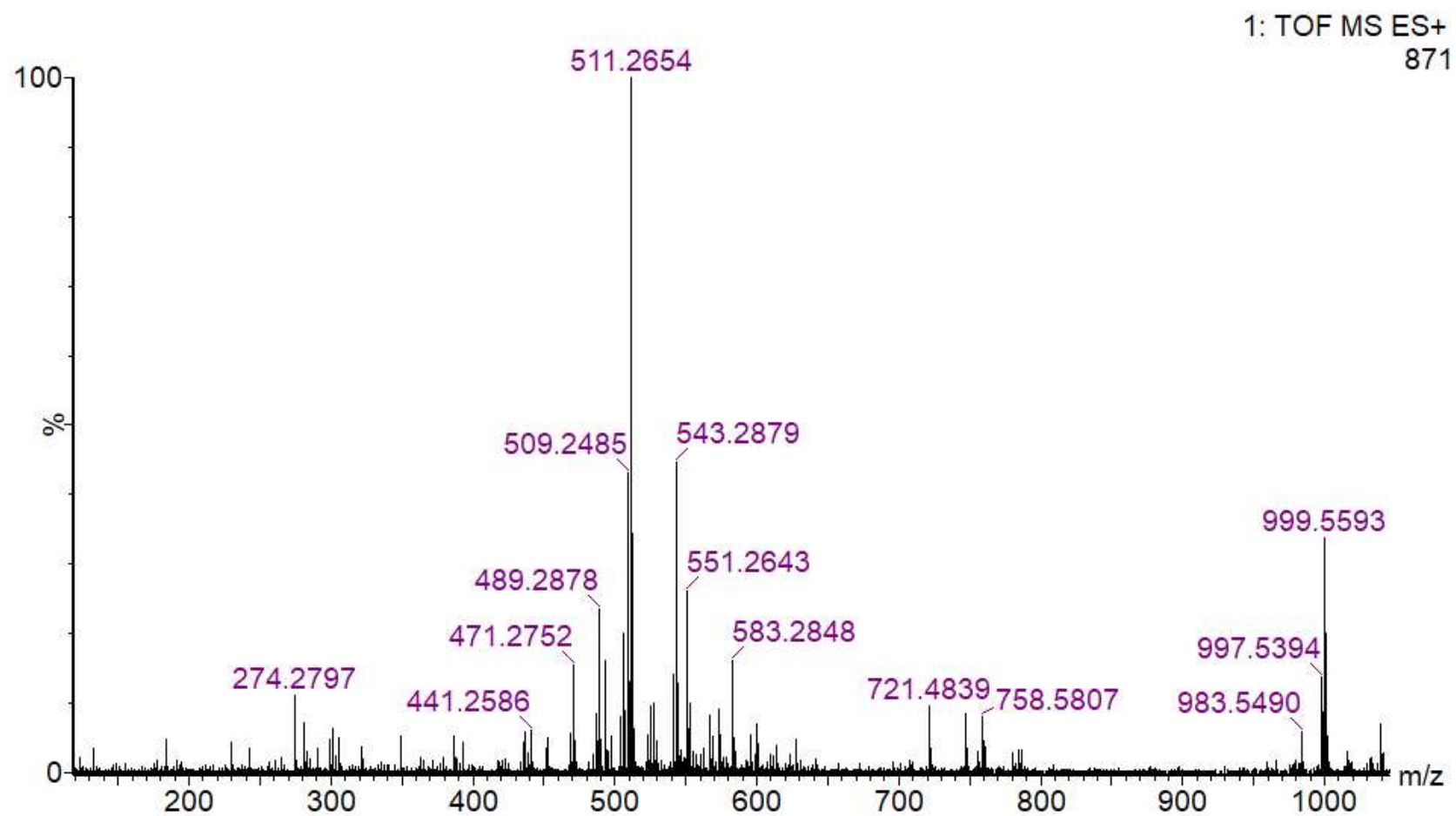
Figure S 21. HRESIMS spectrum of 3.
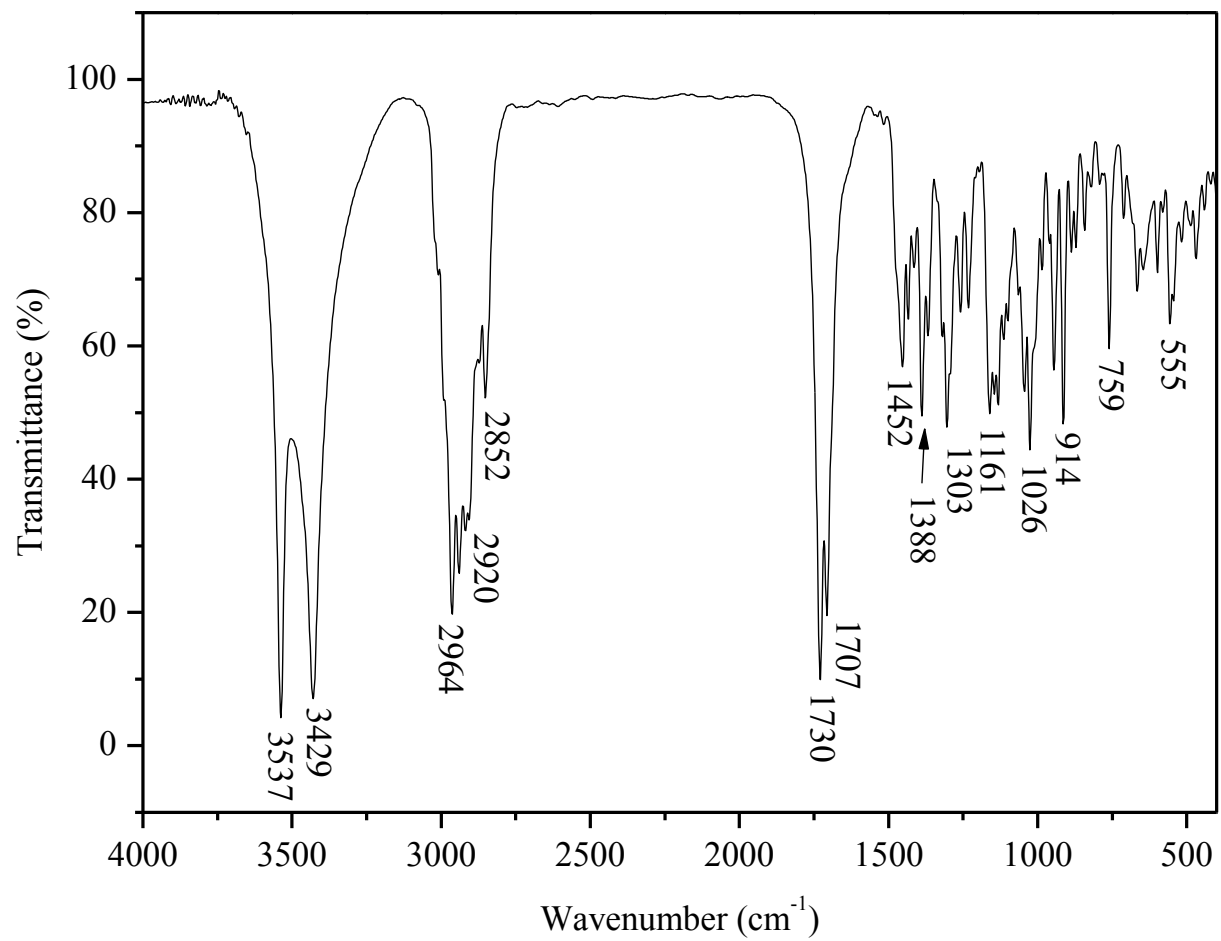
Figure S 22. FTIR spectrum of 4.

Figure S 23. ^{1}H NMR (300.13 MHz) spectrum of 4, in C$_5$D$_5$N.
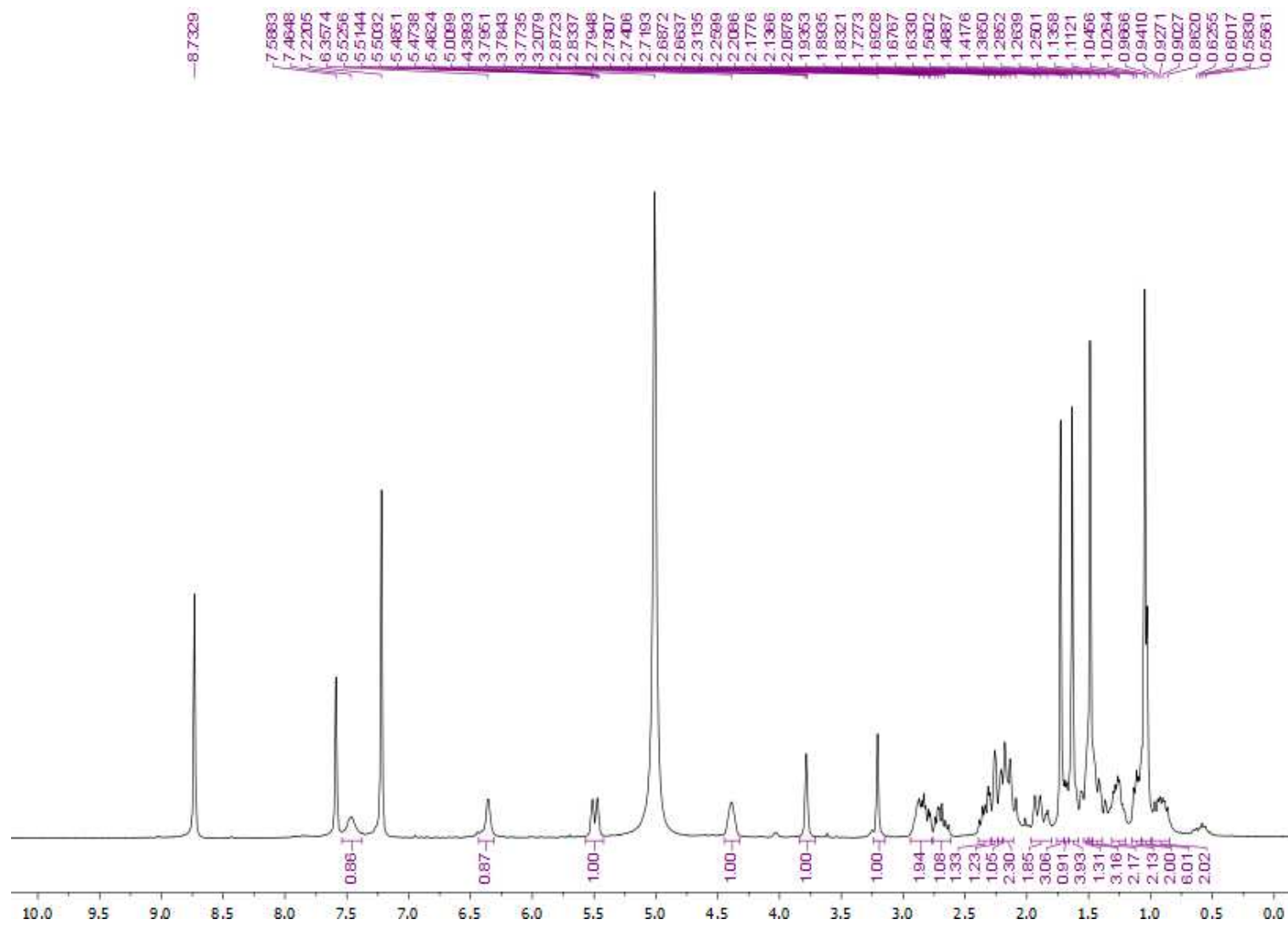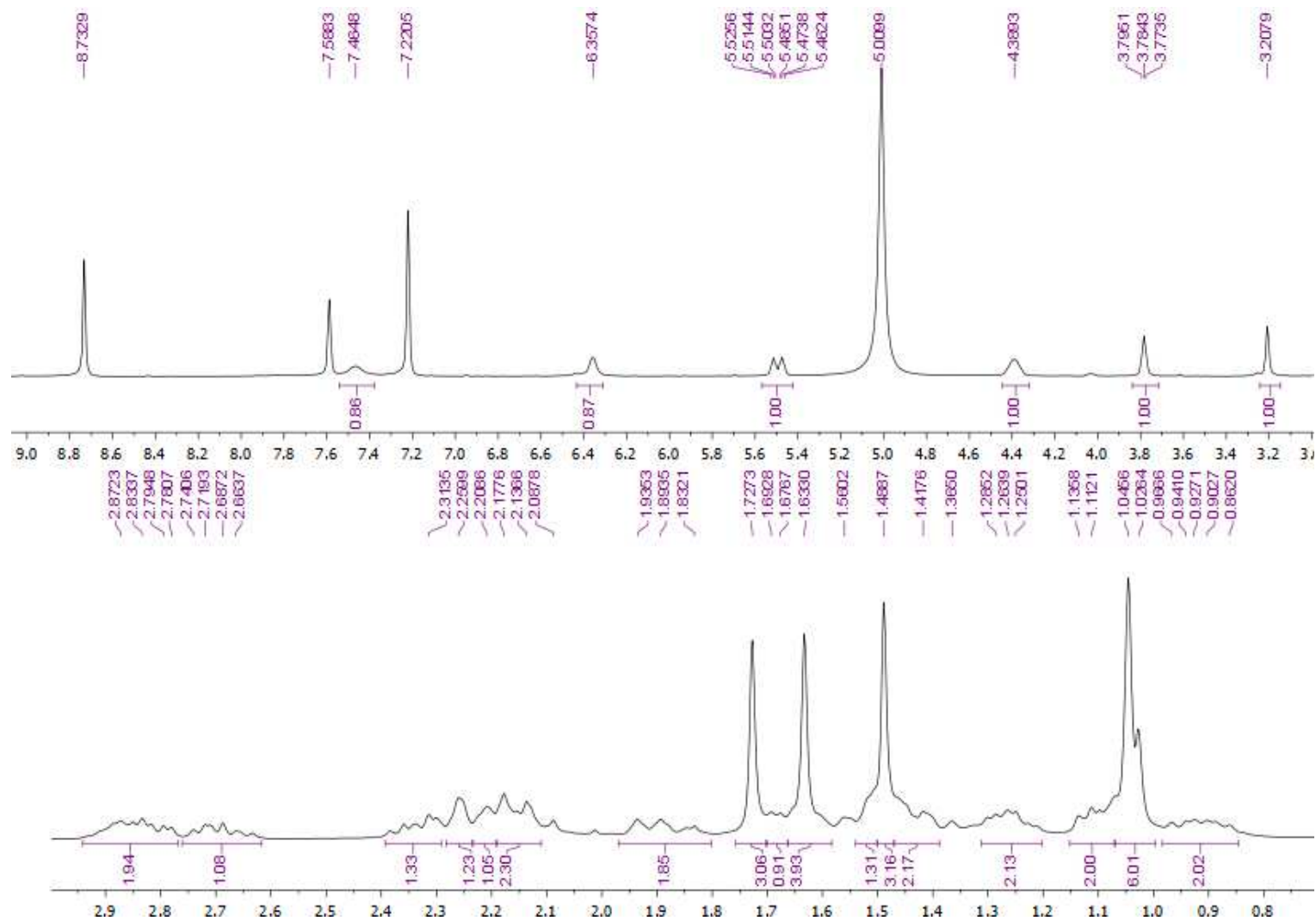
Figure S 24. ^{1}H NMR (300.13 MHz) spectrum of **4**, in C$_5$D$_5$N.
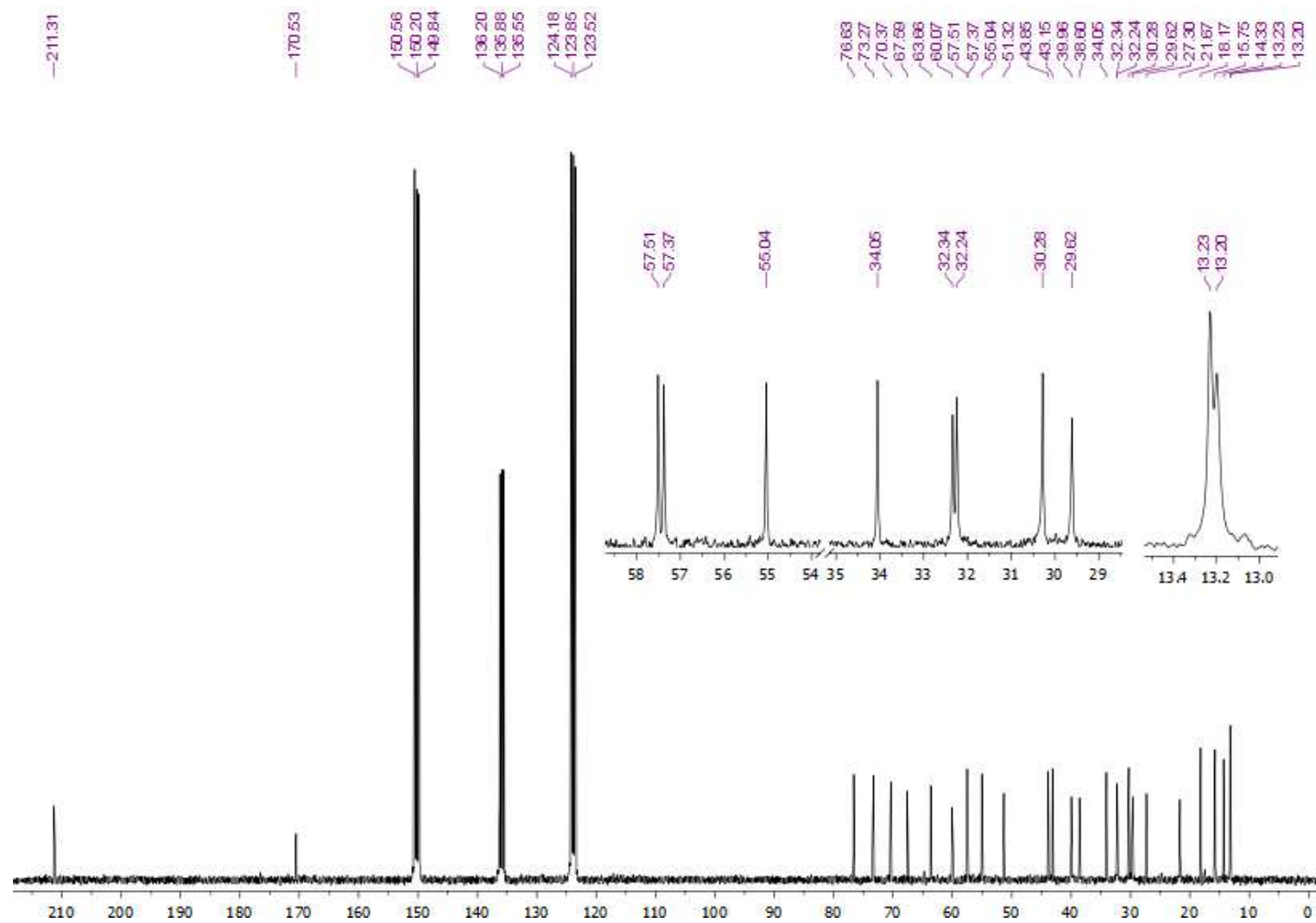
Figure S 25. ^{13}C NMR (75.47 MHz) spectrum of 4, in C$_5$D$_5$N.
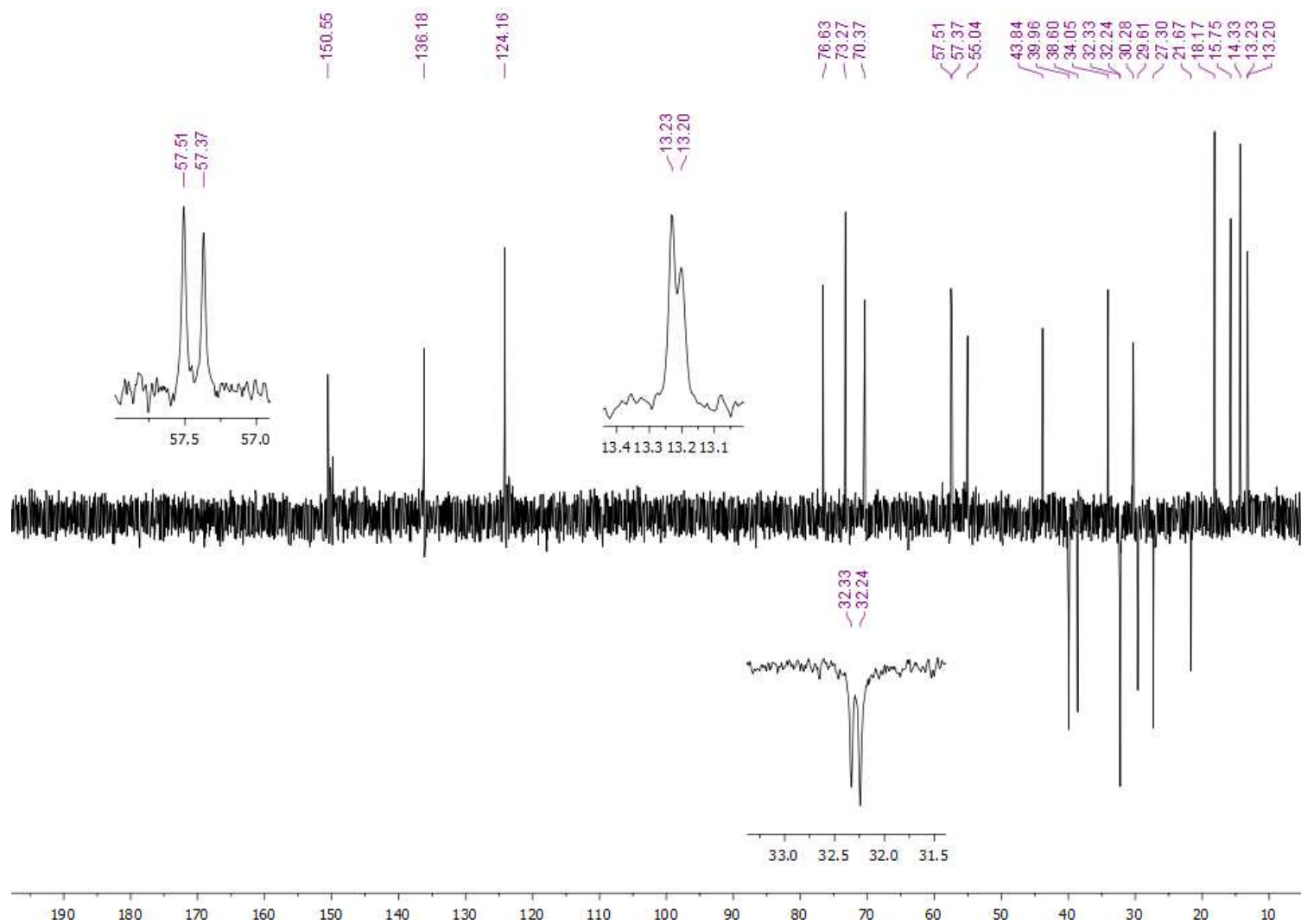
Figure S 26. DEPT 135° NMR (75.47 MHz) spectrum of 4, in C₅D₅N.
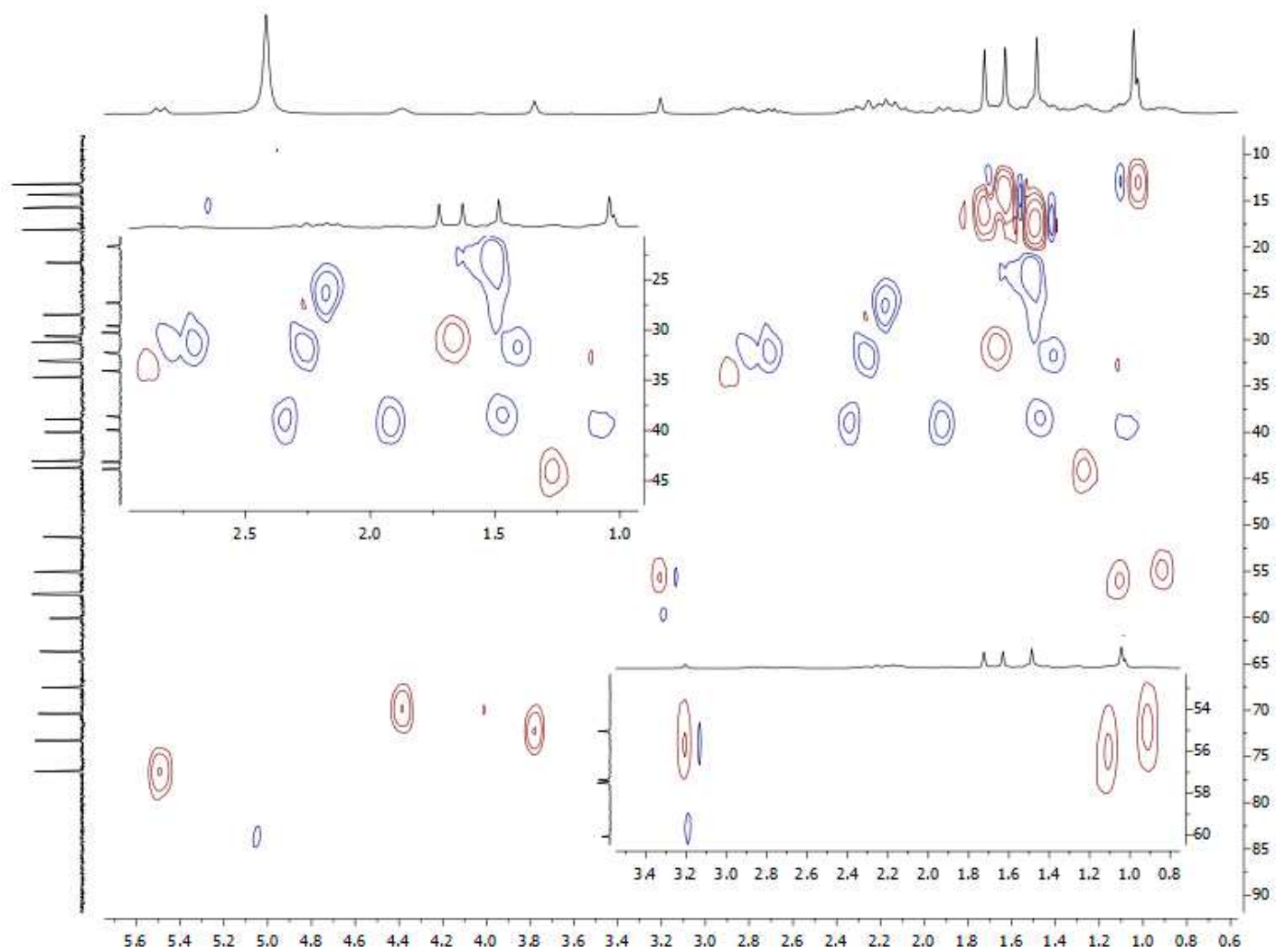
Figure S 27. HSQC NMR spectrum of 4, in C₅D₅N.
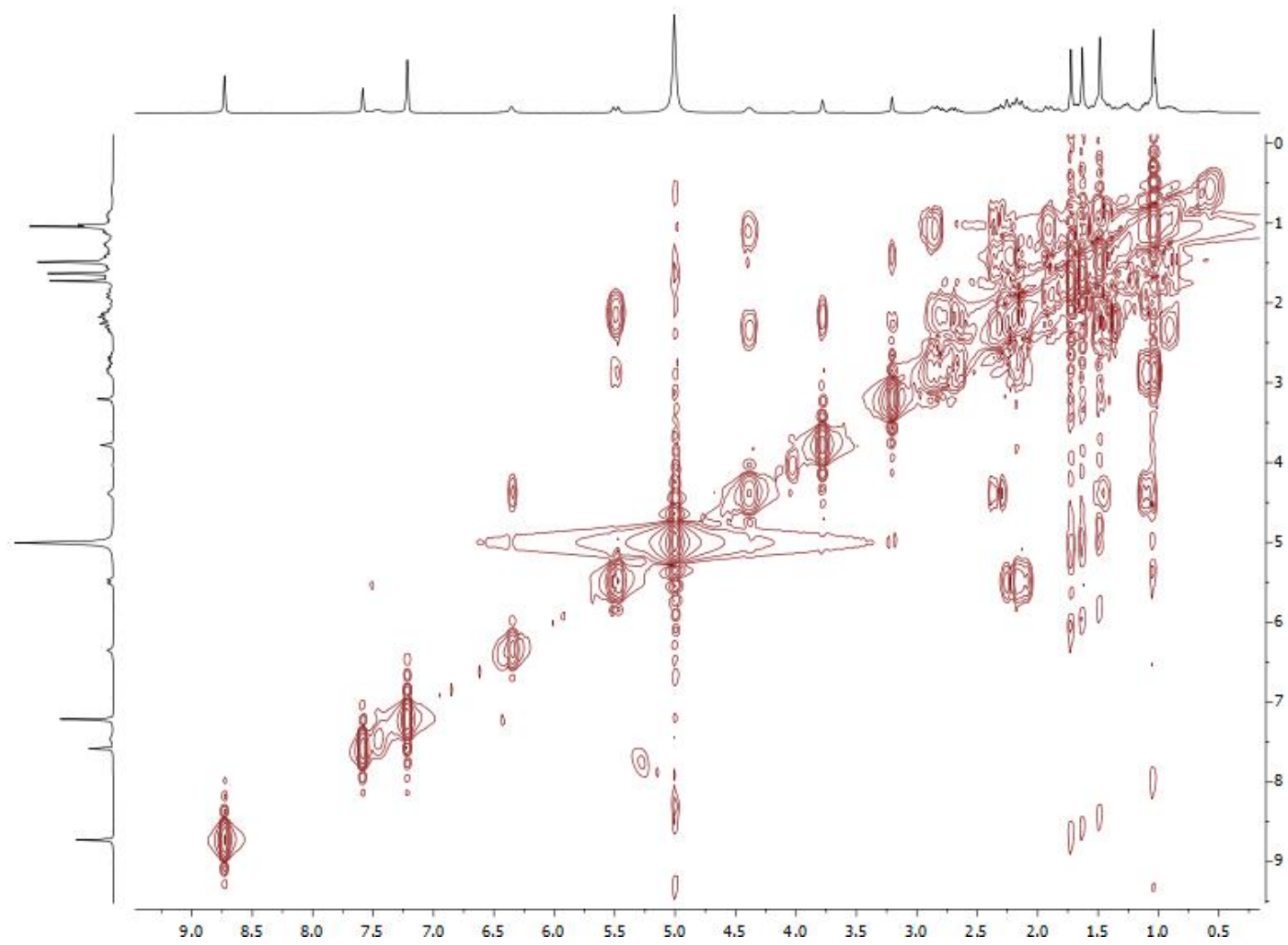
Figure S 28. COSY NMR spectrum of 4, in C$_5$D$_5$N.
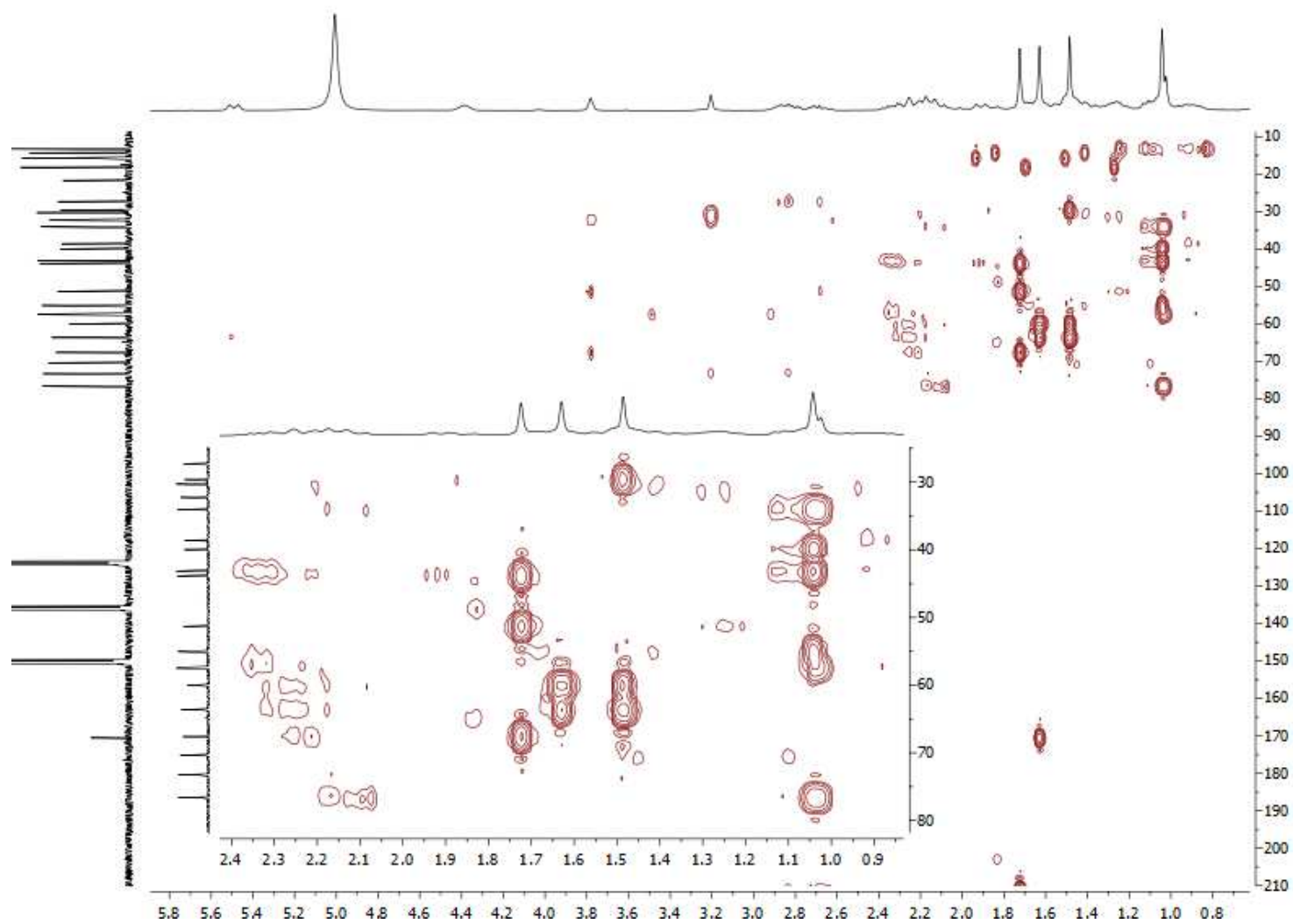
Figure S 29. HMBC NMR spectrum of 4, in C₅D₅N.
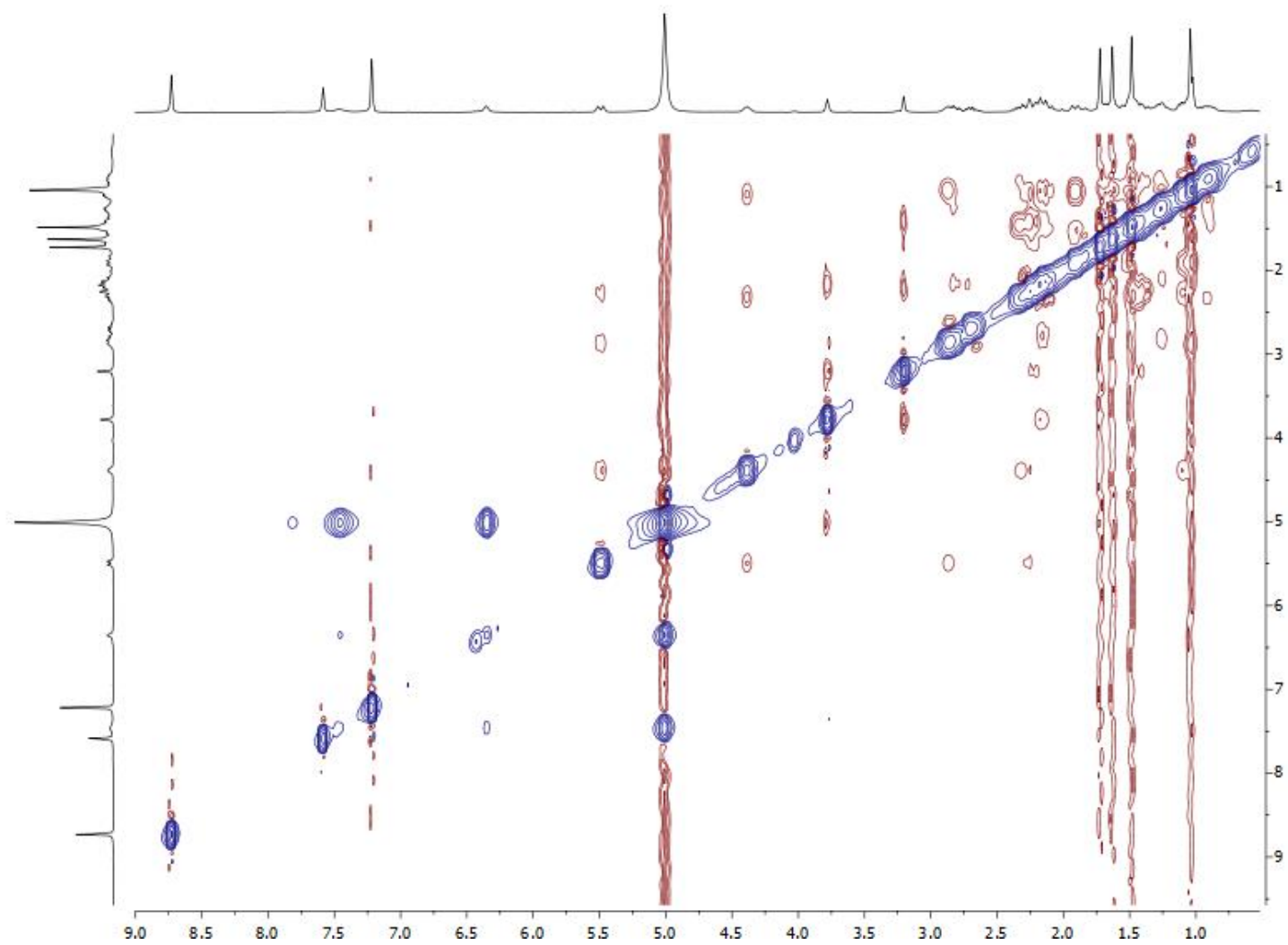
Figure S 30. NOESY NMR spectrum of 4, in C$_5$D$_5$N.
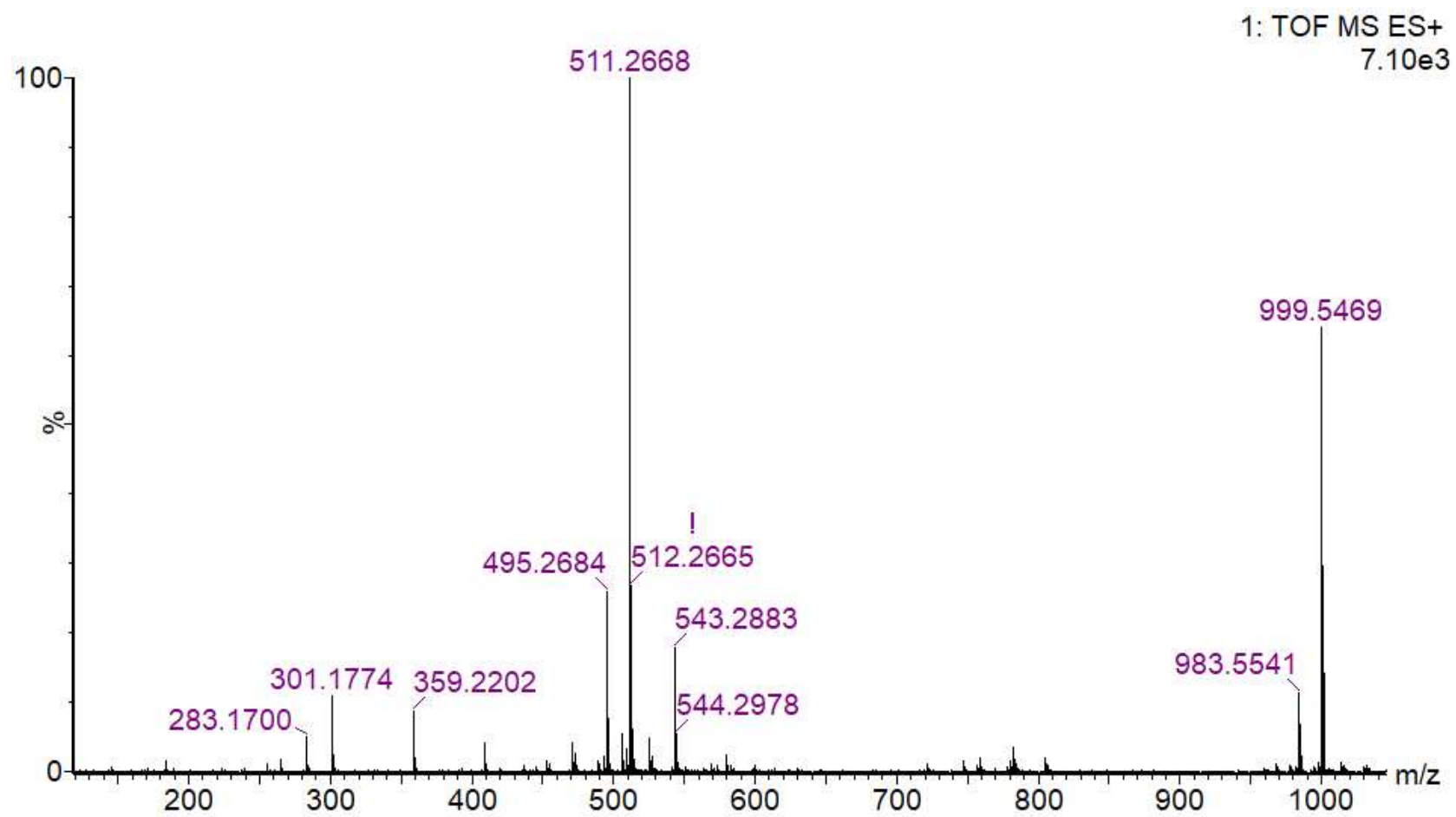
Figure S 31. HRESIMS spectrum of 4.
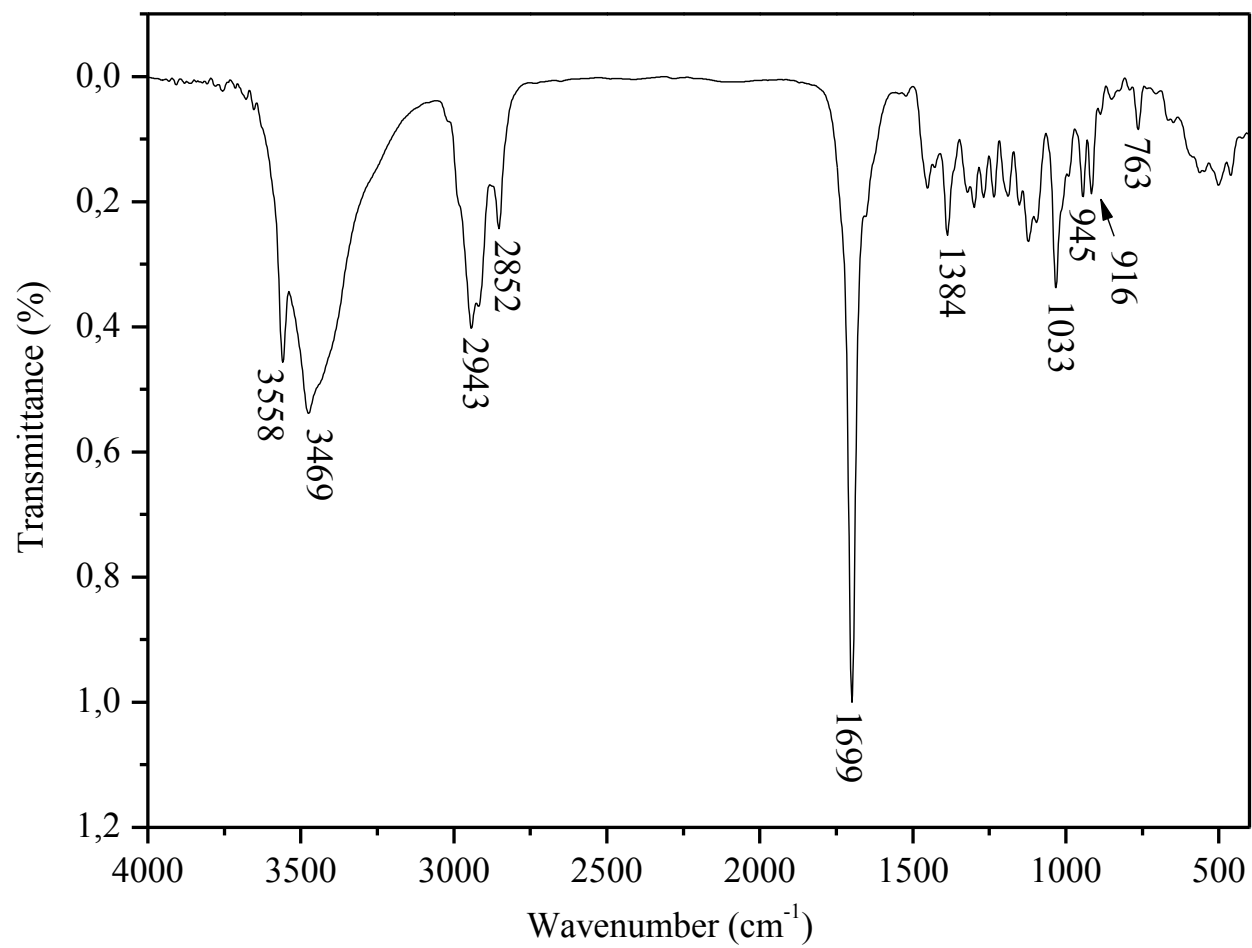
Figure S 32. FTIR spectrum of 5.
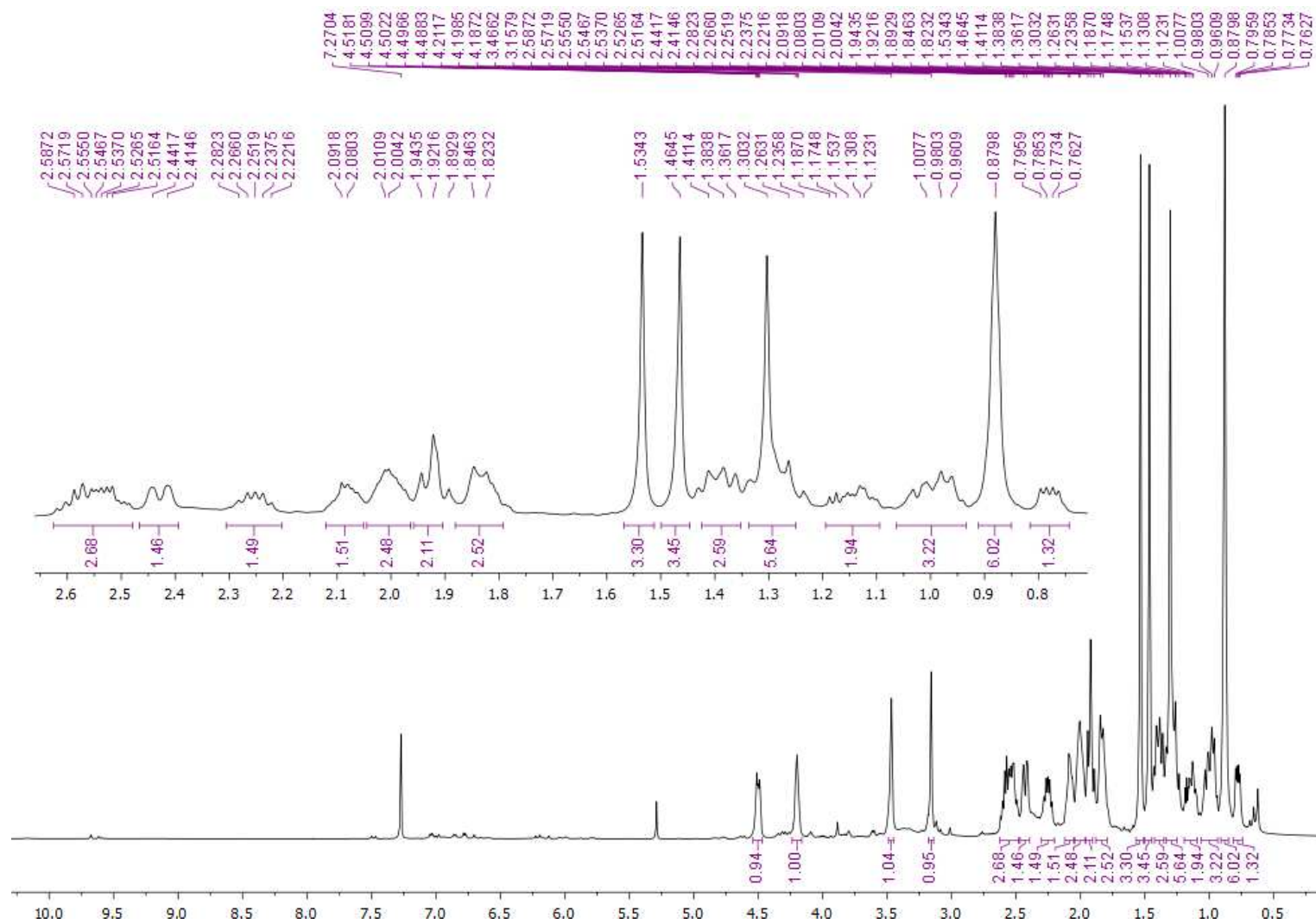
Figure S 33. ^{1}H NMR (300.13 MHz) spectrum of **5**, in CDCl$_3$.
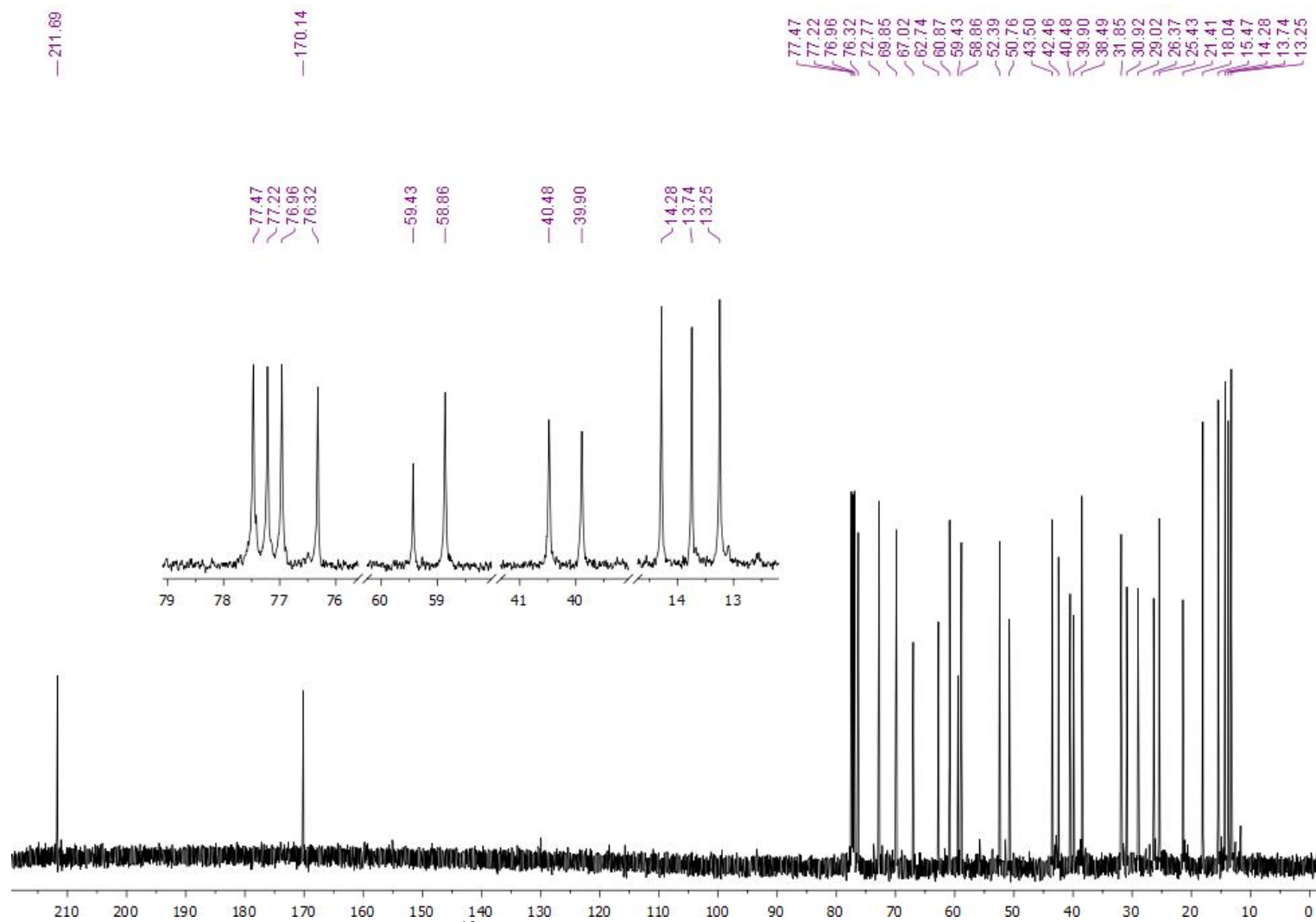
Figure S 34. ^{13}C NMR (75.47 MHz) spectrum of **5**, in CDCl₃.
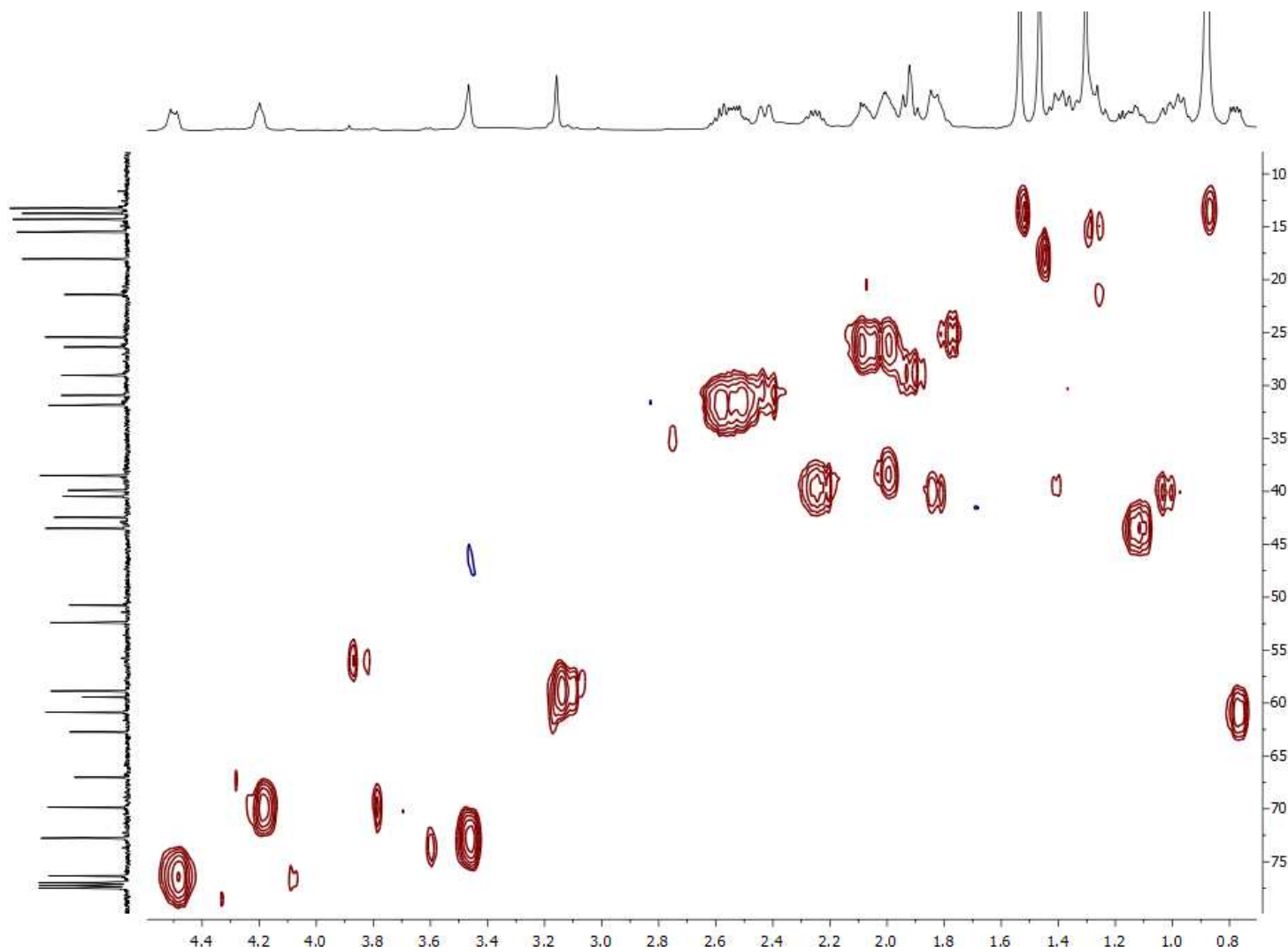
Figure S 35. HSQC NMR spectrum of 5, in CDCl₃.
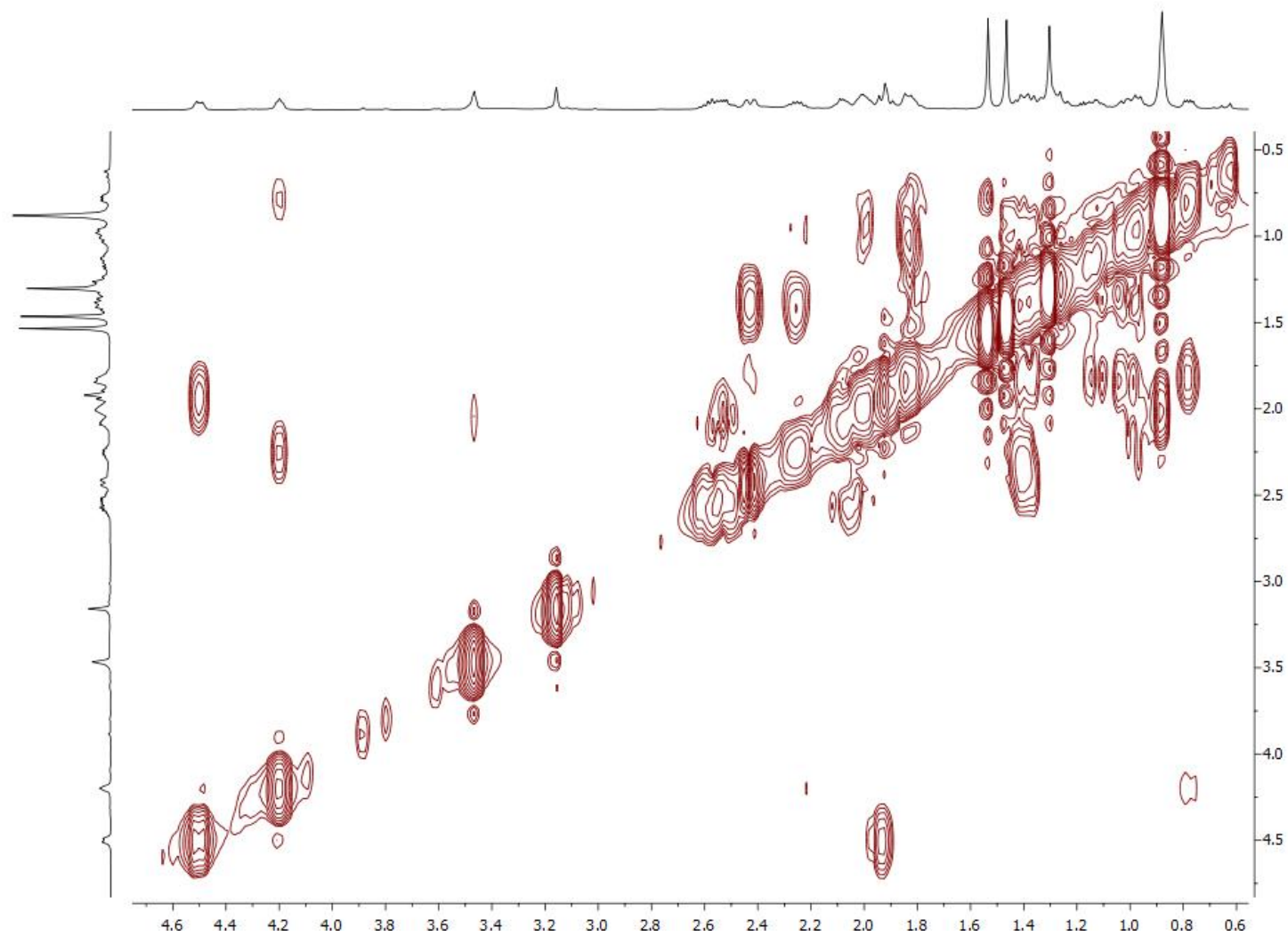
Figure S 36. COSY NMR spectrum of 5, in CDCl₃.
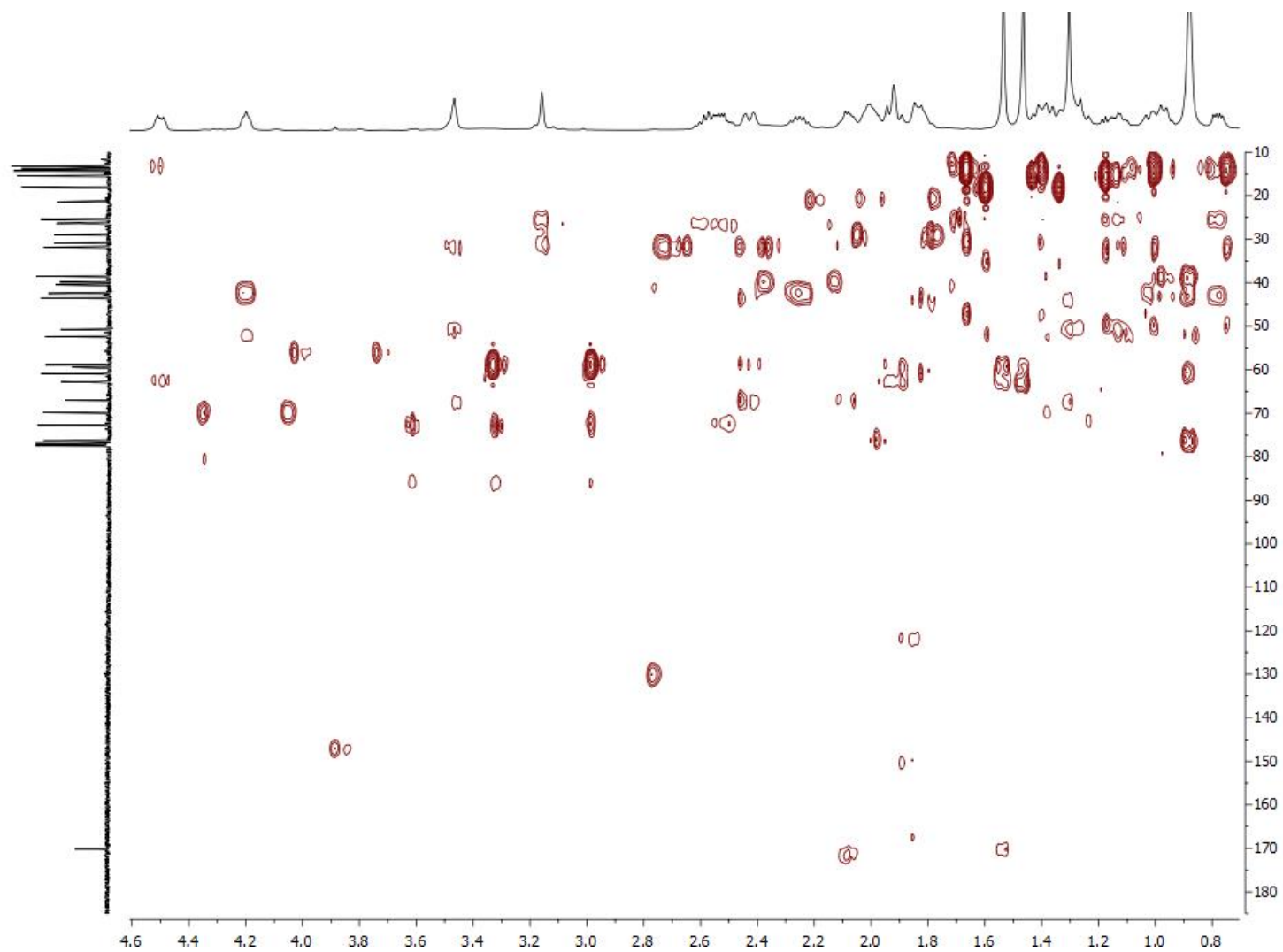
Figure S 37. HMBC NMR spectrum of 5, in CDCl₃.
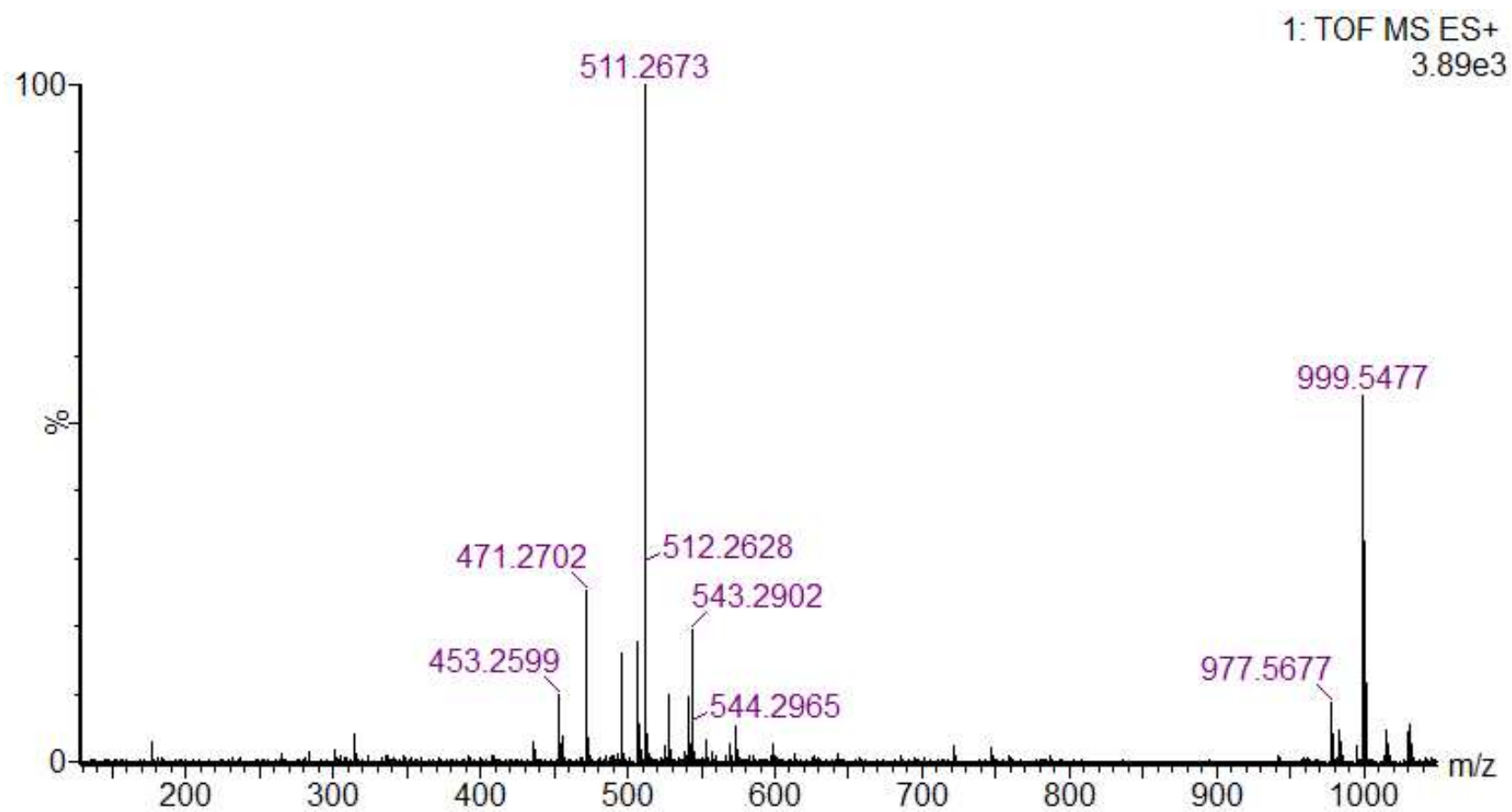
Figure S 38. HRESIMS spectrum of 5.
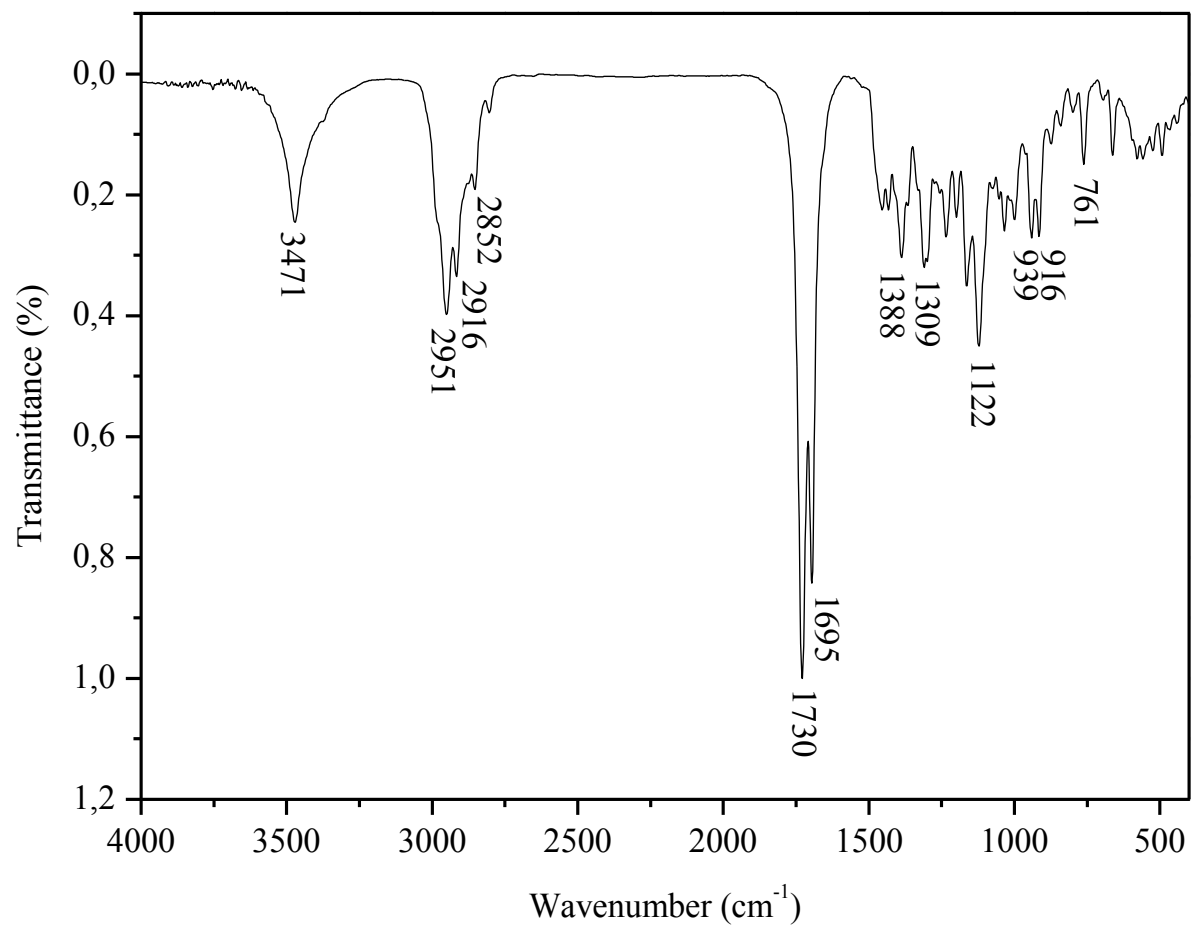
Figure S 39. FTIR spectrum of 6.
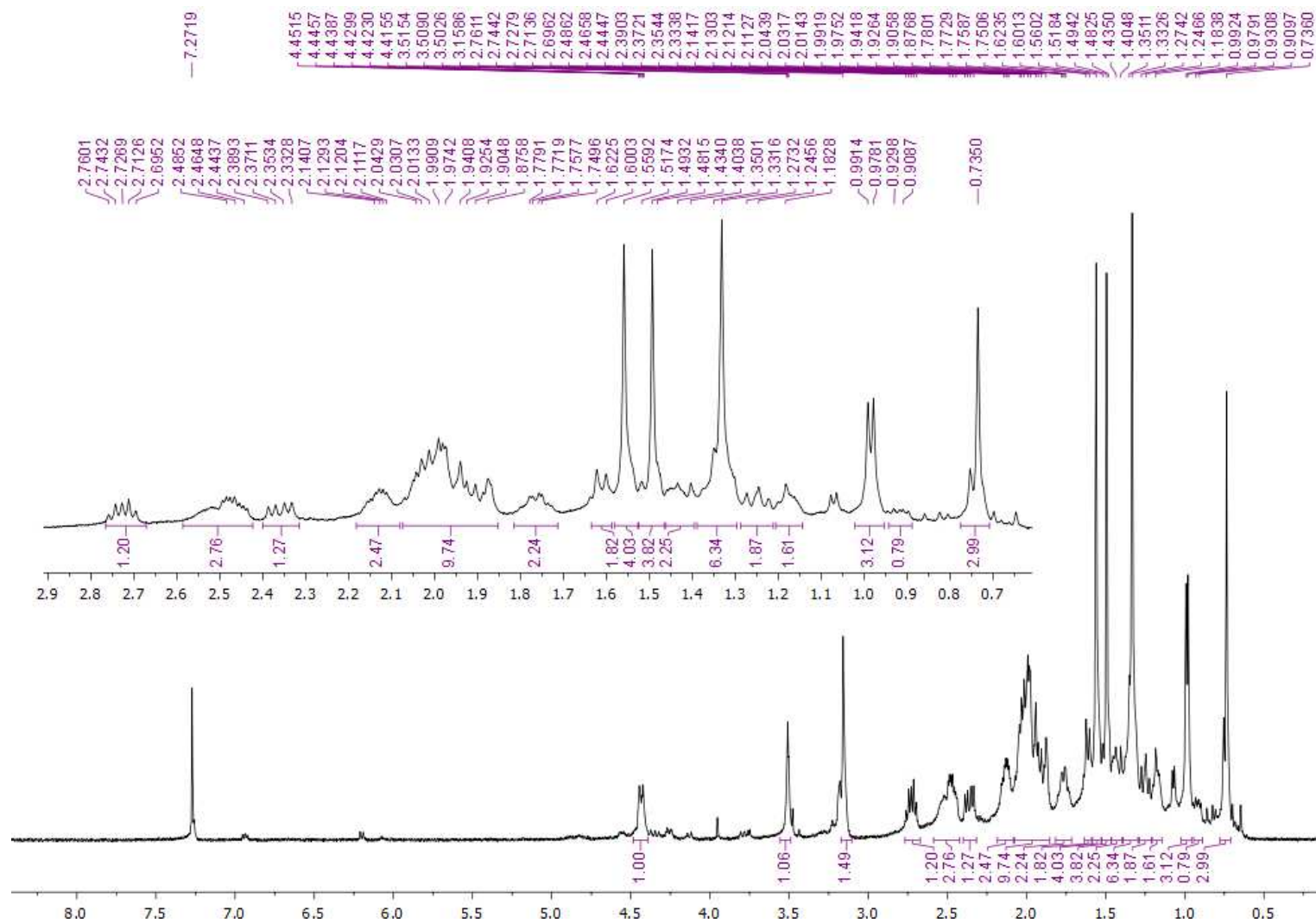
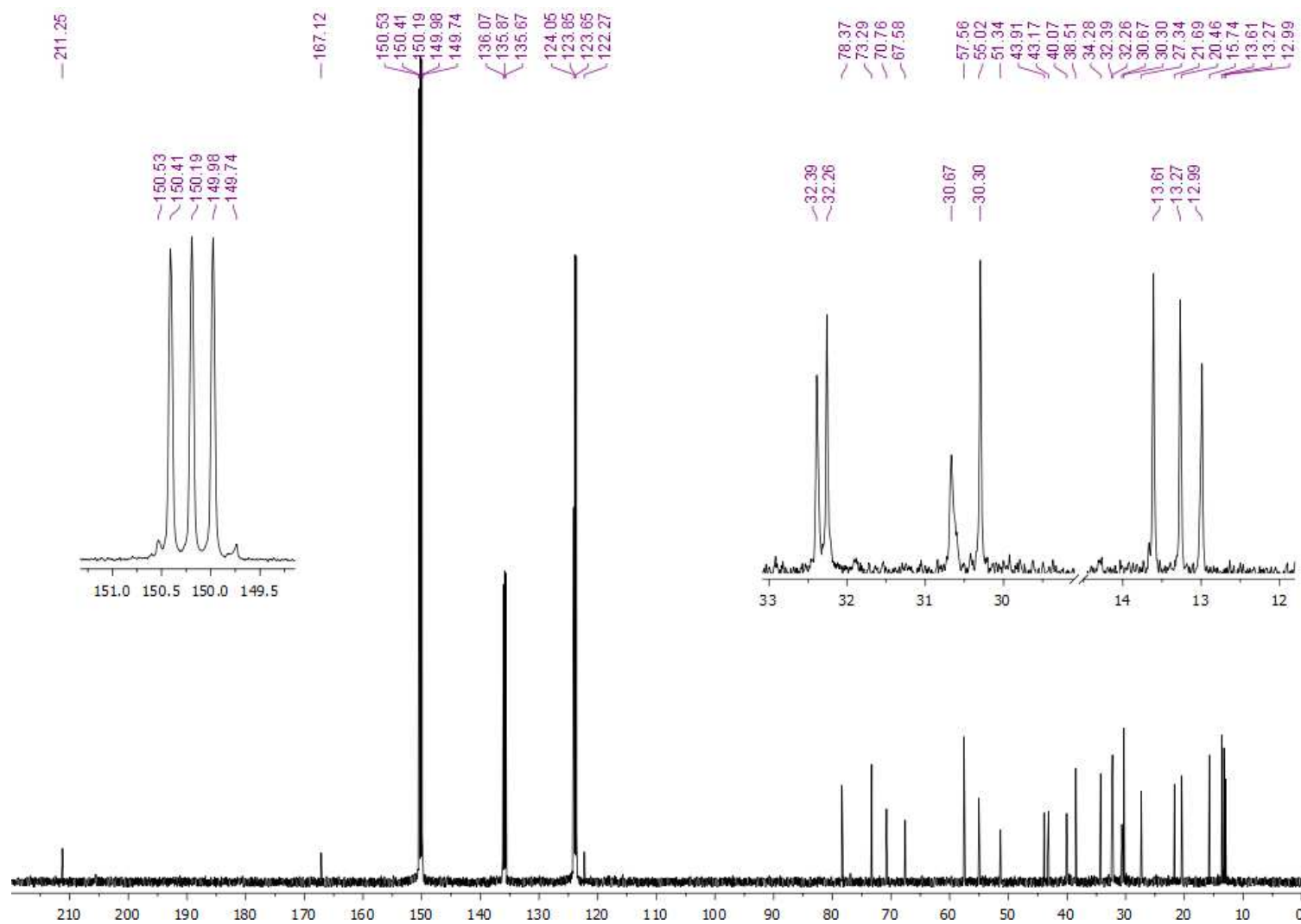**Figure S 40.** ^{1}H NMR (500.13 MHz) spectrum of **6**, in CDCl$_3$.
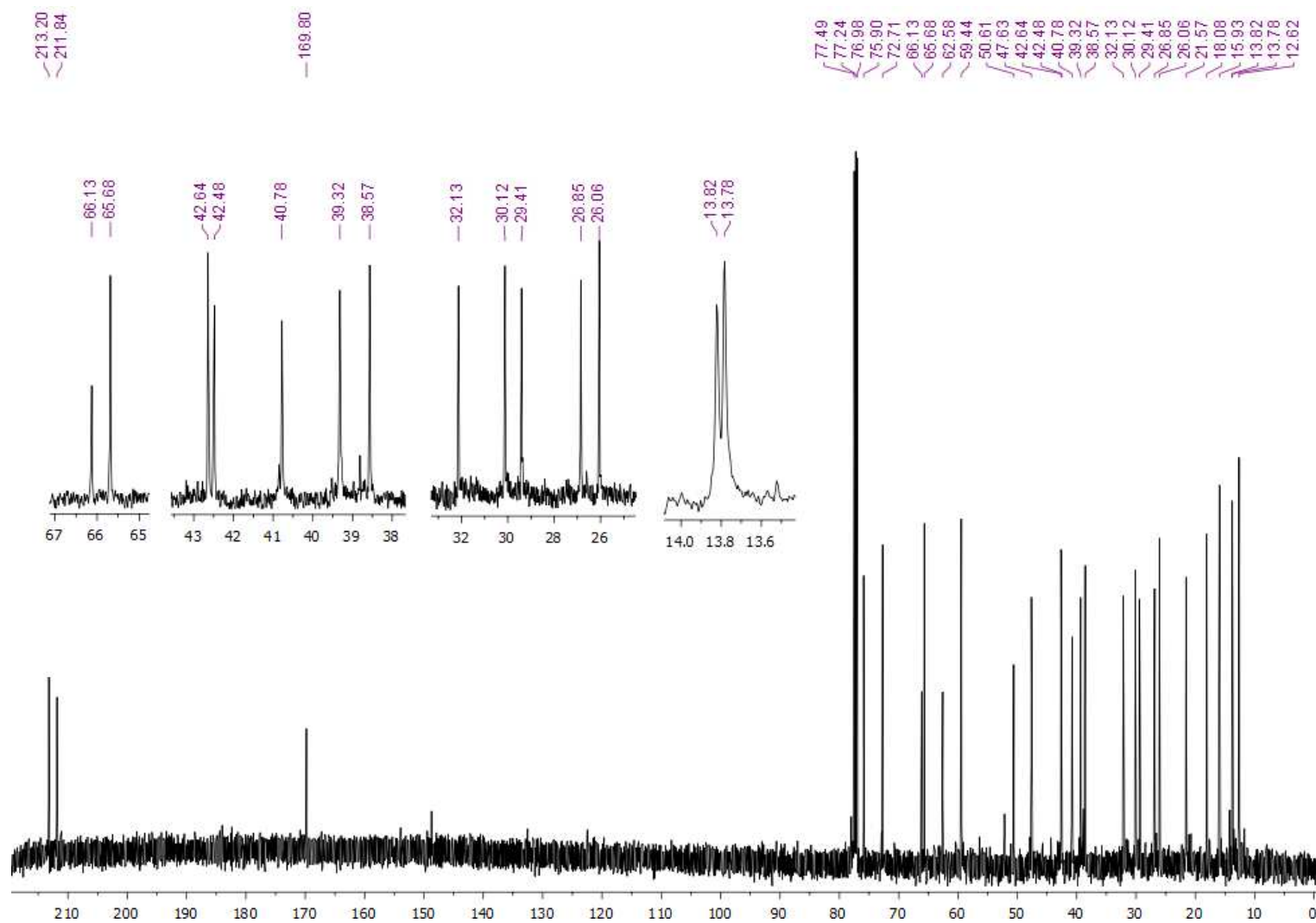
Figure S 41. ^{13}C NMR (125.75 MHz) spectrum of 6, in CDCl$_3$.
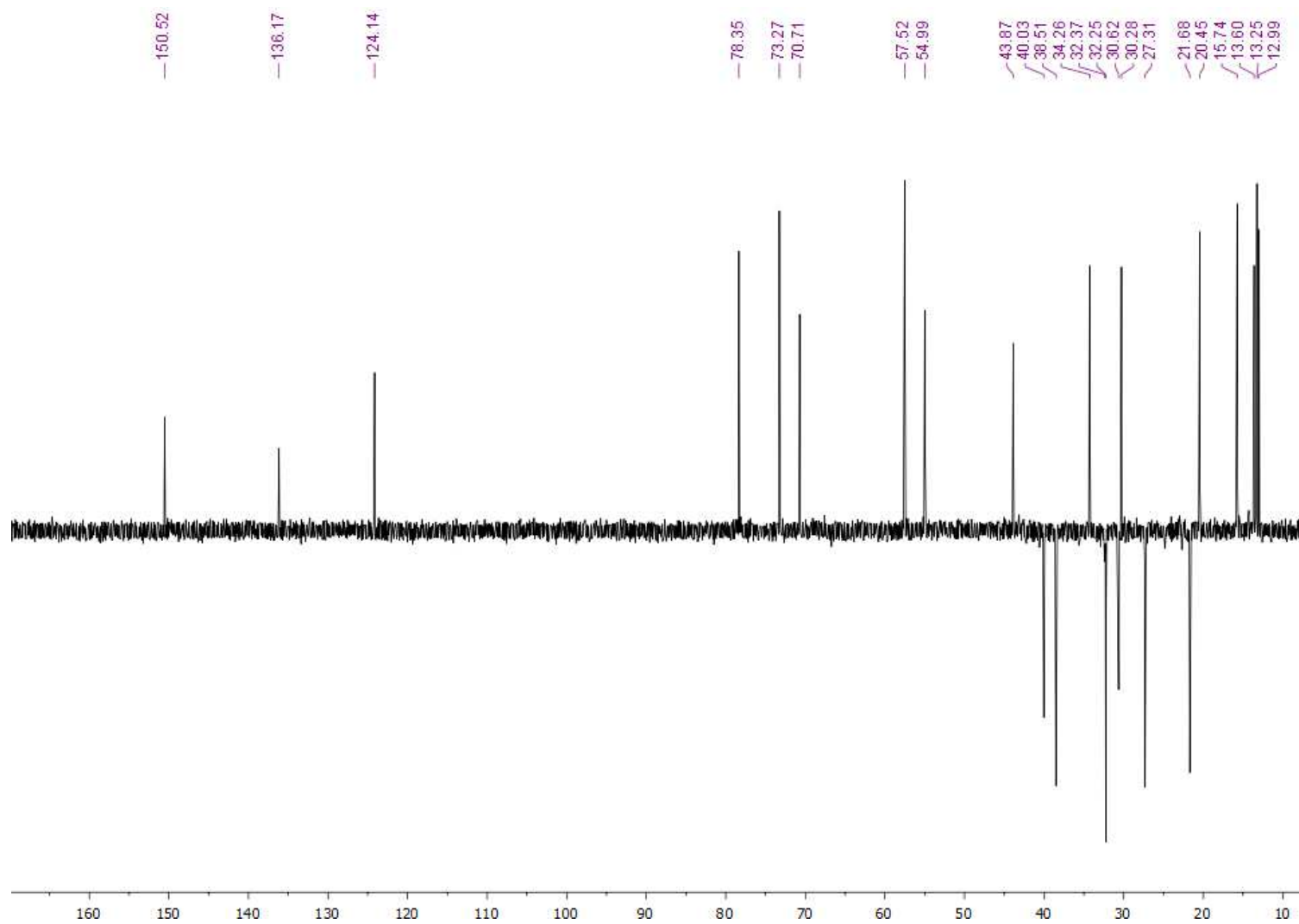
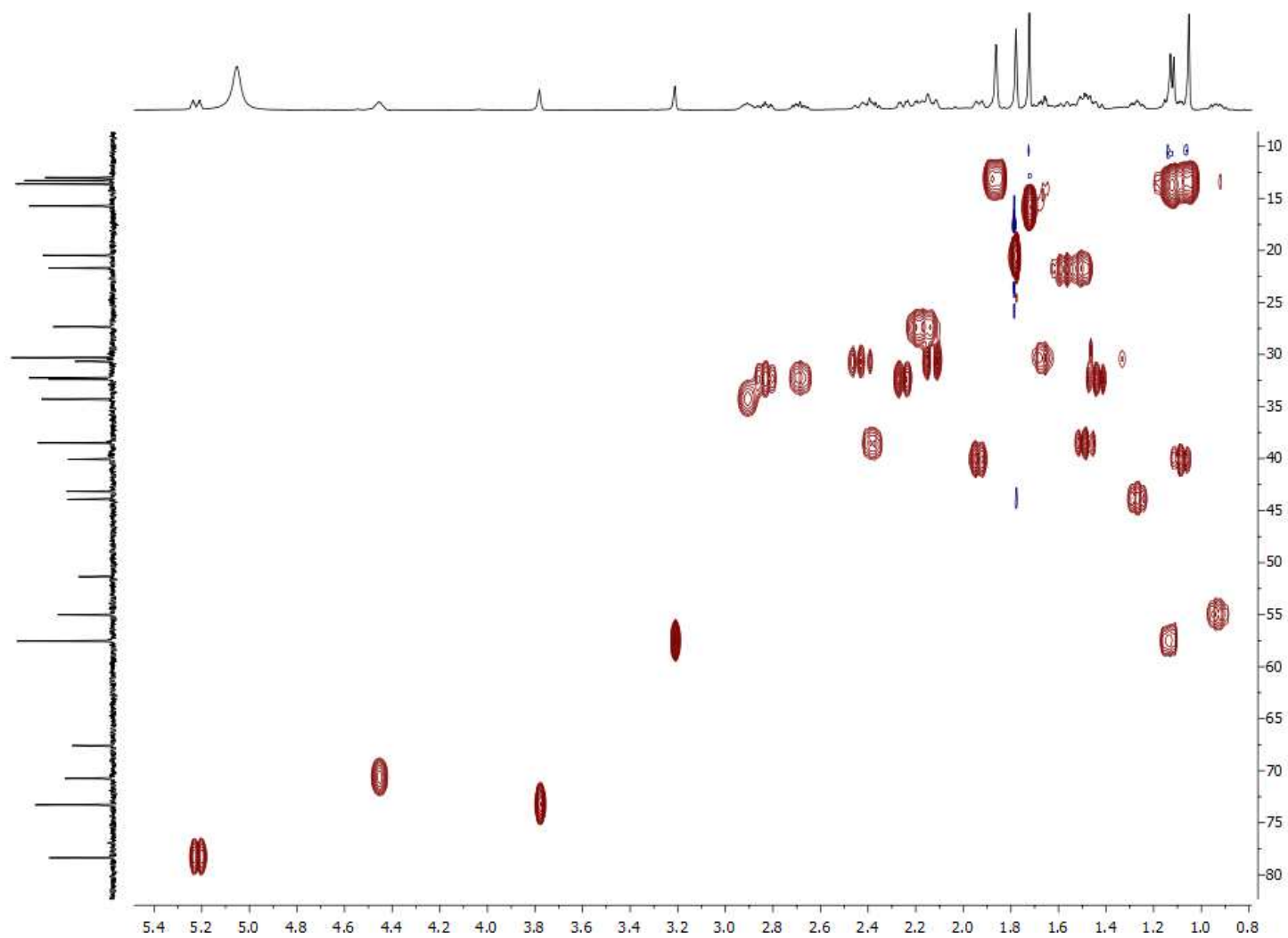**Figure S 42. DEPT 135° NMR (125.75 MHz) spectrum of 6, in CDCl₃.**
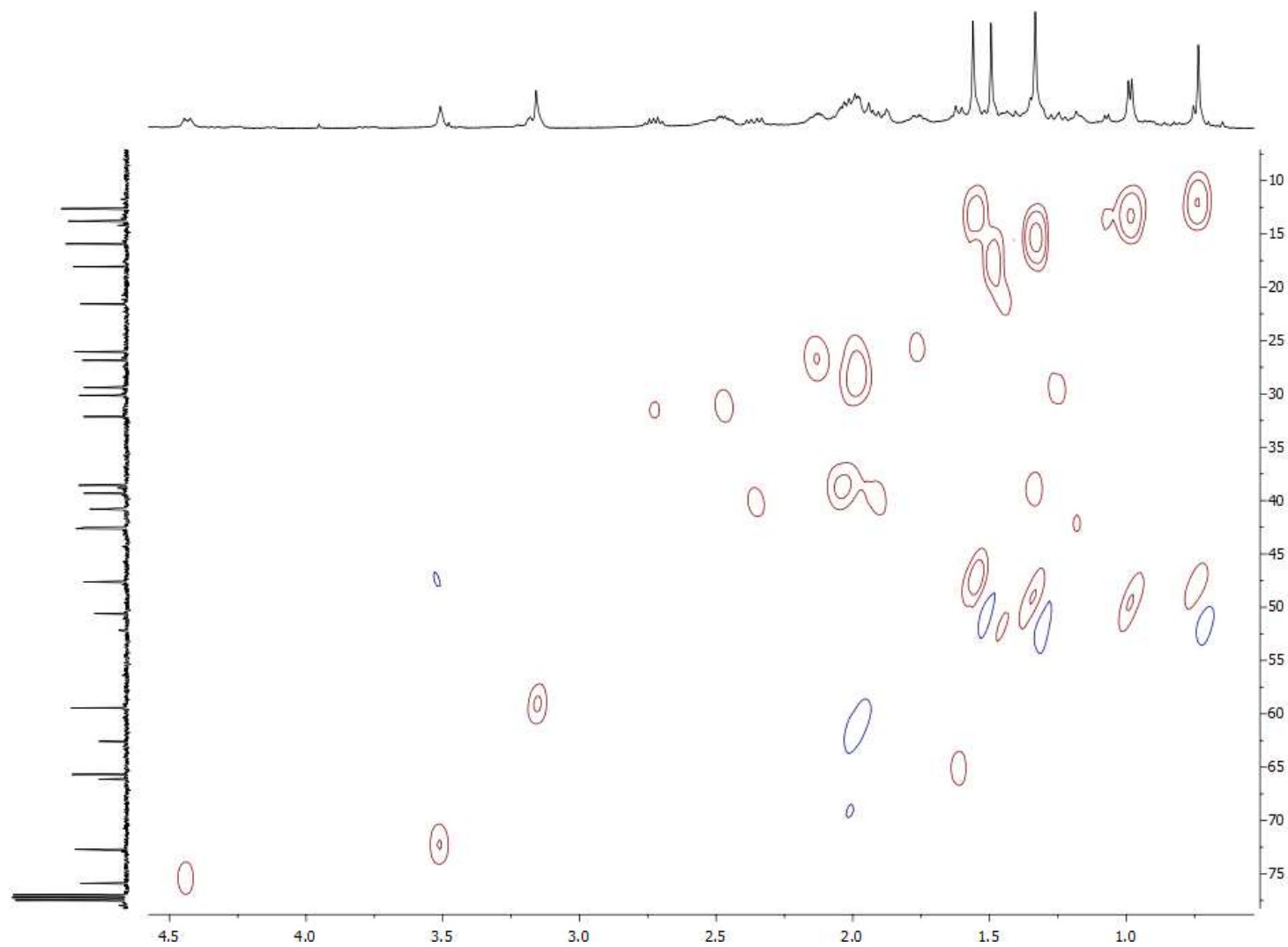
Figure S 43. HSQC NMR spectrum of 6, in CDCl₃.

Figure S 44. COSY NMR spectrum of 6, in CDCl₃

Figure S 45. HMBC NMR spectrum of 6, in CDCl₃.
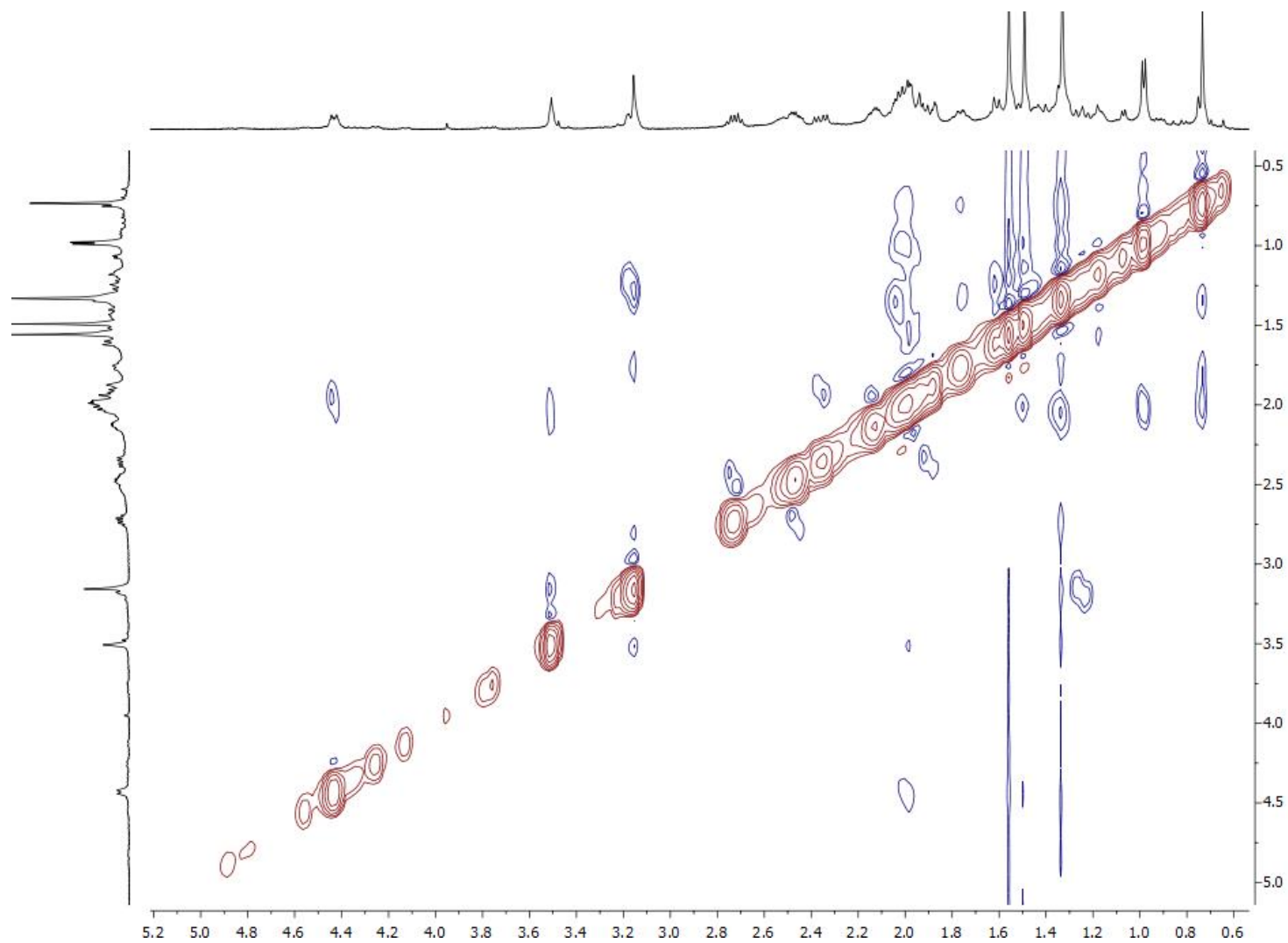
Figure S 46. NOESY NMR spectrum of 6, in CDCl₃.
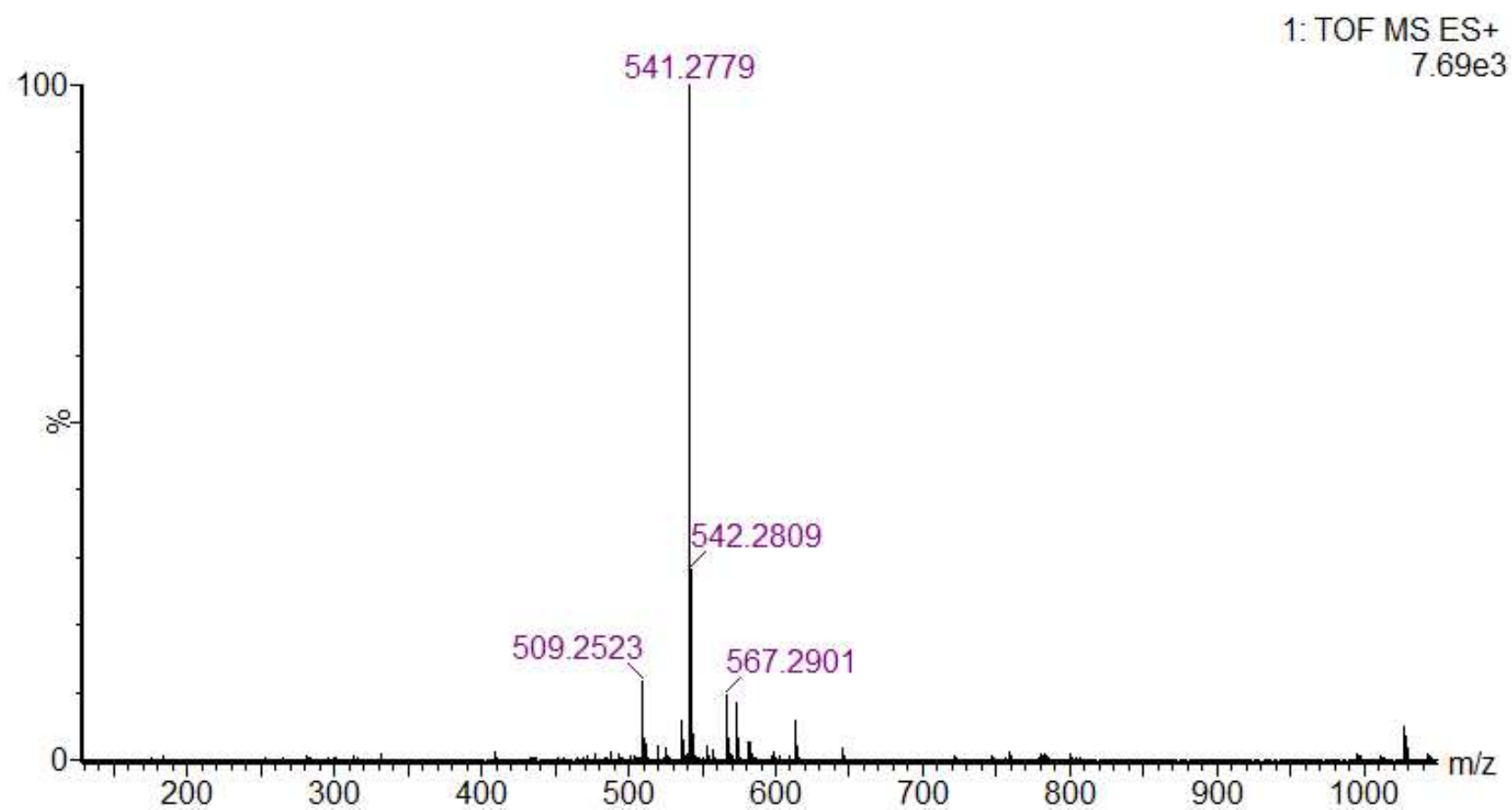
Figure S 47. HRESIMS spectrum of 6.
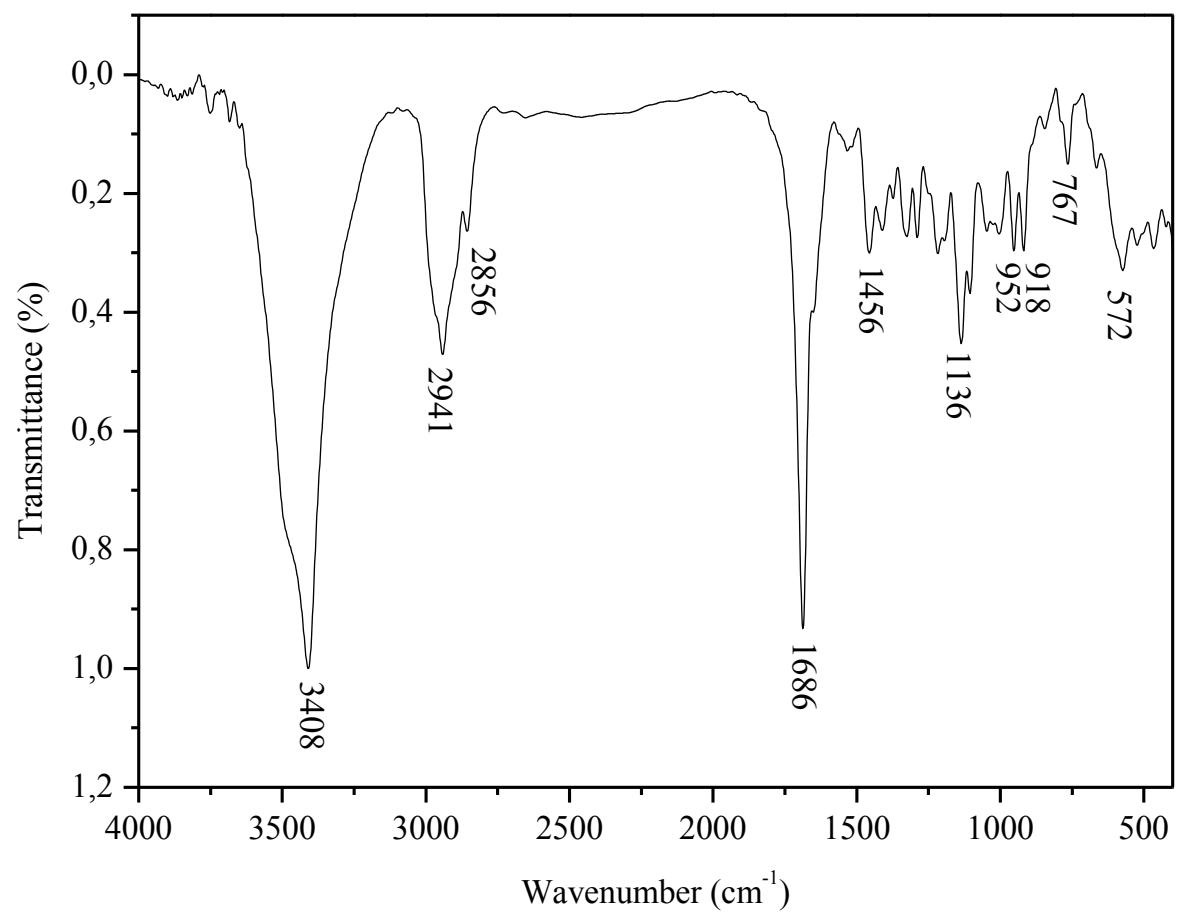
Figure S 48. FTIR spectrum of 7.

Figure S 49. ¹H NMR (500.13 MHz) spectrum of 7, in CDCl₃.
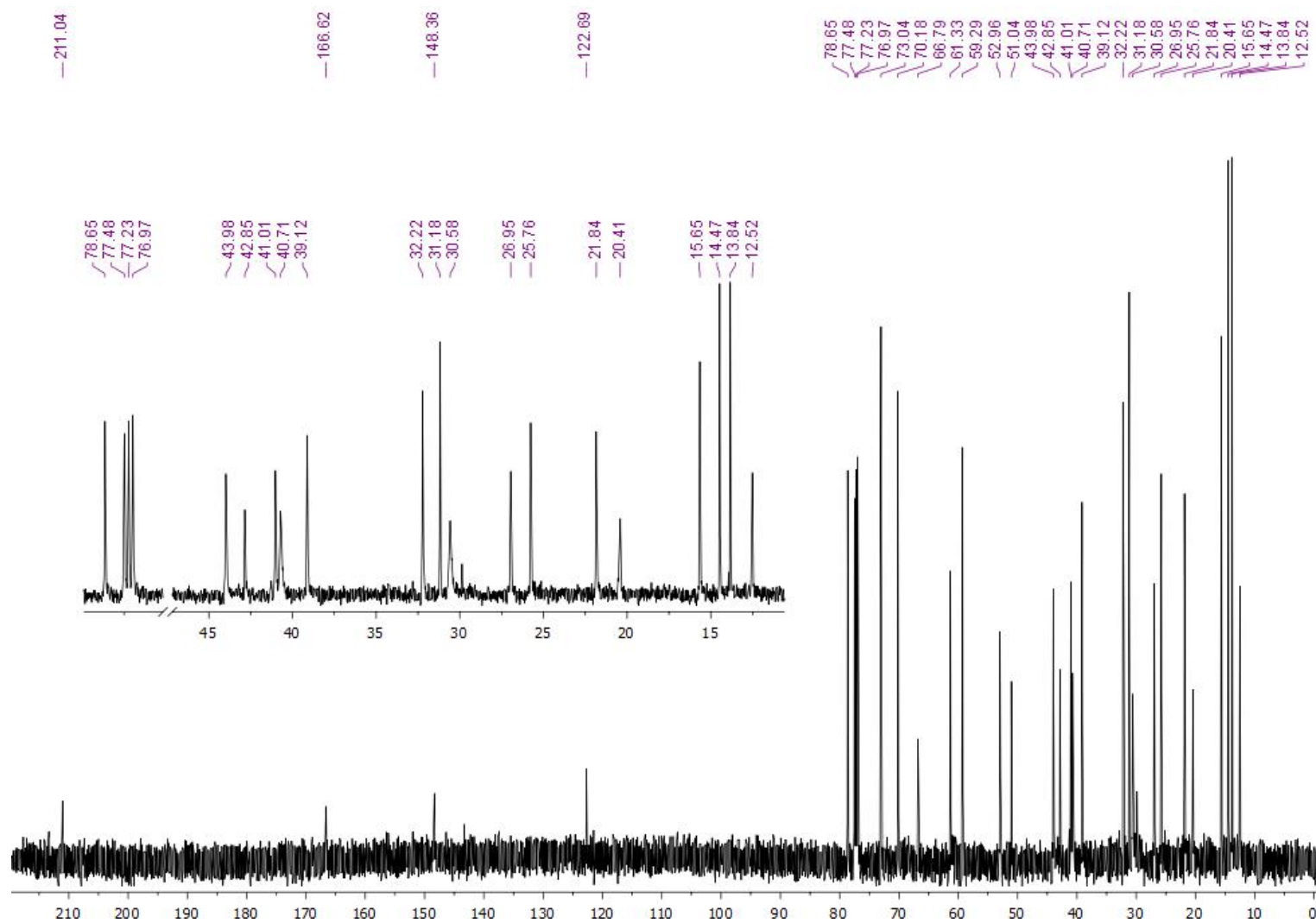
Figure S 50. ^{13}C NMR (125.75 MHz) spectrum of 7, in CDCl₃.
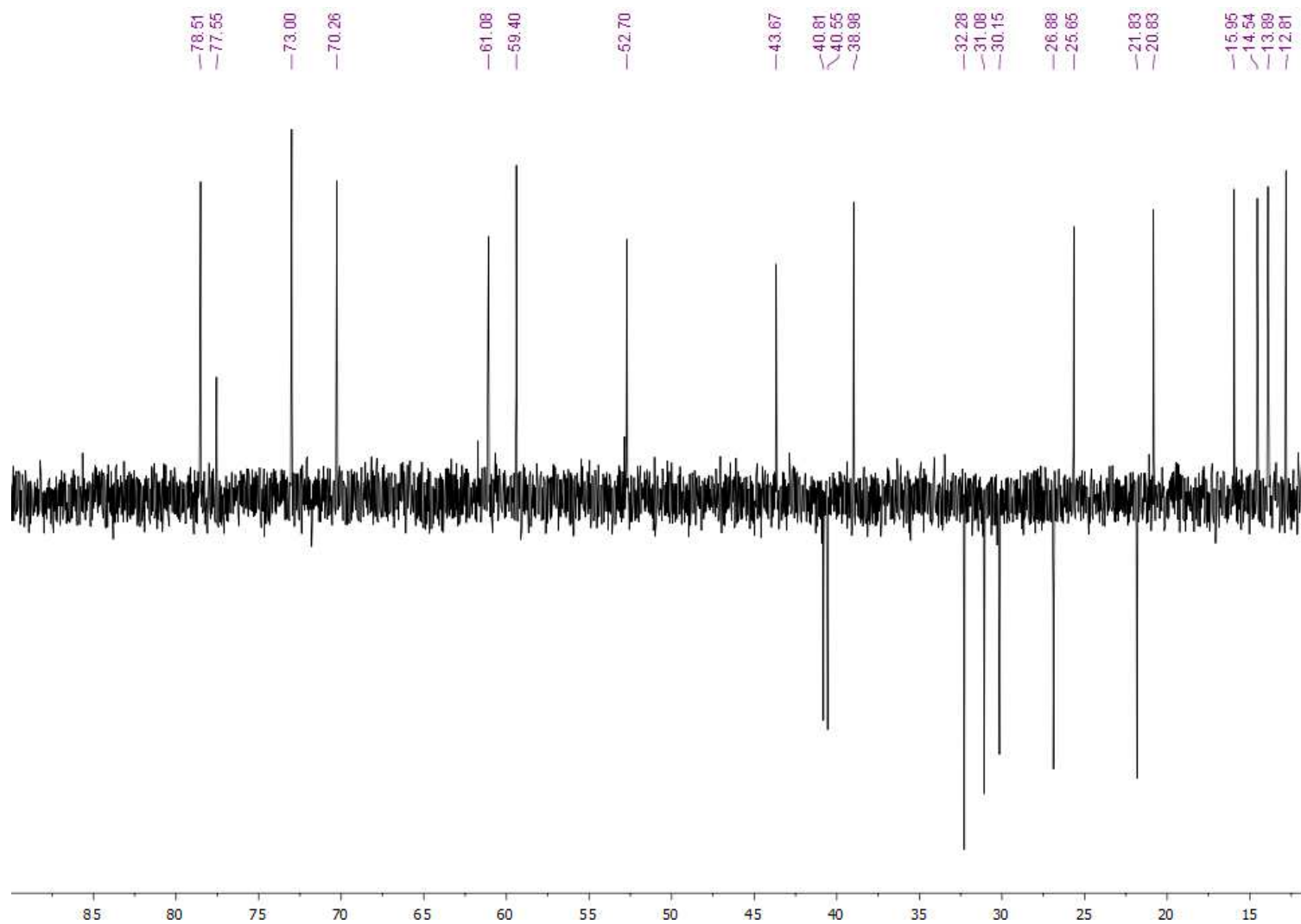
Figure S 51. DEPT 135° NMR (125.75 MHz) spectrum of 7, in CDCl₃.
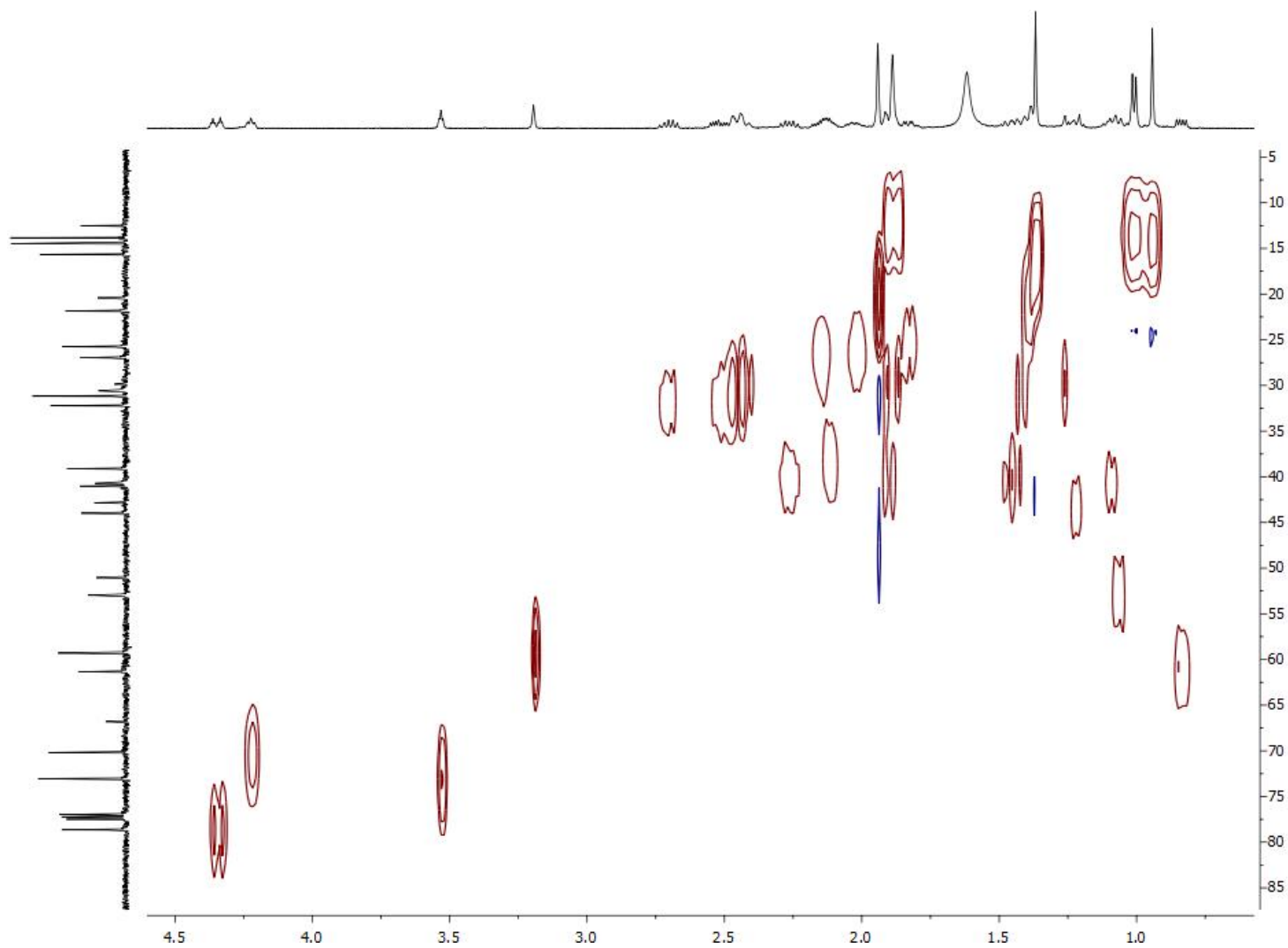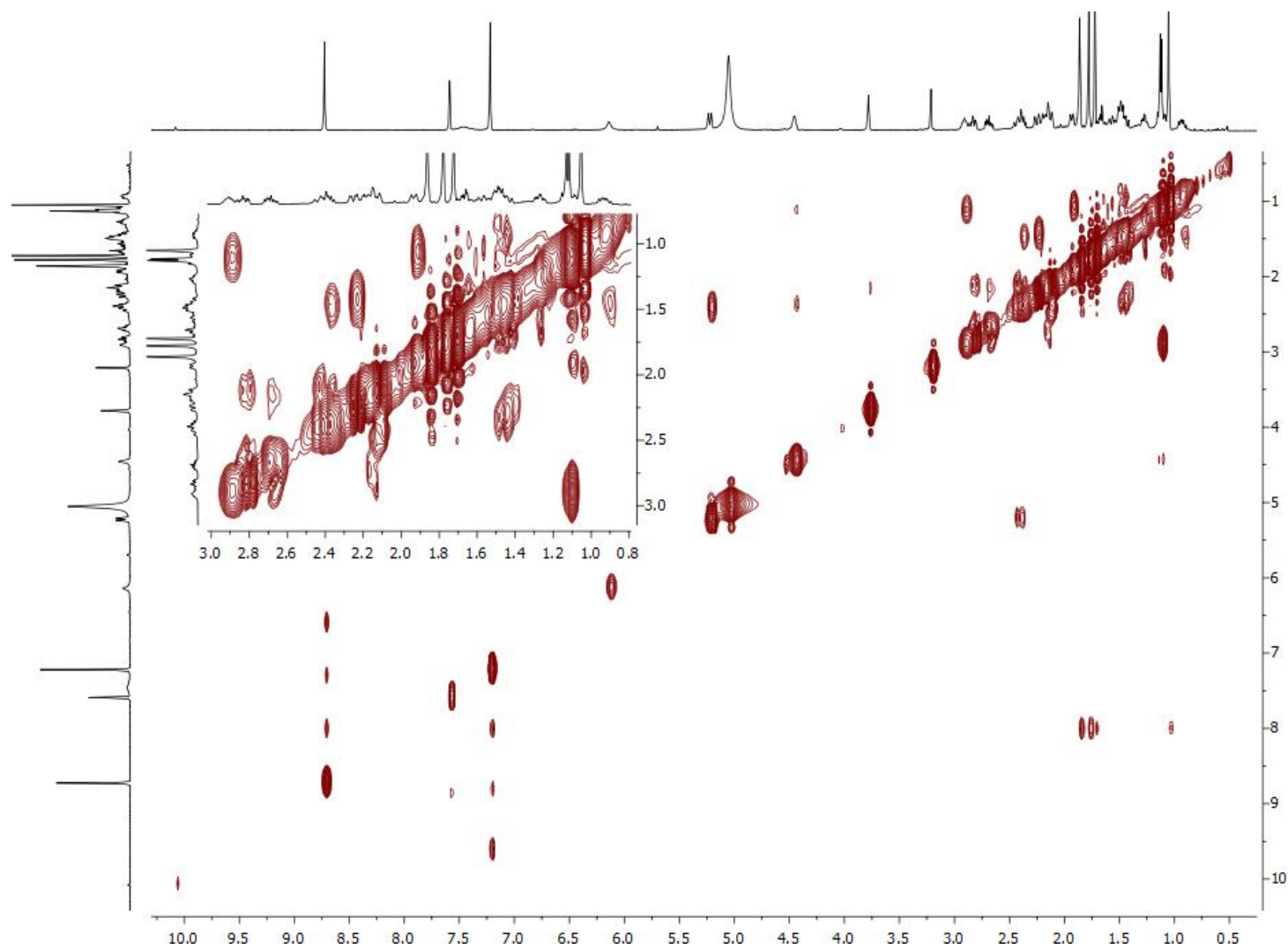
Figure S 52. HSQC NMR spectrum of 7, in CDCl₃.
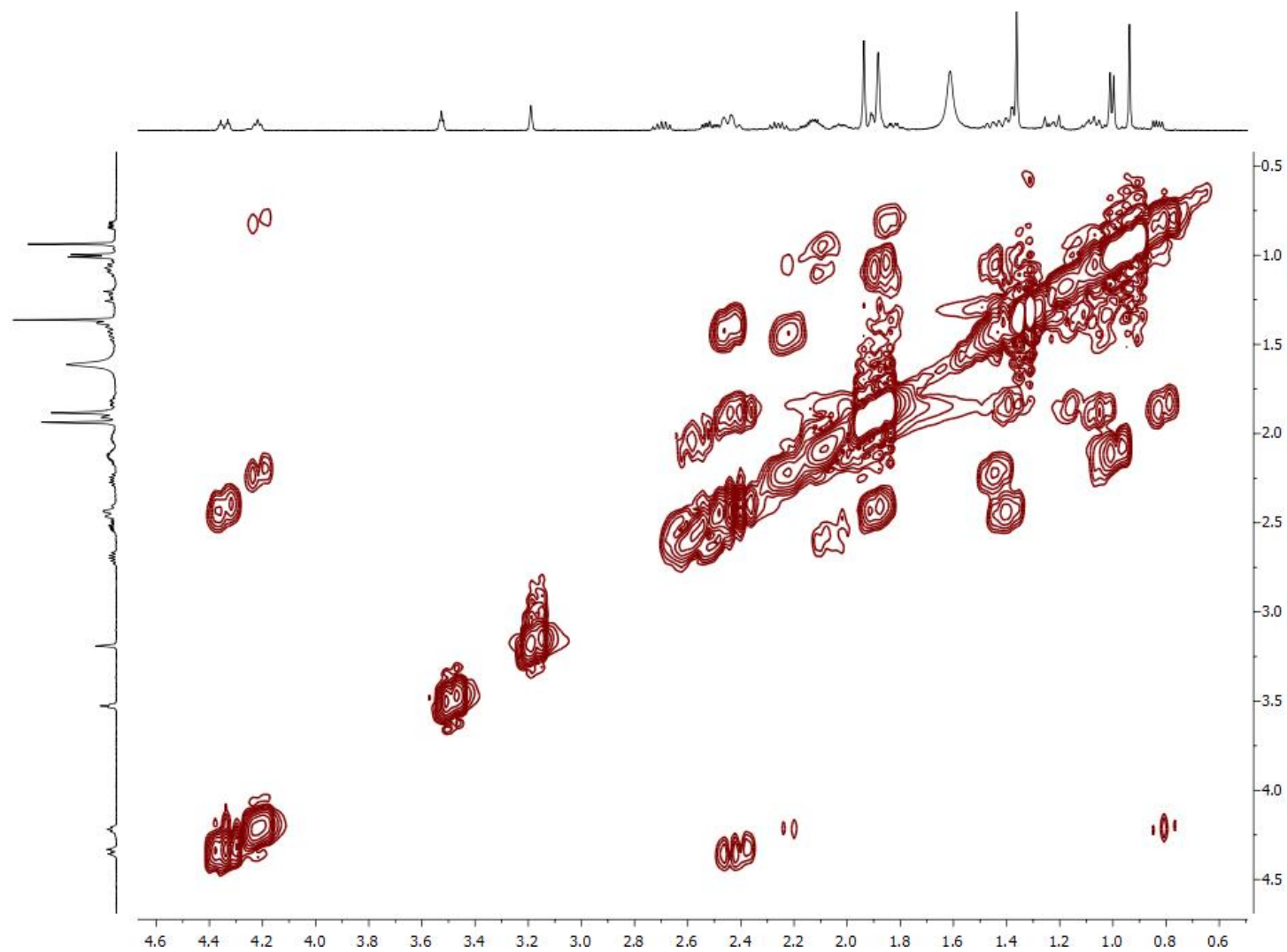
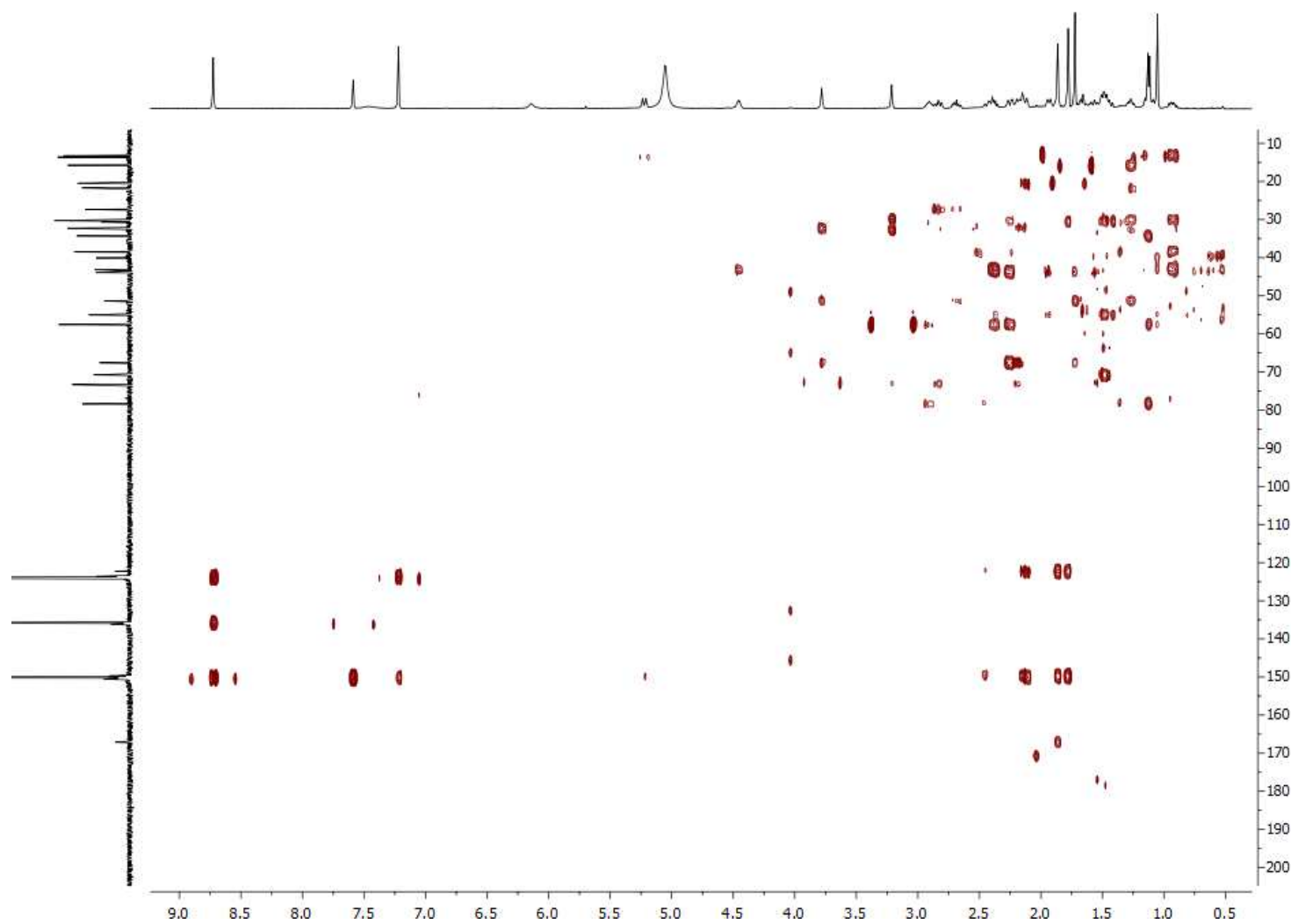**Figure S 53. COSY NMR spectrum of 7, in CDCl₃**
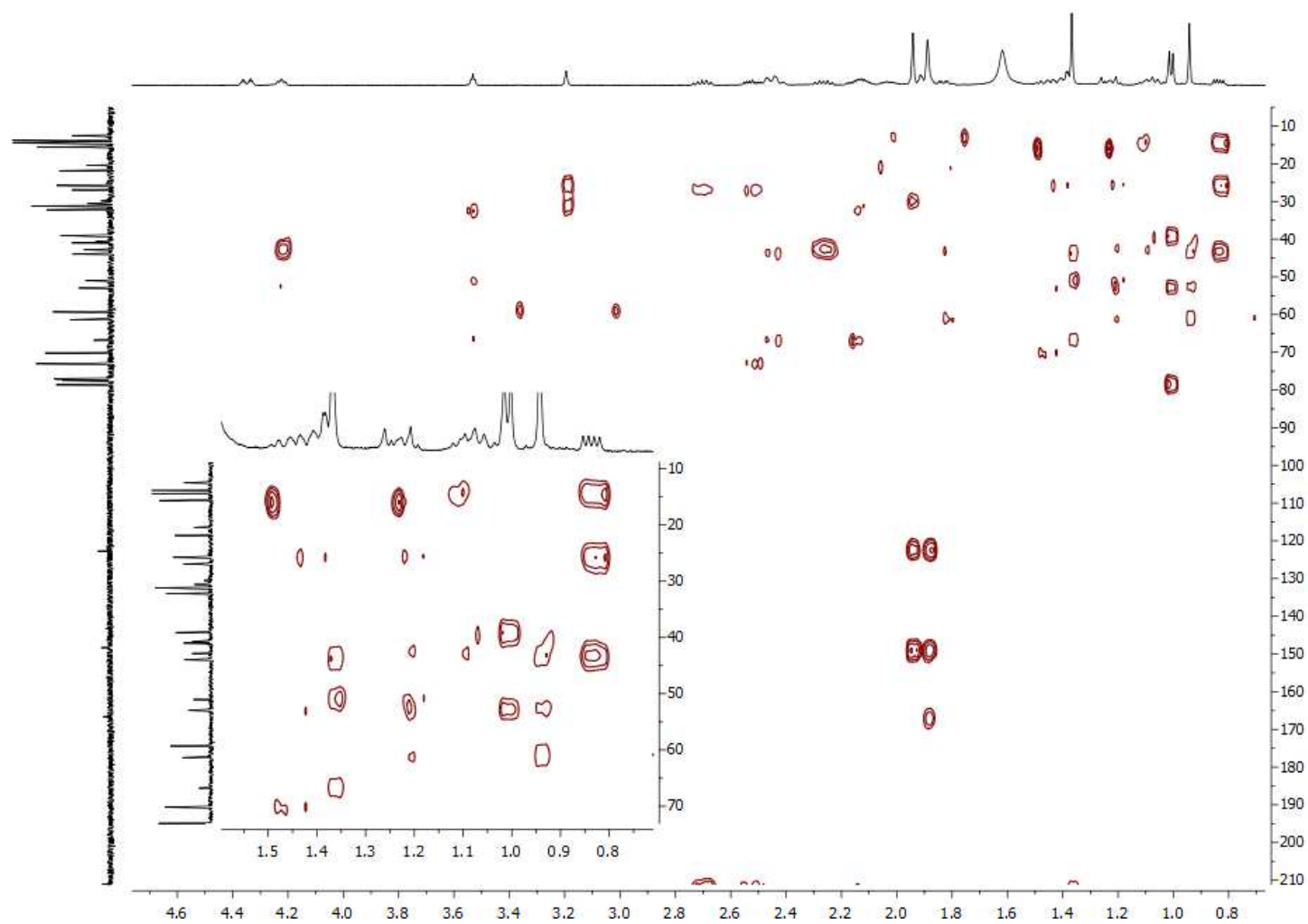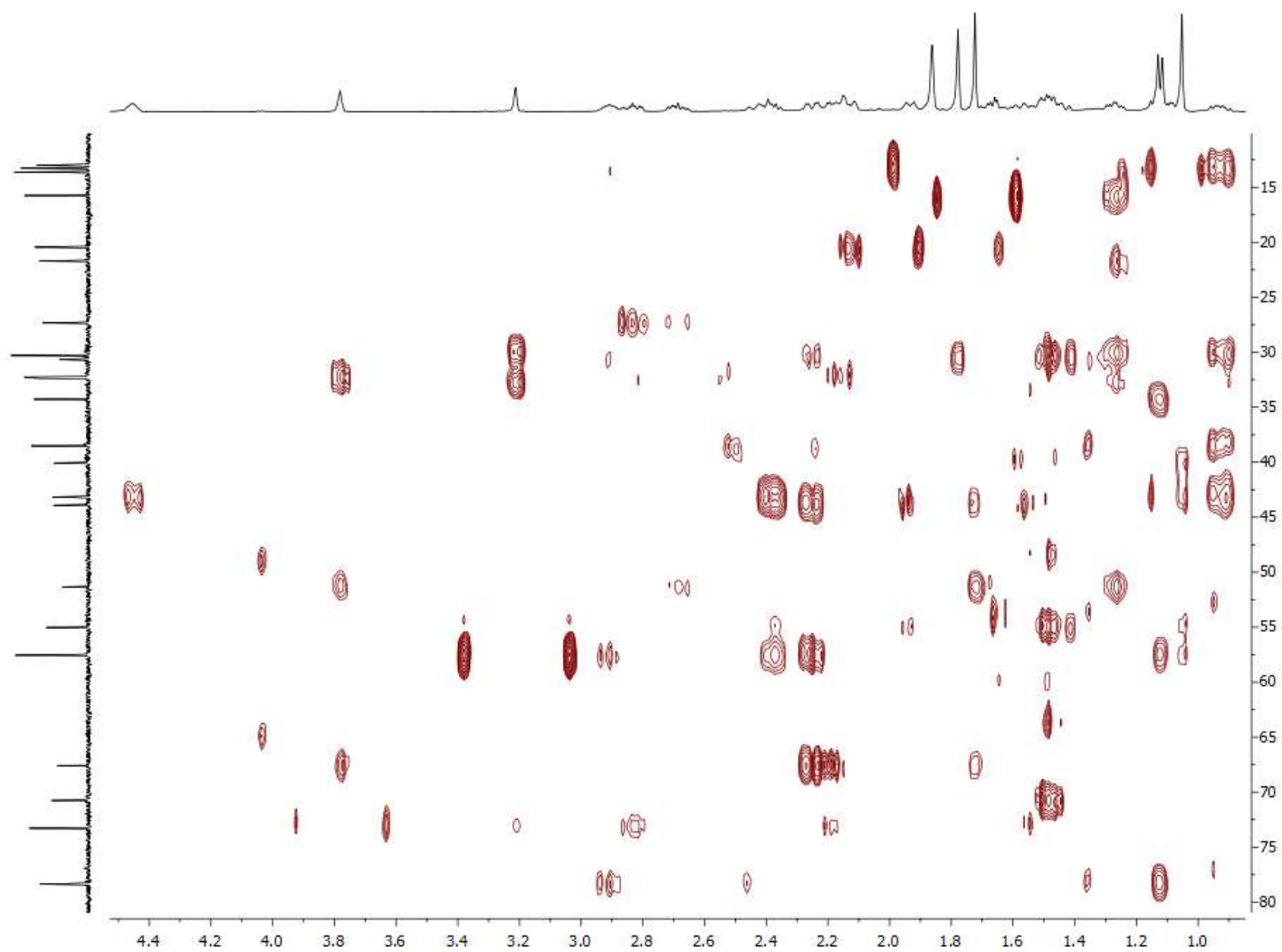
Figure S 54. HMBC NMR spectrum of 7, in CDCl₃.
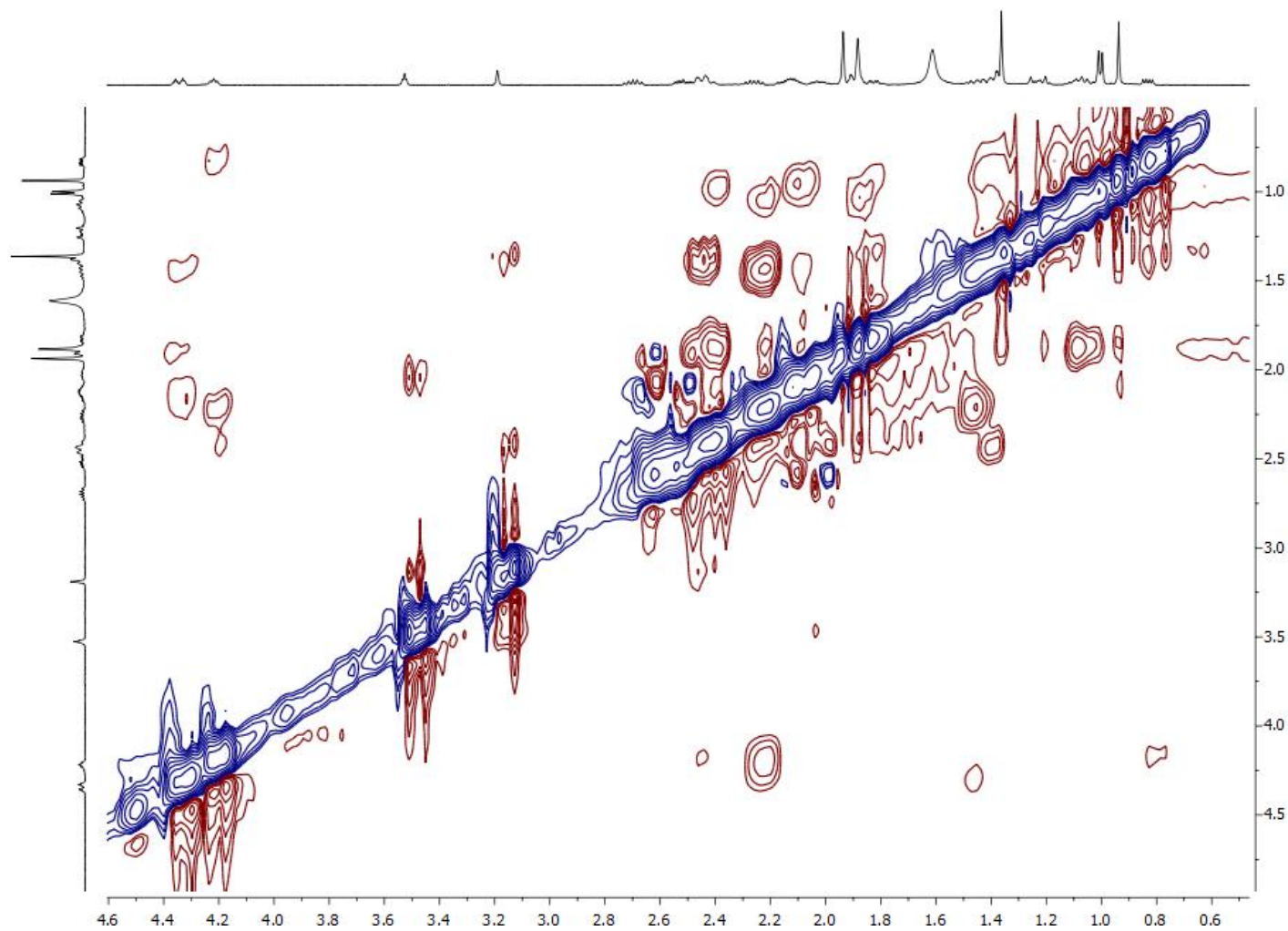
Figure S 55. NOESY NMR spectrum of 7, in CDCl₃.
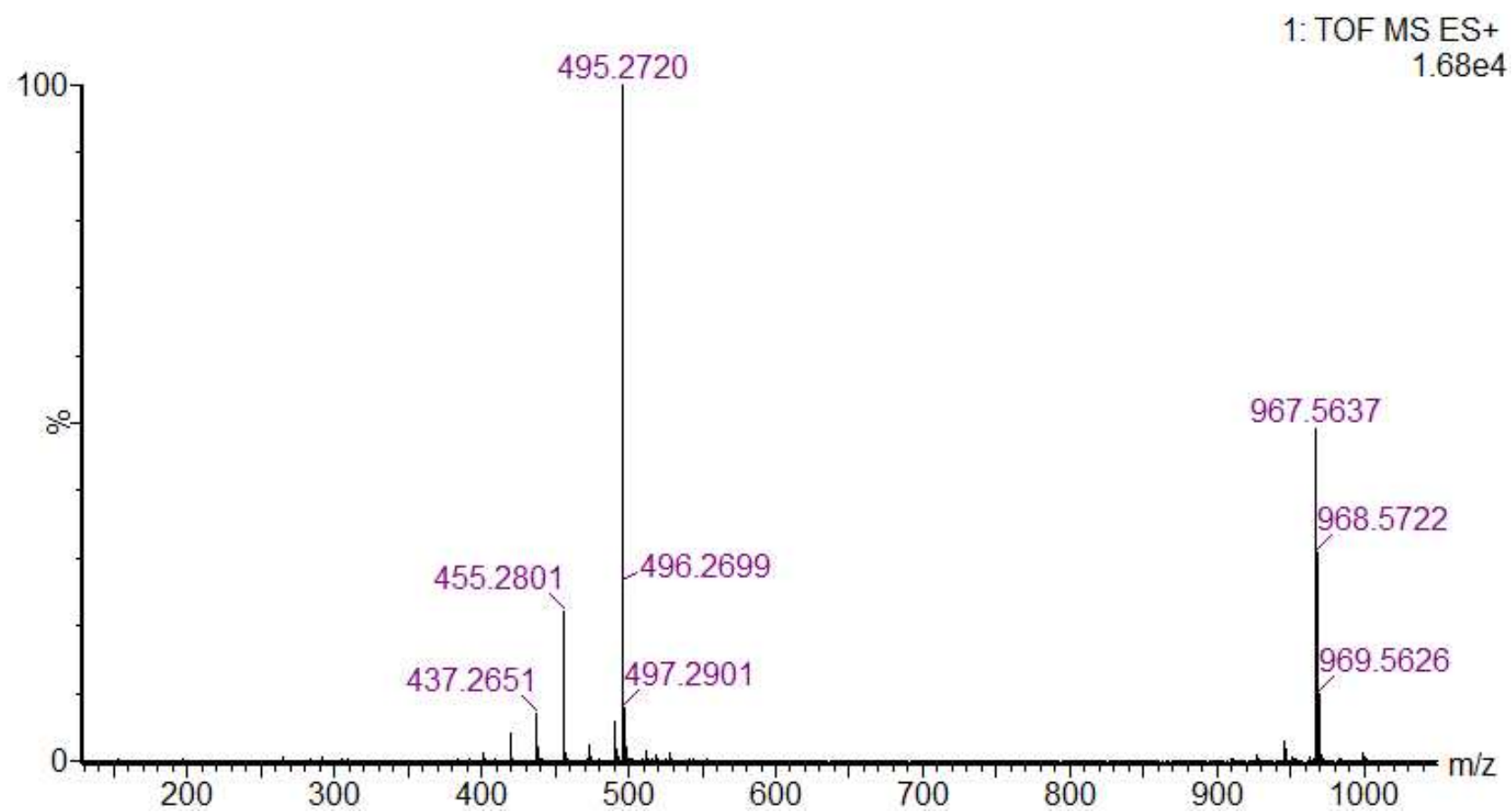
Figure S 56. HRESIMS spectrum of 7.
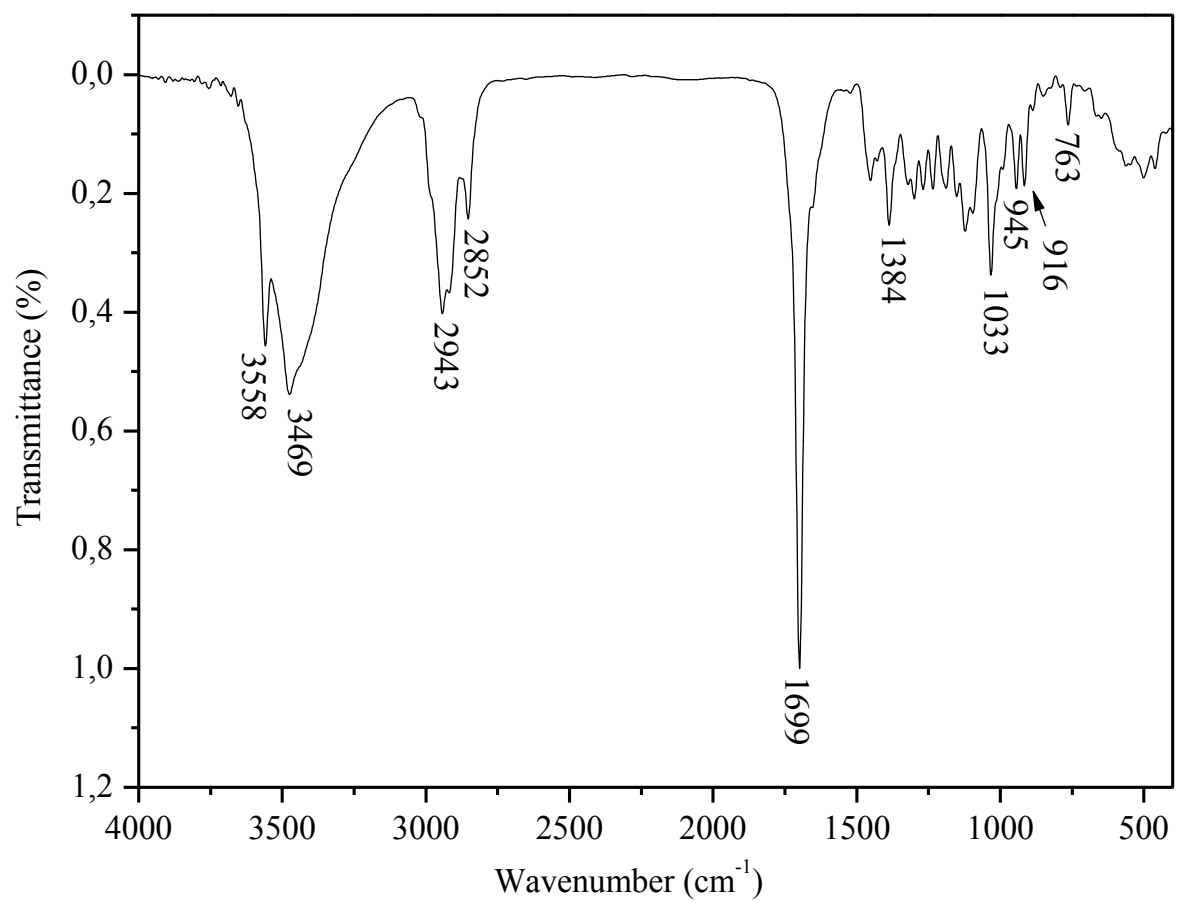
Figure S 57. FTIR spectrum of 8.
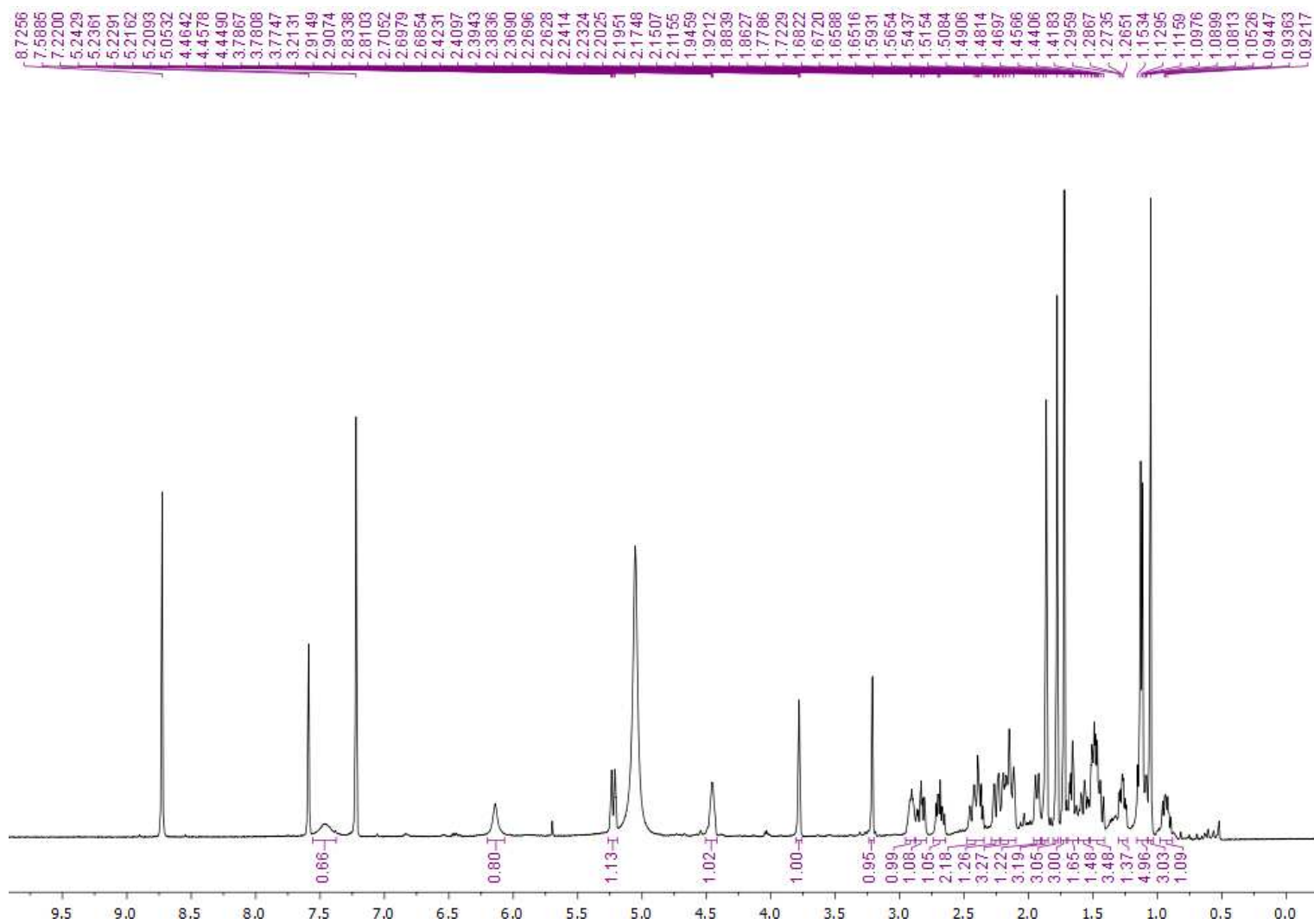
Figure S 58. ^{1}H NMR (500.13 MHz) spectrum of 8, in CDCl$_3$.
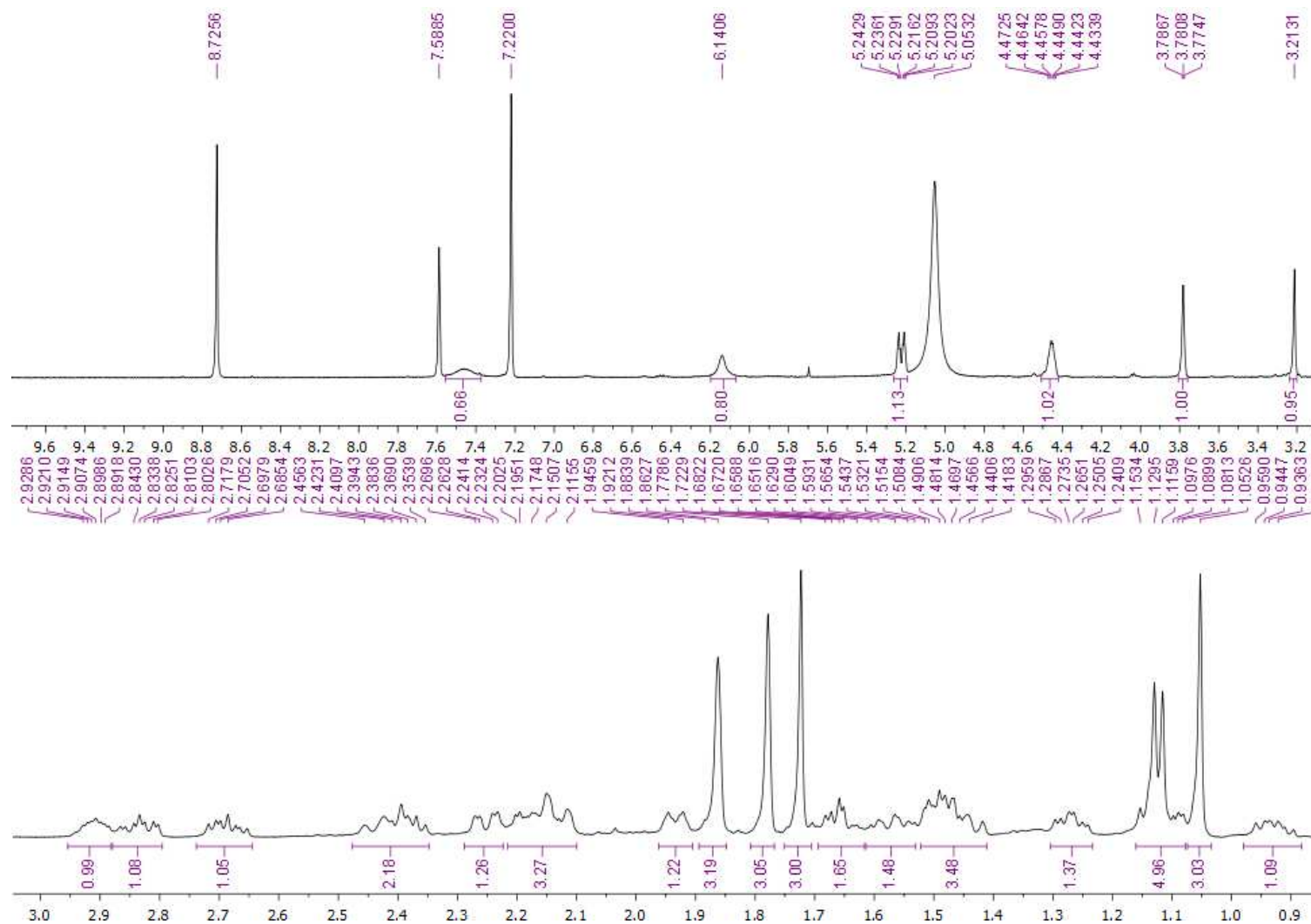
Figure S 59. ¹H NMR expansion of 8, in CDCl₃.

Figure S 60. ^{13}C NMR (125.75 MHz) spectrum of **8**, in CDCl$_3$.

Figure S 61. DEPT 135° NMR (125.75 MHz) spectrum of 8, in CDCl₃.

Figure S 62. HSQC NMR spectrum of 8, in CDCl₃.

Figure S 63. COSY NMR spectrum of 8, in CDCl₃

Figure S 64. HMBC NMR spectrum of 8, in CDCl₃.
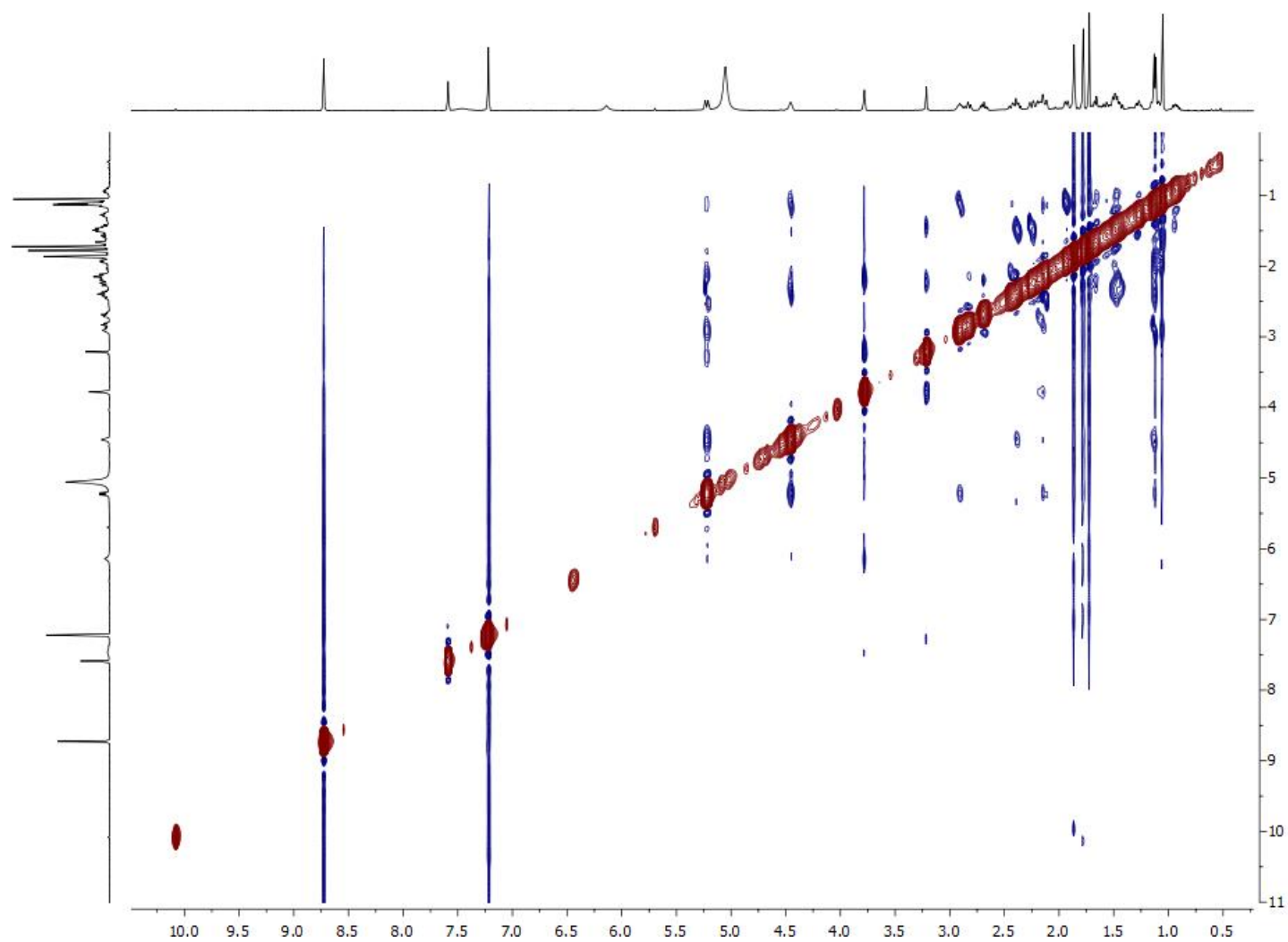
Figure S 65. HMBC expansion of 8, in CDCl₃.
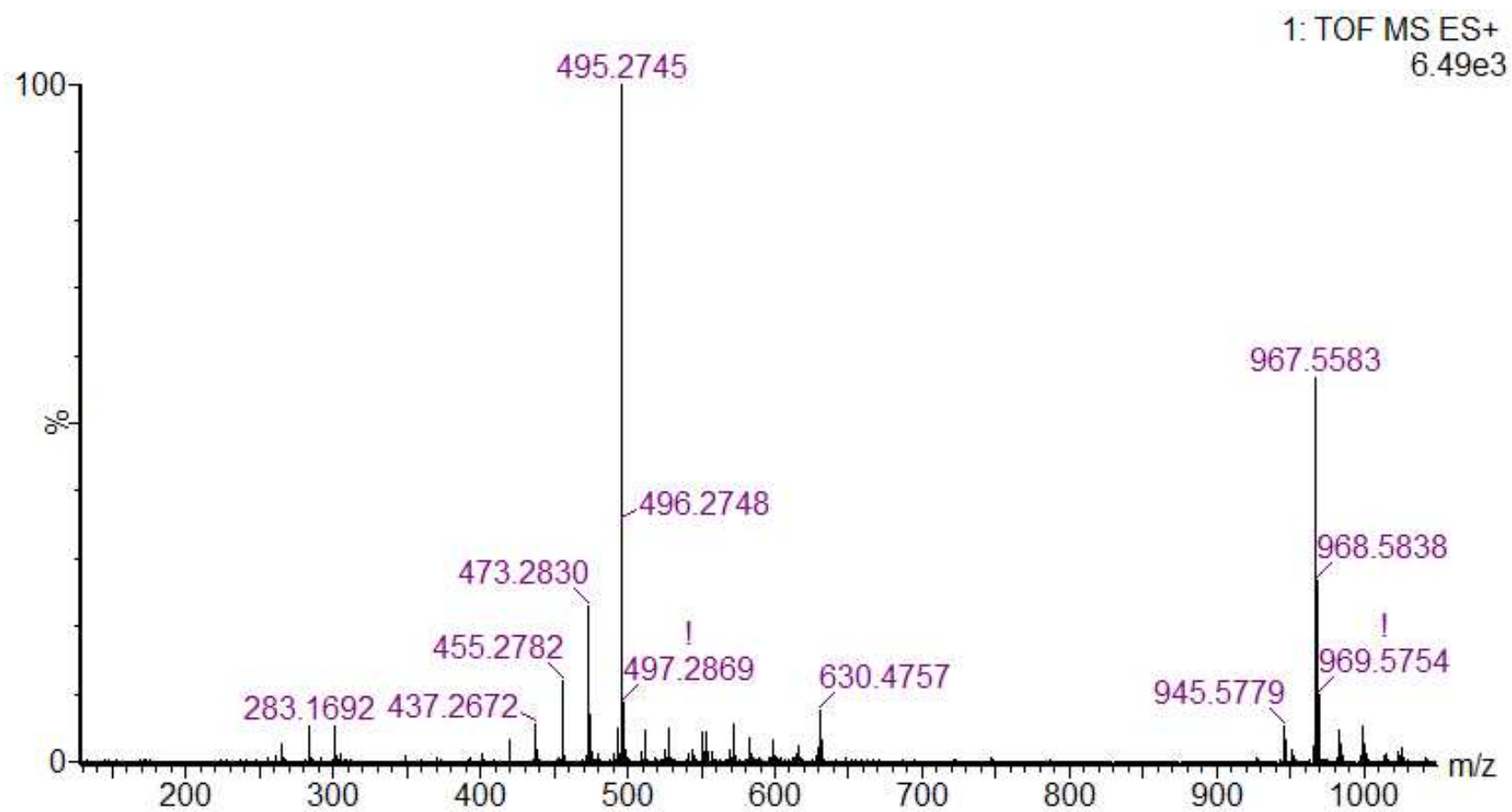
Figure S 66. NOESY NMR spectrum of 8, in CDCl₃.

Figure S 67. HRESIMS spectrum of 8.

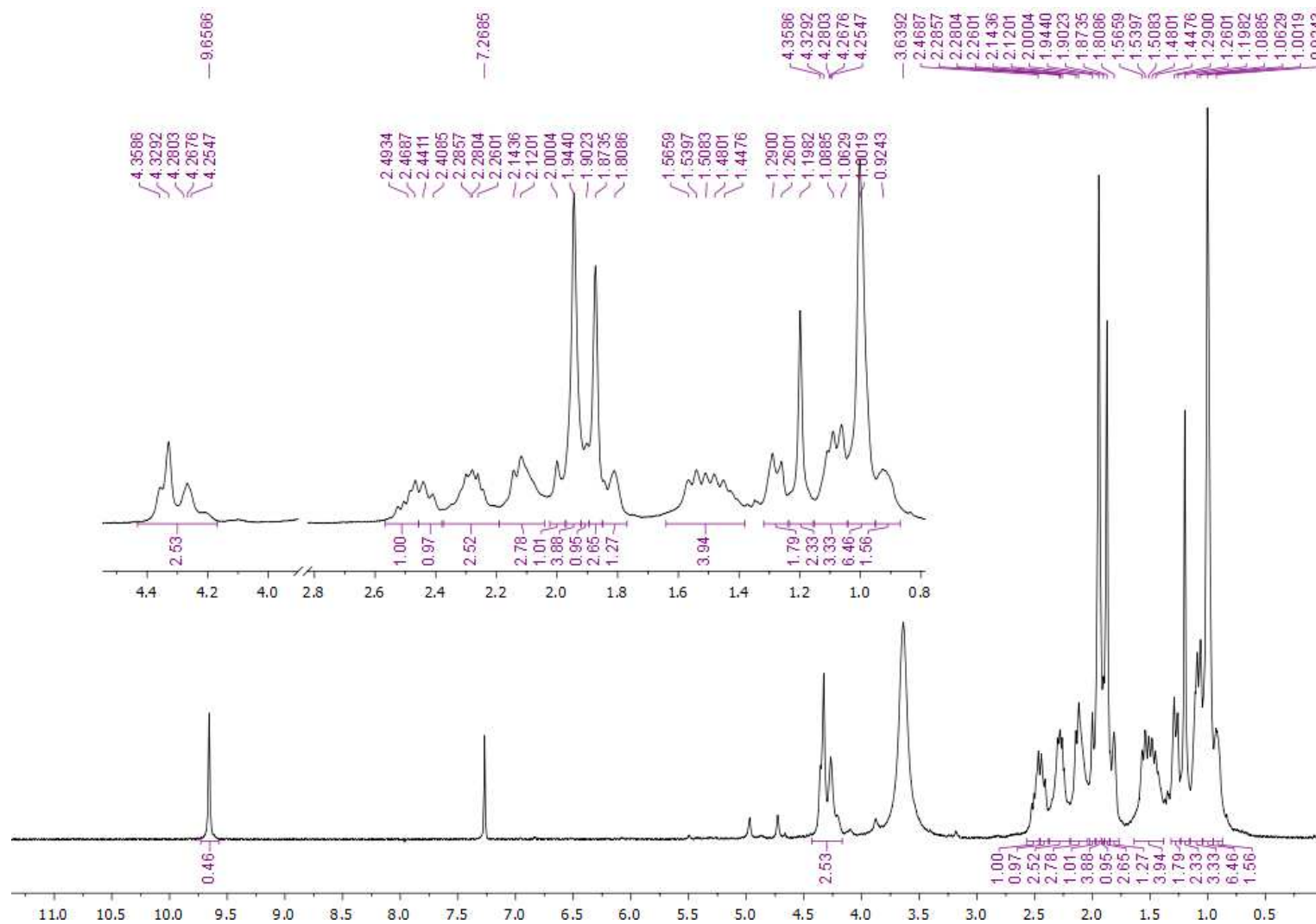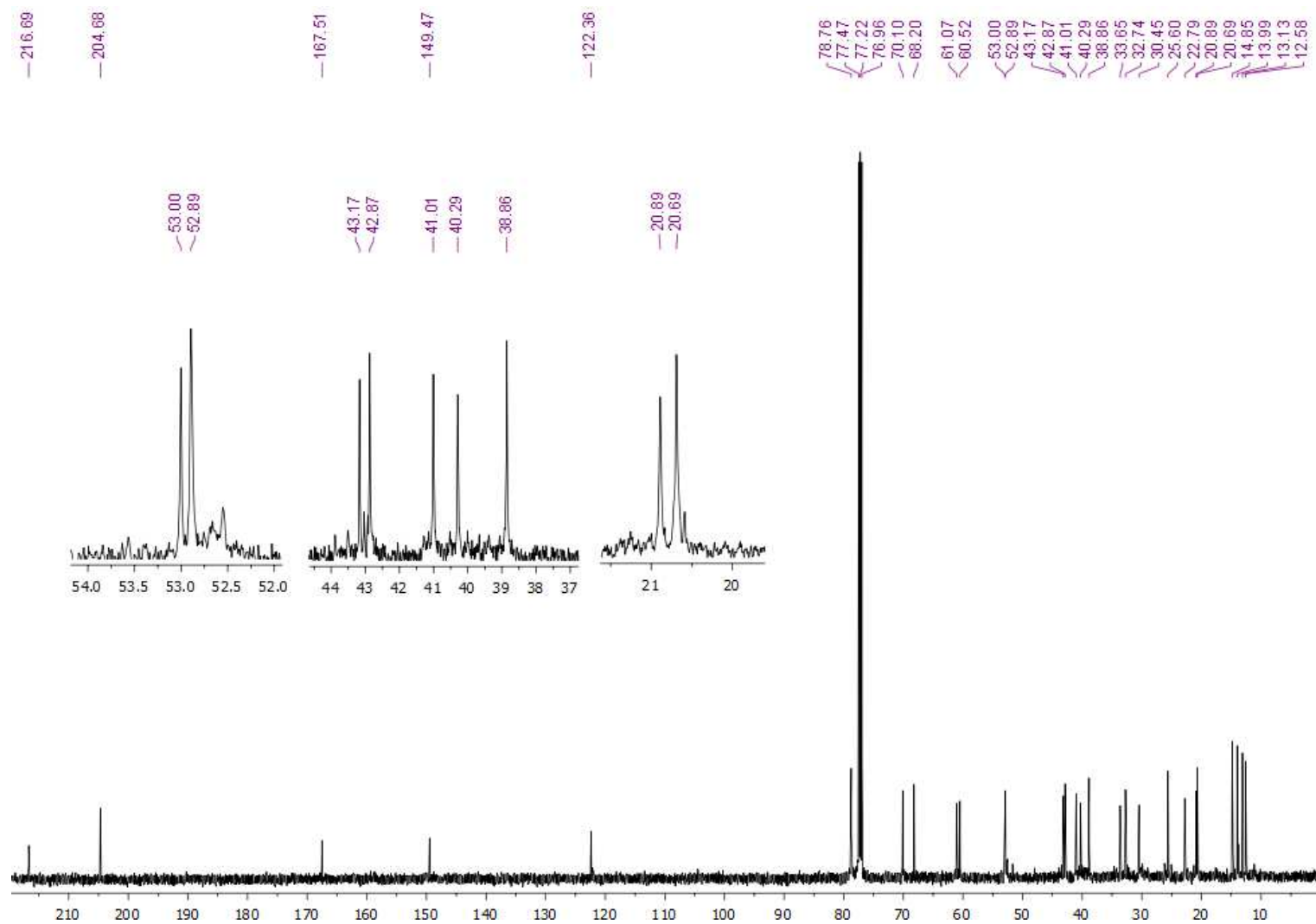**Figure S 68. ¹H NMR (500.13 MHz) spectrum of 9, in CDCl₃.**

Figure S 69. ^{13}C NMR (125.75 MHz) spectrum of **9**, in CDCl$_3$.
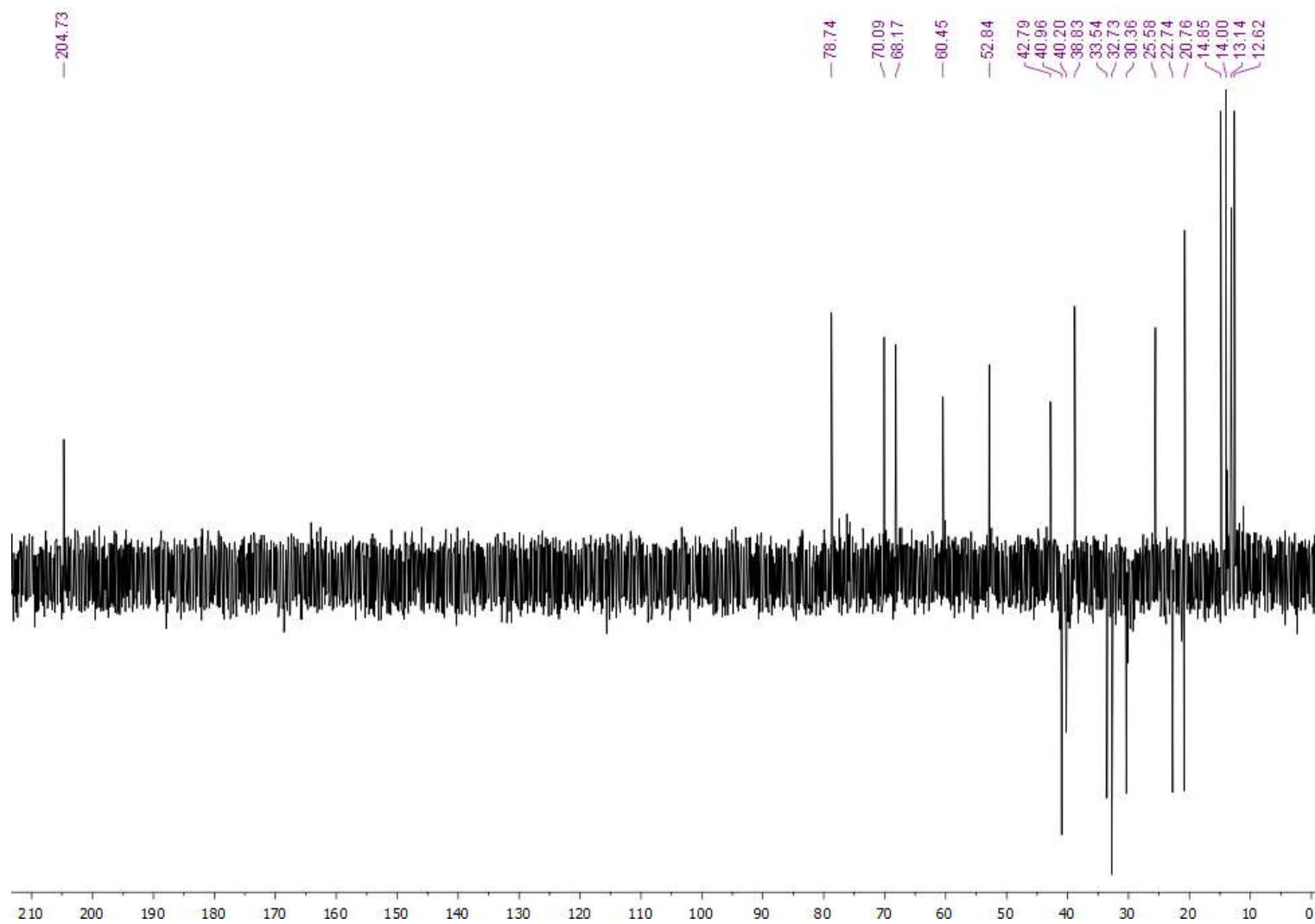
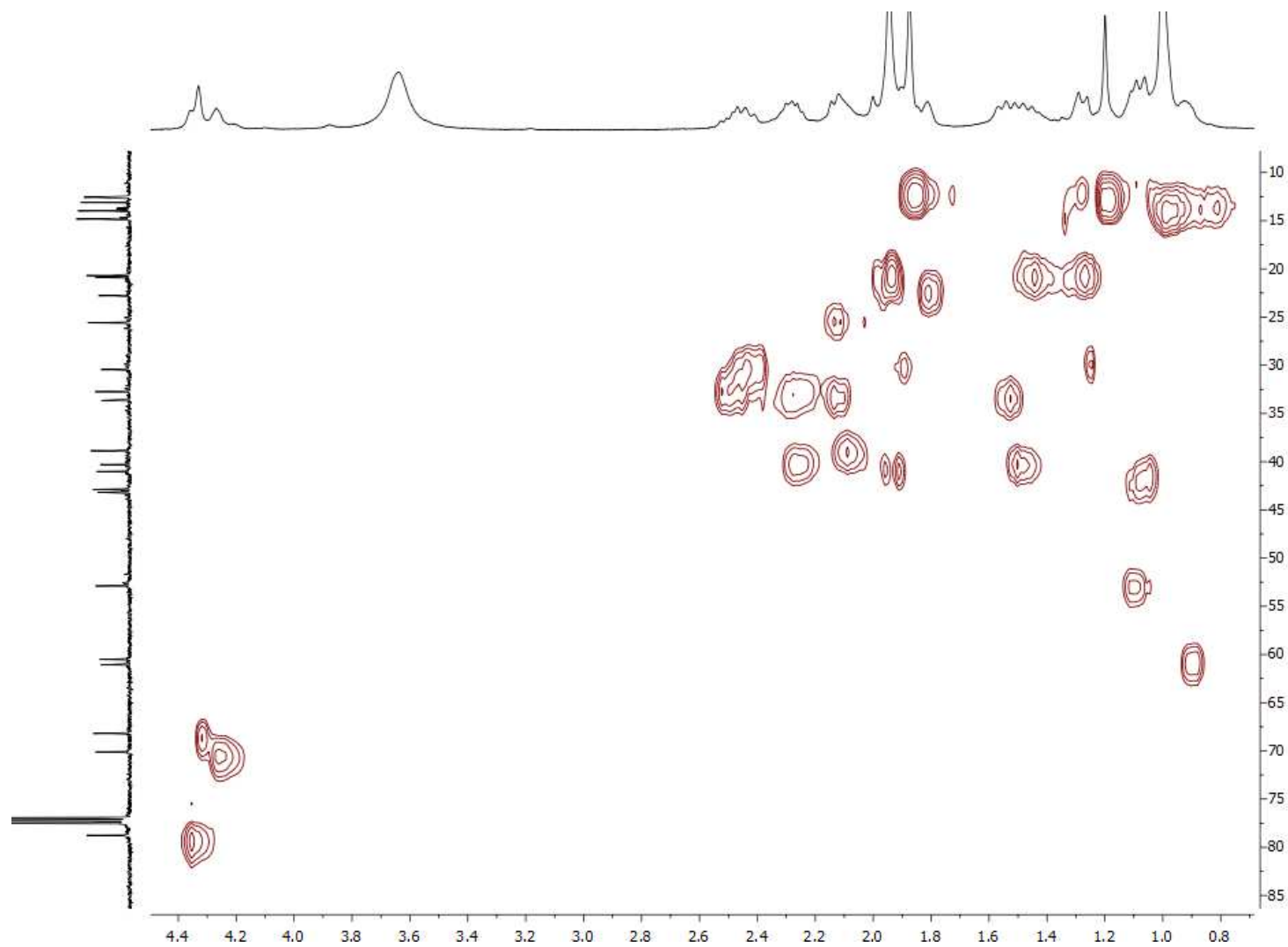**Figure S 70. DEPT 135° NMR (125.75 MHz) spectrum of 9, in CDCl₃.**
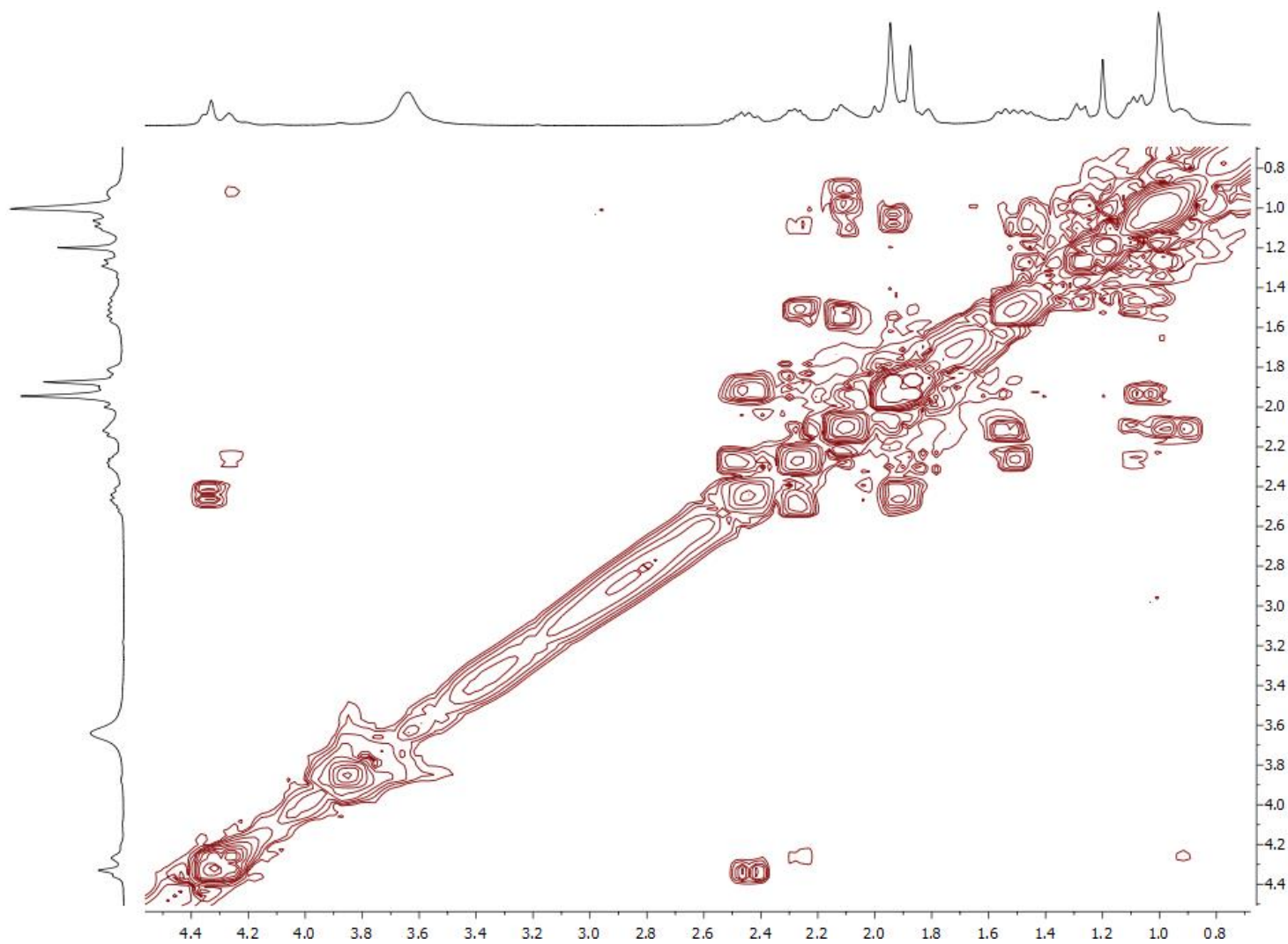
Figure S 71. HSQC NMR spectrum of 9, in CDCl₃.

Figure S 72. COSY NMR spectrum of 9, in CDCl₃

Figure S 73. HMBC NMR spectrum of 9, in CDCl₃.
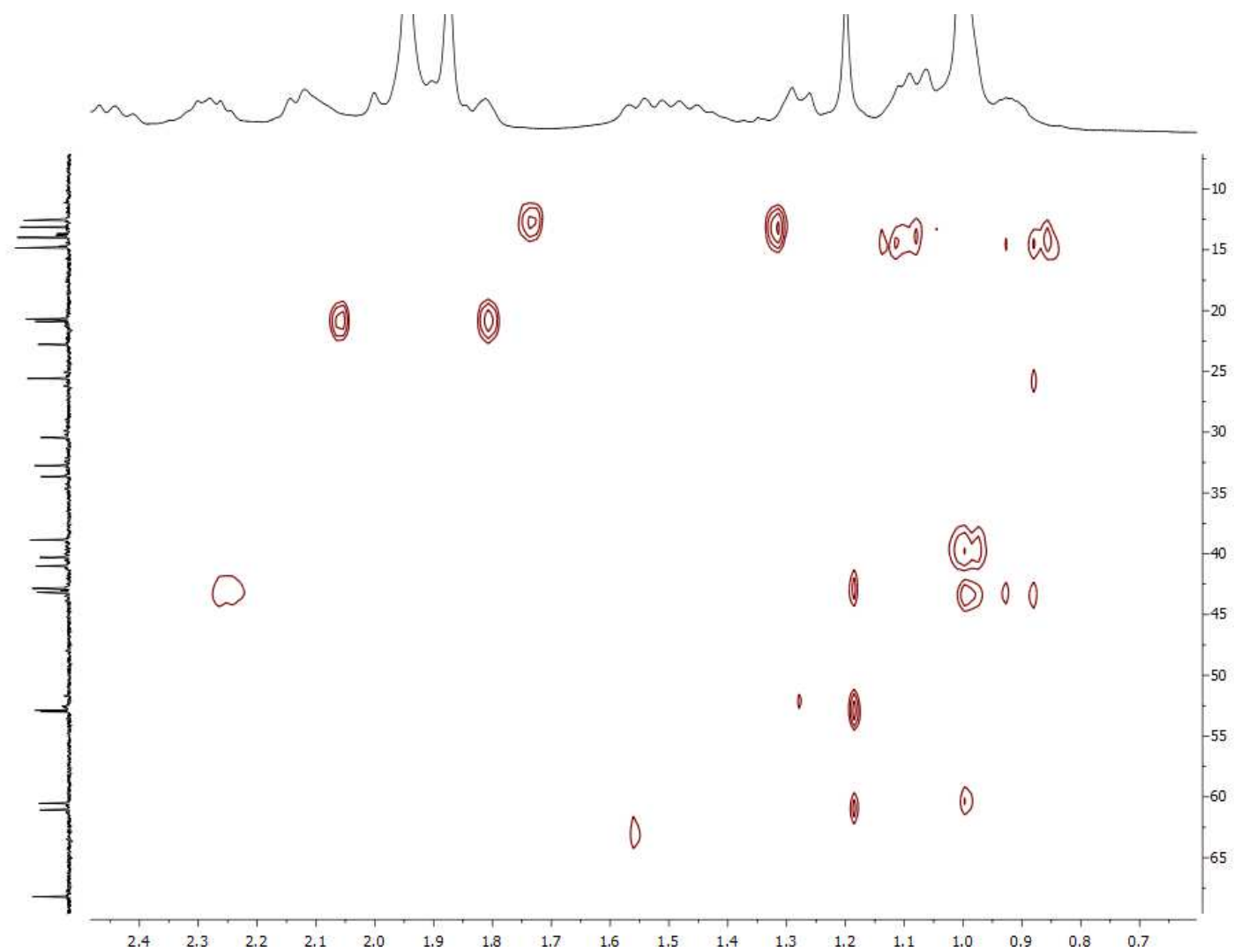
Figure S 74. HMBC expansion of 9, in CDCl₃.
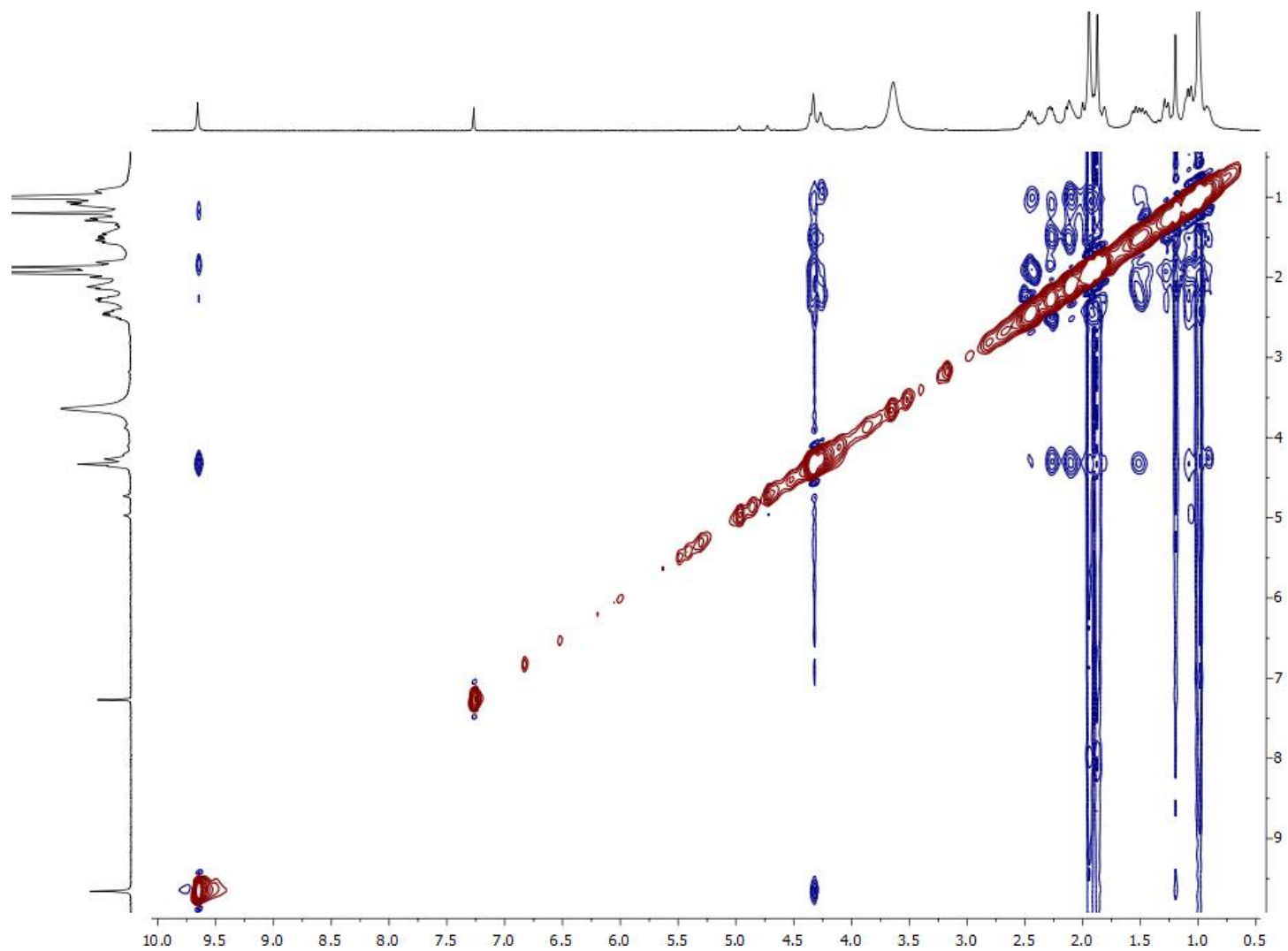
Figure S 75. NOESY NMR spectrum of 9, in CDCl₃.
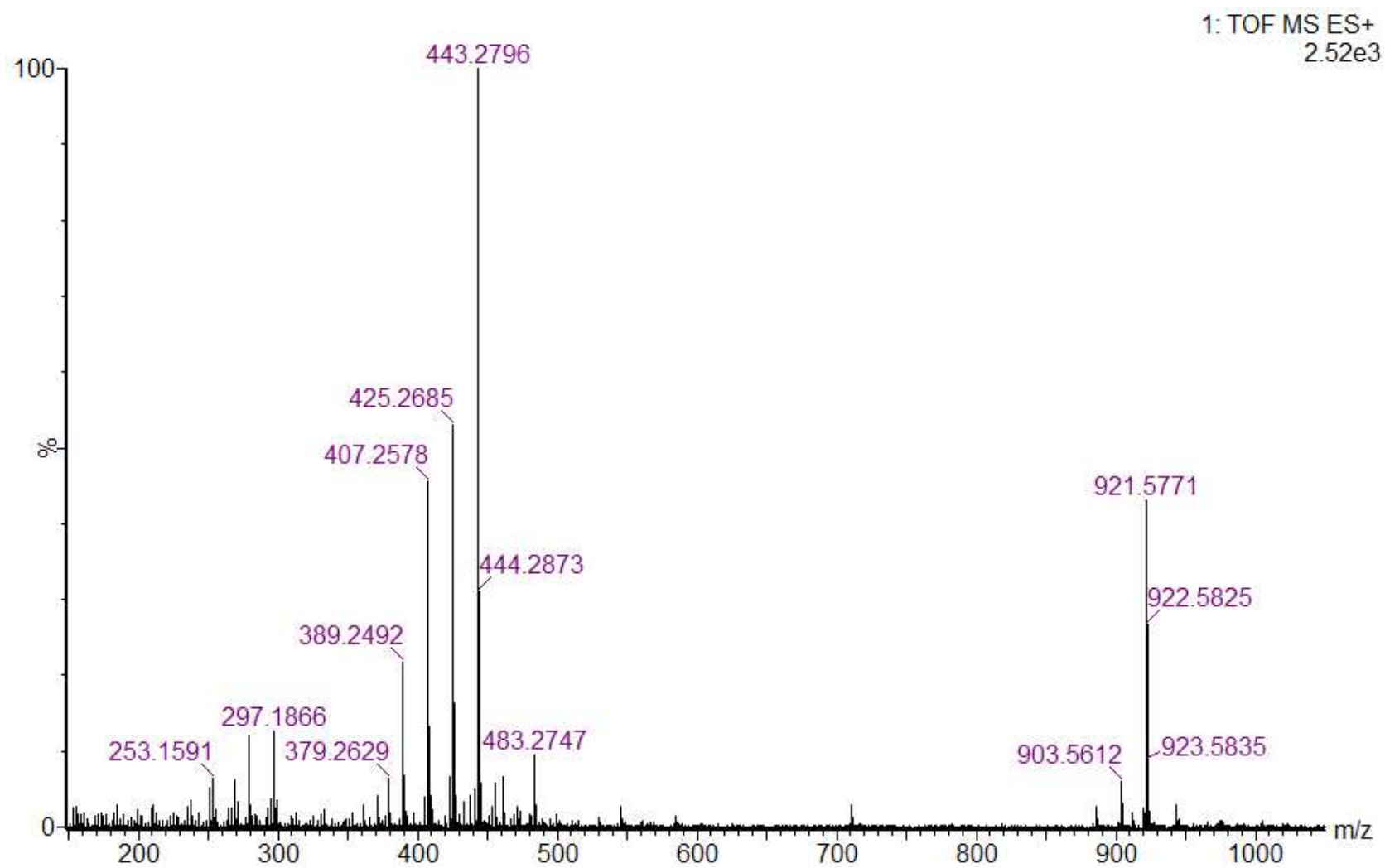
Figure S 76. HRESIMS spectrum of 9.
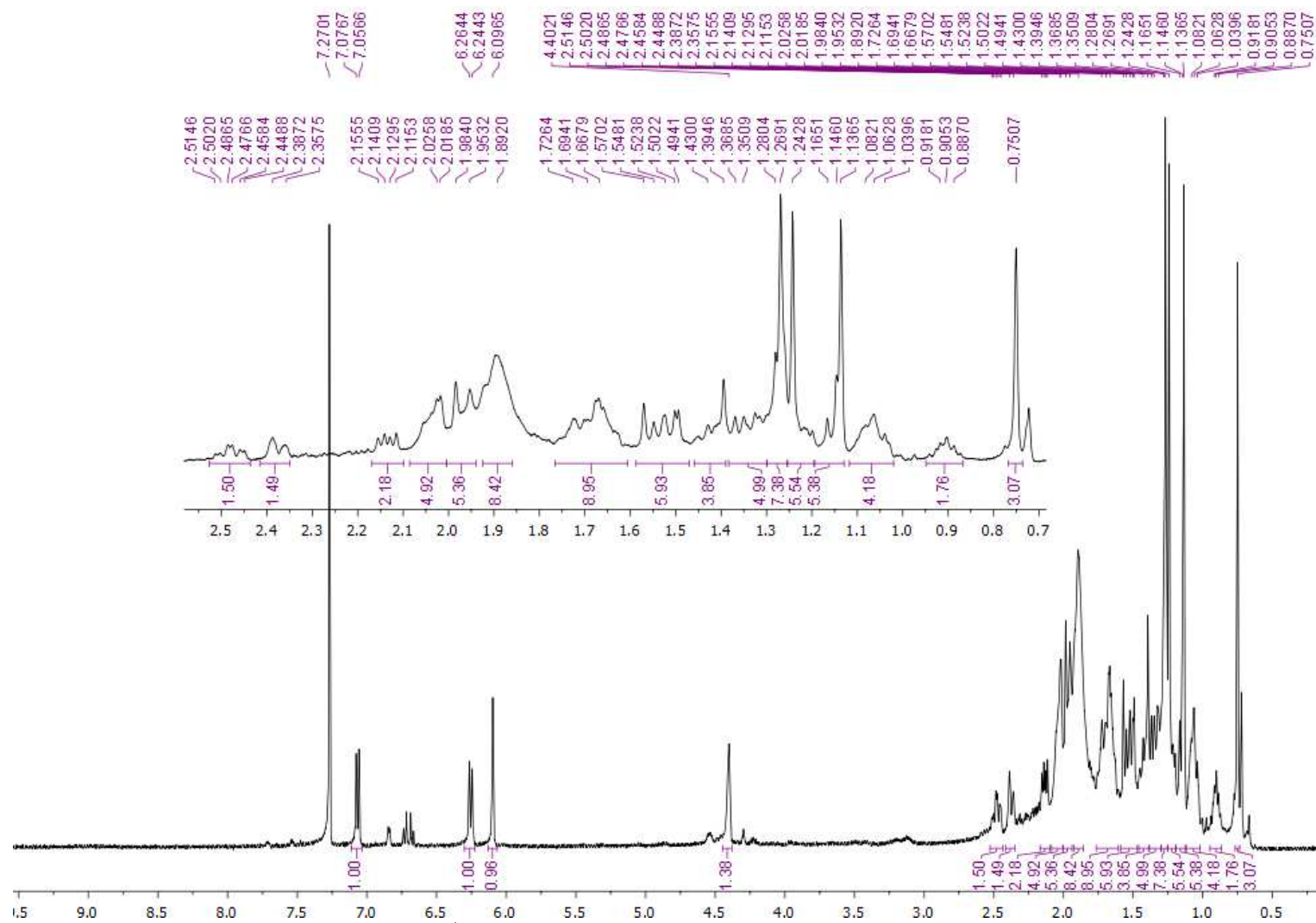
Figure S 77. ^{1}H NMR (500.13 MHz) spectrum of **10**, in CDCl$_3$.
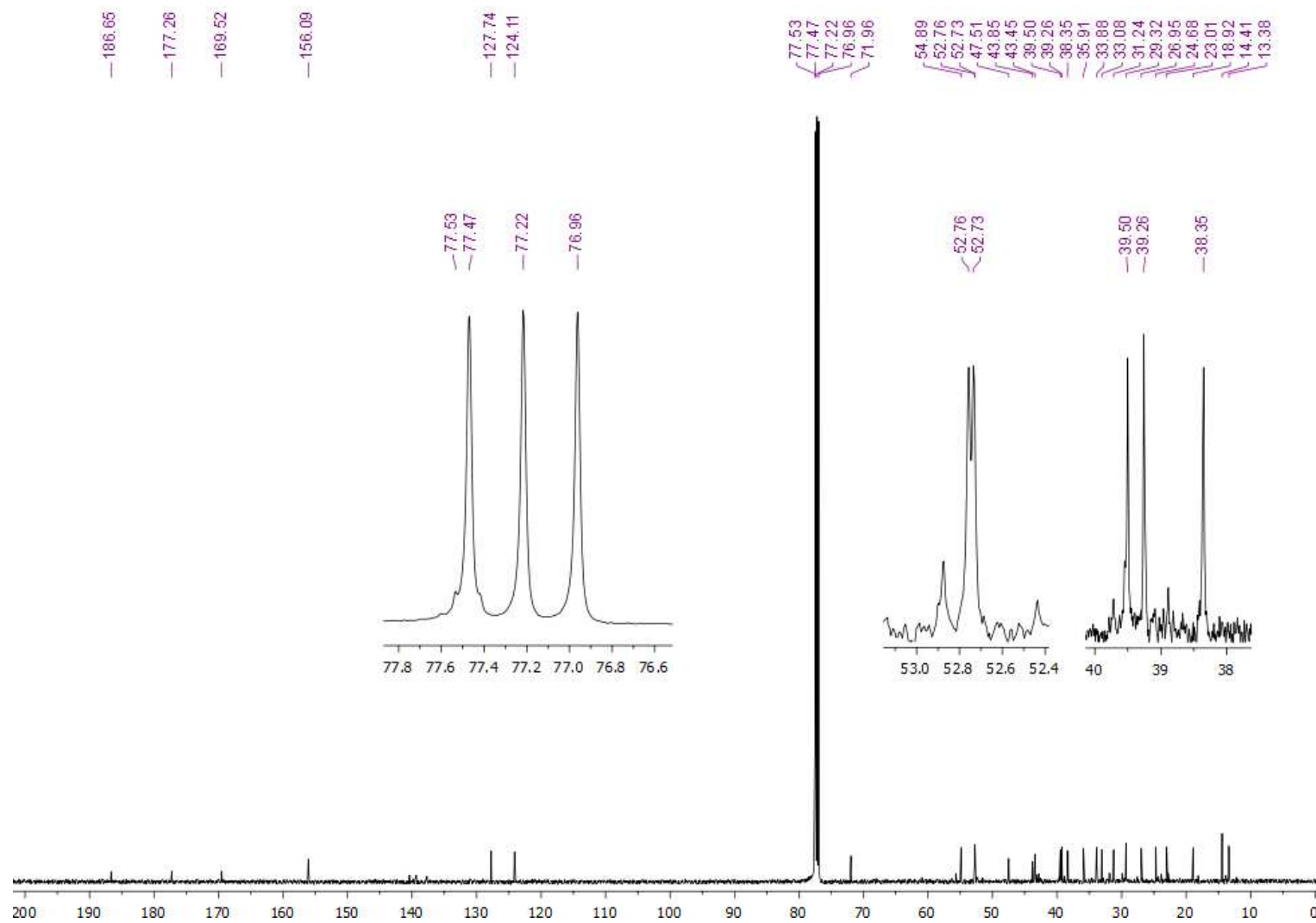
Figure S 78. ^{13}C NMR (125.75 MHz) spectrum of **10**, in CDCl$_3$.

Figure S 79. DEPT 135° NMR (125.75 MHz) spectrum of 10, in CDCl₃.

Figure S 80. HSQC NMR spectrum of 10, in CDCl₃.

Figure S 81. COSY NMR spectrum of 10, in CDCl₃.
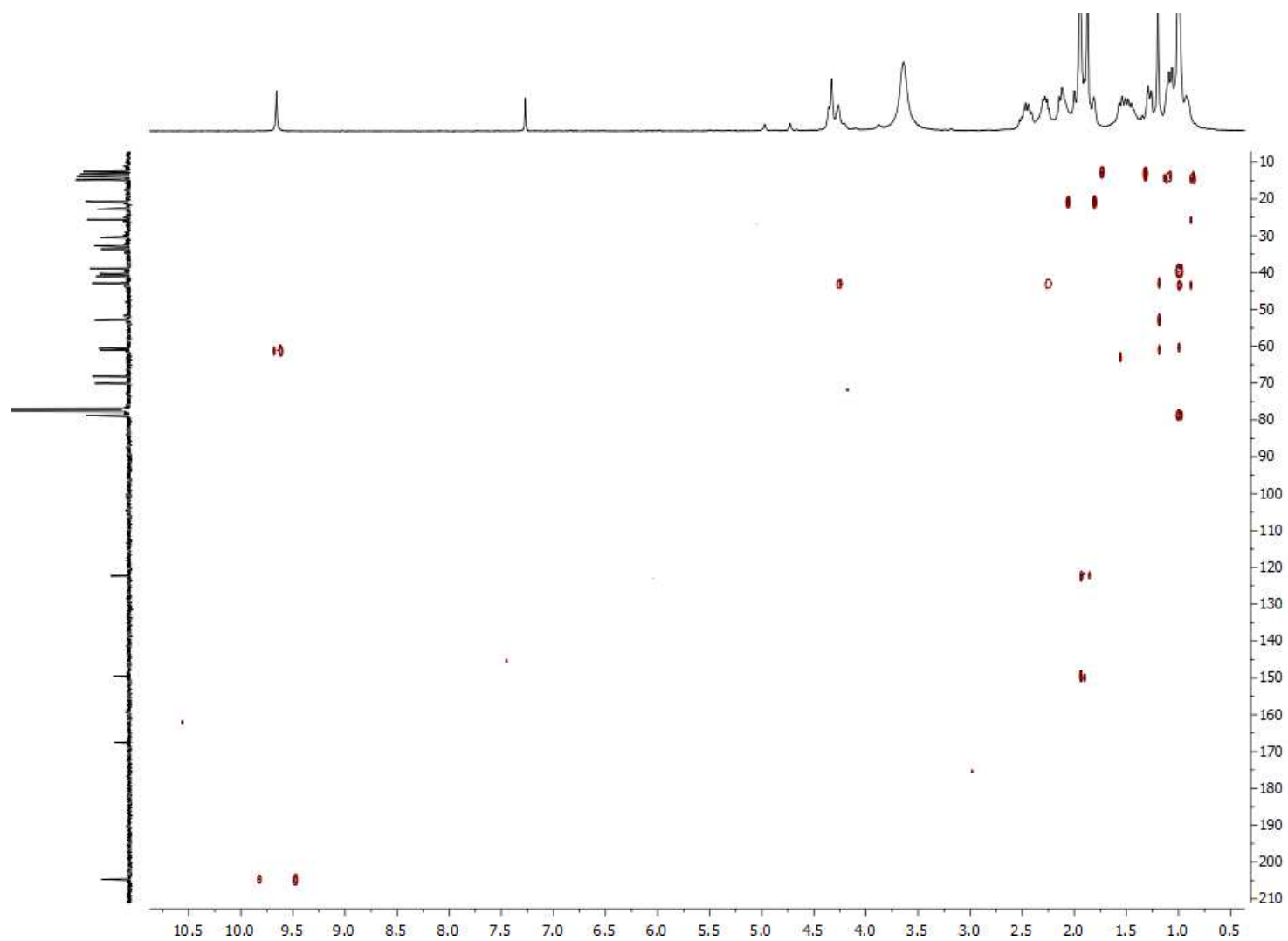
Figure S 82. HMBC NMR spectrum of 10, in CDCl₃.

Figure S 83. HMBC expansion of 10, in CDCl₃.

Figure S 84. NOESY NMR spectrum of 10, in CDCl₃.
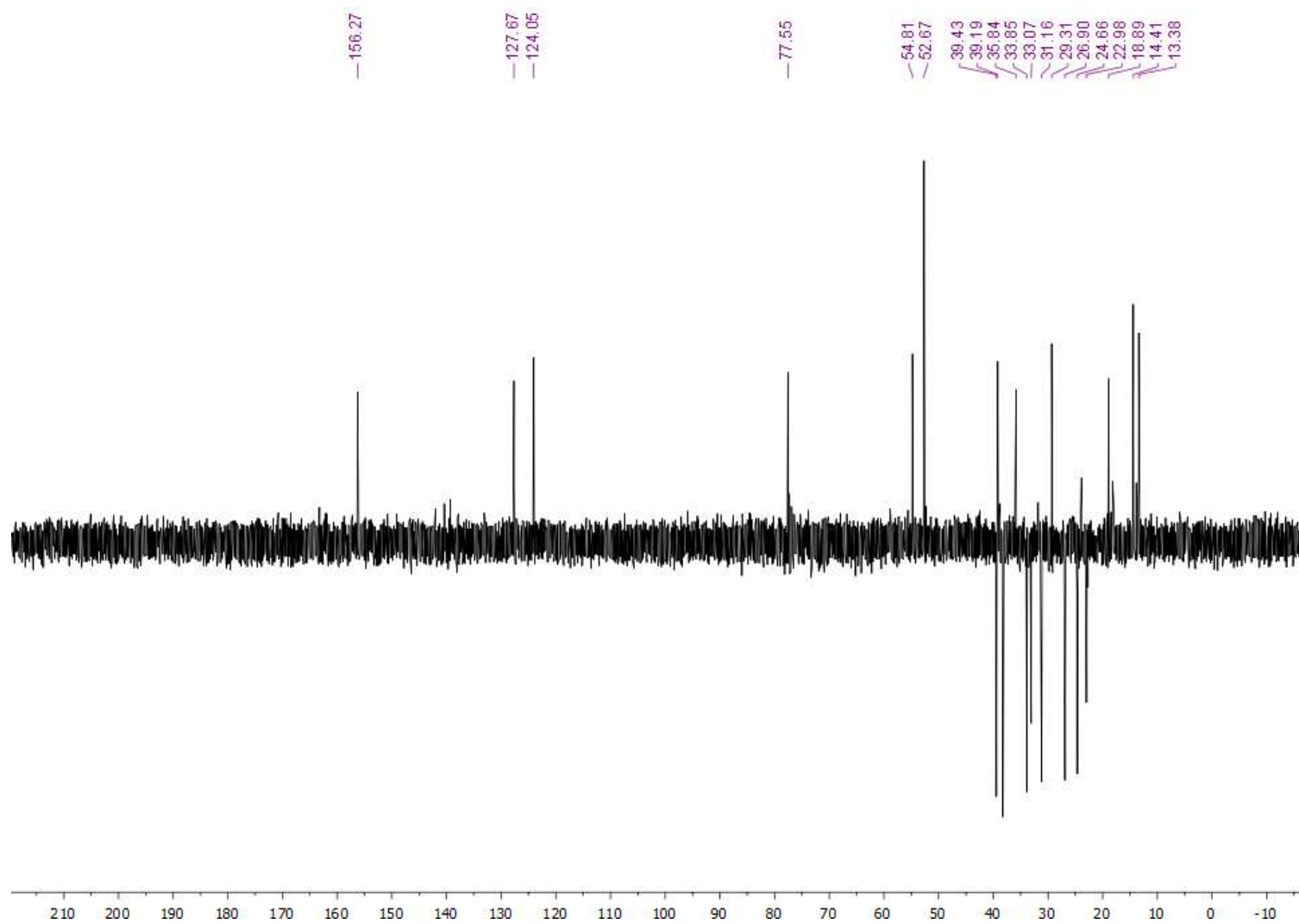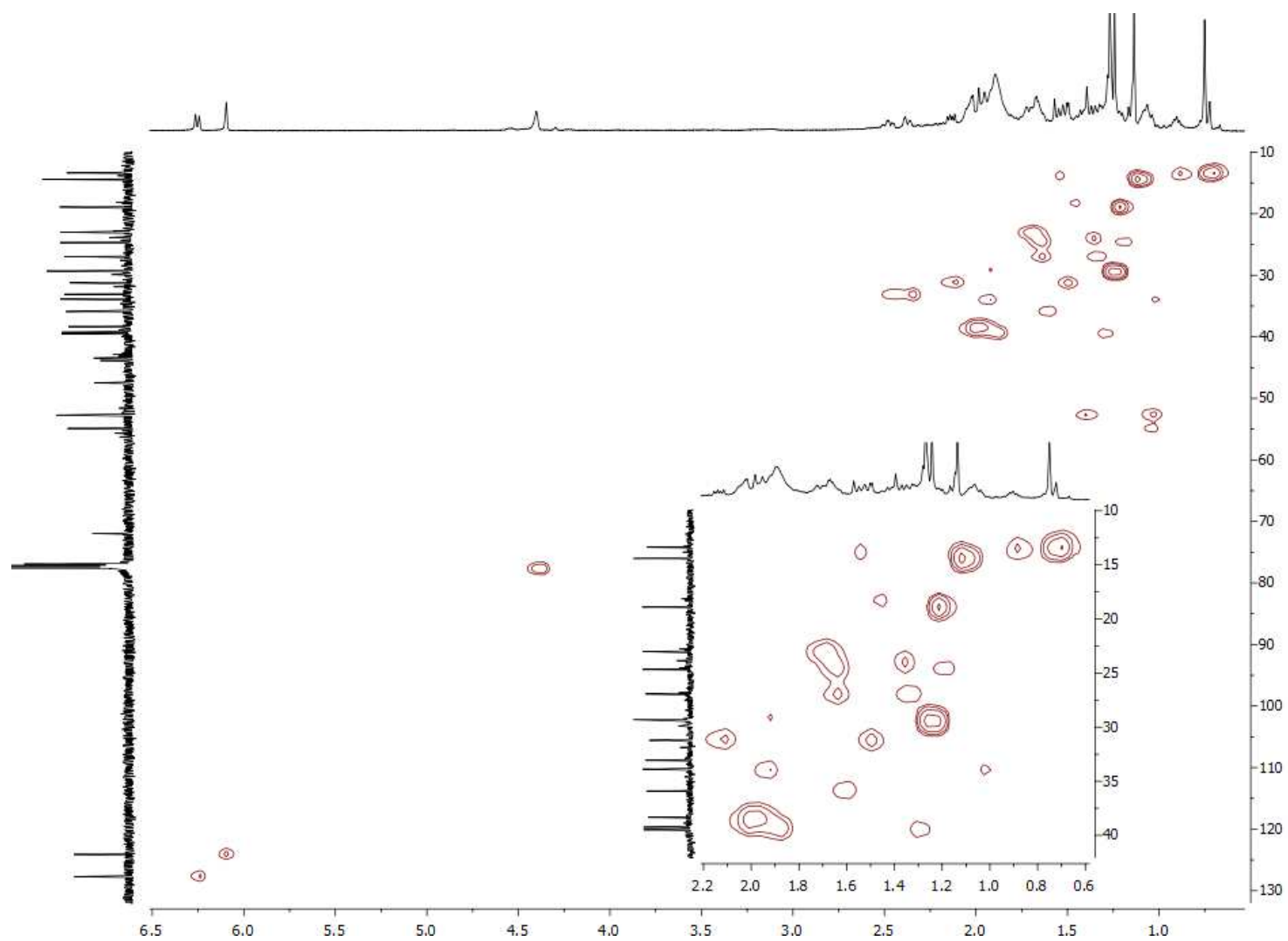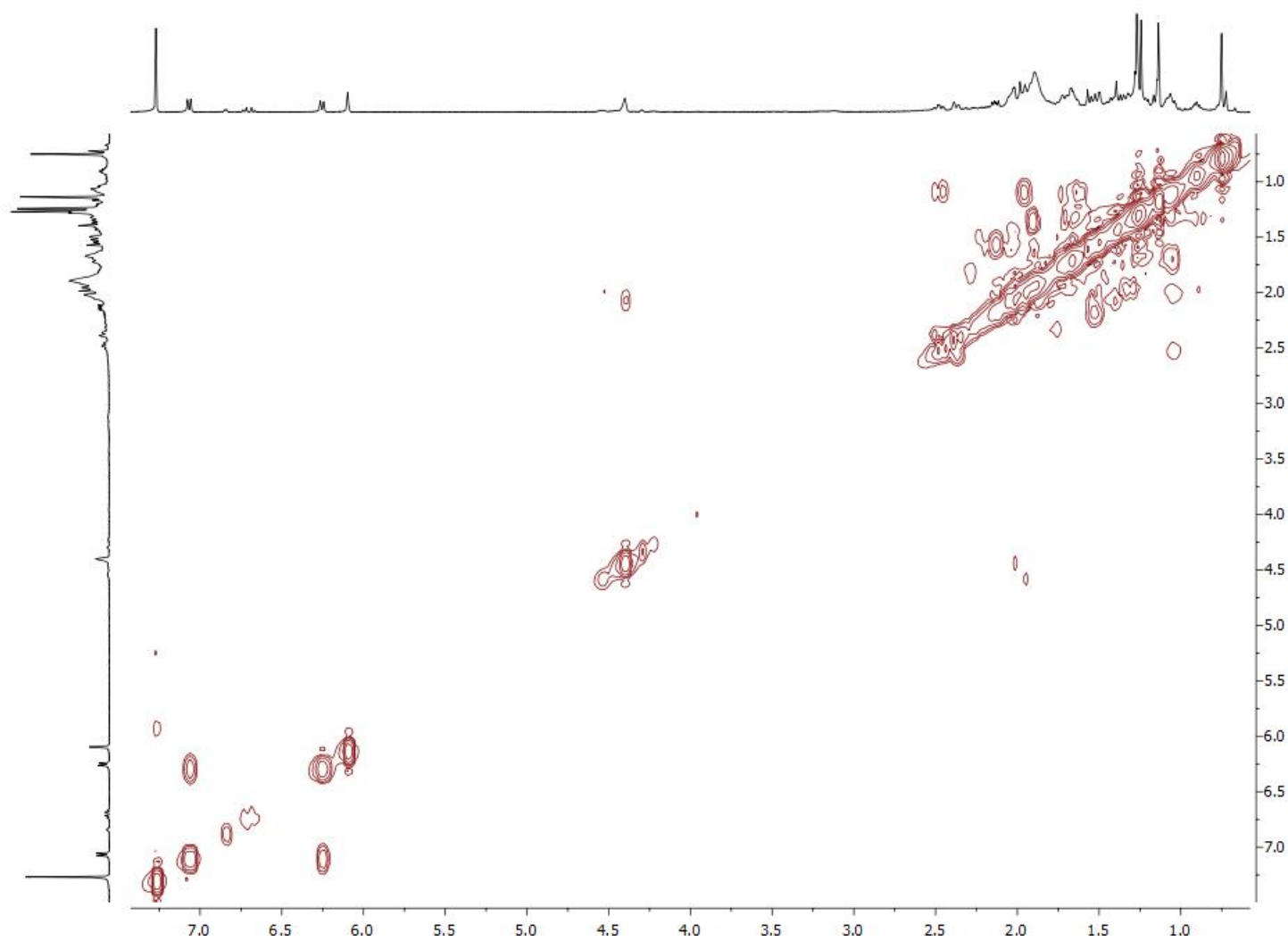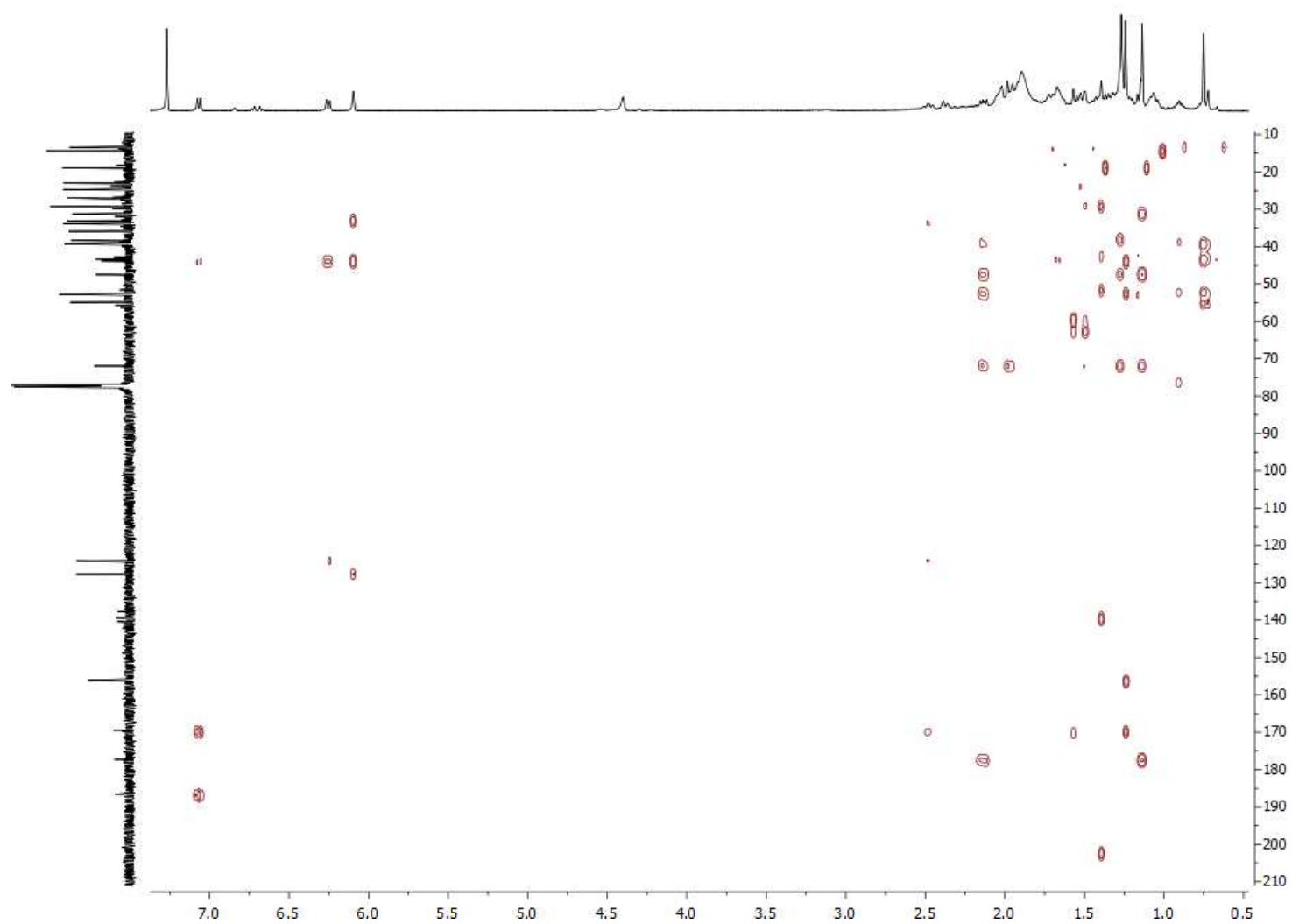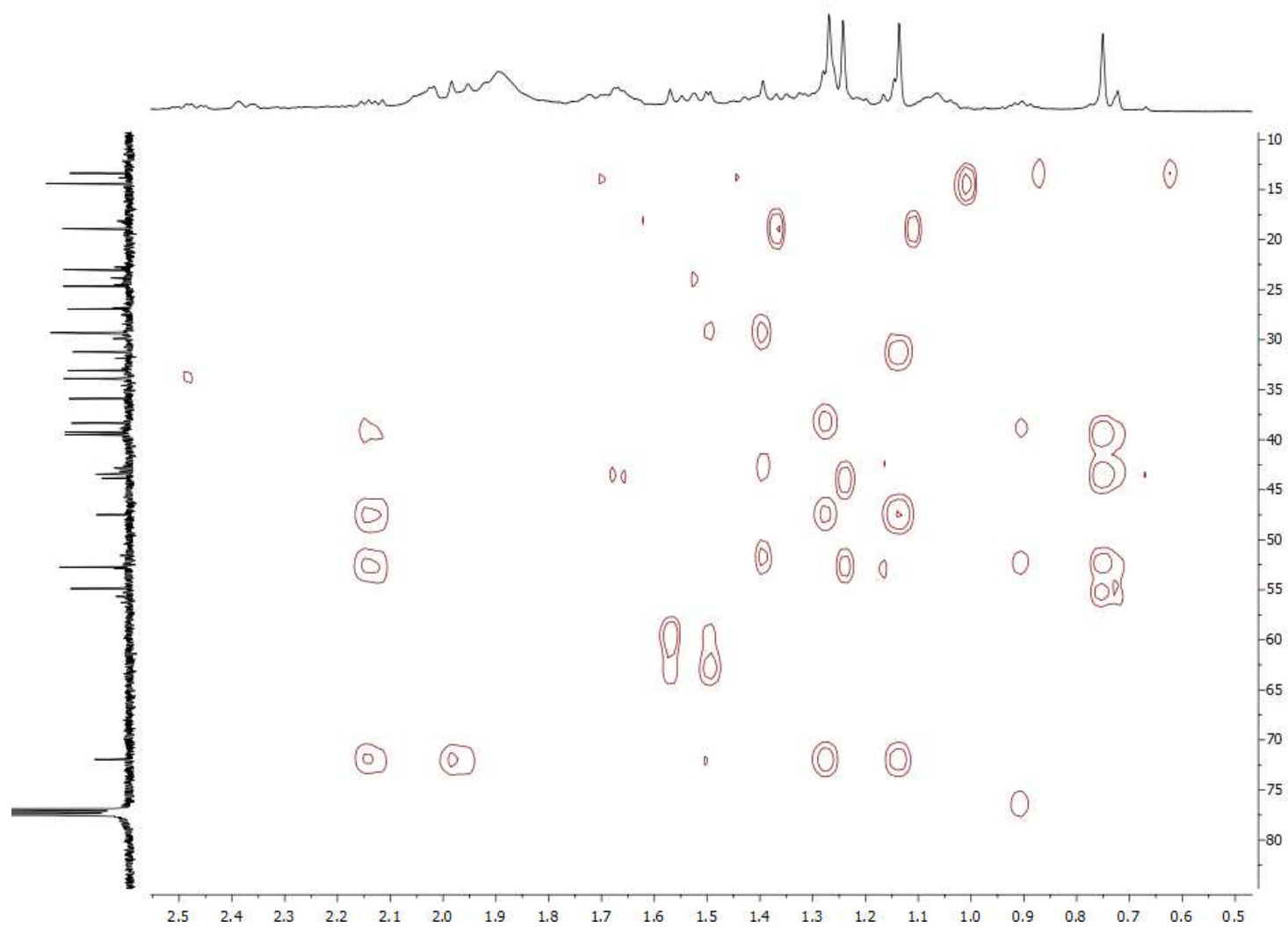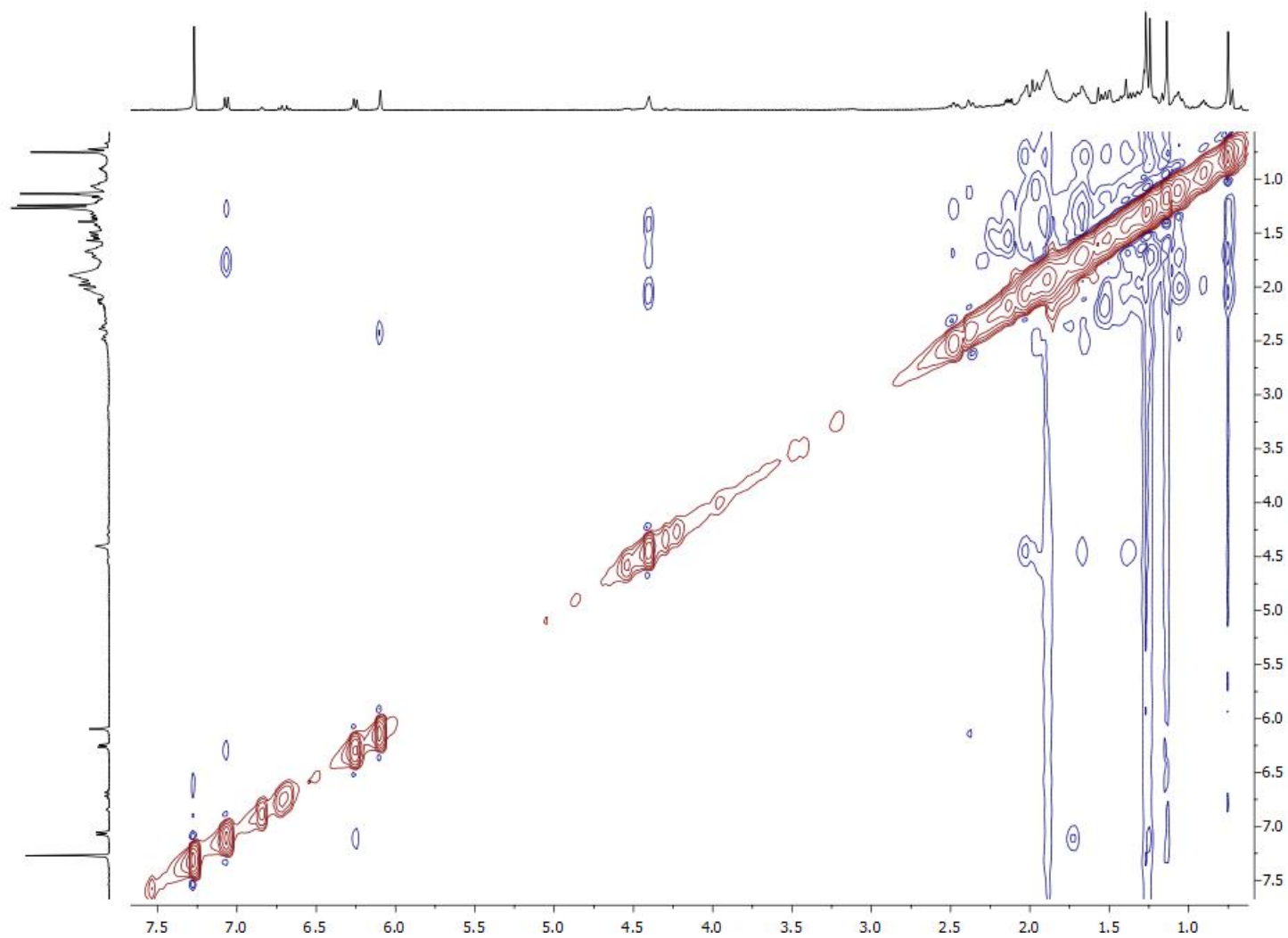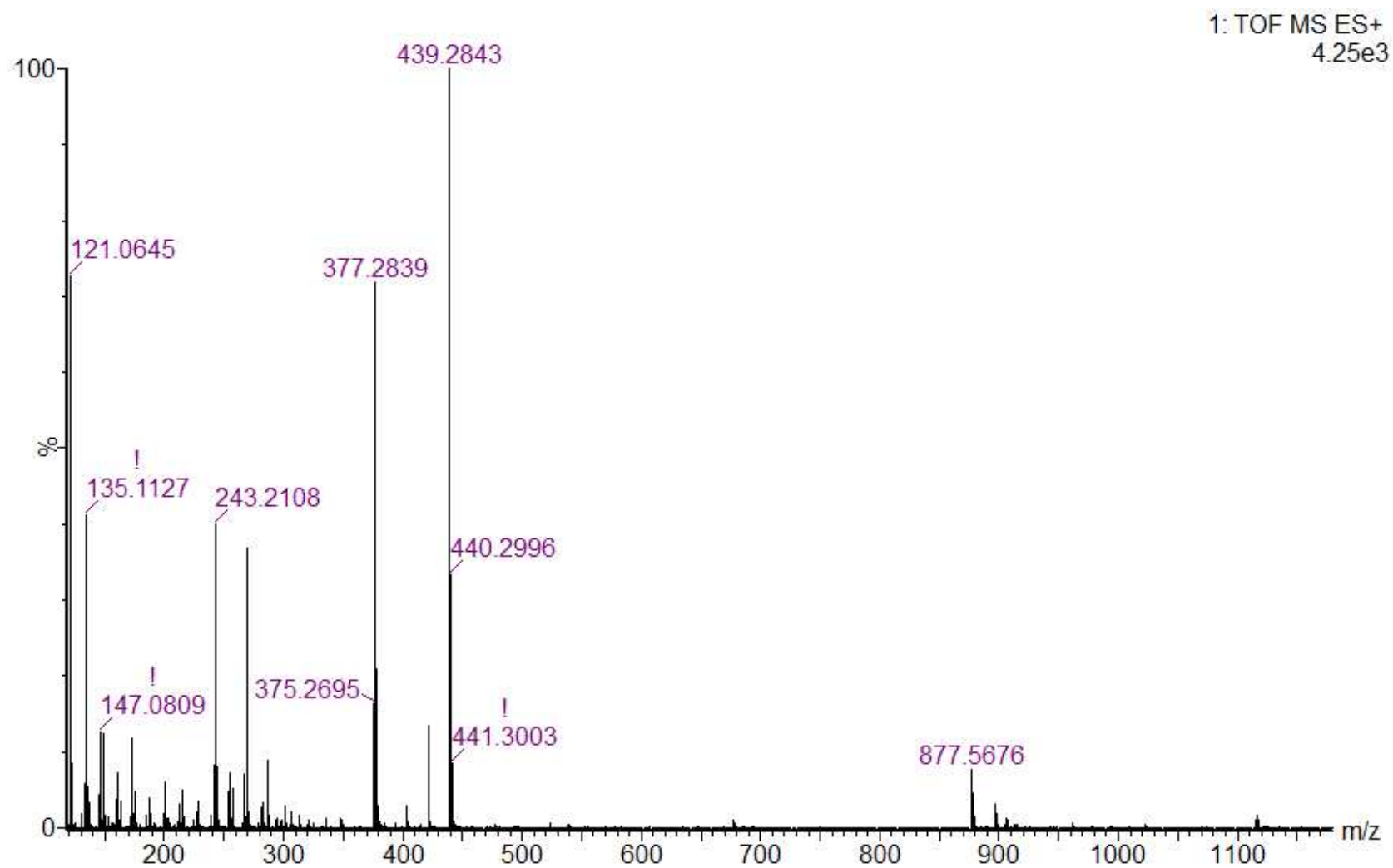
Figure S 85. HRESIMS spectrum of 10

5 CONSIDERAÇÕES FINAIS

Athenaea constitui um pequeno gênero da família Solanaceae ainda pouco explorado sob os aspectos químicos, tendo sido estudadas apenas *Aureliana fasciculata* (*Athenaea fasciculata*), *A. martiana*, e, recentemente, *A. velutina* (Almeida et al., 2019; Dantas Rocha et al., 2022).

A. velutina é a única espécie, dentre as 14 descritas para o gênero, que foi registrada no estado do Ceará, precisamente na localidade Pico Alto, no município de Guaramiranga. A investigação química do extrato hexânico/acetato de etila 1:1 das folhas resultou no isolamento de dezoito vitanolídeos, dentre os quais, quatorze ainda não registrados na literatura. Vale ressaltar, o isolamento de vitajardins, um grupo minoritário de vitanolídeos.

Estudos filogenéticos baseados em sequências de genes e fragmentos de restrição do DNA plastidial, mostram que os gêneros *Athenaea* e *Withania* são muito próximos, e possuem como grupo irmão, o gênero *Tubocapsicum* (ZAMBERLAM, 2012). Baseado em nossos resultados, com o isolamento da vitaferina A e de vários compostos análogos, incluindo os vitajardins, fica confirmado que estes gêneros apresentam uma intrínseca relação que vão além das características botânicas. Dessa forma, os resultados aqui encontrados mostram uma importante contribuição quimiotaxionômica para a espécie.

Um ponto importante e que merece ser destacado, é que, quando uma planta produz vitanolídeos, estes compostos são dominantes, aparecendo tanto nas frações menos polares como nas mais polares. Vale ressaltar que a vitaferina A é um exemplo clássico dos vitanolídeos, considerado uma molécula altamente promissora no campo oncológico, inclusive fazendo parte da lista dos fitoquímicos ativos aprovados na biblioteca do FDA.

No capitulo 1: O Vitanolídeo denominado vitajardin M (AV16), comparativamente a dexametasona, apresentou alta atividade anti-inflamatória, sendo, portanto, um promissor candidato a ser investigado quanto ao potencial anti-inflamatório.

Capítulo 2: Com base nem estudos de dinâmica molecular e simulações de energia livre de ligação, os vitanolides avaliados AV1, AV2 e AV4 mostraram grande estabilidade e alto potencial de interação com o alvo da protease M^{pro}(proteina principal do SARS-CoV-2), com destaque para o composto AV1, sugerindo um promissor agente anti-SARS-CoV-2.

Capítulo 3: Qanto a citotóxicidade, os vitanolídeos foram avaliados frente à um painel de quatro células cancerígenas de humanos. Os compostos AV5, AV10 (vitaferina A) e AV12 exibiram significante atividade com valores de IC_{50} variando entre 0,19 a 3,03. Estes resultados demonstram o potencial anticancer desta grande classe de compostos.

REFERÊNCIAS

ALMEIDA, A. A. *et al*. Screening of plants from the Brazilian Atlantic Forest led to the identification of *Athenaea velutina* (Solanaceae) as a novel source of antimetastatic agents. **Int. J. Exp. Path.** p. 1−16, 2020. https://doi.org/10.1111/iep.12351

ALMEIDA, A. A. *et al*. Withalutin, a new cytotoxic withanolide from *Athenaea velutina* (Sendtn.) D'Arcy, **Nat. Prod. Res.** 2022. https://doi.org/10.1080/14786419.2022.2039135

ALMEIDA-LAFETÁ, R. C. *et al*. Withanolides from *Aureliana fasciculata* var. fasciculata. **Helv. Chim. Acta**. v. 93, p. 2478–2487, 2010.

BAKRIM, W. B. *et al*. Anti-amnesic effects of withaferin A, a steroidal lactone isolated from Withania adpressa, on scopolamine-induced memory impairment in mice. **Arab. J. Chem.** v. 15, 103529, 2022. https://doi.org/10.1016/j.arabjc.2021.103529

BHAT, B. A. *et al*. Isolation, characterization and biological evaluation of datura lactones as potential immunomodulators. **Bioorg. Med. Chem**., v. 13, p. 6672–6677, 2005. https://doi.org/10.1016/j.bmc.2005.07.040

CHAKRABORTY, S. *et al*. The natural products withaferin A and withanone from the medicinal herb *Withania somnifera* are covalent inhibitors of the SARS-CoV-2 main protease. **J. Nat. Prod.** v. 85, p. 2340−2350, 2022. https://doi.org/10.1021/acs.jnatprod.2c00521

CHANDEL, V. *In silico* identification of potent FDA approved drugs against coronavírus COVID-19 main protease: A drug repurposing approach. **Chem. Biol. Lett**. v. 7, n. 3, p. 166–175, 2020. http://thesciencein.org/cbl

CHAUHAN, S. et al. Early selective strategies for higher yielding bio-economic Indian Ginseng based on genotypic study through metabolic and molecular markers, **Saudi J. Biol. Sci.** 2022, doi: https://doi.org/10.1016/j.sjbs.2022.01.030

CHEN, L-X.; HE, H.; QIU, F. Natural withanolides: an overview. **Nat. Prod. Rep.** v. 28, p. 705–740, 2011. https://doi.org/10.1039/c0np00045k

DOM, M.; BERGHE, W. V.; OSTADE, X. V. Broad-spectrum antitumor properties of withaferin A: a proteomic perspective. **RSC Med. Chem**., v. 11, p. 30–50, 2020. https://doi.org/10.1039/c9md00296k

DONG, B. *et al*. Withanolides from *Physalis peruviana* showing nitric oxide inhibitory effects and affinities with iNOS. **Bioorg. Chem**. v. 87, p. 585–593, 2019. https://doi.org/10.1016/j.bioorg.2019.03.051

ECHEVERRI, F. *et al*. Withajardin E, A withanolide from *Deprea orinocensis*. **Phytochemistry**, v. 40, p. 923-925, 1995.

GUO, B. *et al*. Withaferin A promotes white adipose browning and prevents obesity through sympathetic nerve–activated prdm16-FATP1 Axis. **Diabetes**, v. 71, p. 249–263, 2022. https://doi.org/10.2337/db21-0470

GUO, R. *et al*. Withaferin A prevents myocardial ischemia/reperfusion injury by upregulating AMP-activated protein kinase-dependent B-cell lymphoma2 signaling. **Circ. J.** v. 83, p. 1726 – 1736, 2019. https://doi.org/10.1253/circj.CJ-18-1391

KHANCHANDANI, N. *et al*. Antibacterial and antifungal activity of Ashwagandha (*Withania somnifera* L.): A review. **J. Drug Deliv. Ther.** v. 9, n. 5, p. 154−161, 2019. http://dx.doi.org/10.22270/jddt.v9i5-s.3573

KIM, S. *et al*. Cytotoxic withanolides from the roots of indian ginseng (*Withania somnifera*). **J. Nat. Prod.** v. 82, p. 765-773, 2019. https://doi.org/10.1021/acs.jnatprod.8b00665

KIYOTA, N. *et al*. New C28 Steroidal Glycosides from *Tubocapsicum anomalum*. **Chem. Pharm. Bull.** v. 56, p. 1038–1040, 2008. https://doi.org/10.1248/cpb.56.1038

KUPCHAN, S. M. *et al*. Tumor inhibitors. XXXIX. Active principles of *Acnistus arborescens*. Isolation and structural and spectral studies of withaferin A and withacnistin. **J. Org. Chem.** v. 34, n. 12, p. 3858−3866, 1969. https://doi.org/10.1021/jo01264a027

LAVIE, D.; GLOTTER, E.; SHVO, Y. Constituents of *Withania somnifera* Dun. III. The side chain of withaferin A. **J. Chem. Soc.** v. 30, p. 1774-1778, 1965.

LEE, J. *et al*. Withaferin A is a leptin sensitizer with strong antidiabetic properties in mice. **Nat. Med**. v. 22, p. 970–971, 2016. https://doi.org/10.1038/nm.4145

LIMA, S. C. M. *et al*. Leishmanicidal activity of withanolides from *Aureliana fasciculata* var. fasciculata. **Molecules**. v. 23, p. 3160–3171, 2018. https://doi.org/10.3390/molecules23123160

LLANOS, G. G. *et al*. Structure-based design, synthesis, and biological evaluation of withaferin A-analogues as potent apoptotic inducers. **Eur. J. Med. Chem**. v. 140, p. 52–64, 2017. http://dx.doi.org/10.1016/j.ejmech.2017.09.004

LUIZ, J. G. *et al*. Withajardins, withanolides with a new type of skeleton structure of withajardins A, B, C and D absolute configuration of withajardin C. **Tetrahedron**, v. 50, n. 4. p. 1217-1226, 1994.

MALIK, V. *et al*. Computational identification of BCR-ABL oncogenic signaling as a candidate target of withaferin A and withanone. **Biomolecules**, 12, 212. 2022, https://doi.org/10.3390/biom12020212

MINGUZZI, S. *et al*. Cytotoxic withanolides from *Acnistus arborescens*. **Phytochem**. v. 59, p. 635–641, 2002. https://doi.org/10.1016/s0031-9422(02)00022-5

MISICO, R. I. *et al*. **Withanolides and Related Steroids**. Progress in the chemistry of organic natural products, v. 94, Springer-Verlag/Wien p. 128–229. 2011. 103p. https://doi.org/10.1007/978-3-7091-0748-5_3

NICOLÁS, F. G. *et al*. Withanolides with antibacterial activity from *Nicandra john-tyleriana*, **J. Nat. Prod.** v. 78, p. 250-257, 2015. https://doi.org/10.1021/np500824f

RABHI, C. *et al*. Neuroprotective efect of CR-777, a glutathione derivative of withaferin A, obtained through the bioconversion of *Withania somnifera* (L.) Dunal extract by the fungus *Beauveria bassiana*. **Molecules**, v. 24, p. 4599–4617, 2019. https://doi.org/10.3390/molecules24244599

RODRIGUES, I. M. C. *et al*. Pollen morphology in *Athenaea* Sendtn. and *Aureliana* Sendtn. (Solanaceaee) **Palynology**, v. 40, n. 2, p. 202-215, 2016. https://doi.org/10.1080/01916122.2015.1022908

RODRIGUES, I. M. C., KNAPP, S., STEHMANN, J. R. Two new species of *Athenaea* Sendtn. (Solanaceaee) from the Atlantic forests of south-eastern Brazil. **PhytoKeys**, v. 178, p. 1–15, 2021. https://doi.org/10.3897/phytokeys.178.64609

RODRIGUES, I. M. C.; KNAPP, S.; STEHMANN, J. R. The nomenclatural re-establishment of *Athenaea* Sendtn. (Solanaceaee) with a nomenclatural synopsis of the genus. **Taxon**, v. 68 n. 4, p. 839-846, 2019. https://doi.org/10.1002/tax.12089

ROUMY, V. *et al*. Antifungal and cytotoxic activity of withanolides from *Acnistus arborenscens*. **J. Nat. Prod.** v. 73, p. 1313–1317, 2010. https://doi.org/10.1021/np100201p

SAMPAIO, V. S. *et al*. Flora of Ceará, Brazil: Solanum (Solanaceae). **Rodriguésia**, v. 70, e02512017, 2019. http://dx.doi.org/10.1590/2175-7860201970029

SIDDIQUI, B. S. *et al*. Daturacin, a new withanolide from *Datura innoxia*. **Nat. Prod. Res.** v. 19, n. 6, p. 619–623, 2005 https://doi.org/10.1080/147864105123313306200

SILVA, E. L. *et al*. athenolide A, a new steroidal lactone from the leaves of *Athenaea martiana* (Solanaceaee) determined by means of HPLC-HR-MS-SPENMR analysis. **Chem. Biodiversity**, v. 15 e1700455(8p), 2018. https://doi.org/10.1002/cbdv.201700455

SINGH, A. *et al*. Recent advances in the chemistry and therapeutic evaluation of naturally occurring and synthetic withanolides. **Molecules**, v. 27, n. 886, 2022, https://doi.org/10.3390/molecules27030886

STEHMANN, J. R. *et al*. 2015. Solanaceae in lista de espécies da Flora do Brasil. Jardim Botânico do Rio de Janeiro. Disponível em: http://floradobrasil.jbrj.gov.br/jabot/floradobrasil/FB14587

STRAUGHN, A. R., KAKAR, S. S. Withaferin A: a potential therapeutic agente against COVID-19 infection. **J. Ovarian Res.** v. 13, n. 79, 2020. https://doi.org/10.1186/s13048-020-00684-x

TAO, S. *et al*. Withaferin A analogs that target the AAA+ chaperone p97. **ACS Chem. Biol.** v. 10, p. 1916−1924, 2015. https://doi.org/10.1021/acschembio.5b00367

WANG, S-B. *et al*. Cytotoxic withanolides from the aerial parts of *Tubocapsicum anomalum*, **Bioorg. Chem**. v. 81, p. 396-404, 2018. https://doi.org/10.1016/j.bioorg.2018.08.034

WHITE, P.T. *et al*. Natural Withanolides in the Treatment of Chronic Diseases in: S.C. Gupta, S. Prasad, B.B. Aggarwal (Eds.), Anti-inflammatory nutraceuticals and chronic diseases, advances in experimental medicine and biology, Berlin: Springer, p. 329-373, 2016. https://doi.org/10.1007/978-3-319-41334-1_14

WIJERATNE, E. M. K. *et al*. Withaferin A and withanolide D analogues with dual heat-shock-inducing and cytotoxic activities: semisynthesis and biological evaluation. **J. Nat. Prod**. v. 81, p. 825−837, 2018. https://doi.org/10.1021/acs.jnatprod.7b00918

XIA, G.-Y. *et al*. Natural withanolides, an update. **Nat. Prod. Rep.** v. 28, n. 705, 2021. https://doi.org/10.1039/d1np00055a

XIANG, K. *et al*. Withanolides isolated from *Tubocapsicum anomalum* and their antiproliferative activity, **Bioorg. Chem.** 2021. https://doi.org/10.1016/j.bioorg.2021.104809

XU, Y-M. *et al*. 17*β*-Hydroxy-18-acetoxywithanolides from aeroponically grown *Physalis crassifolia* and their potent and selective cytotoxicity for prostate cancer Cells. **J. Nat. Prod**. v. 79, p. 821−830, 2016. https://doi.org/10.1021/acs.jnatprod.5b00911

XU, Y-M. *et al*. 17*β*-Hydroxywithanolides as sensitizers of renal carcinoma cells to tumor necrosis factor‑α related apoptosis inducing ligand (TRAIL) mediated apoptosis: structure−activity relationships. **J. Med. Chem**. v. 60, p. 3039−3051, 2017. https://doi.org/10.1021/acs.jmedchem.7b00069

XU, Y-M. *et al*. Discovery of potent 17*β*-hydroxywithanolides for castration-resistant prostate cancer by high-throughput screening of a natural products library for androgen-induced gene expression inhibitors. **J. Med. Chem**. v. 58, p. 6984−6993, 2015. https://doi.org/10.1021/acs.jmedchem.5b00867

YONEYAMA, T. *et al*. Hedgehog inhibitors from *Withania somnifera*. **Bioorg. Med. Chem. Lett.** v. 25, p. 3541–3544, 2015. http://dx.doi.org/10.1016/j.bmcl.2015.06.081

YOUSEFIAN, Z. *et al*. Production of the anticancer compound withaferin A from genetically transformed hairy root cultures of *Withania Somnifera*. **Nat. Prod. Commun.** v. 13, p. 943–948, 2018.

ZAMBERLAN, P. M. **Estudos filogenéticos e filogeográficos nos gêneros *Athenaea* sendtn. e A*ureliana* sendtn. (solanaceae).** 2012. Tese (Doutorado em Ciências) – Centro de Ciências, Universidade Federal do Rio Grande do Sul, Porto Alegre, 2012.

ZHANG, H. *et al*. Cytotoxic withanolide constituents of *Physalis longifolia*. **J. Nat. Prod**. v. 74, p. 2532–2544, 2011. http://dx.doi.org/10.1021/np200635r